CORA Cork Open Research Archive
Cartlann Taighde Oscailte Chorcaí

Title	Quantum state transfer via invariant based shortcuts to adiabaticity
Authors	Kiely, Anthony
Publication date	2017
Original Citation	Kiely, A. 2017. Quantum state transfer via invariant based shortcuts to adiabaticity. PhD Thesis, University College Cork.
Type of publication	Doctoral thesis
Rights	© 2017, Anthony Kiely. - http://creativecommons.org/licenses/by-nc-nd/3.0/
Download date	2026-10-30 17:13:30
Item downloaded from	https://hdl.handle.net/10468/3877



NATIONAL UNIVERSITY OF IRELAND, CORK



Quantum State Transfer via Invariant based Shortcuts to Adiabaticity

by

Anthony Kiely

A thesis submitted in partial fulfillment for the degree of Doctor of Philosophy

in the Department of Physics

Supervisor: Dr. Andreas Ruschhaupt

Head of Department: Prof. John McInerney

2017

Declaration of Authorship

This is to certify that the work I am submitting is my own and has not been submitted for another degree, either at University College Cork or elsewhere. All external references and sources are clearly acknowledged and identified within the contents. I have read and understood the regulations of University College Cork concerning plagiarism.

Signed: _____

Date: _____

External Examiner
Prof. Daniel Alonso – University of La Laguna, Spain

Internal Examiner
Dr. Bryan Kelleher – University College Cork, Ireland

Abstract

Adiabatic processes in quantum mechanics are very useful to prepare and manipulate quantum states but have the drawback of requiring long operation times. Hence there is a long time for the system to interact with its environment which can lead to a loss of coherence of the final state. This decoherence is problematic for implementing future quantum technologies which require the state's quantum mechanical features. "Shortcuts to Adiabaticity"(STA) provides a toolbox of methods to improve on adiabatic processes. Using these methods one can derive alternative processes which work for much shorter times with perfect fidelity. Since adiabatic processes are ubiquitous in atomic, molecular and optical physics, there is a broad scope of application for STA. In this thesis, STA (especially those using Lewis-Riesenfeld invariants) are applied to a variety of quantum systems for the purpose of quantum state transfer. In particular I show that STA control schemes in two- and three-level systems can be optimised to be more stable against unwanted uncontrollable transitions than adiabatic methods with the same operation time. I also show that STA methods can be applied in a triple well ring system with complex tunnelling, in optical lattices for the purposes of generating a higher orbital state of neutral atoms and in Penning traps to quickly compress or expand the trapped ion wavefunction. Finally I also investigate the effect of classical Poisson white noise on adiabatic processes.

Acknowledgements

There are a tremendous amount of people who have helped me over the last three years. I would like to thank my parents, Dolores and Gerry, for their constant support and encouragement. I also want to thank all the other physics postgraduate students: Danny, Michael, Mark, Bryan, Joe, Donovan, Owen, Psymon, Liam and Declan. There was always great banter at lunch. Lots of thanks must also go to everybody at the UCC mountaineering club. Going hiking and climbing was a great way to escape the routine and clear my mind. I enjoyed all the trips over the years. Special thanks goes to Isobel for numerous delicious baked goods and lots of happy memories. I must also thank all the people I have worked with over the course of my PhD including Gonzalo Muga and Thomas Busch. Although my visit to Bilbao was short I really enjoyed it. Thanks to all those in Okinawa for making my stays there so much fun including Lee, Tara, Steve, Albert, Tadhg, Jérémie, Angela, Mossy and Sawako. I don't think I ever properly acclimatised to the weather but I always felt at home. I'm also thankful to all those in the group. In particular David Rea was a huge help proof reading various papers and boosting morale. Finally I have to thank my supervisor, without whom none of this work would be possible. Andreas has been a great mentor. His boundless optimism is infectious and was an enormous help when tackling the hard problems.

Anthony Kiely
University College Cork
December 2016

List of Publications

This work is based on the following publications which are ordered by appearance in the thesis.

- **A. Kiely** and A. Ruschhaupt
  Inhibiting unwanted transitions in population transfer in two- and three-level quantum systems
  J. Phys. B: At. Mol. Opt. Phys. **47** 115501 (2014)

- A. Benseny, **A. Kiely**, Y. Zhang, T. Busch and A. Ruschhaupt
  Spatial non-adiabatic passage using geometric phases
  ArXiv:1611.02398 (submitted)

- **A. Kiely**, A. Benseny, T. Busch and A. Ruschhaupt
  Shaken, not stirred: creating exotic angular momentum states by shaking an optical lattice
  J. Phys. B: At. Mol. Opt. Phys. **49** 215003 (2016)

- **A. Kiely**, J. P. L. McGuinness, J. G. Muga and A. Ruschhaupt
  Fast and stable manipulation of a charged particle in a Penning trap
  J. Phys. B: At. Mol. Opt. Phys. **48** 075503 (2015)

- **A. Kiely**, J. G. Muga and A. Ruschhaupt
  Effect of Poisson noise on adiabatic quantum control
  Phys. Rev. A **95** 012115 (2017)

". . . it is fair to state that we are not experimenting with single particles, any more than we can raise Ichthyosauria in the zoo."

-Erwin Schrödinger, 1952

Contents

Declaration of Authorship i

Abstract ii

Acknowledgements iii

List of Publications iv

1 Introduction 1

2 Background theory 5
2.1 Quantum optics . . . 5
2.1.1 Interaction of an atom and a classical light field . . . 5
2.1.2 Particle trapping . . . 9
2.1.3 Laser cooling methods . . . 15
2.2 Shortcuts to adiabaticity . . . 17
2.2.1 Adiabatic theorem . . . 18
2.2.2 Lewis–Riesenfeld invariants . . . 22
2.2.3 Counterdiabatic driving . . . 26
2.2.4 Fast–forward approach . . . 28
2.3 Analytical and numerical techniques . . . 29
2.3.1 Example of Hilbert space truncation: the double well . . . 29
2.3.2 Time-dependent perturbation theory . . . 34
2.3.3 Numerical techniques . . . 38

3 Inhibiting unwanted transitions in population transfer in two- and three-level quantum systems 47
3.1 Overview . . . 47
3.2 Introduction . . . 48
3.3 Invariant-based shortcuts in two-level quantum systems . . . 49
3.4 Two-level quantum system with unwanted transition . . . 52

3.4.1 Model . . . 52
3.4.2 Transition sensitivity . . . 54
3.4.3 General properties of the transition sensitivity . . . 56
3.4.4 Reference case: flat π pulse . . . 58
3.4.5 Other examples of π pulses . . . 59
3.4.6 Numerically optimised scheme with $q = 0$ . . . 60
3.4.7 Comparison of the transition probability . . . 61
3.5 Invariant-based shortcuts in three-level systems . . . 63
3.6 Unwanted transitions in three-level systems . . . 65
3.6.1 Model . . . 65
3.6.2 Transition sensitivity . . . 66
3.6.3 General properties of the transition sensitivity . . . 67
3.6.4 Example of schemes . . . 69
3.6.5 Comparison of the transition probability . . . 71
3.7 Conclusion . . . 72

4 Spatial non-adiabatic passage using geometric phases 75
4.1 Overview . . . 75
4.2 Introduction . . . 76
4.3 System model . . . 77
4.4 SNAP in the three-level approximation . . . 80
4.4.1 Adiabatic methods . . . 80
4.4.2 Transitionless quantum driving . . . 81
4.4.3 Invariant-based inverse engineering . . . 82
4.5 Examples of SNAP schemes . . . 84
4.5.1 Transport . . . 85
4.5.2 Creation of a three-trap superposition . . . 87
4.6 SNAP in the continuum model . . . 88
4.7 Conclusions . . . 92

5 Creating exotic angular momentum states by shaking an optical lattice 93
5.1 Overview . . . 93
5.2 Introduction . . . 94
5.3 Model . . . 97
5.3.1 Optical lattice . . . 97
5.3.2 Four–level approximation . . . 99
5.3.3 Initial and target states . . . 102
5.4 Lewis–Riesenfeld invariants for the four–level system . . . 103
5.5 Shaking schemes for preparing an angular momentum state . . . 106
5.5.1 Polynomial scheme . . . 107
5.5.2 Piecewise scheme . . . 108
5.6 Numerical simulations of the shaking schemes . . . 109
5.7 Experimental considerations . . . 114

5.8 Conclusions . . . 115

6 Fast and stable manipulation of a charged particle in a Penning trap 117
6.1 Overview . . . 117
6.2 Introduction . . . 118
6.3 General streamlined formalism . . . 119
6.3.1 Main equations . . . 119
6.3.2 Inverse engineering and boundary conditions . . . 121
6.4 Energy Eigenstates of a Penning trap . . . 123
6.5 Varying the magnetic field strength . . . 125
6.5.1 Streamlined formalism . . . 125
6.5.2 Invariant based approach . . . 128
6.5.3 Numerical Example . . . 131
6.5.4 Superposition . . . 133
6.5.5 Stability . . . 133
6.6 Conclusion . . . 136

7 Effect of Poisson noise on adiabatic quantum control 137
7.1 Overview . . . 137
7.2 Introduction . . . 138
7.3 Master equation for Poisson noise . . . 140
7.3.1 General properties of $\mathcal{L}_0$ and $\mathcal{L}_1$ . . . 143
7.3.2 Special case: Two-level quantum system . . . 145
7.4 Approximations for weak and strong Poisson noise . . . 147
7.4.1 Adiabatic approximation without noise . . . 147
7.4.2 Approximation for weak noise in an adiabatic process . . . 149
7.4.3 Strong noise limit . . . 150
7.5 Poisson noise effect on adiabaticity . . . 152
7.5.1 Phase-changing scheme in a two-level system . . . 152
7.5.2 Population transfer in a two-level system . . . 154
7.5.3 STIRAP process in a three-level system . . . 157
7.6 Conclusion . . . 160

8 Summary and outlook 161
8.1 Inhibiting unwanted transitions . . . 161
8.2 Spatial non-adiabatic passage . . . 162
8.3 Creating exotic angular momentum states . . . 163
8.4 Manipulation of a particle in a Penning trap . . . 164
8.5 Effect of classical Poisson noise . . . 165

A Properties of Lewis–Riesenfeld invariants 167

B Supplementary calculations for chapter 4 171

B.1 Mapping continuum model to the three-level approximation 171

C Supplementary calculations for chapter 5 **175**
C.1 Transformation into lattice frame 175
C.2 Six–level approximation 176

D Supplementary calculations for chapter 6 **179**
D.1 Boundary conditions for $\Phi(t, \vec{r})$ 179
D.2 Solution of the main equations in polar coordinates 180
D.3 Fidelity and sensitivity for arbitrary N and M 181

E Supplementary calculations for chapter 7 **183**
E.1 Commutator recursion relation in two-level systems 183
E.2 Derivation of strong noise limit 185

Bibliography **189**

In memory of Valerie

Chapter 1

Introduction

The theory of quantum mechanics is often regarded as strange or unusual. Despite its accurate predictions in all manner of settings, many notable physicists remained displeased at its counter intuitive nature with Einstein being the most famous [1]. While the theory is far removed from everyday experience, it is now not only widely accepted but also thought to be useful in a variety of applications [2].

Many fundamental theories of physics have later led to important technological revolutions. The exotic physical rules of quantum mechanics provide new opportunities in this respect. Over recent decades there has been great experimental progress in preparing systems which are so small and isolated that they can only be accurately described using quantum mechanics. The unprecedented control of such systems was highlighted with the award of the 2012 Nobel Prize in Physics to Serge Haroche and David J. Wineland "for ground-breaking experimental methods that enable measuring and manipulation of individual quantum systems"[3]. Examples of such quantum systems include nuclear magnetic resonance on molecules [4, 5], neutral atoms in optical traps [6], light in high–finesse cavities [7], the formation of Bose–Einstein condensates [8] and many more. In addition to allowing for the creation of novel technologies, these systems also provide us with the opportunity to investigate fundamental physical phenomenon such as the transition from quantum to classical physics. In particular, realisations of macroscopic superpositions could rule out so called collapse models [9, 10] which postulate an

intrinsic difference between quantum mechanics at microscopic and macroscopic scales.

The applications of technologies using quantum effects span a broad range from those which are already commercially available (such as quantum key distribution [11–13] which guarantees secure communication) to others which have only been realised in a very limited capacity (such as quantum computers [11] which can solve certain problems much faster than traditional classical computers). Several quantum algorithms have already been discovered which demonstrate the supremacy of quantum computers in specific problems such as integer factorization [14] and searching unsorted databases [15]. Quantum effects could also be useful for devices in metrology such as cold atom interferometers [16, 17] (since the de Broglie wavelength of atoms is so small) and atomic clocks [18] which are already commonly used for accurate time keeping.

The coherent manipulation of quantum systems for quantum technologies, fundamental studies, or metrology often requires control protocols of external parameters that are stable with respect to perturbations. In particular the implementation of a quantum computer would require one to create, manipulate and read out quantum states of light or matter. The complete list of required characteristics of a quantum computer are outlined formally in the DiVincenzo checklist [19]. Previously adiabatic methods (where the populations of the instantaneous eigenstates are kept constant by the adiabatic theorem [20]) were used to prepare and manipulate states. While intrinsically stable against many types of noise or systematic error, these methods necessarily require long times. This is typically problematic as there is more time for the state to decohere. That is to say, the system has more time to interact with the enviroment and lose its coherence and hence its quantum mechanical features. This has motivated the development of shortcuts to adiabaticity (STA) [21], which are schemes that reach the fidelities of adiabatic processes in shorter times, keeping or even enhancing their stability. As adiabatic processes have been ubiquitous in atomic, molecular and optical physics, STA processes possess a wide range of applications. These techniques have even

been used outside the realm of non-relativistic quantum mechanics such as work on the Boltzmann equation [22] and the Dirac equation [23, 24].

Apart from STA, there have been several other efforts in this direction such as composite pulses [25–27] and optimal control [28–30]. In the case of the latter the schemes derived are purely numerical and hence it can be difficult to draw any physical intuition from them. As STA schemes are typically analytic in nature, they may provide some insight into what makes certain control schemes more stable than others. They may also provide a means to generate good starting points when optimising over the parameter landscape of all control schemes for very complex systems.

The topic of this thesis is using invariant based STA for the purpose of state transfer in a variety of quantum systems. The remainder of the thesis is structured as follows. In the next chapter I review some of the methods of shortcuts to adiabaticity as well as some other essential background knowledge which is assumed throughout the thesis.

In the subsequent chapters I focus on quantum state transfer in finite dimensional systems. In chapter 3, I show that one can construct fast and stable control schemes for two- and three-level quantum systems using Lewis–Riesenfeld invariants. These schemes are optimised against the presence of an additional, unwanted and uncontrollable transition. In chapter 4, I continue to use shortcuts for three-level systems showing that they can be applied to a system of three tunnel-coupled quantum wells. The key addition to the system is a magnetic field which creates a geometric phase, allowing for complex tunnelling frequencies. In particular, I demonstrate the ability to transport the particle between the different wells and to generate a delocalised superposition between the three traps.

I then move on from state transfer in finite dimensional systems to state transfer in continuous systems. In chapter 5, I proposed a method to create higher orbital states of ultracold atoms in the Mott regime of an optical lattice. This is done by periodically modulating the position of the trap minima (known as shaking) and controlling the interference term of the lasers creating the lattice. In chapter

6, I show how one can derive a streamlined fast–forward method for the minimal coupling equation describing a charged particle in an electromagnetic field. I then use this to design a non-adiabatic change of the magnetic field strength in a Penning trap which changes the radial spread without final excitations.

In chapter 7, in contrast with the rest of the thesis (but still related to the topic of adiabatic evolution), I investigate the effects of classical Poisson white noise on adiabatic processes. In particular, I present a detailed derivation of the master equation for this case and outline its various properties. I also investigate recent claims [31] that this type of noise may improve rather than destroy adiabaticity.

Finally in chapter 8, I summarise the work of the thesis and provide an outlook for future work. Note that there will only be notational consistency within individual chapters but not between them.

Chapter 2

Background theory

In this chapter we will review some important concepts that will be used throughout the thesis. This includes topics in quantum optics, shortcuts to adiabaticity and analytical and numerical techniques often used in quantum mechanics.

2.1 Quantum optics

In this section we review some background material in quantum optics regarding how particles are trapped and cooled using light. We begin by discussing how a classical light field interacts with an atom.

2.1.1 Interaction of an atom and a classical light field

We will briefly review the dynamics of an atom coupled to a classical electromagnetic field. A more detailed discussion can be found in [32]. The minimal coupling equation describes the dynamics of the wavefunction for a charged particle in an electromagnetic field. It is given by

$$i\hbar\frac{\partial}{\partial t}\psi\left(\vec{r},t\right)=\frac{1}{2m}\left[\frac{\hbar}{i}\nabla-q\vec{A}\left(\vec{r},t\right)\right]^{2}\psi\left(\vec{r},t\right)+q\phi\left(\vec{r},t\right)\psi\left(\vec{r},t\right), \tag{2.1}$$

where $\vec{A}(\vec{r},t)$ is the vector potential, $\phi(\vec{r},t)$ is the scalar potential, q is the charge and we have neglected the particle's spin. This type of Schrödinger equation (the minimal coupling equation) can be motivated by considering the usual Schrödinger equation with a general potential $V(\vec{r},t) = q\tilde{\phi}(\vec{r},t)$,

$$i\hbar\frac{\partial}{\partial t}\tilde{\psi}(\vec{r},t) = \left[-\frac{\hbar^2}{2m}\Delta + V(\vec{r},t)\right]\tilde{\psi}(\vec{r},t) \tag{2.2}$$

and enforcing that it must be form invariant under a local gauge transformation of the form

$$\psi(\vec{r},t) = e^{\frac{i}{\hbar}q\Lambda(\vec{r},t)}\tilde{\psi}(\vec{r},t). \tag{2.3}$$

This transformation then leads to the minimal coupling equation (2.1) for the wavefunction. Note that the transformation of the vector and scalar potentials leave the electric and magnetic field unchanged, i.e.,

$$\phi(\vec{r},t) = \tilde{\phi}(\vec{r},t) - \frac{\partial}{\partial t}\Lambda(\vec{r},t), \tag{2.4}$$

$$\vec{A}(\vec{r},t) = \tilde{\vec{A}}(\vec{r},t) + \nabla\Lambda(\vec{r},t). \tag{2.5}$$

For simplicity let us now start with an atom with only two particles (an electron and a proton), namely Hydrogen (although the results can also be extended to more complicated atoms). Using the Coulomb gauge, i.e., $\nabla\cdot\vec{A} = 0$ and $\phi = 0$, we can write the Hamiltonian as

$$\begin{aligned} H = &\frac{\vec{p}_e^{\,2}}{2m_e} - \frac{e}{m_e}\vec{A}(\vec{r}_e,t)\cdot\vec{p}_e + \frac{e^2}{2m_e}\vec{A}^2(\vec{r}_e,t) \\ &+\frac{\vec{p}_p^{\,2}}{2m_p} + \frac{e}{m_p}\vec{A}(\vec{r}_p,t)\cdot\vec{p}_p + \frac{e^2}{2m_p}\vec{A}^2(\vec{r}_p,t) - \frac{1}{4\pi\epsilon_0}\frac{e^2}{|\vec{r}_e - \vec{r}_p|}, \end{aligned} \tag{2.6}$$

where m_e and m_p are the electron and proton mass, $\vec{p}_e$ and $\vec{p}_p$ are the momentum operator of the electron and proton, e is the electron charge and ϵ_0 is the electric permittivity. In order to deal with such a complex Hamiltonian, we make several approximations. Firstly we change to the simpler center of mass and relative

coordinate system. This is defined as

$$\begin{aligned}
\vec{r} &= \vec{r}_e - \vec{r}_p, \\
\vec{R} &= \frac{m_e\vec{r}_e + m_p\vec{r}_p}{m_e + m_p}, \\
M &= m_e + m_p, \\
\mu &= \frac{m_e m_p}{m_e + m_p}, \\
\vec{p}_{cm} &= \vec{p}_e + \vec{p}_p, \\
\vec{p}_r &= \frac{m_p}{M}\vec{p}_e - \frac{m_e}{M}\vec{p}_p.
\end{aligned} \tag{2.7}$$

We then make the dipole approximation which assumes that the external electromagnetic field is approximately constant over the dimensions of the atom, i.e., the size of the atom is much less than the wavelength of the light. This means that $\vec{A}(\vec{R} + \delta\vec{r}) \approx \vec{A}(\vec{R})$. After performing some algebra and a gauge transformation $\exp\left[-\frac{i}{\hbar}e\vec{r}\cdot\vec{A}(\vec{R},t)\right]$ one arrives at the new Hamiltonian

$$\tilde{H} = \frac{1}{2M}\vec{p}_{cm}^{\,2} + H_{atom} - e\vec{r}\cdot\vec{E}(\vec{R},t), \tag{2.8}$$

where

$$H_{atom} = \frac{\vec{p}_r^{\,2}}{2\mu} - \frac{1}{4\pi\epsilon_0}\frac{e^2}{|\vec{r}|} \tag{2.9}$$

and $\vec{E}$ is the electric field. At this point one can see from the form of $\tilde{H}$ why the approximation above is called the dipole approximation. We now make a two–level approximation, i.e. that there are only two relevant eigenstates of this Hamiltonian. More precisely

$$\begin{aligned}
H_{atom} &= \sum_{i=1}^{\infty} \hbar\omega_i |\phi_i\rangle\langle\phi_i| \\
&\approx \hbar\omega_1 |\phi_1\rangle\langle\phi_1| + \hbar\omega_2 |\phi_2\rangle\langle\phi_2|,
\end{aligned} \tag{2.10}$$

where the index i accounts for all different combinations of quantum numbers and the eigenstates are a function of $\vec{r}$ in coordinate representation. We now use these

states as a basis for interaction term

$$\begin{aligned} -e\vec{r}\cdot\vec{E}(\vec{R},t) &= \mathbb{1}(-e\vec{r})\cdot\vec{E}(\vec{R},t)\mathbb{1} \\ &= \sum_{j,k}|\phi_j\rangle\langle\phi_j|(-e\vec{r})|\phi_k\rangle\langle\phi_k|\cdot\vec{E}(\vec{R},t). \end{aligned} \tag{2.11}$$

The diagonal elements of this matrix are zero for parity reasons. Our Hamiltonian is now

$$\tilde{H} = \frac{1}{2M}\vec{p}_{cm} + \hbar\omega_1|\phi_1\rangle\langle\phi_1| + \hbar\omega_2|\phi_2\rangle\langle\phi_2| - (|\phi_1\rangle\langle\phi_2|\vec{\mu}_{12} + \text{h.c.})\cdot\vec{E}(\vec{R},t), \tag{2.12}$$

where h.c. is the Hermitian conjugate and $\vec{\mu}_{12} = \langle\phi_1|e\vec{r}|\phi_2\rangle$ is the dipole moment of the atom. Note that different definitions of the dipole moment can lead to different sign conventions for the Hamiltonian. Consider now classical monochromatic light, e.g., laser light

$$\vec{E}(\vec{R},t) = \text{Re}\left[\vec{E}_0(\vec{R})\, e^{i\vec{k}_L\cdot\vec{R}-i\omega_L t}\right] \tag{2.13}$$

where $\omega_L = c|\vec{k}_L|$. If we now change to the appropriate laser-based interaction picture (using the unitary transformation $\exp(i\omega_L t|\phi_2\rangle\langle\phi_2|)$), and neglects fast oscillating terms of the form $e^{2i\omega_L t}$ (the rotating wave approximation) we arrive at the final form of our Hamiltonian

$$\tilde{H} = \frac{1}{2M}\vec{p}_{cm} - \frac{\hbar}{2}\begin{pmatrix} 0 & \Omega e^{-i\vec{k}_L\cdot\vec{R}} \\ \Omega^* e^{i\vec{k}_L\cdot\vec{R}} & 2\Delta \end{pmatrix} \tag{2.14}$$

using the representation

$$|\phi_1\rangle = \begin{pmatrix} 1 \\ 0 \end{pmatrix},\ |\phi_2\rangle = \begin{pmatrix} 0 \\ 1 \end{pmatrix}. \tag{2.15}$$

We have also shifted the total energy so that $\omega_1 = 0$ and defined the detuning as $\Delta = \omega_L - \omega_2$ and the Rabi frequency as $\Omega = \frac{\vec{\mu}_{12}\cdot\vec{E}_0^*}{\hbar}$.

2.1.2 Particle trapping

Now that we understand how classical light affects an atom, we will consider how this can be exploited to create trapping potentials for particles. Firstly we will use the result from the previous section to show how one can create periodic trapping potentials known as optical lattices for neutral atoms. Secondly we will describe how by using an electromagnetic field one can trap charged particles or ions. In contrast to the case of neutral atoms, these methods do not rely on the internal structure of the ion.

2.1.2.1 Optical lattices

Optical lattices are periodic potentials (formed by interfering monochromatic laser beams) which can trap many ultracold atoms in large arrays (see figure 2.1). They are predicted to be useful quantum simulators for condensed matter physics since they are highly controllable, i.e., one can easily adjust both the periodicity, depth and dimensionality of the potential. They have also found applications in building atomic clocks [33] and as a possible architecture for quantum computing [34–37]. It has even been made possible to perform single site addressing with the invention of the quantum-gas microscope [38, 39]. Detailed reviews of quantum gases in optical lattices can be found in [37, 40, 41].

We now consider the case of a one dimensional optical lattice in detail. We will then comment on generalisations to higher dimensions. The Hamiltonian for a two–level atom in one dimensional motion perpendicular to the laser field (i.e. $\vec{k}_L \cdot \vec{R} = 0$) is given by

$$H = -\frac{\hbar^2}{2m}\frac{\partial^2}{\partial x^2} - \frac{\hbar}{2}\begin{pmatrix} 0 & \Omega(x) \\ \Omega^*(x) & 2\Delta \end{pmatrix}. \tag{2.16}$$

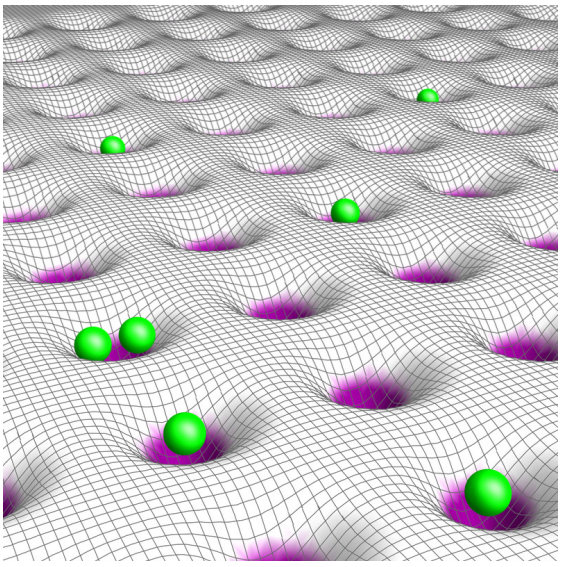


FIGURE 2.1: Diagram of atoms (green spheres) trapped in a two dimensional optical lattice (white mesh surface)

If the wavefunction is given by $\psi(x,t) = [\psi_1(x,t), \psi_2(x,t)]^T$ we can write the Schrödinger equation as

$$i\hbar\frac{\partial}{\partial t}\psi_1 = -\frac{\hbar^2}{2m}\frac{\partial^2}{\partial x^2}\psi_1 - \frac{\hbar}{2}\Omega(x)\psi_2, \tag{2.17}$$

$$i\hbar\frac{\partial}{\partial t}\psi_2 = -\frac{\hbar^2}{2m}\frac{\partial^2}{\partial x^2}\psi_2 - \frac{\hbar}{2}\Omega^*(x)\psi_1 - \hbar\Delta\psi_2. \tag{2.18}$$

By assuming a large detuning, i.e., $|\Delta| \gg 0$, we can write (2.18) as

$$\hbar\Delta\psi_2 \approx -\frac{\hbar}{2}\Omega^*(x)\psi_1. \tag{2.19}$$

Inserting this into (2.17) we get that

$$i\hbar\partial_t\psi_1 = -\frac{\hbar^2}{2m}\frac{\partial^2}{\partial x^2}\psi_1 + V_{eff}(x)\psi_1, \tag{2.20}$$

where our effective potential is now given by $V_{eff}(x) = \frac{\hbar}{4\Delta}|\Omega(x)|^2$. Since the detuning is large, there are effectively no Rabi oscillations between the two levels. In the case of a blue detuned laser ($\omega_L > \omega_2$) we get a repulsive potential $V_{eff}(x) > 0$ and in the case of a red detuned laser ($\omega_L < \omega_2$) we get an attractive potential $V_{eff}(x) < 0$.

From this simple calculation we can see how an electric field can create an effective mechanical potential for an atom. We can now extend this example assuming our electric field is generated by two counter propagating lasers (i.e. two plane waves of the form $\frac{\vec{E}_0}{2}e^{\pm ikx-i\omega t}$). The total electric field is given by

$$\vec{E}_{total} = \cos(kx)\,\mathrm{Re}\left(\vec{E}_0 e^{-i\omega t}\right). \tag{2.21}$$

After the usual approximations (e.g. dipole, rotating wave etc.), we get that (2.16) becomes

$$H = -\frac{\hbar^2}{2m}\frac{\partial^2}{\partial x^2} - \frac{\hbar}{2}\begin{pmatrix} 0 & \Omega_0\cos(kx) \\ \Omega_0\cos(kx) & 2\Delta \end{pmatrix} \tag{2.22}$$

where $\Omega_0 = \frac{\vec{\mu}_{12}\cdot\vec{E}_0^*}{\hbar}$. In the regime of large detuning our effective potential is given by

$$V_{eff}(x) = \frac{\hbar\left|\Omega_0\right|^2}{4\Delta}\cos^2(kx). \tag{2.23}$$

This is the potential of a one dimensional optical lattice. In a three-dimensonal setting, adding two extra pairs of beams in the y and z direction, one obtains a three dimensional potential of the form

$$V(x,y,z) = V_x\cos^2(k_x x) + V_y\cos^2(k_y y) + V_z\cos^2(k_z z). \tag{2.24}$$

In order to suppress interference between the three standing waves it is important to choose mutually orthogonal linear polarizations. In chapter 5, the interference between two orthogonal standing waves will be exploited. While we will only be focussed on the squared geometry of optical lattices, it is also possible to create alternative geometries by setting the laser beams pairs at angles other than the standard right angle configuration. The effects of spontaneous emission can also be neglected as the laser light is highly detuned and hence does not create any excitations of the atom [6].

Neutral atoms loaded into an optical lattice posses two very distinct ground states.

In order to see this, let us very briefly consider a three dimensional optical lattice described using the Bose–Hubbard Hamiltonian [40, 42] (which assumes atoms are only in the lowest energy band)

$$H = -J \sum_{\langle i,j \rangle} a_i^\dagger a_j + \frac{1}{2} U \sum_i n_i(n_i - 1). \tag{2.25}$$

J is the tunneling rate between neighbouring sites $\langle i, j \rangle$ and $a_i^\dagger$ (a_i) creates (destroys) a particle at lattice site i. The first term is the kinetic energy while the second is the onsite interaction U between the particles. $n_i = a_i^\dagger a_i$ counts the number of particles at site i. It is assumed there is no interaction between particles in different sites. The first phase is for the case of weak interactions relative to the kinetic energy, i.e., $U/J \ll 1$. In this case, known as the superfluid phase, each atom is delocalised over the entire lattice. In the other case, known as the Mott insulator phase, the interactions are large relative to the kinetic energy, i.e., $U/J \gg 1$. In this phase each atom is localised to a single site with a fixed particle number per site (e.g. one) in the ideal case. Knowledge of this phase will be required later in chapter 5.

2.1.2.2 Ion traps

The goal of ion traps is to confine the motion of a charged atom to a small region of space. As we have seen in the previous section this is indeed possible with neutral atoms. However the forces acting on ions from electromagnetic field can be much greater which allow for deeper traps and longer storage times.

There are two main types of ion traps. The first is a Paul trap (also known as a Radio Frequency trap) [43] which uses a quadrupole electric field to trap the ion. Due to Earnshaw's theorem, it is not possible to trap the ion with only a static electric field. However if one switches between two potentials at a rate faster than it takes the ion to escape, one can create an average confining potential. This is the principle behind the Paul trap.

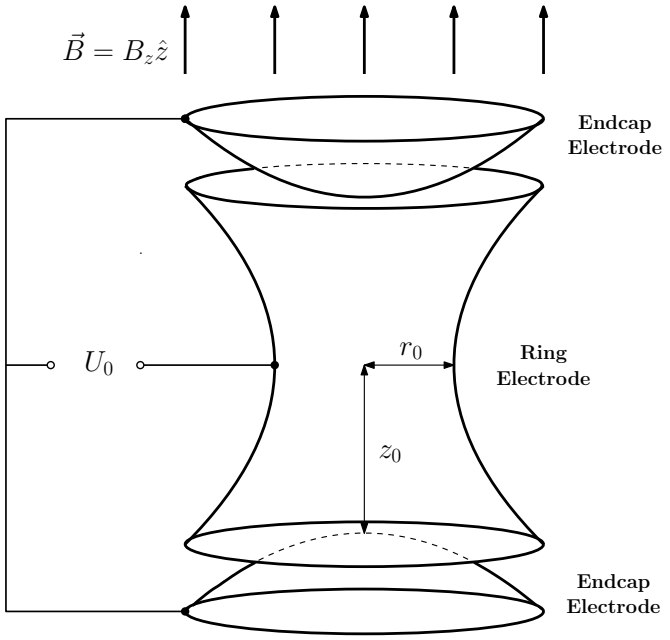


FIGURE 2.2: Diagram of an ideal Penning trap

The second main type is the Penning trap. The general principle of the Penning trap was first described in 1936 [44], however it was not completely developed until 1959 [45, 46]. Unlike the Paul trap, the Penning trap does not require any oscillating fields, avoiding unwanted heating effects. It uses a combination of a uniform and unidirectional magnetic field and an electrostatic quadrupole potential to confine the ion. This harmonic potential is created using three electrodes which are ideally hyperboloids of revolution (see figure 2.2). In practice however this can often be approximated by electrodes with a simpler geometry [47].

The magnetic field is then simply $\vec{B} = B_z\hat{z}$ and the electric field $\vec{E} = -\nabla\phi$ where the scalar potential is $\phi(r,z) = \frac{U_0}{R_0^2}(2z^2 - r^2)$, r is the radial distance in cylindrical coordinates and $R_0^2 \equiv r_0^2 + 2z_0^2$. As can be seen in figure 2.2, r_0 is the distance from the trap centre to the one-sheet hyperboloid (also known as the ring electrode) defined by $2z^2 - r^2 = -r_0^2$, z_0 is the distance from the trap centre to the two-sheet hyperboloid (also known as end cap electrodes) defined by $2z^2 - r^2 = 2z_0^2$ and U_0 is the potential difference between the two surfaces.

Typically the dynamics of an ion in a Penning trap has been treated classically. Considering the classical motion of the ion (using the Lorentz force [48]), one sees

that the z-component decouples leading to harmonic oscillation in this direction with axial frequency $\omega_z = \sqrt{\frac{4qU_0}{mR_0^2}}$. To trap the particle in this direction requires $qU_0 > 0$. The classical motion in the x-y plane has two characteristic frequencies. The modified cyclotron frequency

$$\omega_c' = \frac{\omega_c + \sqrt{\omega_c^2 - 2\omega_z^2}}{2} \tag{2.26}$$

and the magnetron frequency

$$\omega_m = \frac{\omega_c - \sqrt{\omega_c^2 - 2\omega_z^2}}{2} \tag{2.27}$$

where $\omega_c = qB_z/m$ is the cyclotron frequency, i.e., the frequency for the orbits of a charged particle in a uniform magnetic field. We can see that to have a trapping potential, i.e., to have real oscillation frequencies, we require $\omega_c^2 > 2\omega_z^2$. Under the usual operating conditions for a Penning trap [49], the frequencies ω_c', ω_z and ω_m differ by one or several orders of magnitude and one can assume

$$\omega_c' \approx \omega_c \gg \omega_z \gg \omega_m. \tag{2.28}$$

Several techniques have been used to measure these frequencies [50]. The following relations also hold

$$\begin{aligned} \omega_m + \omega_c' &= \omega_c, \\ 2\omega_m\omega_c' &= \omega_z^2, \\ \omega_m^2 + \omega_c'^2 + \omega_z^2 &= \omega_c^2. \end{aligned} \tag{2.29}$$

The last relation is true even if the magnetic field is misaligned with the trap axis [50]. This is useful for high-precision measurements of the mass of trapped ions.

Penning traps are commonly used for accurate measurement of the properties of different charged particles [56, 57], in particular for precise measurements of the electron g-factor [51, 52]. They have also been proposed for applications in quantum information [53–55].

Recent experiments have shown that by resolved-sideband laser cooling, one can achieve a single ion in the motional ground state [58]. This necessitates that one uses a full quantum mechanical treatment of the system (where the frequencies discussed above also naturally arise). In chapter 6, we will show how one can control, in a fast and stable way, the wavefunction of a charged particle in a Penning trap using shortcuts to adiabaticity techniques. This will be done using the minimal coupling equation (outlined in section 2.1.1) to describe how the wavefunction evolves.

2.1.3 Laser cooling methods

While we now know how to trap atoms and ions, a problem still remains. Room temperature atoms or ions simply possess too much kinetic energy to be trapped. The solution to this is to cool the particles down to very low temperatures. This is first done using laser light (known as laser cooling) after which other evaporative techniques may be used. In this section we will review the first step in this process, known as Doppler cooling, to give some insight into how laser cooling works.

The idea that light (in particular laser light), can be used to cool down matter as opposed to heating it up is quite counter intuitive. All methods of laser cooling are based on the premise that light, just like matter, carries momentum. Since this must be conserved, by interacting with matter (absorbing and emitting photons) light can change the momentum of matter. Laser cooling is relevant for both neutral atoms trapped in optical lattices and trapped ions.

We will now outline the main idea. One starts by shining laser light on the atom cloud. Every time an atom absorbs a photon of wavelength λ, the velocity of the atom which absorbs it is changed by the recoil velocity $v_{rec} = \hbar k/m$ (due to conservation of momentum) in the direction of the laser. In this case $k = 2\pi/\lambda$ and m is the mass of the atom. Since the atoms are initially moving (since the cloud has a temperature), the laser light frequency is Doppler shifted for the atoms. This cooling laser is now set to be red-tuned, i.e. it has a frequency less

than that of the resonant frequency of the atom so that the detuning is given by $\Delta = \omega_L - \omega_A < 0$ where ω_A is the frequency of the atomic transition. The laser frequency is then shifted by $-\vec{k}_L \cdot \vec{v}$ where $\vec{k}_L$ is the wave vector of the laser light and $\vec{v}$ is the atomic velocity. Hence an atom moving away from the laser will not absorb a photon (since the light is even more red shifted) whereas an atom moving towards the laser will absorb a photon since it sees blue shifted light which is close to being resonant with the atomic transition. This will have the effect of exciting the internal states of many atoms and reducing their velocity. When an excited atom re-emits a photon it will have a random direction. So by averaging over many atoms this will have no effect on the total momentum of the cloud and hence the temperature. The required detuning decreases as the atomic motion slows down. Of course to achieve total cooling, one needs to apply lasers in all three Cartesian axes, i.e., three orthogonal laser beams which are reflected back in the opposite direction. This type of cooling is most commonly implemented for neutral atoms in a magneto-optical trap (MOT) [59] which prevents a loss of the atoms. This overall loss of kinetic energy can be related to the temperature by the equipartition theorem, which is given by

$$\frac{1}{2}m\langle v^2\rangle = \frac{3}{2}k_B T. \tag{2.30}$$

There is a lower limit for the temperature one can cool to using this method called the Doppler limit [59]. The atoms reach this temperature limit, T_D, when the Doppler cooling is balanced by the heating due to spontaneous emission giving

$$k_B T_D = \frac{1}{2}\hbar\Gamma \tag{2.31}$$

where Γ is the rate of spontaneous emission. The lower limit of laser cooling in general is the recoil limit. The atom will always have at least a momentum equal (in magnitude) to that of a laser photon. To achieve even lower temperatures other special techniques such as evaporative cooling must be used [59–62]. While Doppler cooling is of course also applicable to trapped ions, to cool further a technique known as resolved sideband cooling is typically also used [63, 64].

2.2 Shortcuts to adiabaticity

We now have a much clearer understanding of the quantum systems which are going to be considered in this thesis. The question now is how to control them. For this we review the techniques of shortcuts to adiabaticity (STA).

The term shortcuts to adiabaticity (first introduced in 2010 [65]) describes a variety of methods, typically analytical, which seek to achieve the same outcome as quantum adiabatic processes in significantly shorter times. Each method has certain advantages and disadvantages associated with it.

Much of the activity surrounding STA initially concerned manipulation of harmonic traps in short times with minimal excitations for both single atoms [66–68] and condensates [69–71]. However STA have also been applied to a variety of other tasks now such as atom transport [70, 72, 73], quantum computing [74], quantum simulations [75], wavepacket splitting [76], internal state control [77–81], optical lattice expansion [82, 83], many-body physics [84–87], fast transport of trapped ions [88, 89], phase gates on ion pairs [90] and cooling mechanical resonators [91, 92]. STA have also been used for the classical optics of coupled waveguides [93, 94]. STA may also be useful in probing the validity of so called quantum speed limits [95–97] or the lack of them in the case of some non-Hermitian Hamiltonians [98].

STA were first experimentally used in 2011 for fast decompression and displacement of both a gas of non-interacting cold atoms and an interacting Bose-Einstein condensate [99–101]. They have also been implemented in an effective two-level system comprised of an accelerated Bose-Einstein condensate in an optical lattice [102]. More recently STA methods have been used experimentally for fast control of an electron spin in a single nitrogen-vacancy center in diamond [103], displacement of a trapped ion with minimal excitations [104] and to manipulate the internal states of cold atoms [105].

In the remainder of this section we will outline the different techniques of shortcuts to adiabaticity, but first we briefly review the adiabatic theorem and how this has been used for state transfer.

2.2.1 Adiabatic theorem

The term adiabatic can lead to much confusion in physics as it has two distinct meanings. In the case of thermodynamics, an adiabatic process refers to one where no heat is exchanged between the system and the environment. In quantum mechanics however it has a different meaning. It refers to when there is a negligible probability of having transitions between the instantaneous eigenstates of a Hamiltonian.

In this section, we will briefly review the adiabatic theorem in quantum mechanics. It was originally derived by Born and Fock in 1928 [20] and later refined by others, e.g., [106–108]. A simply summary of it is the following: a system will remain in its instantaneous eigenstate provided the Hamiltonian changes slowly enough in time and there is a gap between the eigenvalue and the rest of the Hamiltonian's spectrum.

We will now present an overview of the proof of the adiabatic theorem. We start with a time-dependent Hamiltonian $H(t)$ with a discrete, non-degenerate spectrum

$$H(t)|n(t)\rangle = E_n(t)|n(t)\rangle. \tag{2.32}$$

The time dependent Schrödinger equation (TDSE) is given by

$$i\hbar\partial_t|\psi(t)\rangle = H(t)|\psi(t)\rangle. \tag{2.33}$$

To prove the adiabatic theorem, we choose the following ansatz

$$|\psi(t)\rangle = \sum_n c_n(t)e^{i\theta_n(t)}|n(t)\rangle, \tag{2.34}$$

such that $\sum_n |c_n(t)|^2 = 1$ and $\theta_n(t) = -\frac{1}{\hbar}\int_0^t E_n(s)ds$ is the dynamical phase. Putting this into the TDSE (2.33), we get

$$i\hbar \sum_n \left(\dot{c}_n|n\rangle + c_n|\dot{n}\rangle + ic_n\dot{\theta}_n|n\rangle \right) e^{i\theta_n} = \sum_n c_n H|n\rangle e^{i\theta_n}, \tag{2.35}$$

where the dot indicates a time derivative. Taking into account the form of θ_n and (2.32), this becomes

$$\sum_n \dot{c}_n|n\rangle e^{i\theta_n} = -\sum_n c_n|\dot{n}\rangle e^{i\theta_n}. \tag{2.36}$$

If we now apply $\langle m|$ from the left, we get that

$$\begin{aligned} \dot{c}_m &= -\sum_n c_n \langle m|\dot{n}\rangle e^{i(\theta_n - \theta_m)} \\ &= -c_m\langle m|\dot{m}\rangle - \sum_{n\neq m} c_n\langle m|\dot{n}\rangle e^{i(\theta_n-\theta_m)}. \end{aligned} \tag{2.37}$$

If one now differentiates (2.32) and applies $\langle m|$ from the left the result is

$$\langle m|\dot{n}\rangle = \frac{\langle m|\dot{H}|n\rangle}{E_n - E_m}. \tag{2.38}$$

Inserting this into (2.37) we see that

$$\dot{c}_m = -c_m\langle m|\dot{m}\rangle - \sum_{n\neq m} c_n \frac{\langle m|\dot{H}|n\rangle}{E_n - E_m} e^{i(\theta_n-\theta_m)}. \tag{2.39}$$

Up until this point the result is exact. We now make the adiabatic approximation, i.e., that the Hamiltonian changes slowly in time. Since we are assuming $\dot{H}$ is small we drop the last term. For a more rigorous justification for this step see [109]. This leaves us now with

$$\dot{c}_m(t) = -c_m\langle m|\dot{m}\rangle. \tag{2.40}$$

This has the solution

$$c_m(t) = c_m(0)e^{i\gamma_m(t)}, \tag{2.41}$$

where

$$\gamma_m(t) = i\int_0^t \langle m(s)|\partial_s m(s)\rangle ds, \tag{2.42}$$

is the geometric phase. Note that one can show that γ_m is real using the fact that $|m\rangle$ is normalised. Hence given an initial state $|\psi(0)\rangle = \sum_n c_n(0)|n(0)\rangle$, the solution for a time t in the adiabatic limit is given by

$$|\psi(t)\rangle \approx \sum_n c_n(0)e^{i\theta_n(t)}e^{i\gamma_n(t)}|n(t)\rangle. \tag{2.43}$$

From this we can see that apart from accumulating both a dynamical and geometric phase, the populations of the instantaneous eigenstates remain unchanged.

Typically the adiabatic criterion used is given by [110]

$$\hbar\left|\frac{\langle m|\dot{H}|n\rangle}{(E_n - E_m)^2}\right| \ll 1 \ \forall n, m \tag{2.44}$$

although it is not applicable in all circumstances [111]. This type of adiabatic condition is utilised in a method not discussed in this thesis known as fast quasiadiabatic dynamics [112]. By designing a process which is equally adiabatic across all instances of time, one can reduce the total time needed for the process.

Perhaps the most famous example of an adiabatic process is quantum-optical technique known as stimulated Raman adiabatic passage (STIRAP) [113]. This is a process whereby population is transferred between two stable atomic states which cannot be directly coupled in a 3-level lambda system. This was first introduced to avoid losses due to spontaneous emission from the intermediate state [114]. The

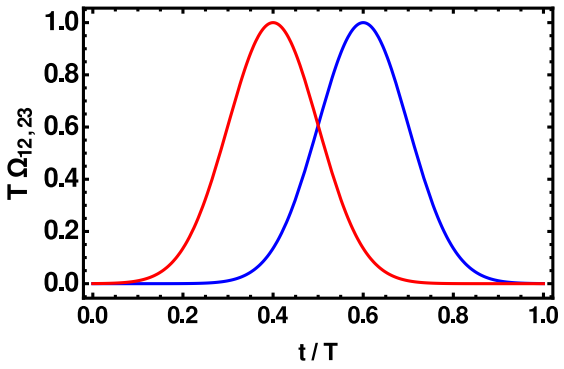


FIGURE 2.3: Example of counterintuitive pulse sequence used in STIRAP; Ω_{12} (blue) and Ω_{23} (red).

Hamiltonian for this system is given by

$$H = \frac{\hbar}{2}\begin{pmatrix} 0 & \Omega_{12} & 0 \\ \Omega_{12} & 0 & \Omega_{23} \\ 0 & \Omega_{23} & 0 \end{pmatrix} \tag{2.45}$$

where Ω_{12} is known as the pump field and Ω_{23} is known as the Stokes field. Note that Rabi frequencies are time-dependent. We have assumed that both lasers are resonant with the respective transition (although this need not be the case) and the Rabi frequencies are real. This Hamiltonian has an instantaneous eigenstate

$$|d\rangle = \cos\theta|1\rangle - \sin\theta|3\rangle, \tag{2.46}$$

which is known as a dark state and θ is known as the mixing angle defined as $\tan\theta = \Omega_{12}/\Omega_{23}$. This state has no component of the intermediate state $|2\rangle$. Note that the states $|1\rangle$, $|2\rangle$ and $|3\rangle$ are time independent basis states for the system and not necessarily eigenstates. By adiabatically changing the mixing angle θ from 0 ($\Omega_{23} \gg \Omega_{12}$) to $\pi/2$ ($\Omega_{23} \ll \Omega_{12}$) one can effectively transfer between state $|1\rangle = (1,0,0)^T$ to $|3\rangle = (0,0,1)^T$ without any population in state $|2\rangle$. This is done by a counterinuitive pulse sequence where the unpopulated states ($|2\rangle$ and $|3\rangle$) are coupled first (see figure 2.3). While STIRAP was originally used in the case of internal atomic states, it is also applicable to general three-level quantum systems in particular those describing tunnel coupled traps [115]. This will be

further explored in chapter 4.

Having considered an example of how the adiabatic theorem may be used to perform state transfer we now move on to the methods of shortcuts to adiabaticity. These will allow us to derive non-adiabatic state transfers. We start with methods based on Lewis-Riesenfeld invariants.

2.2.2 Lewis–Riesenfeld invariants

Originally discovered in 1969, a Lewis–Riesenfeld invariant [116] for a Hamiltonian $H(t)$ is a Hermitian operator $I(t)$ which satisfies

$$\frac{\partial I}{\partial t} + \frac{i}{\hbar}[H, I] = 0. \tag{2.47}$$

Non–Hermitian invariants and Hamiltonians have been considered in [117–120]. Since $I(t)$ is a constant of motion it can be shown that it has time–independent eigenvalues and that a particular solution of the Schrödinger equation,

$$i\hbar\frac{\partial}{\partial t}\left|\psi_n(t)\right\rangle = H(t)\left|\psi_n(t)\right\rangle, \tag{2.48}$$

can be written as

$$\left|\psi_n(t)\right\rangle = e^{i\beta_n(t)}\left|\phi_n(t)\right\rangle. \tag{2.49}$$

Here $\left|\phi_n(t)\right\rangle$ is an instantaneous eigenstate of $I(t)$ and

$$\beta_n(t) = \frac{1}{\hbar}\int_0^t \left\langle\phi_n(s)\left|[i\hbar\partial_s - H(s)]\right|\phi_n(s)\right\rangle ds, \tag{2.50}$$

is the Lewis–Riesenfeld phase. Hence a general solution to the Schrödinger equation can be written as

$$\left|\psi(t)\right\rangle = \sum_n c_n\left|\psi_n(t)\right\rangle \tag{2.51}$$

where the c_n are independent of time. See Appendix A for full details. We have assumed a discrete non–degenerate spectrum for the invariant. Invariants have also been used to control mixed states [121].

It should be noted that for a given Hamiltonian there are many possible invariants. For example, the density operator describing the evolution of a system is a dynamical invariant. The choice of which particular invariant to use is made on the basis of mathematical convenience.

These invariants were originally used to solve for the state of a time-dependent system. In shortcuts to adiabaticity this idea is reversed. One first prescribes the particular state evolution and then determines the time dependence of the Hamiltonian. The idea is that instead of approximately following the instantaneous eigenstate of the Hamiltonian (as in the adiabatic case), one exactly follows the instantaneous eigenstate of the invariant (up to the Lewis–Riesenfeld phase). Formally this amounts to wanting a time evolution operator of the form

$$U = \sum_n e^{i\alpha_n(t)} |\phi_n(t)\rangle\langle\phi_n(0)|. \tag{2.52}$$

Since the time evolution operator also obeys the Schrödinger equation it then follows that one needs to implement a Hamiltonian $H(t) = i\hbar\dot{U}U^\dagger$. Demanding that the invariant and the Hamiltonian commute at the start and the end of the process, i.e., $[I(0), H(0)] = [I(T), H(T)] = 0$, one ensures that the eigenstates of the invariant and the Hamiltonian coincide at initial and final times. This leaves the freedom to choose how the state evolves in the intermediate time and then use (2.47) to determine how the Hamiltonian should vary with time to ensure such a state evolution. Note that the same control Hamiltonian will work for all energy eigenstates.

This idea can also be formulated in terms of Lie algebras [122]. Let's assume our Hamiltonian $H(t)$ can be written as a linear combinations of Hermitian operators G_a (which will later be referred to as generators)

$$H(t) = \sum_{a=1}^{N} h_a(t) G_a. \tag{2.53}$$

These generators form a closed Lie algebra (also called a dynamical algebra). Since they are closed under the commutator, we have that

$$[G_b, G_c] = \sum_{a=1}^{N} \alpha_{abc} G_a, \tag{2.54}$$

where α_{abc} is known as a structure constant. If the invariant exists, we can also write it in terms of this algebra as follows

$$I(t) = \sum_{a=1}^{N} f_a(t) G_a. \tag{2.55}$$

Note that not every h_a and f_a is necessarily non-zero. If we now insert this into (2.47), we get that

$$\dot{f}_a(t) - \sum_{b=1}^{N} A_{ab}(t) h_b(t) = 0 \tag{2.56}$$

where the $N \times N$ matrix A is defined by

$$A_{ab} \equiv \frac{1}{i\hbar} \sum_{c=1}^{N} \alpha_{abc} f_c(t). \tag{2.57}$$

This can be more naturally written as a matrix equation

$$\partial_t \vec{f}(t) = A\vec{h}(t) \tag{2.58}$$

where the vectors $\vec{f}(t)$ and $\vec{h}(t)$ represent the invariant and Hamiltonian respectively. We now want to do the same trick as before, whereby the auxiliary functions $\vec{f}(t)$ (and therefore the state evolution) is chosen first and the time evolution of the Hamiltonian is inferred from this. Doing this requires that one can invert (2.58), i.e., that A^{-1} exists. In some cases, one can still determine $\vec{h}(t)$ (corresponding to the physical potentials to be experimentally implemented) even when A^{-1} does not exist [122].

Note that for long times the dynamics prescribed by this method will approach adiabatic dynamics. This can be roughly seen by noting that for long times (2.47)

can be written as

$$\frac{i}{\hbar}\left[H, I\right] \approx 0 \tag{2.59}$$

Hence for long times, H and I have approximately a common eigenbasis for all times.

The most well studied invariant is of course the class of quadratic in momentum invariants. Consider a one-dimensional Hamiltonian $H = p^2/2m + V(q,t)$ where the potential has a Lewis-Leach form [123]

$$V(q,t) = -F(t)q + \frac{m}{2}\omega^2(t)q^2 + \frac{1}{\rho(t)^2}U\left[\frac{q - q_c(t)}{\rho(t)}\right]. \tag{2.60}$$

The arbitrary functions of time ρ, q_c, ω and F satisfy the following auxiliary equations

$$\begin{aligned} \ddot{\rho} + \omega^2(t)\rho &= \frac{\omega_0^2}{\rho^3}, \\ \ddot{q_c} + \omega^2(t)q_c &= F(t)/m, \end{aligned} \tag{2.61}$$

with ω_0 a constant. The first equation is known as the Ermakov equation [124] while the second is the Newtonian equation of motion for a forced harmonic oscillator. In this case the Hamiltonian posses an invariant given by

$$I = \frac{1}{2m}\left[\rho\left(p - m\dot{q_c}\right) - m\dot{\rho}\left(q - q_c\right)\right]^2 + \frac{1}{2}m\omega_0^2\left(\frac{q - q_c}{\rho}\right)^2 + U\left(\frac{q - q_c}{\rho}\right). \tag{2.62}$$

In this case we can explicitly calculate the Lewis-Riesenfeld phase

$$\alpha_n = -\frac{1}{\hbar}\int_0^t dt' \left[\frac{\lambda_n}{\rho^2} + \frac{m\left(\dot{q_c}\rho - q_c\dot{\rho}\right)^2}{2\rho^2}\right] \tag{2.63}$$

and the eigenvectors in coordinate representation

$$\phi_n(q,t) = \exp\left\{\frac{im}{\hbar}\left[\dot{\rho}q^2/2\rho + \left(\dot{q_c}\rho - q_c\dot{\rho}\right)q/\rho\right]\right\}\rho^{-1/2}\underbrace{\Phi_n\left(\frac{q - q_c}{\rho}\right)}_{=\Phi_n(\sigma)} \tag{2.64}$$

where $\Phi_n(\sigma)$ is a solution of the following Schrödinger equation

$$\left[-\frac{\hbar^2}{2m}\frac{\partial^2}{\partial\sigma^2}+\frac{1}{2}m\omega_0^2\sigma^2+U\left(\sigma\right)\right]\Phi_n=\lambda_n\Phi_n. \tag{2.65}$$

This invariant has been instrumental in designing many of the schemes which manipulate harmonic trapping potentials. One first designs the functions ρ (which determines the wavefunction width) and q_c (which is the classical particle trajectory) which fulfil the necessary boundary conditions. Using these, one can then determine the physical quantities $F(t)$ and $\omega(t)$, using (2.61).

2.2.3 Counterdiabatic driving

The method of counterdiabatic driving (or transitionless tracking as it is also known) was first developed by Berry [125], and also independently by Demirplak and Rice [126]. We start with the following general time dependent Hamiltonian

$$H_0(t)=\sum_n E_n(t)|n(t)\rangle\langle n(t)|. \tag{2.66}$$

The adiabatic solution under the dynamics of H_0 is given by

$$|\psi_n^{(ad)}(t)\rangle=e^{i\xi_n(t)}|n(t)\rangle \tag{2.67}$$

where the additional phase is given by

$$\xi_n(t)=-\frac{1}{\hbar}\int_0^t dsE_n(s)+i\int_0^t ds\langle n(s)|\dot{n}(s)\rangle. \tag{2.68}$$

We want that the wavefunction evolution is exactly "adiabatic" for arbitrary times. The time evolution operator for this case is given by

$$U(t)=\sum_n e^{i\xi_n(t)}|n(t)\rangle\langle n(0)|. \tag{2.69}$$

The Hamiltonian associated with this time evolution operator is given by

$$\begin{aligned} H &= i\hbar\dot{U}U^{\dagger} \\ &= i\hbar\left(\sum_n i\dot{\xi}_n e^{i\xi_n(t)}|n(t)\rangle\langle n(0)| + e^{i\xi_n(t)}|\dot{n}(t)\rangle\langle n(0)|\right) \\ &\times \left(\sum_m e^{-i\xi_m(t)}|m(0)\rangle\langle m(t)|\right) \\ &= i\hbar\sum_n i\dot{\xi}_n|n(t)\rangle\langle n(t)| + |\dot{n}(t)\rangle\langle n(t)| \end{aligned} \tag{2.70}$$

Now using (2.68) for the additional adiabatic phase, the Hamiltonian becomes

$$H = \underbrace{\sum_n E_n(t)|n(t)\rangle\langle n(t)|}_{H_0(t)} + \underbrace{i\hbar\sum_n |\dot{n}(t)\rangle\langle n(t)| - \langle n(t)|\dot{n}(t)\rangle|n(t)\rangle\langle n(t)|}_{H_{cd}(t)}. \tag{2.71}$$

From this we can see that by adding the additional driving H_{cd} to the original Hamiltonian H_0, we will follow the adiabatic solutions of H_0 alone for arbitrary times. One can see, in a heuristic way, how more energy is required to achieve faster state evolution since an extra Hamiltonian is needed. The energetic cost of this additional Hamiltonian has been examined in [127, 128]. Note that one could also consider other choices for $\xi_n(t)$ than the adiabatic phase such as $\xi_n(t) = 0$ [125]. This method can be connected with the method of Lewis–Riesenfeld invariants by noting that the Hamiltonian one gets from the invariant method is the same as (2.70) if one reinterprets $\xi_n(t)$ as the Lewis–Riesenfeld phase and $|n(t)\rangle$ as an eigenstate of the invariant.

This method has also been extended to non-Hermitian Hamiltonians [120], many body systems [86, 129] and to open systems [130]. A well known problem with this method is that it requires additional Hamiltonians which may not be experimentally realisable. This has been combated by changing to a suitable interaction picture in which the correction is more useful [131] and by approximating the correction as good as possible with the limited set of observables one can implement [132, 133].

2.2.4 Fast–forward approach

The basic fast-forward formalism for a particle in a time dependent potential was first introduced by Masuda and Nakamura in 2008 [134, 135]. The original formulation was somewhat involved and cumbersome. This led to a streamlined version of the formalism being developed [136]. This streamlined formalism has been applied for example to engineering of fast and stable splitting of matter waves [76] and to achieve rapid loading of a Bose-Einstein condensate into an optical lattice [137]. We present the streamlined version of the basic formalism below.

We start with the usual Schrödinger equation

$$i\hbar\frac{\partial}{\partial t}\psi(\vec{r},t) = -\frac{\hbar^2}{2m}\nabla^2\psi(\vec{r},t) + V(\vec{r},t). \tag{2.72}$$

We now make an ansatz for the wavefunction $\psi(\vec{r},t) = \alpha(\vec{r},t)e^{i\beta(\vec{r},t)}$ where $\alpha(\vec{r},t)$, $\beta(\vec{r},t) \in \mathbb{R}$. We can now solve (2.72) for the potential

$$\mathrm{Re}\left[V(\vec{r},t)\right] = -\hbar\dot{\beta} + \frac{\hbar^2}{2m}\left(\frac{\nabla^2\alpha}{\alpha} - (\nabla\beta)^2\right), \tag{2.73}$$

$$\mathrm{Im}\left[V(\vec{r},t)\right] = \hbar\frac{\dot{\alpha}}{\alpha} + \frac{\hbar^2}{2m}\left(\frac{2\nabla\beta\cdot\nabla\alpha}{\alpha} + \nabla^2\beta\right). \tag{2.74}$$

We first design $\alpha(\vec{r},t)$ and by enforcing that the potential is real, solve for $\beta(\vec{r},t)$ using (2.74). We can then calculate the required potential from (2.73). The method is essentially an inversion of the Schrödinger equation.

For the case of the Schrödinger equation of a Lewis-Leach potential [123], the potential is the same for all modes, just as in the case of the Lewis–Riesenfeld invariant. Hence the invariant based method can be thought of as a special case of the fast–forward approach [136].

A fast-forward formalism including an electromagnetic field was introduced in [138]. In chapter 6, we will show how the fast-forward formalism including an electromagnetic field can be streamlined and applied to the case of a Penning trap.

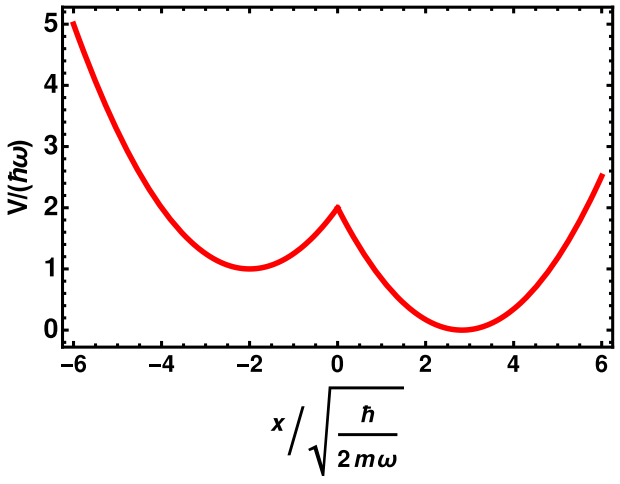


FIGURE 2.4: The double well potential with $a = b = 2\sqrt{\frac{\hbar}{2m\omega}}$

This work was later extended to design schemes which filter ions with respect to charge and mass in a Penning trap [139].

2.3 Analytical and numerical techniques

To conclude the background theory required we review some analytical and numerical techniques used in the thesis.

2.3.1 Example of Hilbert space truncation: the double well

A particle in a double well potential is, along with the interaction of an atom and a classical light field neglecting the atomic motion (see section 2.1.1), a typical example of a system that can be well approximated using a two-level model. This will provide an illustrative example that truncating a Hilbert space for the purpose of approximation can be a useful tool for designing schemes which change the motional states of atoms. This idea will be used later in chapter 4 and 5. Chapter 4 is particularly similar as in that case the basis states are also coupled by means of quantum tunnelling.

We will now outline the mapping in detail. Let us start with the following asymmetric one dimensional double-well potential [140],

$$V(x,t) = \begin{cases} \frac{1}{2}m\omega^2 \left\{ [x + a(t)]^2 + b(t)^2 \right\} & x \leq 0 \\ \frac{1}{2}m\omega^2 \left[x - \sqrt{a(t)^2 + b(t)^2} \right]^2 & x \geq 0 \end{cases}. \tag{2.75}$$

This is shown in figure 2.4. This potential could be approximately implemented using optical dipole traps (see sections 2.1.1 and 2.1.2.1 or [141] for example). We now set $\hbar = \omega = 1$, $m = \frac{1}{2}$ for this section and make the following change of variables

$$\tilde{a}(t) = \frac{1}{2}\left[a(t) + \sqrt{a(t)^2 + b(t)^2} \right], \tag{2.76}$$

$$\tilde{b}(t) = a(t) - \sqrt{a(t)^2 + b(t)^2}. \tag{2.77}$$

This allows us to write the potential as $V(x,t) = V_s(x,t) + V_{as}(x,t)$, i.e., its symmetric and antisymmetric parts,

$$V_s(x,t) = \frac{1}{4} \begin{cases} [x + \tilde{a}(t)]^2 & x \leq 0 \\ [x - \tilde{a}(t)]^2 & x \geq 0 \end{cases}, \tag{2.78}$$

$$V_{as}(x,t) = \frac{1}{4}\tilde{b}(t)\, x. \tag{2.79}$$

The Hamiltonian for this system can now be written as

$$\begin{aligned} H(t) &= -\frac{d^2}{dx^2} + V_s(x,t) + V_{as}(x,t) \\ &= H_0(t) + V_{as}(x,t). \end{aligned} \tag{2.80}$$

The instantaneous eigenstates of $H_0(t)$ are known [140]. The first two eigenstates (which must be symmetric and antisymmetric) are given by

$$\psi_s(x) = N_s \begin{cases} \phi_1(x,\nu_s) & x \leq 0 \\ \phi_2(x,\nu_s) & x \geq 0 \end{cases}, \tag{2.81}$$

$$\psi_{as}(x) = N_{as} \begin{cases} \phi_1(x,\nu_{as}) & x \leq 0 \\ -\phi_2(x,\nu_{as}) & x \geq 0 \end{cases}, \tag{2.82}$$

where

$$\phi_1(x,\nu) = D_\nu\left[-(x+\tilde{a})\right], \tag{2.83}$$

$$\phi_2(x,\nu) = D_\nu(x-\tilde{a}). \tag{2.84}$$

N_s and N_{as} are real normalization constants and $D_\nu(y)$ is a Parabolic Cylinder function [142]. The values of ν_s and ν_{as} are found by solving the following equations

$$D'_{\nu_s}(-\tilde{a}) = 0, \tag{2.85}$$

$$D_{\nu_{as}}(-\tilde{a}) = 0, \tag{2.86}$$

(where the prime denotes a derivative) and the energies are given by $E_i = \nu_i + 1/2$ with $i = s, as$. We now write $H(t)$ in the basis of instantaneous eigenvectors of $H_0(t)$,

$$\begin{aligned} H(t) &= H_0(t) + V_{as}(x) \\ &= \sum_i E_i |i\rangle\langle i| + \sum_{j,k} |j\rangle\langle j| V_{as}(x) |k\rangle\langle k| \\ &\approx \sum_{i=s,as} E_i |i\rangle\langle i| + \langle as| V_{as}(x) |s\rangle |as\rangle\langle s| + \langle s| V_{as}(x) |as\rangle |s\rangle\langle as| \end{aligned} \tag{2.87}$$

where in the last step we have made a two-level approximation. We now define a new basis of left and right states (which are chosen to be real),

$$|L\rangle = \frac{1}{\sqrt{2}}\left(|s\rangle + |as\rangle\right), \tag{2.88}$$

$$|R\rangle = \frac{1}{\sqrt{2}}\left(|s\rangle - |as\rangle\right), \tag{2.89}$$

where $\langle x|s\rangle = \psi_s(x)$ and so on. If we change to the time-dependent basis $\{|L[\tilde{a}(t)]\rangle, |R[\tilde{a}(t)]\rangle\}$ we get

$$H_{2L}(t) = \begin{pmatrix} \langle L|H|L\rangle & \langle L|H|R\rangle \\ \langle R|H|L\rangle & \langle R|H|R\rangle \end{pmatrix} - i\hbar \begin{pmatrix} \langle L|\dot{L}\rangle & \langle L|\dot{R}\rangle \\ \langle R|\dot{L}\rangle & \langle R|\dot{R}\rangle \end{pmatrix} \tag{2.90}$$

where the second term is due to the time dependence of the new basis. From the fact that the new basis vectors are real and normalised we get that $\langle L|\dot{L}\rangle = \langle R|\dot{R}\rangle = 0$ and since they are orthogonal $\langle L|\dot{R}\rangle = -\langle R|\dot{L}\rangle$. After this we must simply evaluate all the components individually, e.g.,

$$\langle L|H|L\rangle = \frac{1}{2}\left(E_s + E_{as} + 2\langle s|V_{as}|as\rangle\right). \tag{2.91}$$

We finally arrive at the two-level Hamiltonian

$$H_{2L}(t) = \frac{1}{2}\left(E_s + E_{as}\right)\mathbb{1} + \frac{1}{2}\begin{pmatrix} -\Delta & \Omega_R - i\Omega_I \\ \Omega_R + i\Omega_I & \Delta \end{pmatrix} \tag{2.92}$$

where

$$\Delta(t) = -2\left\langle s[\tilde{a}(t)]\right| V_{as}(x,t)\left|as[\tilde{a}(t)]\right\rangle, \tag{2.93}$$

$$\Omega_R(t) = E_s[\tilde{a}(t)] - E_{as}[\tilde{a}(t)], \tag{2.94}$$

$$\Omega_I(t) = \left\langle L[\tilde{a}(t)]\right| \partial_t \left|R[\tilde{a}(t)]\right\rangle = \left\langle L(\tilde{a})\right| \partial_{\tilde{a}} \left|R(\tilde{a})\right\rangle \left(\frac{\partial \tilde{a}}{\partial t}\right). \tag{2.95}$$

The first term of the Hamiltonian is just a shift in energy and can be ignored.

For the the states $\psi_s(x)$and $\psi_{as}(x)$ to be normalized we demand that for $i = s, as$ we have

$$\begin{aligned} & \int_{-\infty}^{\infty} |\psi_i(x)|^2 dx = 1, \\ \Longrightarrow \quad & N_i^2 \left\{ \int_{-\infty}^{0} D_{\nu_i}[-(x+\tilde{a})]^2 dx + \int_0^{\infty} D_{\nu_i}(x-\tilde{a})^2 dx \right\} = 1, \\ \Longrightarrow \quad & 2N_i^2 \int_0^{\infty} D_{\nu_i}(x-\tilde{a})^2 dx = 1. \end{aligned} \tag{2.96}$$

From this we get that

$$N_i = \left[2 \int_0^{\infty} D_{\nu_i}(x-\tilde{a})^2 dx \right]^{-\frac{1}{2}}. \tag{2.97}$$

The detuning is given as

$$\begin{aligned} \Delta &= -2 \langle s | V_{as}(x) | as \rangle \\ &= -\frac{\tilde{b}}{2} \int_{-\infty}^{\infty} \psi_s(x) x \psi_{as}(x) dx. \end{aligned} \tag{2.98}$$

By making the substitutions $\alpha = -(x+\tilde{a})$ and $\beta = x - \tilde{a}$ we can write

$$\begin{aligned} \int_{-\infty}^{\infty} \psi_s(x) x \psi_{as}(x) dx &= N_s N_{as} \int_{\infty}^{-\tilde{a}} D_{\nu_s}(\alpha)(\alpha+\tilde{a}) D_{\nu_{as}}(\alpha) d\alpha \\ &- N_s N_{as} \int_{-\tilde{a}}^{\infty} D_{\nu_s}(\beta)(\beta+\tilde{a}) D_{\nu_{as}}(\beta) d\beta \\ &= -2 N_s N_{as} \int_{-\tilde{a}}^{\infty} D_{\nu_s}(\alpha)(\alpha+\tilde{a}) D_{\nu_{as}}(\alpha) d\alpha. \end{aligned} \tag{2.99}$$

Finally we get

$$\Delta = \tilde{b} N_s N_{as} \int_{-\tilde{a}}^{\infty} D_{\nu_s}(\alpha)(\alpha+\tilde{a}) D_{\nu_{as}}(\alpha) d\alpha. \tag{2.100}$$

One now has clear analytic expressions for all the parameters of the two-level Hamiltonian. It can be found numerically that $\Omega_I / (\partial_t \tilde{a}) \ll \Omega_R$ in the range of $\tilde{a} \in (0, 7)$. Hence it can often be effectively neglected.

2.3.2 Time-dependent perturbation theory

We now review the method of time-dependent perturbation theory in quantum mechanics. Typically in textbooks this is derived if the reference Hamiltonian (for which the solutions are known) is time-independent and the perturbing Hamiltonian is time-dependent [143, 144]. In our case however both Hamiltonians are time-dependent. Hence we will now outline perturbation theory in this case.

We wish to approximate the solutions of the following Schrödinger equation

$$i\hbar\partial_t|\psi_s(t)\rangle = H_s(t)|\psi_s(t)\rangle, \tag{2.101}$$

where $H_s(t) = H_0(t) + H_1(t)$ and the solutions for just $H_0(t)$ are known. The subscript s refers to the fact that we are working in the Schrödinger picture. Equation (2.101) can of course also be written using the time evolution operator U as follows

$$|\psi_s(t)\rangle = U(t,t_0)|\psi_s(t_0)\rangle, \tag{2.102}$$

where

$$i\hbar\partial_t U(t,t_0) = H_s(t)U(t,t_0), \tag{2.103}$$

and $U(t_0,t_0) = \mathbb{1}$. The time evolution operator also has the properties that $U^\dagger(t',t) = U^{-1}(t',t) = U(t,t')$ and $U(t,t')U(t',t'') = U(t,t'')$. By repeated integration of this equation we can see that

$$\begin{aligned} U(t,t_0) &= \mathbb{1} - \frac{i}{\hbar}\int_{t_0}^{t} dt' H_s(t')U(t',t_0) \\ &= \mathbb{1} - \frac{i}{\hbar}\int_{t_0}^{t} dt' H_s(t')\left[\mathbb{1} - \frac{i}{\hbar}\int_{t_0}^{t'} dt'' H_s(t'')U(t'',t_0)\right] \\ &= \cdots \\ &= \sum_{n=0}^{\infty}\tilde{U}_n(t,t_0) \end{aligned} \tag{2.104}$$

where

$$\tilde{U}_n(t,t_0) = \left(-\frac{i}{\hbar}\right)^n \int_{t_0}^{t} dt_n \int_{t_0}^{t_n} dt_{n-1} \ldots \int_{t_0}^{t_2} dt_1 H_s(t_n) \ldots H_s(t_1), \qquad (2.105)$$

$\tilde{U}_0(t,t_0) = \mathbb{1}$ and $t \geq t_n \geq t_{n-1} \geq \ldots \geq t_1$. From this it can be seen that the time evolution operator can be written as

$$U(t,t_0) = \mathcal{T} \exp\left[-\frac{i}{\hbar}\int_{t_0}^{t} dt' H_s(t')\right], \qquad (2.106)$$

where $\mathcal{T}$ is the time ordering operator. We can now change to the interaction picture by defining the state $|\psi_i(t)\rangle$ as

$$\begin{aligned} |\psi_i(t)\rangle &\equiv U_0^\dagger(t,t_0)|\psi_s(t)\rangle \\ &= U_0^\dagger(t,t_0)U(t,t_0)|\psi_s(t_0)\rangle \end{aligned} \qquad (2.107)$$

where $U_0(t,t_0) = \mathcal{T}\exp\left[-\frac{i}{\hbar}\int_{t_0}^{t} dt' H_0(t')\right]$ is the time-evolution operator for the individual Hamiltonian $H_0(t)$. We now set about finding the Hamiltonian in this interaction picture

$$\begin{aligned} i\hbar\partial_t|\psi_i(t)\rangle &= i\hbar\partial_t\left[U_0^\dagger(t,t_0)|\psi_s(t)\rangle\right] \\ &= \left[i\hbar\partial_t U_0^\dagger(t,t_0)\right]|\psi_s(t)\rangle + U_0^\dagger(t,t_0)i\hbar\partial_t|\psi_s(t)\rangle \end{aligned} \qquad (2.108)$$

We now focus our attention on the first term of the right hand side. Using

$$[i\hbar\partial_t U_0(t,t_0)]^\dagger = [H_0(t)U_0(t,t_0)]^\dagger \qquad (2.109)$$

it can be rewritten as

$$\left[i\hbar\partial_t U_0^\dagger(t,t_0)\right]|\psi_s(t)\rangle = -U_0^\dagger(t,t_0)H_0(t)U_0(t,t_0)|\psi_i(t)\rangle. \qquad (2.110)$$

The second term can be rewritten as follows

$$\begin{aligned} U_0^\dagger(t,t_0)i\hbar\partial_t|\psi_s(t)\rangle &= U_0^\dagger(t,t_0)H_s(t)|\psi_s(t)\rangle \\ &= U_0^\dagger(t,t_0)H_s(t)U_0(t,t_0)U_0^\dagger(t,t_0)|\psi_s(t)\rangle \\ &= U_0^\dagger(t,t_0)H_s(t)U_0(t,t_0)|\psi_i(t)\rangle. \end{aligned} \tag{2.111}$$

Therefore one gets that

$$\begin{aligned} i\hbar\partial_t|\psi_i(t)\rangle &= U_0^\dagger(t,t_0)\left[H_s(t)-H_0(t)\right]U_0(t,t_0)|\psi_i(t)\rangle \\ &= U_0^\dagger(t,t_0)H_1(t)U_0(t,t_0)|\psi_i(t)\rangle \\ &= H_i(t)|\psi_i(t)\rangle \end{aligned} \tag{2.112}$$

where $H_i(t)$ is the Hamiltonian in the interaction picture. We now integrate (2.112) to get that

$$|\psi_i(t)\rangle = |\psi_i(t_0)\rangle - \frac{i}{\hbar}\int_{t_0}^{t} dt' H_i(t')|\psi_i(t')\rangle. \tag{2.113}$$

Using the fact that $|\psi_i(t_0)\rangle = |\psi_s(t_0)\rangle$ we change back to the Schrödinger picture

$$U_0^\dagger(t,t_0)|\psi_s(t)\rangle = |\psi_s(t_0)\rangle - \frac{i}{\hbar}\int_{t_0}^{t} dt' U_0^\dagger(t',t_0)H_1(t')U_0(t',t_0)U_0^\dagger(t',t_0)|\psi_s(t')\rangle. \tag{2.114}$$

Multiplying across by $U_0(t,t_0)$ we get that

$$\begin{aligned} |\psi_s(t)\rangle &= U_0(t,t_0)|\psi_s(t_0)\rangle - \frac{i}{\hbar}\int_{t_0}^{t} dt' U_0(t,t_0)U_0^\dagger(t',t_0)H_1(t')|\psi_s(t')\rangle \\ &= U_0(t,t_0)|\psi_s(t_0)\rangle - \frac{i}{\hbar}\int_{t_0}^{t} dt' U_0(t,t_0)U_0(t_0,t')H_1(t')|\psi_s(t')\rangle \\ &= U_0(t,t_0)|\psi_s(t_0)\rangle - \frac{i}{\hbar}\int_{t_0}^{t} dt' U_0(t,t')H_1(t')|\psi_s(t')\rangle. \end{aligned} \tag{2.115}$$

We now set $H_1(t) = \lambda V(t)$ where $\lambda \in \mathbb{R}$. If we then substitute this into (2.115) and repeat the integration as before we obtain

$$\begin{aligned}
|\psi_s(t)\rangle &= U_0(t,t_0)|\psi_s(t_0)\rangle - \frac{i}{\hbar}\lambda \int_{t_0}^{t} dt' U_0(t,t')V(t')|\psi_s(t')\rangle \\
&= U_0(t,t_0)|\psi_s(t_0)\rangle + \left(-\frac{i}{\hbar}\right)\lambda \int_{t_0}^{t} dt' U_0(t,t')V(t')U_0(t',t_0)|\psi_s(t_0)\rangle \\
&\quad + \left(-\frac{i}{\hbar}\right)^2 \lambda^2 \int_{t_0}^{t} dt' \int_{t_0}^{t'} dt'' U_0(t,t')V(t')U_0(t',t'')V(t'')|\psi_s(t'')\rangle + \ldots \\
&= \left[U_0(t,t_0) + \sum_{n=1}^{\infty} \lambda^n U_{0,n}(t,t_0)\right]|\psi_s(t_0)\rangle \qquad (2.116)
\end{aligned}$$

where we define

$$\begin{aligned}
U_{0,n}(t,t_0) &= \left(-\frac{i}{\hbar}\right)^n \int_{t_0}^{t} dt_n \int_{t_0}^{t_n} dt_{n-1} \ldots \int_{t_0}^{t_2} dt_1 U_0(t,t_n)V(t_n)U_0(t_n,t_{n-1}) \\
&\quad \times \ldots U_0(t_2,t_1)V(t_1)U_0(t_1,t_0). \qquad (2.117)
\end{aligned}$$

We arrive now at the final result. Given an initial state $|\psi_s(t_0)\rangle$ governed by time-dependent Hamiltonian $H(t) = H_0(t) + \lambda V(t)$, the state at time $t > t_0$ is given by

$$|\psi_s(t)\rangle = \left[U_0(t,t_0) + \sum_{n=1}^{\infty} \lambda^n U_{0,n}(t,t_0)\right]|\psi_s(t_0)\rangle \qquad (2.118)$$

This result is exact. In practice one assumes that $\lambda \ll 1$, i.e., that $H_1(t)$ is only a perturbation to the known dynamics of $H_0(t)$. In this case one can then approximate the time evolution operator by truncating the power series up to some fixed order of λ. This result will be exploited in chapter 3 where perturbation theory will be used to derive the transition sensitivity for different protocols in the presence of unwanted transitions.

2.3.3 Numerical techniques

Suppose we have a system described by the Hamiltonian

$$H(t) = -\frac{\hbar^2}{2m}\nabla^2 + V\left(\vec{r}, t\right), \tag{2.119}$$

and we would like to numerically determine its ground state at initial time and the subsequent time evolution of the wavefunction. In the following we show how the so called split operator method allows one to compute the evolution of the wavefunction and that by evolving a trial wavefunction in imaginary time one obtains the ground state of the system. We also show how one can use the finite difference approximation for derivatives to perform exact numerical diagonlisation of such a Hamiltonian. These methods will be used in chapter 5.

2.3.3.1 Split Operator Method

We will now give an overview of the split operator method [145] which allows one to numerically evolve the wavefunction. The Schrödinger equation for our system is given by

$$i\hbar\partial_t|\psi(t)\rangle = H(t)|\psi(t)\rangle. \tag{2.120}$$

where the Hamiltonian can be written as $H(t) = T + V(t)$ and $T = -\frac{\hbar^2}{2m}\nabla^2$ is the kinetic energy. For the case where $H(t)$ is time independent, i.e., $V(t) = V$, we can write down the time evolution of the wavefunction over a time Δt as

$$|\psi(t_0 + \Delta t)\rangle = \exp\left(-\frac{i}{\hbar}H\Delta t\right)|\psi(t_0)\rangle. \tag{2.121}$$

We now claim that

$$\exp\left(-\frac{i}{\hbar}H\Delta t\right) = \exp\left(-\frac{i}{\hbar}\frac{V}{2}\Delta t\right)\exp\left(-\frac{i}{\hbar}T\Delta t\right)\exp\left(-\frac{i}{\hbar}\frac{V}{2}\Delta t\right) + \mathcal{O}(\Delta t^3). \tag{2.122}$$

The error in this method of splitting is of order Δt^3 which can be neglected for small enough time steps, i.e., for $\Delta t \ll 1$. Hence this particular way of splitting the operator is very accurate and as we will see later, much easier to implement than other methods. We will now prove this claim by considering the series expansion of these matrix exponentials, i.e., $e^X = \sum_{k=o}^{\infty} \frac{1}{k!} X^k$. The exact time evolution operator can be expressed as

$$\exp\left(-\frac{i}{\hbar} H \Delta t\right) = \mathbb{1} - \frac{i}{\hbar}(T+V)\Delta t + \frac{1}{2}\left[-\frac{i}{\hbar}(T+V)\Delta t\right]^2 + \mathcal{O}(\Delta t^3). \tag{2.123}$$

The series expansion of the right hand term can be written as

$$\begin{aligned} &\exp\left(-\frac{i}{\hbar}\frac{V}{2}\Delta t\right)\exp\left(-\frac{i}{\hbar}T\Delta t\right)\exp\left(-\frac{i}{\hbar}\frac{V}{2}\Delta t\right) = \\ &\left[\mathbb{1} - \frac{i}{\hbar}\frac{V}{2}\Delta t + \frac{1}{2}\left(-\frac{i}{\hbar}\frac{V}{2}\Delta t\right)^2 + \mathcal{O}(\Delta t^3)\right] \\ \times &\left[\mathbb{1} - \frac{i}{\hbar}T\Delta t + \frac{1}{2}\left(-\frac{i}{\hbar}T\Delta t\right)^2 + \mathcal{O}(\Delta t^3)\right] \\ \times &\left[\mathbb{1} - \frac{i}{\hbar}\frac{V}{2}\Delta t + \frac{1}{2}\left(-\frac{i}{\hbar}\frac{V}{2}\Delta t\right)^2 + \mathcal{O}(\Delta t^3)\right]. \end{aligned} \tag{2.124}$$

After multiplying out and neglecting terms of order Δt^3 or higher this becomes

$$\begin{aligned} &\exp\left(-\frac{i}{\hbar}\frac{V}{2}\Delta t\right)\exp\left(-\frac{i}{\hbar}T\Delta t\right)\exp\left(-\frac{i}{\hbar}\frac{V}{2}\Delta t\right) = \\ &\mathbb{1} - \frac{i}{\hbar}(T+V)\Delta t + \frac{1}{2}\left(-\frac{i}{\hbar}\right)^2 \Delta t^2\left(T^2 + TV + VT + V^2\right) + \mathcal{O}(\Delta t^3). \end{aligned} \tag{2.125}$$

By comparing (2.123) and (2.125), we can see that the splitting is the same up to higher order terms. However, we wish to be able to perform this same splitting for a time dependent Hamiltonian. The question then arises, at what time to evaluate the potential term $V(t)$ in the spitting so that we retain the same accuracy. For the time dependent case we claim that the time evolution operator over a time Δt

can be approximated by

$$\mathcal{T}\exp\left[-\tfrac{i}{\hbar}\int_{t_0}^{t_0+\Delta t}H(t')dt'\right] = \exp\left(-\tfrac{i}{\hbar}\tfrac{V_m}{2}\Delta t\right)\exp\left(-\tfrac{i}{\hbar}T\Delta t\right)\exp\left(-\tfrac{i}{\hbar}\tfrac{V_m}{2}\Delta t\right)+\mathcal{O}(\Delta t^3) \tag{2.126}$$

where

$$V_m = \frac{V(t_0+\Delta t)+V(t_0)}{2} \tag{2.127}$$

is a linear approximation of the midpoint value of the potential over the two extremal times and $\mathcal{T}$ is the time ordering operator. Note that V_m depends on Δt. We will now prove this approximation. Using the results from the previous case, the series expansion of the term on the right hand sides gives us

$$\exp\left(-\frac{i}{\hbar}\frac{V_m}{2}\Delta t\right)\exp\left(-\frac{i}{\hbar}T\Delta t\right)\exp\left(-\frac{i}{\hbar}\frac{V_m}{2}\Delta t\right) = \mathbb{1}-\frac{i}{\hbar}\left(T+V_m\right)\Delta t+\frac{1}{2}\left(-\frac{i}{\hbar}\right)^2\Delta t^2\left[T^2+TV(t_0)+V(t_0)T+V(t_0)^2\right]+\mathcal{O}(\Delta t^3) \tag{2.128}$$

Here we have used a series expansion of $V(t)$ about t_0

$$V(t_0+\Delta t) = V(t_0)+\Delta t V'(t_0)+\frac{(\Delta t)^2}{2}V''(t_0)+\mathcal{O}(\Delta t^3) \tag{2.129}$$

on the last part of the expression and neglected terms which are of order Δt^3 or higher. The exact time evolution operator however is expressed as a Dyson series

$$\mathcal{T}\exp\left[-\frac{i}{\hbar}\int_{t_0}^{t_0+\Delta t}H(t')dt'\right] = \mathbb{1}+\left(-\frac{i}{\hbar}\right)\int_{t_0}^{t_0+\Delta t}H(t_1)dt_1+\left(-\frac{i}{\hbar}\right)^2\int_{t_0}^{t_0+\Delta t}\int_{t_0}^{t_1}H(t_1)H(t_2)dt_2dt_1+\mathcal{O}(\Delta t^3) \tag{2.130}$$

This can be rewritten as

$$\mathcal{T}\exp\left[-\frac{i}{\hbar}\int_{t_0}^{t_0+\Delta t}H(t')dt'\right] = \mathbb{1} + \left(-\frac{i}{\hbar}\right)\int_{t_0}^{t_0+\Delta t}\left[T+V(t_1)\right]dt_1 + \left(-\frac{i}{\hbar}\right)^2\int_{t_0}^{t_0+\Delta t}\int_{t_0}^{t_1}\left[T^2+V(t_1)T+TV(t_2)+V(t_1)V(t_2)\right]dt_2dt_1+\mathcal{O}(\Delta t^3). \tag{2.131}$$

We now approximate these integrals using the trapezoidal rule (see for example [146]). Firstly we get that

$$\int_{t_0}^{t_0+\Delta t}V(t_1)dt_1 = V_m\Delta t+\mathcal{O}(\Delta t^3). \tag{2.132}$$

Secondly we get that

$$\begin{aligned}\int_{t_0}^{t_0+\Delta t}\int_{t_0}^{t_1}V(t_1)Tdt_2dt_1 &= \int_{t_0}^{t_0+\Delta t}V(t_1)T\left(t_1-t_0\right)dt_1\\ &= \frac{1}{2}V(\Delta t+t_0)T\Delta t^2+\mathcal{O}(\Delta t^3).\end{aligned} \tag{2.133}$$

The third integral is given by

$$\begin{aligned}\int_{t_0}^{t_0+\Delta t}\int_{t_0}^{t_1}TV(t_2)dt_2dt_1 &= \frac{1}{2}\int_{t_0}^{t_0+\Delta t}T\left[V(t_1)+V(t_0)\right](t_1-t_0)dt_1+\mathcal{O}(\Delta t^3)\\ &= \frac{1}{2}\Delta t^2TV_m+\mathcal{O}(\Delta t^3).\end{aligned} \tag{2.134}$$

The final integral is given by

$$\begin{aligned}\int_{t_0}^{t_0+\Delta t}\int_{t_0}^{t_1}V(t_1)V(t_2)dt_2dt_1 &= \int_{t_0}^{t_0+\Delta t}V(t_1)\left[\frac{V(t_1)+V(t_0)}{2}\right](t_1-t_0)dt_1+\mathcal{O}(\Delta t^3)\\ &= \frac{\Delta t^2}{4}\left[V(t_0+\Delta t)^2+V(t_0+\Delta t)V(t_0)\right]+\mathcal{O}(\Delta t^3).\end{aligned} \tag{2.135}$$

If we put this all together now we see that the Dyson expansion now looks like

$$\mathcal{T}\exp\left[-\frac{i}{\hbar}\int_{t_0}^{t_0+\Delta t}H(t')dt'\right] = \mathbb{1} + \left(-\frac{i}{\hbar}\right)(T+V_m)\,\Delta t + \left(-\frac{i}{\hbar}\right)^2\Delta t^2\left[\frac{T^2}{2} + \frac{V(\Delta t+t_0)T}{2} + \frac{1}{2}TV_m + \frac{1}{4}V(t_0+\Delta t)^2 + \frac{1}{4}V(t_0+\Delta t)V(t_0)\right] + \mathcal{O}(\Delta t^3). \tag{2.136}$$

In the same way as before we Taylor expand $V(t)$ about t_0 in the last term and neglect any terms that are order Δt^3 or higher. This leaves us with

$$\mathcal{T}\exp\left[-\frac{i}{\hbar}\int_{t_0}^{t_0+\Delta t}H(t')dt'\right] = \mathbb{1} + \left(-\frac{i}{\hbar}\right)(T+V_m)\,\Delta t + \left(-\frac{i}{\hbar}\right)^2\frac{\Delta t^2}{2}\left[T^2 + V(t_0)T + TV(t_0) + V(t_0)^2\right] + \mathcal{O}(\Delta t^3). \tag{2.137}$$

By comparing (2.128) and (2.125), we can see that this splitting is accurate to $\mathcal{O}(\Delta t^3)$.

We are now in a position to see why this splitting is so useful numerically. The individual operators V_m and T are diagonal in position and momentum representation respectively. Hence is it simple to perform both the matrix exponential and the multiplication on the wavefunction in these particular representations. Hence this splitting can be easily applied by changing between position and momentum representations. In order to see this explicitly, we now define the Fourier transformation $\mathcal{F}[\cdot]$ going from position space to momentum space. In three dimensions, this is given by

$$\mathcal{F}[\langle\vec{r}|\psi(t)\rangle](\vec{p}) = \frac{1}{(2\pi\hbar)^{3/2}}\int_{-\infty}^{\infty}\langle\vec{r}|\psi(t)\rangle e^{-i\vec{p}\cdot\vec{r}/\hbar}d^3\vec{r}. \tag{2.138}$$

We can see that one can propagate the wavefunction in position representation by Δt by doing the following

$$\langle\vec{r}|\psi(t_0+\Delta t)\rangle = \exp\left(-\frac{i}{\hbar}\frac{V_m}{2}\Delta t\right)\mathcal{F}^{-1}\left[\exp\left(-\frac{i}{\hbar}T\Delta t\right)\mathcal{F}\left[\exp\left(-\frac{i}{\hbar}\frac{V_m}{2}\Delta t\right)\langle\vec{r}|\psi(t_0)\rangle\right]\right]. \tag{2.139}$$

It is clear here that to propagate the wavefunction in time the Fourier transform must be used many times. As Graphic Processing Units (GPUs) are very suitable to parallel tasks such as Fourier transforms, they can be much faster for numerically implementing this method. In our case, the CUDA architecture created by NVIDIA was used [147].

2.3.3.2 Imaginary time evolution

Suppose we would like to determine the ground state of the stationary Hamiltonian

$$H_0 = -\frac{\hbar^2}{2m}\nabla^2 + V\left(\vec{r}, 0\right). \tag{2.140}$$

We start with a trial wavefunction

$$|\chi(0)\rangle = \sum_n c_n |\phi_n\rangle \tag{2.141}$$

where $|\phi_n\rangle$ is the eigenstate of H_0 with energy E_n. The time evolution of the trial wavefunction under H_0 is given by

$$\begin{aligned} |\chi(t)\rangle &= \exp\left(-\frac{i}{\hbar}H_0 t\right)|\chi(0)\rangle \\ &= \sum_n c_n \exp\left(-\frac{i}{\hbar}H_0 t\right)|\phi_n\rangle \\ &= \sum_n c_n \exp\left(-\frac{i}{\hbar}E_n t\right)|\phi_n\rangle. \end{aligned} \tag{2.142}$$

If the process is now done in imaginary time $\tau \in \mathbb{R}$ (which is completely unphysical) we get that

$$|\chi(\tau)\rangle = \sum_n c_n \exp\left(-\frac{1}{\hbar}E_n \tau\right)|\phi_n\rangle. \tag{2.143}$$

This can be rewritten as

$$|\chi(\tau)\rangle = c_0 \exp\left(-\frac{1}{\hbar}E_0\tau\right)\left\{|\phi_0\rangle + \sum_{n\neq 0} c_0^{-1}c_n \exp\left[-\frac{1}{\hbar}\left(E_n - E_0\right)\tau\right]|\phi_n\rangle\right\}. \tag{2.144}$$

For long imaginary times, the last term in brackets will tend towards $|\phi_0\rangle$. The first term however tends towards 0. This is offset by renormalising the wavefunction after every time step. Note that evolution in imaginary time is a non unitary process. Hence for long imaginary times, the trial wavefunction will tend towards the ground state. This effect is independent of the initial trial wavefunction as long as it has a non-zero overlap with the ground state. This method is exceptionally useful as any numerical method for computing the evolution of the wavefunction can be easily adapted to work in imaginary time.

2.3.3.3 Finite difference method for exact numerical diagonalisation

Here we will review how the finite difference method [148] is used for numerically exact diagonalisation. This method will allow us to obtain all eigenvalues and eigenvectors of the Hamiltonian. We will only consider the one dimensional case in this thesis as that is the only case that is required for our purposes. The Hamiltonian is given by

$$H = -\frac{\hbar^2}{2m}\frac{d^2}{dx^2} + V(x). \tag{2.145}$$

We must now discretise the x coordinate into points x_m with spacing $\Delta x = x_{m+1} - x_m$ where $m = 0, 1, 2, ..., N$. Using the finite difference approximation [148] we can write the second derivative as

$$-\frac{\hbar^2}{2m}\frac{d^2}{dx^2}\psi(x_m) \approx \frac{\hbar^2}{2m\left(\Delta x\right)^2}\left[-\psi(x_{m+1}) + 2\psi(x_m) - \psi(x_{m-1})\right] \tag{2.146}$$

with an error of order $(\Delta x)^2$. In matrix form this can be written as

$$-\frac{\hbar^2}{2m}\frac{d^2}{dx^2}\psi(x) = \frac{\hbar^2}{2m\left(\Delta x\right)^2}\begin{pmatrix} 2 & -1 & 0 & \cdots & 0 \\ -1 & 2 & -1 & \cdots & \vdots \\ 0 & -1 & 2 & \ddots & 0 \\ \vdots & \vdots & \ddots & \ddots & -1 \\ 0 & \cdots & 0 & -1 & 2 \end{pmatrix}\begin{pmatrix} \psi(x_0) \\ \psi(x_1) \\ \psi(x_2) \\ \vdots \\ \psi(x_N) \end{pmatrix}. \quad (2.147)$$

Note that this assumes as boundary conditions that the wavefunction is exactly zero outside the discretised space. Since we are working in position space the potential is diagonal in matrix form

$$V(x) = \begin{pmatrix} V(x_0) & 0 & 0 & \cdots & 0 \\ 0 & V(x_1) & 0 & \cdots & 0 \\ 0 & 0 & V(x_2) & \ddots & \vdots \\ \vdots & \vdots & \ddots & \ddots & 0 \\ 0 & 0 & \cdots & 0 & V(x_N) \end{pmatrix}. \quad (2.148)$$

Finally if we define $C_m = 2 + \frac{2m(\Delta x)^2}{\hbar^2}V(x_m)$, our final Hamiltonian can be written as

$$H = \frac{\hbar^2}{2m\left(\Delta x\right)^2}\begin{pmatrix} C_0 & -1 & 0 & \cdots & 0 \\ -1 & C_1 & -1 & \cdots & \vdots \\ 0 & -1 & C_2 & \ddots & 0 \\ \vdots & \vdots & \ddots & \ddots & -1 \\ 0 & \cdots & 0 & -1 & C_N \end{pmatrix}. \quad (2.149)$$

We can now obtain the corresponding eigenvalues and eigenvectors of the Hamiltonian by diagonalising this matrix provided $\Delta x \ll 1$.

This concludes the background theory for the thesis. The next chapter starts by looking at STA in finite level systems.

Chapter 3

Inhibiting unwanted transitions in population transfer in two- and three-level quantum systems

3.1 Overview

In this chapter, we construct fast and stable control schemes for two- and three-level quantum systems. These schemes result in an almost perfect population transfer even in the presence of an additional, unwanted and uncontrollable transition. Such schemes are developed by first using the techniques of "Shortcuts to Adiabaticity" and then introducing and examining a measure of the scheme's sensitivity to an unwanted transition. We optimise the schemes to minimise this sensitivity and provide examples of shortcut schemes which lead to a nearly perfect population inversion even in the presence of unwanted transitions.

This chapter is based on the following publication:
A. Kiely and A. Ruschhaupt,
Inhibiting unwanted transitions in population transfer in two- and three-level quantum systems,
J. Phys. B: At. Mol. Opt. Phys. **47** 115501 (2014).

3.2 Introduction

The manipulation of the state of a quantum system with time-dependent interacting fields is a fundamental operation in atomic and molecular physics. Modern applications of this quantum control such as quantum information processing [11, 149] require fast schemes with a high fidelity (typically with an error lower than 10^{-4} [11, 149]) which must also be very stable with respect to imperfections of the system or fluctuations of the control parameters.

Most methods used may be classified into two major groups: fast, resonant, fixed-area pulses, and slow adiabatic methods such as "Rapid" Adiabatic Passage (RAP). Fixed area pulses are traditionally considered to be fast but unstable with respect to perturbations. For two-level systems, an example of a fixed area pulse is a π pulse. A π pulse may be fast but is highly sensitive to variations in the pulse area and to inhomogeneities in the sample [150]. An alternative to a single π pulse are composite pulses [151–153], which still need an accurate control of pulse phase and intensity. On the other hand, the canonical robust option is to perform operations adiabatically [154–156]. Nevertheless, such schemes are slow and therefore likely to be affected by decoherence or noise over the long times required and do not lead to an exact transfer.

A compromise is to use "shortcuts to adiabaticity" (STA). In particular, STA for two- and three-level systems are developed in [77, 79, 131, 158, 159] and [78] respectively. Nonetheless, in an experimental implementation the system is never an ideal two- or three-level system. There may be unwanted couplings to other levels. Many other effects can limit the ability to quickly and robustly manipulate these few level systems , such as noise and systematic error in the control parameters i.e. calibration imperfections. STA schemes are developed in [160] which are stable against dephasing noise and systematic frequency error.

In this chapter, we develop STA inversion schemes which lead to nearly perfect population inversion even in the case of such unwanted uncontrollable transitions. To achieve this we examine the effect of unwanted couplings to STA in two- and

three-level quantum systems and we develop STA schemes with minimal sensitivity to unwanted and uncontrollable transitions. Note that this is different from [161]; in that paper the effect of such unwanted transitions for composite pulses has been examined and optimised where it was also assumed that the phase of the unwanted coupling to another level could be controlled in a time-dependent way.

The remainder of this chapter is structured as follows. In the subsequent section, we briefly review STA for two-level systems. In section 3.4, we examine the sensitivity of STA schemes to unwanted transitions and develop schemes to minimise this sensitivity (which leads to nearly perfect population inversion for these schemes). In section 3.5, we review STA for three-level systems. We examine their sensitivity to unwanted transitions in section 3.6 and we also develop schemes in the three-level case leading to nearly perfect population inversion in the case of additional unwanted, uncontrollable transitions.

3.3 Invariant-based shortcuts in two-level quantum systems

Here we will review the derivation of invariant-based STA schemes in two-level quantum systems. We assume our two-level system (see also figure 3.1(a)) has a Hamiltonian of the form

$$H_{2L}(t) = \frac{\hbar}{2}\begin{pmatrix} -\delta_2(t) & \Omega_R(t) - i\Omega_I(t) \\ \Omega_R(t) + i\Omega_I(t) & \delta_2(t) \end{pmatrix} \tag{3.1}$$

expressed in the "bare basis" of the two-level system

$$|1\rangle = \begin{pmatrix} 1 \\ 0 \end{pmatrix} \text{ and } |2\rangle = \begin{pmatrix} 0 \\ 1 \end{pmatrix}. \tag{3.2}$$

We also assume $\delta_2(t) = \Omega_R(t) = \Omega_I(t) = 0$ for $t < 0$ and for $t > T$.

An example of such a quantum system would be a semi-classical coupling of two atomic levels with a laser in a laser-adapted interaction picture (using the dipole and rotating-wave approximations. Recall section 2.1.1). In this setting, $|1\rangle$ might represent the ground state and $|2\rangle$ a meta-stable excited state of the atom. $\Omega(t) = \Omega_R(t) + i\Omega_I(t)$ would be the complex Rabi frequency (where Ω_R and Ω_I are the real and imaginary parts) and δ_2 would be the time-dependent detuning between transition and laser frequencies. To simplify the language we will assume this setting for convenience in the following, noting that our reasoning will still pertain to any other two-level system such as electron spin in a quantum dot [80] or a Bose-Einstein condensate on an accelerated optical lattice [102]. In other settings, $\Omega(t)$ and $\delta_2(t)$ will correspond to different physical quantities.

The goal is to achieve perfect population inversion in a short time in a two-level quantum system. The system should start at $t = 0$ in state $|1\rangle$ and end in state $|2\rangle$ (up to a phase) at final time T. In order to design a scheme to achieve this goal i.e. to design a STA, we make use of Lewis-Riesenfeld invariants [116]. Recall from section 2.2.2 that a Lewis-Riesenfeld invariant of H_{2L} is a Hermitian Operator $I(t)$ such that

$$\frac{\partial I}{\partial t} + \frac{i}{\hbar}[H_{2L}, I] = 0\,. \tag{3.3}$$

In this case $I(t)$ is given by

$$I(t) = \frac{\hbar}{2}\begin{pmatrix} \cos(\theta(t)) & \sin(\theta(t))\, e^{-i\alpha(t)} \\ \sin(\theta(t))\, e^{i\alpha(t)} & -\cos(\theta(t))\,. \end{pmatrix} \tag{3.4}$$

The functions $\theta(t)$ and $\alpha(t)$ must satisfy the following equations:

$$\dot{\theta} = \Omega_I \cos\alpha - \Omega_R \sin\alpha, \tag{3.5}$$

$$\dot{\alpha} = -\delta_2 - \cot\theta\,(\Omega_R \cos\alpha + \Omega_I \sin\alpha)\,. \tag{3.6}$$

The eigenvectors of $I(t)$ are

$$|\phi_+(t)\rangle = \begin{pmatrix} \cos(\theta/2)\, e^{-i\alpha/2} \\ \sin(\theta/2)\, e^{i\alpha/2} \end{pmatrix}, \tag{3.7}$$

$$|\phi_-(t)\rangle = \begin{pmatrix} \sin(\theta/2)\, e^{-i\alpha/2} \\ -\cos(\theta/2)\, e^{i\alpha/2} \end{pmatrix} \tag{3.8}$$

with eigenvalues $\pm\frac{\hbar}{2}$. One can write a general solution of the Schrödinger equation

$$i\hbar\frac{d}{dt}|\Psi(t)\rangle = H_{2L}(t)\,|\Psi(t)\rangle \tag{3.9}$$

as a linear combination of the eigenvectors of $I(t)$ i.e. $|\Psi(t)\rangle = c_+ e^{i\kappa_+(t)}\,|\phi_+(t)\rangle + c_- e^{i\kappa_-(t)}\,|\phi_-(t)\rangle$ where $c_\pm \in \mathbb{C}$ and $\kappa_\pm(t)$ are the Lewis-Riesenfeld phases [116]

$$\dot{\kappa}_\pm(t) = \frac{1}{\hbar}\,\langle\phi_\pm(t)\,|(i\hbar\partial_t - H_{2L}(t))|\,\phi_\pm(t)\rangle\ . \tag{3.10}$$

Therefore, it is possible to construct a solution

$$|\psi(t)\rangle = |\phi_+(t)\rangle\, e^{-i\gamma(t)/2} \tag{3.11}$$

where $\gamma = \pm 2\kappa_\pm$. From (3.10) we get

$$\dot{\gamma} = \frac{1}{\sin\theta}\left(\Omega_R\cos\alpha + \Omega_I\sin\alpha\right)\ . \tag{3.12}$$

For population inversion it must be the case that $\theta(0) = 0$ and $\theta(T) = \pi$. This ensures that $|\psi(0)\rangle = |1\rangle$ and $|\psi(T)\rangle = |2\rangle$ up to a phase. Note, that this method is not limited to going from state $|1\rangle$ to state $|2\rangle$; the initial and final states can be determined by changing the boundary conditions on θ and α. Using Eqs. (3.5), (3.6) and (3.12) we can retrieve the physical quantities:

$$\Omega_R = \cos\alpha\sin\theta\,\dot{\gamma} - \sin\alpha\,\dot{\theta}\,, \tag{3.13}$$

$$\Omega_I = \sin\alpha\sin\theta\,\dot{\gamma} + \cos\alpha\,\dot{\theta}\,, \tag{3.14}$$

$$\delta_2 = -\cos\theta\,\dot{\gamma} - \dot{\alpha}\,. \tag{3.15}$$

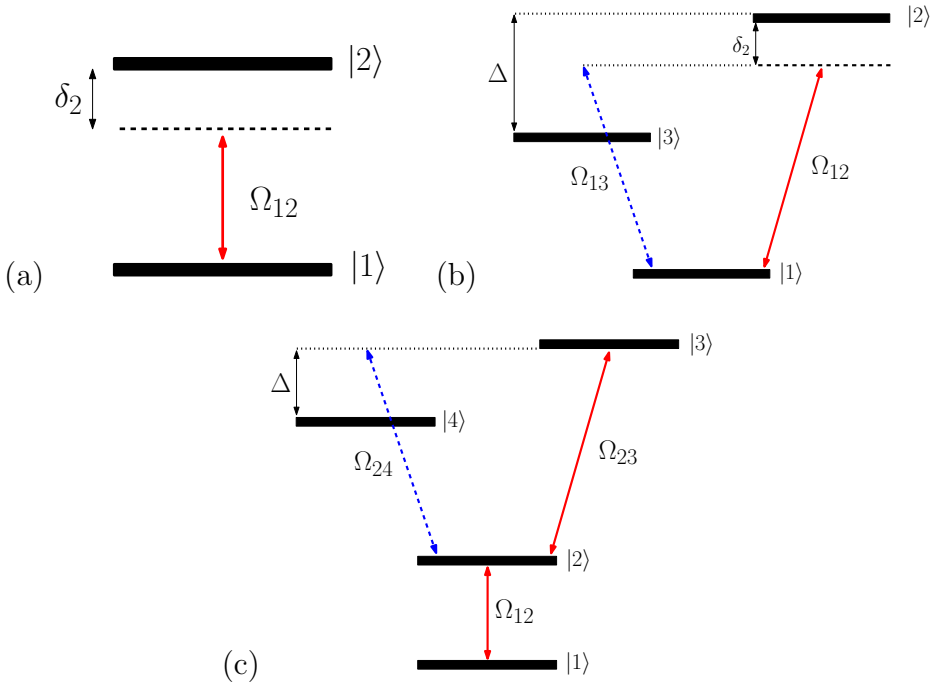


FIGURE 3.1: Schematic of level structure: (a) Ideal two-level system; (b) two-level system with an unwanted coupling (blue dotted arrow) to a third level; (c) three-level system with an unwanted coupling (blue dotted arrow) to a fourth level.

From this we can see that if the functions α, γ, and θ are chosen with the appropriate boundary conditions, perfect population inversion would be achieved at a time T assuming no perturbation or unwanted transitions. These functions will henceforth be referred to as ancillary functions. The angles α and θ can be thought of as spherical coordinates on the Bloch sphere. In the following section we assume that there is an additional unwanted coupling to a third level.

3.4 Two-level quantum system with unwanted transition

3.4.1 Model

We assume there are in fact three levels in the atom as shown in figure 3.1(b) and the energy of level $|j\rangle$ is $\hbar\omega_j$ where $j = 1, 2, 3$. Without loss of generality we set

$\omega_1 = 0$. The frequency of the laser coupling levels $|1\rangle$ and $|2\rangle$ is denoted by ω_L. The detuning with the second level is given by

$$\delta_2 = \omega_2 - \omega_L \,. \tag{3.16}$$

We assume that this laser is also unintentionally coupling levels $|1\rangle$ and $|3\rangle$. With this in mind, we assume that the Rabi frequency $\Omega_{13}(t)$ differs from $\Omega_{12}(t)$ by a constant complex number, i.e.

$$\Omega_{13}\,(t) = \beta e^{i\zeta}\Omega_{12}(t) \tag{3.17}$$

where ζ, β are real unknown constants, $\beta \ll 1$. $\Omega_{12}(t)$ is the Rabi frequency coupling levels $|1\rangle$ and $|2\rangle$.

A possible motivation for these assumptions in a quantum-optics setting might be the following: assume that one needs right circularly polarised light in order to couple states $|1\rangle$ and $|2\rangle$ and one needs left circularly polarised light to couple states $|1\rangle$ and $|3\rangle$. If the laser light is -instead of exactly right polarised- elliptically polarised, this would cause unwanted transitions to level $|3\rangle$. Other motivations for these assumptions are possible, especially in other quantum systems (different from the quantum-optics setting of an atom and a classical laser). Note, that these assumptions are also used in [161] with the only difference that in that paper a controllable, time-dependent phase ζ has been assumed.

The three levels or bare states of our atom have the following state representation:

$$|1\rangle = \begin{pmatrix} 1 \\ 0 \\ 0 \end{pmatrix} , |2\rangle = \begin{pmatrix} 0 \\ 1 \\ 0 \end{pmatrix} , |3\rangle = \begin{pmatrix} 0 \\ 0 \\ 1 \end{pmatrix} . \tag{3.18}$$

Hence our Hamiltonian for the three-level system is

$$H(t) = \frac{\hbar}{2} \begin{pmatrix} -\delta_2(t) & \Omega_{12}^*(t) & \beta e^{-i\zeta}\Omega_{12}^*(t) \\ \Omega_{12}(t) & \delta_2(t) & 0 \\ \beta e^{i\zeta}\Omega_{12}(t) & 0 & -2\Delta + \delta_2(t) \end{pmatrix} \tag{3.19}$$

where $\Delta = \omega_2 - \omega_3$ is the frequency difference between level $|2\rangle$ and $|3\rangle$. The phase ζ can be absorbed in a redefinition of the basis state for the third level and therefore in the following we will just set $\zeta = 0$. We also assume that $\delta_2(t) = \Omega_{12}(t) = 0$ for $t \leq 0$ and $t > T$.

Using the formalism presented in Sect. 3.3, we can construct schemes which result in full population inversion in the case of no unwanted transition. There is a lot of freedom in choosing the ancillary functions. The goal will be to find the schemes which are very robust against unwanted transitions, i.e. schemes which result in a nearly perfect population inversion even in the presence of an unwanted transition.

3.4.2 Transition sensitivity

We can write solutions of the time-dependent Schrödinger equation for the Hamiltonian in (3.19) if $\beta = 0$ as follows

$$\begin{aligned} |\psi_0(t)\rangle &= \begin{pmatrix} \cos(\theta/2)\, e^{-i\alpha/2} \\ \sin(\theta/2)\, e^{i\alpha/2} \\ 0 \end{pmatrix} e^{-i\gamma/2}, \\ |\psi_1(t)\rangle &= \begin{pmatrix} \sin(\theta/2)\, e^{-i\alpha/2} \\ -\cos(\theta/2)\, e^{i\alpha/2} \\ 0 \end{pmatrix} e^{i\gamma/2}, \\ |\psi_2(t)\rangle &= \begin{pmatrix} 0 \\ 0 \\ e^{-i\Gamma(t)} \end{pmatrix} \end{aligned} \tag{3.20}$$

where $\dot{\Gamma} = \frac{1}{2}(-2\Delta + \delta_2)$. These solutions form an orthonormal basis at every time t. The ancillary functions θ, α, γ must fulfil Eqs. (3.5), (3.6) and (3.12).

This unwanted coupling to the third level can be regarded as a perturbation using the approximation that β is small. We can write our Hamiltonian (3.19) as

$$H(t) = H_0(t) + \beta V(t) \tag{3.21}$$

where β is the strength of the perturbation, $H_0(t) = H(t)|_{\beta=0}$ and

$$V(t) = \frac{\hbar}{2}\begin{pmatrix} 0 & 0 & \Omega_{12}^*(t) \\ 0 & 0 & 0 \\ \Omega_{12}(t) & 0 & 0 \end{pmatrix}. \tag{3.22}$$

Using time-dependent perturbation theory (see section 2.3.2) we can calculate the probability of being in state $|2\rangle$ at time T as

$$P_2 = 1 - \beta^2 q + \mathcal{O}\left(\beta^4\right) \tag{3.23}$$

where

$$q = \frac{1}{\hbar^2}\sum_{k=0}^{2}\left|\int_0^T dt\,\langle\psi_0(t)|V(t)|\psi_k(t)\rangle\right|^2. \tag{3.24}$$

If we substitute in the expression for the perturbation (3.22) then we get

$$\begin{aligned} q &= \frac{1}{4}\left|\int_0^T dt\,\cos\left(\frac{\theta}{2}\right)\left(\sin\theta\,\dot{\gamma} - i\dot{\theta}\right)e^{iF(t)+i\Delta t}\right|^2 \\ &= \left|\int_0^T dt\,\frac{d}{dt}\left[\sin\left(\frac{\theta(t)}{2}\right)e^{iF(t)}\right]e^{i\Delta t}\right|^2 \end{aligned} \tag{3.25}$$

where $F(t) = \frac{1}{2}\int_0^t ds\,(1+\cos\theta(s))\dot{\gamma}(s)$. The q quantifies how sensitive a given protocol (determined by the ancillary functions) is concerning the unwanted transition to level $|3\rangle$. Therefore we will call q *transition sensitivity* in the following. Our goal will be to determine protocols or schemes which would maximise P_2 or equivalently minimise q.

3.4.3 General properties of the transition sensitivity

We will begin by examining some general properties of the transition sensitivity q. First, we note that q is always independent of α. In the case where $\dot{\gamma} = 0$ the transition sensitivity is symmetric about $\Delta \leftrightarrow -\Delta$.

In the case of $\Delta = 0$, the integral in (3.25) can be easily evaluated by taking into account that $\theta(T) = \pi$ and $\theta(0) = 0$. From this we see that

$$q = 1 \text{ if } \Delta = 0\,. \tag{3.26}$$

This means there is no possibility in the case of $\Delta = 0$ to completely reduce the influence of the unwanted transition.

In the following, we will show that even for $|\Delta| < 1/T$ the transition probability q cannot be zero. By partial integration, we get

$$q = |1 - i\Delta M|^2 = 1 + 2\Delta \mathrm{Im}(M) + \Delta^2 |M|^2 \tag{3.27}$$

where

$$M = \int_0^T dt\, \sin\left(\frac{\theta(t)}{2}\right) \exp\left(i(t-T)\Delta - \frac{i}{2}\int_t^T ds\,(1+\cos\theta(s))\dot{\gamma}(s)\right). \tag{3.28}$$

We have $q \geq (1 + \Delta \mathrm{Im}(M))^2$ and

$$|\mathrm{Im}(M)| \leq \int_0^T dt \left|\sin\left(\frac{\theta(t)}{2}\right)\right| \leq T\,. \tag{3.29}$$

Let us assume $|\Delta|T < 1$ then

$$q \geq (1 - |\Delta||\mathrm{Im}(M)|)^2 \geq \left(1 - |\Delta| \int_0^T dt \left|\sin\left(\frac{\theta(t)}{2}\right)\right|\right)^2 \geq (1 - |\Delta|T)^2\,. \tag{3.30}$$

So we get $q > 0$ if $|\Delta|T < 1$, i.e. this means that a necessary condition for $q = 0$ is $T \geq 1/|\Delta|$.

The next question which we will address is whether there could be a scheme (independent of Δ) which results in $q = 0$ for all $|\Delta| > 1/T$. For this we would need

$$H(\Delta) \equiv \int_0^T dt \, \frac{d}{dt} \left[G\left(t\right) \right] e^{i\Delta t} \stackrel{!}{=} 0 \tag{3.31}$$

for all $|\Delta| > 1/T$, where $G(t) = \sin\left(\theta(t)/2\right) e^{iF(t)}$. The left-hand side of this equation, $H(\Delta)$, is simply the Fourier transform of $h(t) = \chi_{[0,T]}(t) \frac{d}{dt} \left[G\left(t\right) \right]$ (where $\chi_{[0,T]}(t) = 1$ for $0 \leq t \leq T$ and zero otherwise). $h(t)$ has compact support. If (3.31) would be true then this would mean that the Fourier transform $H(\Delta)$ of the compactly supported function $h(t)$ also has compact support. This is not possible and therefore there can be no (Δ-independent) protocol which results in $q = 0$ for all $|\Delta| > 1/T$. Nevertheless, we will show below that for a fixed Δ there are schemes resulting in $q = 0$.

It is also important to examine general properties for $|\Delta| \gg 1/T$. From the previous remark (and the property that a Fourier transform of any function vanishes at infinity) it is immediately clear that we get $q \to 0$ for $|\Delta| \to \infty$. Using partial integration we can derive a series expansion of q in $1/\Delta$. We use

$$\begin{aligned} \int_0^T dt \dot{G}(t) e^{i\Delta t} &= -\frac{i}{\Delta} \left[\dot{G}(t) e^{i\Delta t} \right]_0^T + \frac{i}{\Delta} \int_0^T dt \ddot{G}(t) e^{i\Delta t} \\ &= -\frac{i}{\Delta} \left[\dot{G}(t) e^{i\Delta t} \right]_0^T + o\left(\frac{1}{\Delta} \right). \end{aligned} \tag{3.32}$$

Hence, in the case where $|\Delta| \gg 1/T$ the transition sensitivity is

$$q = \frac{1}{\Delta^2} \frac{1}{4} \dot{\theta}(0)^2 + ... \tag{3.33}$$

where we have taken into account that $\theta(0) = 0$ and $\theta(T) = \pi$. By repeating partial integration, we get the higher orders in this $1/\Delta$ series.

If we demand

$$\dot{\theta}(0) = \dot{\theta}(T) = \ddot{\theta}(0) = 0 \tag{3.34}$$

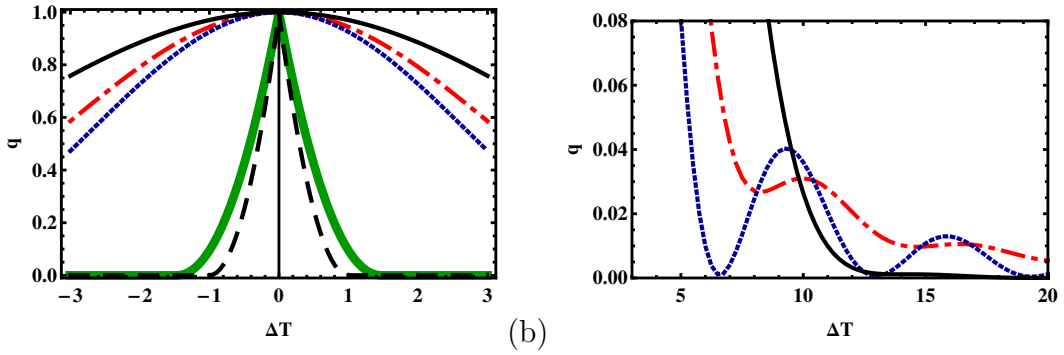


FIGURE 3.2: Transition sensitivity q versus ΔT for different schemes; reference case of a flat π pulse (red, dot-dashed line); other π pulse given by (3.41) (blue, dotted line); scheme given by (3.42) (black, solid line); also in (a): scheme in (3.43) with numerically optimised parameters c_0 and c_1 (green, thick, solid line); lower bound for q as in (3.30) (black, dashed line).

then this first term and the next terms in the $1/\Delta$ series expansion of the transition sensitivity vanish. The first non-vanishing term is now

$$q = \frac{1}{\Delta^6} \dddot{\theta}(0)^2 + ... \tag{3.35}$$

3.4.4 Reference case: flat π pulse

As a reference case we will consider a flat π pulse with

$$\Omega_R = -\frac{\pi}{T} \sin\alpha, \; \Omega_I = \frac{\pi}{T} \cos\alpha \tag{3.36}$$

with a constant phase α. This scheme corresponds to $\theta(t) = \pi \frac{t}{T}$ and $\gamma(t) = 0$.

The transition sensitivity can be easily calculated

$$q = \left| \int_0^T dt \, \frac{d}{dt} \left[\sin\left(\frac{\pi t}{2T} \right) \right] e^{i\Delta t} \right|^2 = \frac{\pi^2 \left(4\Delta^2 T^2 - 4\pi \Delta T \sin(\Delta T) + \pi^2 \right)}{\left(\pi^2 - 4\Delta^2 T^2 \right)^2} . \tag{3.37}$$

This transition sensitivity q is plotted in figure 3.2(a) and (b). It can be seen that q is one for $\Delta = 0$ and it goes to zero for large $|\Delta|$ as is expected. The transition sensitivity for the flat π pulse is never exactly zero.

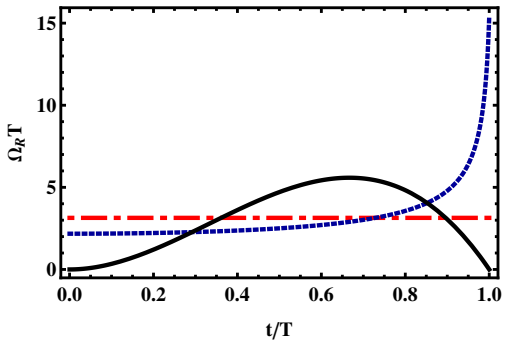


FIGURE 3.3: Rabi frequencies $\Omega_R(t)$ versus time for different scheme: reference case of a flat π pulse (red, dot-dashed, line); other π pulse given by (3.41) (blue, dotted line); scheme given by (3.42) (black, solid line).

3.4.5 Other examples of π pulses

Let us examine two other examples of protocols. Suppose $\gamma(t) = 0$, $\theta(t) = 2\arcsin\left(\frac{t}{T}\right)$. Then we get

$$q = \left| \frac{\left(1 - e^{i\Delta T}\right)}{\Delta T} \right|^2 . \tag{3.38}$$

In order to achieve $q = 0$ one must have $T = \frac{2n\pi}{\Delta}$. We also set α constant and then the associated physical quantities for this protocol are

$$\delta_2(t) = 0\,, \;\; \Omega_{12}(t) = \frac{2ie^{i\alpha}}{T\sqrt{1 - \frac{t^2}{T^2}}}\,. \tag{3.39}$$

This is a type of π pulse. Unfortunately the Rabi frequency Ω_{12} diverges at $t = T$. To stop divergence we set

$$\theta(t) = \frac{\pi}{\arcsin(1-\epsilon)} \arcsin\left((1-\epsilon)\frac{t}{T}\right) \tag{3.40}$$

where $0 < \epsilon \ll 1$. By setting $\alpha = -\pi/2$ the corresponding Rabi frequency is real (i.e. $\Omega_I(t) = 0$) and

$$\Omega_R(t) = \frac{\pi(1-\epsilon)}{\arcsin(1-\epsilon)\,T\sqrt{1 - \frac{t^2(\epsilon-1)^2}{T^2}}}\,. \tag{3.41}$$

It also follows that $\delta_2 = 0$. The corresponding transition sensitivity with $\epsilon = 0.01$ is also plotted in figure 3.2(a) and (b). Note that this scheme converges for $\epsilon \to 1$ to a flat π pulse.

We also construct a scheme fulfilling Eqs. (3.34) which results in a low q value for large $|\Delta|$. For this scheme we set

$$\theta(t) = -\frac{3\pi t^4}{T^4} + \frac{4\pi t^3}{T^3} \tag{3.42}$$

and $\gamma = 0$. The corresponding transition probability can be seen in figure 3.2(a) and (b). The transition sensitivity for this scheme is lower than that of the flat π-pulse for $\Delta T > 10$, meaning it is less sensitive to unwanted transitions. If we set $\alpha = -\pi/2$ then we get $\Omega_R(t) = \frac{12\pi t^2(T-t)}{T^4}$, $\Omega_I = 0$ and $\delta_2 = 0$.

3.4.6 Numerically optimised scheme with $q = 0$

In the following we will present an example of a class of schemes which can be optimised to achieve a zero transition sensitivity for a fixed Δ. We use the ansatz

$$\begin{aligned} \gamma(t) &= c_0\theta(t)\,, \\ \theta(t) &= (\pi - c_1)t/T + c_1 t^3/T^3 \end{aligned} \tag{3.43}$$

where the parameters c_0 and c_1 were numerically calculated in order to minimise q for a given Δ. The result is shown in figure 3.2(a). As it can be seen, we can construct schemes which make q vanish for $|\Delta|T \geq 1.5$.

$\alpha(t)$ is chosen so that the Rabi frequency is real. The corresponding Rabi frequency Ω_R and the detuning δ_2 is shown in figure 3.4 for different values of ΔT.

Note that we pick the ansatz (3.43) because it is simple. It is still possible to optimise the ansatz further for example with the goal of minimising the maximal Rabi frequency. Moreover, the ansatz could be modified so that the Rabi frequency is zero at initial and final times.

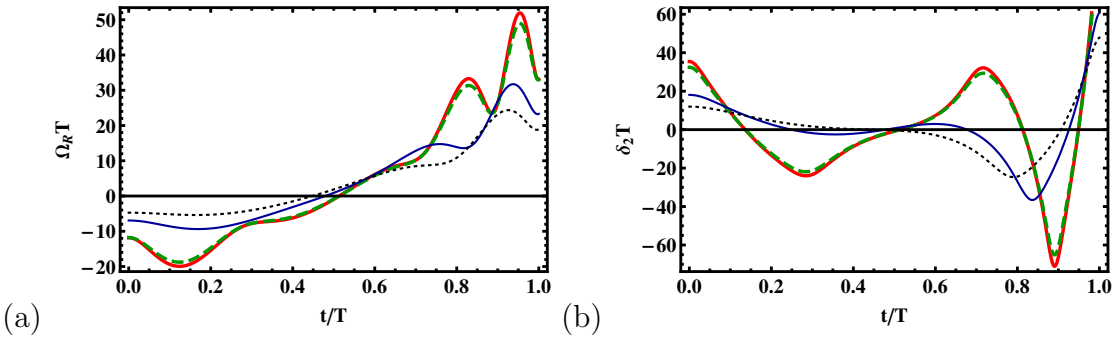


FIGURE 3.4: Physical potentials for the numerically optimised schemes in (3.43) versus time t. (a) Rabi frequency Ω_R; (b) detuning δ_2. $\Delta T = 0.2$ (red, thick, solid line), $\Delta T = 1.0$ (green, dashed line), $\Delta T = 2.0$ (blue, thin, solid line), $\Delta T = 3.0$ (black, dotted line).

3.4.7 Comparison of the transition probability

In the following we compare the effectiveness of the different schemes. To do this we compare the exact (numerically calculated) transition probability P_2 for the different schemes versus β for different values of Δ. This can be seen in figure 3.5. From this we see that the transition sensitivity is a good indicator of a stable scheme. This is however not the only useful quantity to know about a particular scheme. We also consider the area of the pulse $A \equiv \int_0^T dt \sqrt{\Omega_R^2 + \Omega_I^2}$ and its energy $E \equiv \hbar \int_0^T dt \ (\Omega_R^2 + \Omega_I^2)$. The values for the different schemes are shown in table 3.1. It can be seen that the numerically optimised schemes require a higher energy than three different variations of a π pulse.

For completeness we also include the following sinusoidal adiabatic scheme [162, 163] in our comparison:

$$\begin{aligned} \Omega_{12}(t) &= \Omega_0 \sin\left(\tfrac{\pi t}{T}\right) , \\ \delta_2(t) &= -\delta_0 \cos\left(\tfrac{\pi t}{T}\right) . \end{aligned} \tag{3.44}$$

We have chosen Ω_0 so that the adiabatic scheme requires the same energy as the numerically optimised scheme. In addition, we have also optimised the δ_0 to maximise the value of P_2 for the error-free case $\beta = 0$. The energy is high enough that the adiabatic scheme results in a nearly perfect population inversion in the

	$A[\pi]$	$E[\pi^2\hbar/T]$
Flat π pulse	1	1
Critical timing scheme($\epsilon = 0.01$), (3.41)	1	1.28
Large Δ scheme, (3.42)	1	$\frac{48}{35}$
Numerically optimised scheme, (3.43)		
$\Delta T = 1.0$ ($c_0 = 1.376, c_1 = 14.927$)	4.79	36.56
$\Delta T = 3.0$ ($c_0 = 1.266, c_1 = 7.873$)	2.49	10.51
Adiabatic Scheme	$2T\Omega_0\pi^{-2}$	$\frac{1}{2}\pi^{-2}T^2\Omega_0^2$
$\Delta T = 1.0$	5.44	36.56
$\Delta T = 3.0$	2.92	10.51

TABLE 3.1: Pulse area A and energy E for different protocols.

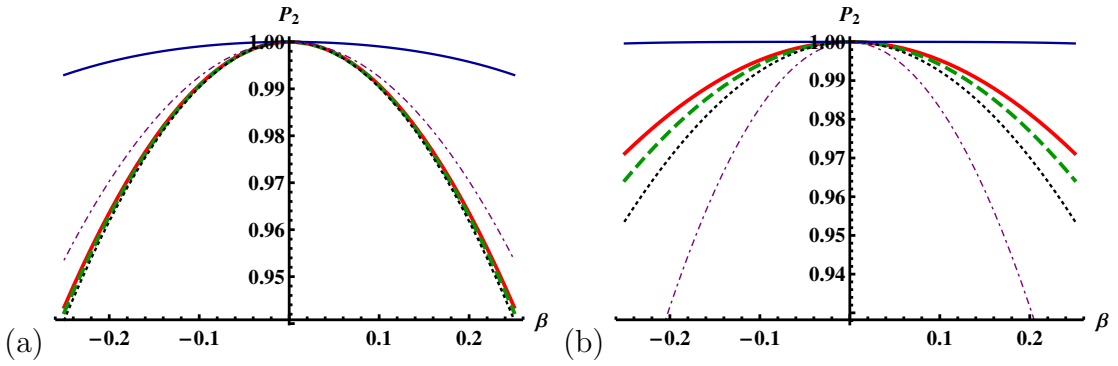


FIGURE 3.5: Transition probability P_2 versus perturbation strength β for different schemes: reference case of a flat π pulse (green, thick, dashed line); other π pulse given by (3.41) (red, thick, solid line); scheme given by (3.42) (black, thin, dashed line); scheme in (3.43) with numerically optimised parameters c_0 and c_1 (blue, thin, solid line); adiabatic scheme (purple, thin, dot-dashed line); (a) $\Delta T = 1.0$, (b) $\Delta T = 3.0$.

error-free case. Nevertheless, the numerically optimised scheme is less sensitive to unwanted transitions, i.e. the numerically optimised scheme results in a higher P_2 for non-zero β.

3.5 Invariant-based shortcuts in three-level systems

In this section, we will review the derivation of invariant-based STA in three-level systems [78] (for an application see for example [94]). We use a different notation than [78] to underline the connection between the two and three-level Hamiltonians in (3.1) and (3.45) respectively (see for example [164]). In addition, we will introduce different boundary conditions for the ancillary functions than those used in [78].

We assume our three-level system has a Hamiltonian of the form

$$H_{3L}(t) = \frac{\hbar}{2}\begin{pmatrix} 0 & \Omega_{12}(t) & 0 \\ \Omega_{12}(t) & 0 & \Omega_{23}(t) \\ 0 & \Omega_{23}(t) & 0 \end{pmatrix} \tag{3.45}$$

where Ω_{12} and Ω_{23} are real. We also assume that $\Omega_{12}(t) = \Omega_{23}(t) = 0$ for $t < 0$ and $t > T$.

This could for example describe a three-level atom with two on resonance lasers (one coupling states $|1\rangle$ and $|2\rangle$ and the other coupling states $|2\rangle$ and $|3\rangle$). The Lewis-Riesenfeld invariant for this Hamiltonian is

$$I(t) = \frac{\hbar}{2}\begin{pmatrix} 0 & -\sin\theta\sin\alpha & -i\cos\theta \\ -\sin\theta\sin\alpha & 0 & -\sin\theta\cos\alpha \\ i\cos\theta & -\sin\theta\cos\alpha & 0 \end{pmatrix}. \tag{3.46}$$

The ancillary functions $\alpha(t)$ and $\theta(t)$ satisfy

$$\dot{\theta} = \frac{1}{2}\left(\Omega_{12}\cos\alpha - \Omega_{23}\sin\alpha\right), \tag{3.47}$$

$$\dot{\alpha} = -\frac{1}{2}\cot\theta\left(\Omega_{23}\cos\alpha + \Omega_{12}\sin\alpha\right). \tag{3.48}$$

Note the similarity with Eqs. (3.5) and (3.6). This is due to the aforementioned connection between the two- and three-level Hamiltonians. The eigenstates of $I(t)$

are

$$|\phi_0(t)\rangle = \begin{pmatrix} -\sin\theta\cos\alpha \\ -i\,\cos\theta \\ \sin\theta\sin\alpha \end{pmatrix} \text{ and } |\phi_\pm(t)\rangle = \frac{1}{\sqrt{2}} \begin{pmatrix} \cos\theta\cos\alpha \pm i\,\sin\alpha \\ -i\,\sin\theta \\ -\cos\theta\sin\alpha \pm i\,\cos\alpha \end{pmatrix} \quad (3.49)$$

with eigenvalues $\lambda_0 = 0$ and $\lambda_\pm = \pm 1$ i.e. $I(t)\,|\phi_n(t)\rangle = \lambda_n\,|\phi_n(t)\rangle$ and the label $n = 0, \pm$. The Lewis-Riesenfeld phases $\kappa_n(t)$ are $\kappa_0 = 0$ and

$$\kappa_\pm = \mp \int_0^t dt' \left(\dot{\alpha}\cos\theta - \frac{1}{2}\left(\Omega_{12}\sin\alpha + \Omega_{23}\cos\alpha\right)\sin\theta \right). \quad (3.50)$$

A solution of the time-dependent Schrödinger equation with the Hamiltonian (3.45) is now $|\Psi(t)\rangle = |\phi_0(t)\rangle$. In order for the solution $|\Psi(t)\rangle$ to evolve from the initial state $|1\rangle$ to the final state $|3\rangle$ we must impose the following boundary conditions on α and θ:

$$\theta(0) = -\frac{\pi}{2}\,,\ \theta(T) = \frac{\pi}{2}\,,\ \alpha(0) = 0\,,\ \alpha(T) = \frac{\pi}{2}\,. \quad (3.51)$$

One could impose the following additional boundary conditions in order to make the Rabi frequencies have a finite limit at the initial and final times

$$\dot{\alpha}(0) = 0\,,\ \dot{\alpha}(T) = 0\,,\ \dot{\theta}(0) \neq 0\,,\ \dot{\theta}(T) \neq 0\,. \quad (3.52)$$

Note that the boundary conditions given by Eqs. (3.51) and (3.52) are an alternative choice to the ones imposed in [78].

Using Eqs. (3.47) and (3.48) we can calculate the Rabi frequencies

$$\Omega_{12}(t) = 2\left(-\dot{\alpha}\tan\theta\sin\alpha + \dot{\theta}\cos\alpha\right), \quad (3.53)$$

$$\Omega_{23}(t) = -2\left(\dot{\alpha}\tan\theta\cos\alpha + \dot{\theta}\sin\alpha\right). \quad (3.54)$$

If the functions α and θ fulfil Eqs. (3.51) and (3.52), then the corresponding Rabi frequencies will lead to full population inversion $|1\rangle \to |3\rangle$.

3.6 Unwanted transitions in three-level systems

3.6.1 Model

Now we assume that there is an unwanted coupling to a fourth level as shown in figure 3.1(c). Analogous to section 3.4, we assume that the laser coupling levels $|2\rangle$ and $|3\rangle$ also unintentionally couples levels $|2\rangle$ and $|4\rangle$ as well. Hence we assume for the Rabi frequency

$$\Omega_{24}(t) = \beta e^{i\nu}\Omega_{23}(t) \tag{3.55}$$

where $\beta, \nu \in \mathbb{R}$ are unknown constants and $\beta \ll 1$. The Hamiltonian for this four-level system is given by

$$H(t) = \frac{\hbar}{2}\begin{pmatrix} 0 & \Omega_{12} & 0 & 0 \\ \Omega_{12} & 0 & \Omega_{23} & \beta e^{-i\nu}\Omega_{23} \\ 0 & \Omega_{23} & 0 & 0 \\ 0 & \beta e^{i\nu}\Omega_{23} & 0 & -2\Delta \end{pmatrix} \tag{3.56}$$

where $\Delta = \omega_3 - \omega_4$ and $\hbar\omega_j$ is the energy of state $|j\rangle$. As in the previous case, one can redefine the state $|4\rangle$ to remove the phase. Hence we set $\nu = 0$ in the following.

Using the formalism presented in Sect. 3.5, we can construct schemes which result in full population inversion in the case of no unwanted transitions. Again, there is a lot of freedom in choosing the ancillary functions and the goal will be to find the schemes which are stable concerning these unwanted transitions.

3.6.2 Transition sensitivity

We once again regard this unwanted transition as a perturbation. To treat it as such we write the Hamiltonian as

$$H(t) = H_0(t) + \beta V(t) \tag{3.57}$$

where $H_0(t) = H(t)|_{\beta=0}$ and

$$V(t) = \frac{\hbar}{2}\begin{pmatrix} 0 & 0 & 0 & 0 \\ 0 & 0 & 0 & \Omega_{23} \\ 0 & 0 & 0 & 0 \\ 0 & \Omega_{23} & 0 & 0 \end{pmatrix}. \tag{3.58}$$

If $\beta = 0$ then the time-dependent Schrödinger equation for $H(t)$ has the following set of orthonormal solutions:

$$\begin{aligned}
|\psi_0(t)\rangle &= \begin{pmatrix} -\sin\theta\cos\alpha \\ -i\,\cos\theta \\ \sin\theta\sin\alpha \\ 0 \end{pmatrix} e^{i\kappa_0}, \\
|\psi_1(t)\rangle &= \frac{1}{\sqrt{2}}\begin{pmatrix} \cos\theta\cos\alpha + i\,\sin\alpha \\ -i\,\sin\theta \\ -\cos\theta\sin\alpha + i\,\cos\alpha \\ 0 \end{pmatrix} e^{i\kappa_+}, \\
|\psi_2(t)\rangle &= \frac{1}{\sqrt{2}}\begin{pmatrix} \cos\theta\cos\alpha - i\,\sin\alpha \\ -i\,\sin\theta \\ -\cos\theta\sin\alpha - i\,\cos\alpha \\ 0 \end{pmatrix} e^{i\kappa_-}, \\
|\psi_3(t)\rangle &= \begin{pmatrix} 0 \\ 0 \\ 0 \\ e^{i\Delta t} \end{pmatrix}.
\end{aligned} \tag{3.59}$$

Using time-dependent perturbation theory similar to section 3.4.2, we get for the probability P_3 to end in the state $|3\rangle$ at time $t = T$ that

$$P_3 = 1 - \beta^2 Q + \mathcal{O}\left(\beta^4\right) . \tag{3.60}$$

where

$$Q = \left| \int_0^T dt\, e^{i\Delta t} \left(\dot{\alpha} \sin\theta \cos\alpha + \dot{\theta} \cos\theta \sin\alpha \right) \right|^2 = \left| \int_0^T dt\, e^{i\Delta t} \frac{d}{dt} \left(\sin\theta \sin\alpha \right) \right|^2 . \tag{3.61}$$

Similar to Sect. 3.4, the Q quantifies how sensitive a given protocol is concerning the unwanted transition to level $|4\rangle$. As before we will call Q *transition sensitivity* in the following and our goal will be to determine protocols or schemes which would minimise Q.

3.6.3 General properties of the transition sensitivity

We start by examining some general properties of the transition sensitivity Q given by (3.61) by noting that Q is independent of the sign of Δ. By taking into account the boundary conditions for $\theta(t)$ and $\alpha(t)$ we find that

$$Q = 1 \text{ if } \Delta = 0 . \tag{3.62}$$

Similar to Sect. 3.4.3, we get by partial integration

$$Q = |1 - i\Delta N|^2 = 1 + 2\Delta \mathrm{Im} N + \Delta^2 |N|^2 \tag{3.63}$$

where

$$N = \int_0^T dt\, e^{i\Delta(t-T)} \sin\theta \sin\alpha . \tag{3.64}$$

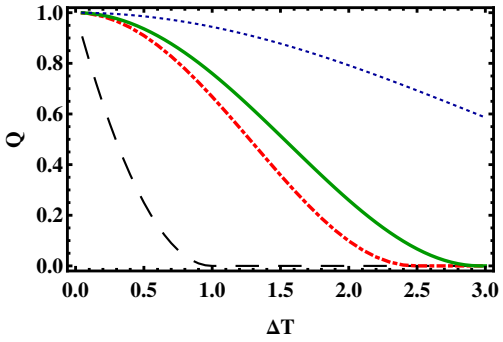


FIGURE 3.6: Transition sensitivity Q versus ΔT for different schemes; reference example($\epsilon = 0.002$) from [78] (blue, thin, dotted line); numerical scheme 1 given by (3.70) (red, thick, dot-dashed line); numerical scheme 2 given by (3.71) (green, solid line); lower bound for Q as in (3.66) (black, dashed line).

Therefore $Q \geq (1 + \Delta \mathrm{Im}\,(N))^2$ and

$$\begin{aligned} |\mathrm{Im}\,(N)| &\leq \left| \int_0^T dt\, \sin\left(\Delta\,(t-T)\right) \sin\theta \sin\alpha \right| \\ &\leq \int_0^T dt\, \left|\sin\left(\Delta\,(t-T)\right) \sin\theta \sin\alpha\right| \leq T\,. \end{aligned} \tag{3.65}$$

Let's assume $|\Delta|\,T < 1$ then as before we get

$$Q \geq (1 - |\Delta||\mathrm{Im}(N)|)^2 \geq (1 - |\Delta|T)^2\,. \tag{3.66}$$

So $Q > 0$ if $|\Delta|\,T < 1$, i.e. a necessary condition for $Q = 0$ is $T \geq \frac{1}{|\Delta|}$.

Using similar arguments to the ones in Sect. 3.4.3, we see that in this case as well there can be no Δ-independent scheme with $Q = 0$ for all $|\Delta| > 1/T$. Moreover, an approximation of Q in the case of $|\Delta|T \gg 1$ can be derived in a similar way as in the previously mentioned section. So we get for $|\Delta|T \gg 1$ that

$$Q = \frac{1}{\Delta^2}\dot{\alpha}(0)^2 + ... \tag{3.67}$$

taking into account the boundary conditions.

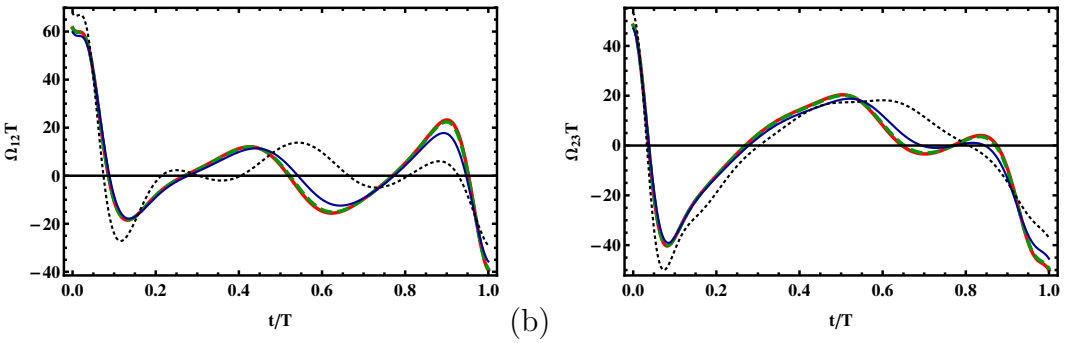


FIGURE 3.7: Rabi frequencies for the numerically optimised scheme 1 in (3.70) versus time t; (a) Rabi frequency Ω_{12}; (b)Rabi frequency Ω_{23}; $\Delta T = 0.2$ (red, thick, solid line), $\Delta T = 1.0$ (green, dashed line), $\Delta T = 2.0$ (blue, thin, solid line), $\Delta T = 3.0$ (black, dotted line).

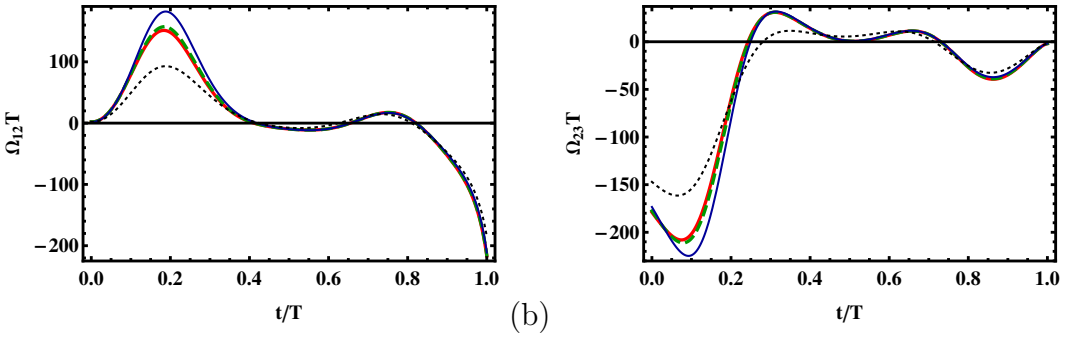


FIGURE 3.8: Rabi frequencies for the numerically optimised scheme 2 in (3.71) versus time t; (a) Rabi frequency Ω_{12}; (b)Rabi frequency Ω_{23}; $\Delta T = 0.2$ (red, thick, solid line), $\Delta T = 1.0$ (green, dashed line), $\Delta T = 2.0$ (blue, thin, solid line), $\Delta T = 3.0$ (black, dotted line).

3.6.4 Example of schemes

As a reference case we consider one of the protocols given in [78]. In this protocol, the following ancillary functions are used

$$\theta(t) = \epsilon - \frac{\pi}{2}, \alpha(t) = \frac{\pi t}{2T} \tag{3.68}$$

where $0 < \epsilon \ll 1$ and the only difference in boundary conditions being that now $\theta(T) = -\frac{\pi}{2}$. It should be noted that this protocol does not have perfect population transfer since the boundary conditions are not exactly fulfilled for a non-zero ϵ. In [78] $\epsilon = 0.002$ was deemed sufficient. This protocol has the following Rabi

frequencies:

$$\begin{aligned}\Omega_{12}(t) &= \frac{\pi}{T}\cot\epsilon\sin\left(\frac{\pi t}{2T}\right),\\ \Omega_{23}(t) &= \frac{\pi}{T}\cot\epsilon\cos\left(\frac{\pi t}{2T}\right).\end{aligned} \tag{3.69}$$

The transition sensitivity for this scheme is shown in figure 3.6. Here we note that the derivation of the transition sensitivity is based on exact population transfer in the error free case. Hence it is not strictly correct to consider the transition sensitivity for this protocol. However for the purposes of comparison we include it.

In the following we provide two examples of numerically optimised schemes leading to zero transition sensitivity for some range of Δ. For the first scheme we use the ansatz

$$\begin{aligned}\theta(t) &= -\frac{\pi}{2}+(\pi-c_0-c_1)\frac{t}{T}+c_0\left(\frac{t}{T}\right)^2+c_1\left(\frac{t}{T}\right)^3,\\ \alpha(t) &= \frac{\pi}{4}\sin(\theta(t))+\frac{\pi}{4}\end{aligned} \tag{3.70}$$

where the parameters c_0 and c_1 were numerically calculated in order to minimise Q for a given Δ. Note that this ansatz automatically avoids any divergences of the corresponding physical potentials for $0 \leq t \leq T$. The resulting transition sensitivity Q is shown in figure 3.6. As it can be seen, we can construct schemes which make Q vanish for $|\Delta|T \geq 2.5$. The corresponding Rabi frequencies Ω_{12} and Ω_{23} are shown in figure 3.7 for different values of ΔT.

Another example of a scheme is the following

$$\begin{aligned}\theta(t) &= -\frac{\pi}{2}-\frac{8(\pi-2d_0)t^4}{T^4}+\frac{2t^3(-16d_0+1+7\pi)}{T^3}-\frac{t^2(-16d_0+3+5\pi)}{T^2}+\frac{t}{T},\\ \alpha(t) &= \frac{1}{2}(2\pi d_1+3\pi)\frac{t^2}{T^2}+\left(\frac{1}{2}(-2\pi d_1-3\pi)+\frac{3\pi}{2}\right)\frac{t}{T}+d_1\sin\left(\frac{\pi t}{T}\right)-\pi\frac{t^3}{T^3}\end{aligned} \tag{3.71}$$

where the parameters d_0 and $d_1$were numerically calculated to minimise Q for a

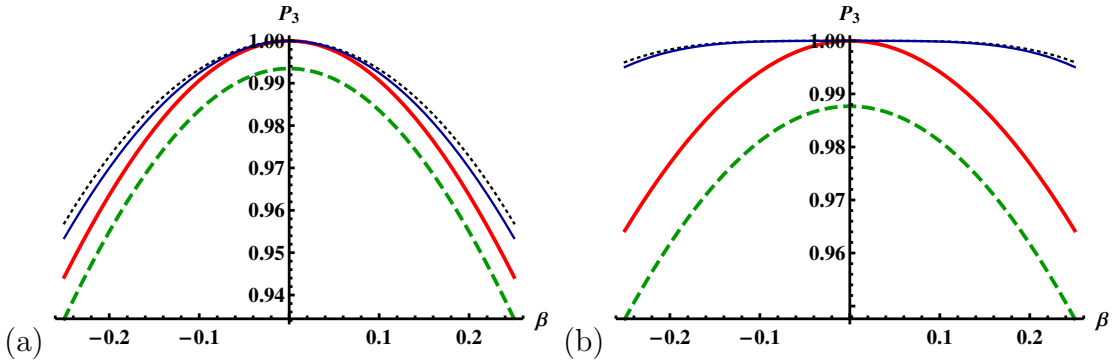


FIGURE 3.9: Transition probability P_3 versus perturbation strength β for different schemes: reference example($\epsilon = 0.002$) from [78] (red, thick, solid line); numerical scheme 1 given by (3.70) (black, dotted line); numerical scheme 2 given by (3.71) (blue, thin, solid line); adiabatic scheme (green, thick, dashed line); (a) $\Delta T = 1.0$, (b) $\Delta T = 3.0$.

given Δ. d_0 was restricted to the range $0.55 \leq d_0 \leq 2.5$ to avoid divergence of the Rabi frequencies for all $0 \leq t \leq T$. The transition sensitivity Q for this scheme is shown in figure 3.6. It achieves $Q = 0$ at $\Delta T = 3$. The corresponding Rabi frequencies are shown in figure 3.8.

3.6.5 Comparison of the transition probability

In order to compare the schemes we once again look at the exact (numerically calculated) transition probability P_3 as a function of β as in figure 3.9. We compare the scheme of the schemes proposed in [78] as a reference scheme, the numerical scheme 1 given by (3.70) and the numerical scheme 2 given by (3.71). Once again we see that the transition sensitivity is a good indicator of a stable scheme. We also consider the area of the pulse and its energy which in this case is defined as $A \equiv \int_0^T dt \sqrt{\Omega_{12}^2 + \Omega_{23}^2}$ and $E \equiv \hbar \int_0^T dt \, (\Omega_{12}^2 + \Omega_{23}^2)$ respectively. These values are shown for each scheme in table 3.2.

	$A[\pi]$	$E[\pi^2\hbar/T]$
Scheme of [78] ($\epsilon = 0.002$)	500.00	249999
Numerical Scheme 1, (3.70)		
$\Delta T = 1.0$ ($c_0 = -76.546, c_1 = 49.040$)	6.71	70.29
$\Delta T = 3.0$ ($c_0 = -76.735, c_1 = 46.054$)	6.61	73.61
Numerical Scheme 2, (3.71)		
$\Delta T = 1.0$ ($d_0 = 0.794, d_1 = -15.633$)	24.34	1171.7
$\Delta T = 3.0$ ($d_0 = 0.852, d_1 = -13.204$)	18.65	663.17
Adiabatic Scheme, (3.73)	$\Omega_0 T \pi^{-1}$	$\Omega_0^2 T^2 \pi^{-2}$
$\Delta T = 1.0$	8.38	70.29
$\Delta T = 3.0$	8.58	73.61

TABLE 3.2: Pulse area A and energy E for different protocols.

For completeness we also include the following adiabatic STIRAP-like scheme in our comparison [113]:

$$\Omega_{12} = \Omega_0 \sin\left(\frac{\pi t}{2T}\right), \tag{3.72}$$

$$\Omega_{23} = \Omega_0 \cos\left(\frac{\pi t}{2T}\right). \tag{3.73}$$

Ω_0 was chosen so that the adiabatic scheme has the same energy as the numerical scheme 1.

Both numerically-optimised schemes result in the largest P_3 in figure 3.9(a) if $\beta \neq 0$ for $\Delta T = 1.0$. If $\Delta T = 3.0$, see figure 3.9(b), then both numerical-optimised schemes result in nearly full population transfer even in the case of $-0.1 < \beta < 0.1$. It can be seen that a full population transfer is not achieved in both cases by this adiabatic scheme for $\beta = 0$.

3.7 Conclusion

In this chapter, we have developed STA schemes in two- and three-level quantum systems which lead to nearly perfect population inversion even in the presence of an additional unwanted and uncontrollable transition. For the two-level case as well as for the three-level case, this has been based on the definition of a

transition sensitivity which quantifies how sensitive a given scheme is concerning these unwanted couplings to another level. We have provided examples of shortcut schemes leading to a zero transition sensitivity (and hence almost full population inversion) in certain regimes.

The developed shortcut schemes can easily be adapted to other quantum settings. Additionally, the proposed schemes may be simpler to implement experimentally than previous methods which require a control of the phase of the unwanted transition. Hence, the results of this chapter could be important in quantum information processing or other applications which require fast quantum control with high fidelity.

The approach of this chapter could be even further generalised; one could construct different shortcut schemes fulfilling even further constraints apart from vanishing transition sensitivity similar to [158]. This work could also be generalised to different level structures of the unwanted transitions or to multiple unwanted transition channels. In the latter case, one might expect to find that the unwanted transition with lowest detuning would dominate.

Chapter 4

Spatial non-adiabatic passage using geometric phases

4.1 Overview

We introduce a set of non-adiabatic protocols for spatial state preparation, which yield the same fidelity as their adiabatic counterparts, but on fast timescales. In particular, we consider a charged particle in a system of tunnel-coupled quantum wells, where the presence of a magnetic field can induce a geometric phase during the tunnelling processes. We show that this leads to the appearance of complex tunnelling frequencies and allows for the implementation of spatial non-adiabatic passage. We demonstrate the ability of such a system to transport a particle between two different wells and to generate a delocalised superposition between the three traps with high fidelity in short times.

This chapter is based on the following publication:
A. Benseny, A. Kiely, Y. Zhang, T. Busch and A. Ruschhaupt,
Spatial non-adiabatic passage using geometric phases,
ArXiv:1611.02398 (submitted).
I derived the phase induced by the magnetic field, the invariant for the 3-level Hamiltonian and the associated schemes. I also worked out the mapping of the

continuous case to the three-level model (in Appendix B.1) and performed the numerical calculations associated with this. Albert Benseny performed the simulations of the continuous model and made the figures. Yongping Zhang contributed in the initial discussions. All authors contributed to the writing of the manuscript.

4.2 Introduction

Adiabatic techniques are widely used for the manipulation of quantum states. They typically yield high fidelities and possess a high degree of robustness. One paradigmatic example is stimulated Raman adiabatic passage (STIRAP) in three-level atomic systems [113]. STIRAP-like techniques have been successfully applied to a wide range of problems, and in particular, to the control of the centre-of-mass states of atoms in microtraps. This spatial analogue of STIRAP is called spatial adiabatic passage (SAP) and it relies on coupling different spatial eigenstates via a controllable tunnelling interaction [115]. It has been examined for cold atoms in optical traps [165–168] and for electrons trapped in quantum dots [169, 170]. The ability to control the spatial degrees of freedom of trapped particles is an important goal for using these systems in future quantum technologies such as atomtronics [171] and quantum information processing [172]. SAP has also been suggested for a variety of tasks such as interferometry [167], creating angular momentum [168], and velocity filtering [173]. It is also applicable to the classical optics of coupled waveguides [174].

However, the high fidelity and robustness of adiabatic techniques comes at the expense of requiring long operation times. This is problematic as the system will have a long time to interact with an environment leading to losses or decoherence. To avoid this problem, we will show how one can speed-up processes that control the centre-of-mass state of quantum particles and introduce a new class of techniques which we refer to as spatial non-adiabatic passage (SNAP). The underlying foundation for these are shortcuts to adiabaticity (STA) techniques, which have been developed to achieve high fidelities in much shorter total times, for a

review see [21, 157]. Moreover, shortcuts are known to provide the freedom to optimise against undesirable effects such as noise, systematic errors or transitions to unwanted levels [79, 157, 175].

Implementing the STA techniques for spatial control requires complex tunnelling frequencies. However, tunnelling frequencies are typically real. To solve this, we show that the application of a magnetic field to a triple well system containing a single charged particle (which could correspond to a quantum dot system [176–179]) can achieve complex tunnelling frequencies through the addition of a geometric phase. This then allows one to implement a counter-diabatic driving term [21, 77, 125, 126, 157] or, more generally, to design dynamics using Lewis–Riesenfeld invariants [116].

The chapter is structured as follows. In the next section, we present the model we examine, namely a charged particle in a triple well ring system with a magnetic field in the centre. In section 4.4, we introduce the spatial adiabatic passage technique in a three-level system and show that making one of the couplings imaginary allows the implementation of transitionless quantum driving. We then show, in section 4.4.3, how to create inverse-engineering protocols in this system using Lewis–Riesenfeld invariants. Results for two such protocols, namely transport and generation of a three-trap superposition, are given in section 4.5. Section 4.6 presents a more realistic one-dimensional continuum model for the system, where the same schemes are implemented. Finally, in section 4.7, we review and summarise the results of this chapter.

4.3 System model

We consider a charged particle trapped in a system of three localised potentials, between which the tunnel coupling can be changed in a time-dependent manner. Such a model could, for example, correspond to an electron trapped in an arrangement of quantum dots, where gate electrodes can be used to change the

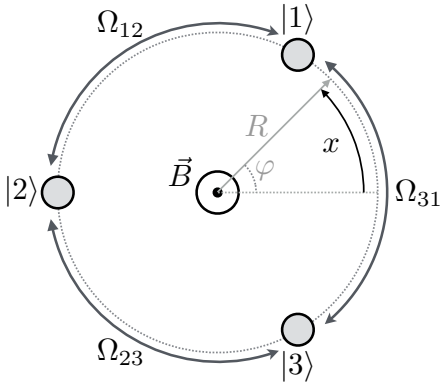


FIGURE 4.1: Diagram of the system consisting of three coupled quantum wells and a localised magnetic field in the centre. The basis states and the couplings strengths used in the three-level approximation are indicated. The coordinate system for the continuous model in section 4.6 is also shown. The distance between two traps along the ring is defined as l, so that the total circumference of the ring is $3l$.

tunnelling between different traps [180], or an ion trapped in an array of micro-surface traps [181], where the distance between traps can be controlled. In order to have coupling between all traps, they are assumed to be arranged along a ring and a magnetic field exists perpendicular to the plane containing the traps, see figure 4.1. The particle will initially be located in one of the traps and we will show how to design SNAP protocols where a specific final state can be reached within a finite time and with high fidelity.

Let us start by considering the single-particle Schrödinger equation

$$i\hbar\frac{\partial\psi}{\partial t} = \frac{1}{2m}\left(-i\hbar\nabla - q\vec{A}\right)^2\psi + V\psi, \tag{4.1}$$

where m and q are the mass and charge of the particle, respectively, and V corresponds to the potential describing the trapping geometry. We assume that the vector potential is originating from an idealised point-like and infinitely long solenoid at the origin (creating a magnetic flux Φ_B) and it is therefore given by $\vec{A} = \frac{\Phi_B}{2\pi r}\hat{e}_\varphi$ (for $\vec{r} \neq 0$). Here r, φ, z are cylindrical coordinates and $\hat{e}_\varphi$ is a unit vector in the φ direction.

At low energies such a system can be approximated by a three-level model (similar

to the example presented in section 2.3.1), where each basis state, $|j\rangle$, corresponds to the localised ground state in one of the trapping potentials (see figure 4.1). These states are isolated when a high barrier between them exists, but when the barrier is lowered the tunnelling rate Ω_{jk} between states $|j\rangle$ and $|k\rangle$ becomes significant.

The presence of the magnetic field leads to the particle acquiring an Aharonov–Bohm phase [182] whenever it moves (tunnels) between two different positions (traps). This phase is given by $\phi_{j,k} = \frac{q}{\hbar}\int_{\vec{r}_j}^{\vec{r}_k} \vec{A}(\vec{r}) \cdot d\vec{r}$, where $\vec{r}_j$ is the position of the j-th trap, and for consistency, we always chose the direction of the path of the integration to be anti-clockwise around the pole of the vector potential (at $\vec{r} = 0$). The effects of this phase on the tunnelling rates is given through the Peierls phase factors [183], $\exp(i\phi_{j,k})$, and the Hamiltonian for the three-level system can be written as

$$H = -\frac{\hbar}{2}\begin{pmatrix} 0 & \Omega_{12}e^{i\phi_{1,2}} & \Omega_{31}e^{-i\phi_{3,1}} \\ \Omega_{12}e^{-i\phi_{1,2}} & 0 & \Omega_{23}e^{i\phi_{2,3}} \\ \Omega_{31}e^{i\phi_{3,1}} & \Omega_{23}e^{-i\phi_{2,3}} & 0 \end{pmatrix}. \tag{4.2}$$

Here the Ω_{jk} are the coupling coefficients in the absence of any vector potential. The total phase around a closed path containing the three traps is then given by

$$\Phi \equiv \phi_{1,2} + \phi_{2,3} + \phi_{3,1} = \frac{q}{\hbar}\oint \vec{A}(\vec{r}) \cdot d\vec{l} = \frac{q}{\hbar}\Phi_B, \tag{4.3}$$

and is non-zero due to the pole of the vector potential $\vec{A}$ at the origin.

To simplify the Hamiltonian (4.2) one can use the following unitary transformation, which only employs local phases,

$$U = \begin{pmatrix} 1 & 0 & 0 \\ 0 & e^{-i\phi_{1,2}} & 0 \\ 0 & 0 & e^{-i(\phi_{1,2}+\phi_{2,3})} \end{pmatrix}, \tag{4.4}$$

and transforms the Hamiltonian as

$$H \to U^\dagger H U = -\frac{\hbar}{2}\begin{pmatrix} 0 & \Omega_{12} & \Omega_{31}e^{-i\Phi} \\ \Omega_{12} & 0 & \Omega_{23} \\ \Omega_{31}e^{i\Phi} & \Omega_{23} & 0 \end{pmatrix}, \tag{4.5}$$

so that two of the tunnelling rates become real-valued.

A case of particular interest is when $\Phi = \pi/2$, i.e., when the magnetic flux is $\Phi_B = \pi\hbar/2q$. In this case the Hamiltonian becomes

$$H = -\frac{\hbar}{2}\Big(\Omega_{12}K_1 + \Omega_{23}K_2 + \Omega_{31}K_3\Big), \tag{4.6}$$

where each K_j is a spin 1 angular momentum operator defined as

$$K_1 = \begin{pmatrix} 0 & 1 & 0 \\ 1 & 0 & 0 \\ 0 & 0 & 0 \end{pmatrix}, \; K_2 = \begin{pmatrix} 0 & 0 & 0 \\ 0 & 0 & 1 \\ 0 & 1 & 0 \end{pmatrix}, \; K_3 = \begin{pmatrix} 0 & 0 & -i \\ 0 & 0 & 0 \\ i & 0 & 0 \end{pmatrix}, \tag{4.7}$$

satisfying $[K_j, K_k] = i\epsilon_{jkl}K_l$ and ϵ_{jkl} is the Levi-Civita symbol [184]. This means that the tunnel coupling between $|3\rangle$ and $|1\rangle$ becomes purely imaginary. We will show in the next section that this allows for the implementation of SNAP processes by either applying a transitionless quantum driving protocol or by using Lewis–Riesenfeld invariants.

4.4 SNAP in the three-level approximation

4.4.1 Adiabatic methods

A series of spatial adiabatic passage (SAP) techniques have been developed in recent years, which allows one to manipulate and control the external degrees of freedom of quantum particles in localised potentials with high fidelity [115]. The standard SAP protocol for the transport of a single particle in a triple well

system [165, 169] is the spatial analogue of the quantum-optical STIRAP technique [113]. It involves three linearly arranged, degenerate trapping states, $|j\rangle$ with $j = 1$, 2 and 3, that can be coupled through tunnelling by either changing the distance between the traps or lowering the potential barrier between them. The system in the three-level approximation is described by the Hamiltonian

$$H_0 = -\frac{\hbar}{2}\left(\Omega_{12}K_1 + \Omega_{23}K_2\right), \tag{4.8}$$

which has a zero-energy eigenstate of the form

$$|\lambda_0\rangle = \cos\theta|1\rangle - \sin\theta|3\rangle \quad \text{with} \quad \tan\theta = \Omega_{12}/\Omega_{23}. \tag{4.9}$$

This state is often called the *dark state* and SAP consists of adiabatically following $|\lambda_0\rangle$ from $|1\rangle$ (at $t = 0$) to $-|3\rangle$ (at a final time $t = T$), effectively transporting the particle between the outer traps one and three. This corresponds to changing θ from 0 ($\Omega_{23} \gg \Omega_{12}$) to $\pi/2$ ($\Omega_{23} \ll \Omega_{12}$). Hence in the case of ideal adiabatic following, trap two (located in the middle) is never populated.

4.4.2 Transitionless quantum driving

The main drawback of SAP is that it requires the process to be carried out adiabatically and therefore slowly compared to the energy gap [115]. If this requirement is not met, unwanted excitations will lead to imperfect transport. One way to specifically cancel possible diabatic transitions in STIRAP was discussed in [185] and a general approach for recovering adiabatic dynamics in a non-adiabatic regime is to use shortcuts to adiabaticity, such as transitionless quantum driving [77, 125, 126]. Recall from section 2.2.3, that this technique consists of adding a counter-diabatic term to the original Hamiltonian, whose particular form is given as

$$H_{\mathrm{CD}} = i\hbar\sum_n \Big(|\partial_t\lambda_n\rangle\langle\lambda_n| - \langle\lambda_n|\partial_t\lambda_n\rangle|\lambda_n\rangle\langle\lambda_n|\Big), \tag{4.10}$$

where the $|\lambda_n\rangle$ are the eigenstates of H_0. For the reference Hamiltonian in (4.8) this gives [77]

$$H_{\mathrm{CD}} = -\frac{\hbar\Omega_{31}(t)}{2}K_3, \quad \text{with} \quad \Omega_{31}(t) = 2\dot{\theta}(t) = 2\left(\frac{\Omega_{23}\dot{\Omega}_{12} - \Omega_{12}\dot{\Omega}_{23}}{\Omega_{12}^2 + \Omega_{23}^2}\right). \quad (4.11)$$

We will see in section 4.5.1 how this exact same scheme can also be obtained using Lewis–Riesenfeld invariants.

Shortcuts to adiabaticity have been studied in the context of STIRAP [77, 105], i.e., population transfer between internal levels. Its spatial analogue is more challenging as it requires that the additional tunnelling coupling between sites one and three is imaginary (see the definition of K_3 in (4.7)). However, the system we have presented here is ideal for this, as the system Hamiltonian (4.6) is already equal to the total Hamiltonian $H_0 + H_{\mathrm{CD}}$. Other methods to implement the imaginary coupling could be, for example, the use of artificial magnetic fields [186] or angular momentum states [187].

A heuristic but not rigorous explanation of why the coupling needs to be imaginary can be obtained by examining the two "paths" the particle can take to move from trap one to trap three. The first is via SAP and leads to $|1\rangle \to -|3\rangle$ whereas the second is via the direct coupling the shortcut introduces, which leads to $|1\rangle \to ie^{i\Phi}|3\rangle$. One can then immediately see that for constructive interference of these two terms the phase needs to have the value $\Phi = \pi/2$, which corresponds to the required imaginary coupling between states $|1\rangle$ and $|3\rangle$. It is also interesting to note that the coupling between traps one and three in the shortcut has the form of a π-pulse

$$\int_0^T \Omega_{31}(t)dt = 2\int_0^T \dot{\theta}(t)dt = 2\left[\theta(T) - \theta(0)\right] = \pi. \quad (4.12)$$

4.4.3 Invariant-based inverse engineering

Recall from section 2.2.2, that another method of designing shortcuts to adiabaticity is by means of inverse-engineering using Lewis–Riesenfeld invariants [65, 116].

In this section we will briefly review these methods and then apply them to our particular system to both transport the particle and create a superposition between the three wells.

A Lewis–Riesenfeld invariant for a Hamiltonian $H(t)$ is a Hermitian operator $I(t)$ satisfying [116]

$$\frac{\partial I}{\partial t} + \frac{i}{\hbar}[H, I] = 0. \tag{4.13}$$

The idea behind inverse engineering using Lewis–Riesenfeld invariants is not to follow an instantaneous eigenstate of the $H(t)$ as one would in the adiabatic case, but rather follow an eigenstate of $I(t)$ (up to the Lewis–Riesenfeld phase). To guarantee that the eigenstates coincide at the beginning and the end of the process, it is necessary that the invariant and the Hamiltonian commute at these times, i.e.,

$$[I(0), H(0)] = [I(T), H(T)] = 0. \tag{4.14}$$

One is then free to choose how the state evolves in the intermediate time and once this is fixed, (4.13) determines how the Hamiltonian should vary with time to achieve those dynamics.

A Lewis–Riesenfeld invariant for a three-level system described by (4.6) can be written as

$$I = -\sin\beta\sin\alpha K_1 - \sin\beta\cos\alpha K_2 + \cos\beta K_3. \tag{4.15}$$

where α and β are time dependent functions which must fulfil the following relations (imposed by (4.13))

$$\dot{\alpha} = \frac{\Omega_{12}\sin\alpha + \Omega_{23}\cos\alpha}{2\tan\beta} + \frac{\Omega_{31}}{2}, \tag{4.16}$$

$$\dot{\beta} = \frac{1}{2}(\Omega_{23}\sin\alpha - \Omega_{12}\cos\alpha). \tag{4.17}$$

The eigenstates of this invariant are

$$|\phi_0(t)\rangle = \begin{pmatrix} -\sin\beta\cos\alpha \\ -i\cos\beta \\ \sin\beta\sin\alpha \end{pmatrix}, \tag{4.18}$$

$$|\phi_\pm(t)\rangle = \frac{1}{\sqrt{2}} \begin{pmatrix} \cos\beta\cos\alpha \pm i\sin\alpha \\ -i\sin\beta \\ -\cos\beta\sin\alpha \pm i\cos\alpha \end{pmatrix}, \tag{4.19}$$

with respective eigenvalues $\mu_0 = 0$ and $\mu_\pm = \pm 1$. One solution of the time-dependent Schrödinger equation is then given by $|\Psi(t)\rangle = |\phi_0(t)\rangle$ as the corresponding Lewis–Riesenfeld phase is zero in this case. Note that this invariant is a generalisation of the invariant considered in [78] where a third coupling Ω_{31} was not taken into account.

After fixing the boundary conditions using (4.14), one is free to choose the functions $\alpha(t)$ and $\beta(t)$. Moreover, in this case, one is also free to directly choose the function Ω_{31}. By inverting (4.16) and (4.17), the other coupling coefficients are then given by

$$\Omega_{12} = 2\dot{\alpha}\sin\alpha\tan\beta - 2\dot{\beta}\cos\alpha - \Omega_{31}\sin\alpha\tan\beta, \tag{4.20}$$

$$\Omega_{23} = 2\dot{\alpha}\cos\alpha\tan\beta + 2\dot{\beta}\sin\alpha - \Omega_{31}\cos\alpha\tan\beta. \tag{4.21}$$

4.5 Examples of SNAP schemes

In the following we will discuss two examples of SNAP derived from Lewis–Riesenfeld invariant based inverse engineering in the three-level approximation. The first one is the transport between two different traps, which is shown to be equivalent to the transitionless quantum driving method from section 4.4 in some cases. The second scheme will create an equal superposition of the particle in all three traps.

4.5.1 Transport

The first example of control we examine is the population transfer determined by

$$|\Psi(0)\rangle = |1\rangle \quad \rightarrow \quad |\Psi_{\text{target}}\rangle = \Psi(T) = -|3\rangle, \tag{4.22}$$

which was considered in the optical regime in [77]. This can be achieved by choosing auxiliary functions that fulfil the boundary conditions

$$\beta(0) = \beta(T) = -\frac{\pi}{2}, \quad \alpha(0) = 0, \quad \text{and} \quad \alpha(T) = \frac{\pi}{2}. \tag{4.23}$$

The experimentally required tunnelling frequencies are then explicitly given by (4.20) and (4.21).

For the special choice of $\beta(t) = -\pi/2$, one can show that $\langle 2|\Psi(t)\rangle = 0$ for all times, i.e. trap two is never occupied during the process. This choice then results in

$$\tan\alpha = \frac{\Omega_{12}}{\Omega_{23}} \quad \text{and} \quad \Omega_{31} = 2\dot{\alpha}. \tag{4.24}$$

By identifying α with θ (see (4.9)) one can immediately see that this is the same pulse as in the STA scheme derived in section 4.4.2.

The transport scheme can be implemented by the choosing the counterintuitive SAP pulses Ω_{12} and Ω_{23} to have a Gaussian profile [115]

$$\Omega_{12}(t) = \Omega_0 \exp\left[-100\,(t/T - 1/2)^2\right], \tag{4.25}$$

$$\Omega_{23}(t) = \Omega_0 \exp\left[-100\,(t/T - 1/3)^2\right], \tag{4.26}$$

and then calculating Ω_{31} from (4.24). The resulting pulses and associated dynamical populations are shown in figure 4.2. As expected the system follows exactly the dark state, transferring the population between states $|1\rangle$ and $|3\rangle$ without populating state $|2\rangle$.

The fidelity of the transport process as a function of the total time and the phase Φ generated by the magnetic field is shown in figure 4.3(a). Transport can be seen

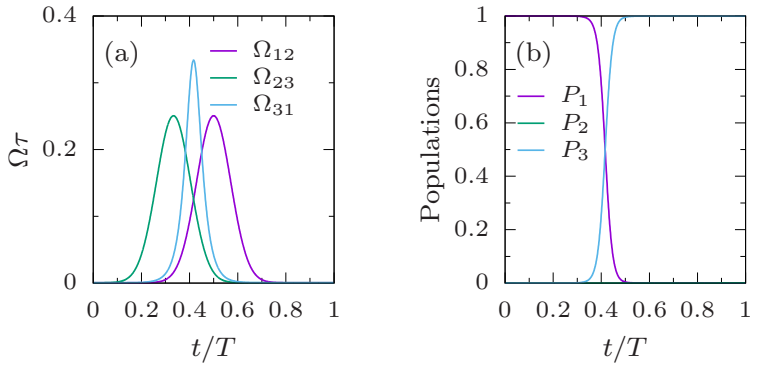


FIGURE 4.2: SNAP transport in the three-level approximation. $T/\tau = 100$ for $\Omega_0\tau = 0.25$. (a) Tunnelling rates. (b) Evolution of the populations $P_i = |\langle i|\Psi(t)\rangle|^2$. The time unit τ is defined as $\tau = ml^2/\hbar$.

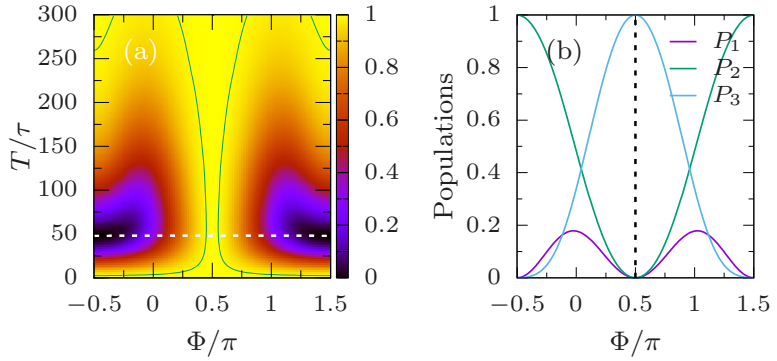


FIGURE 4.3: SNAP transport process $|1\rangle \to -|3\rangle$ in the three-level approximation. (a) Fidelity as a function of the total time and the total magnetic phase traversing the system. The green contour line is defined by $P_3 = 99\%$. (b) Probabilities of population in each of the traps for $T/\tau = 48$ (indicated by a dashed white line in (a)) as a function of the total magnetic phase traversing the system. The dashed black line indicates the optimal value of the phase $\Phi = \pi/2$

to occur with perfect fidelity for any value of the total time if the phase takes the appropriate value $\Phi = \pi/2$. It can also be seen that the shortcut is successful for any value of the phase in the limit of very short or very long times. The latter one is not surprising, as Ω_{31} can be neglected in the adiabatic limit, and hence its phase becomes irrelevant. A similar effect occurs for short total times, where the roles are reversed. In this limit Ω_{31} is the largest of all three couplings, and hence the phase relation between it and the other couplings becomes inconsequential. As Ω_{31} is a π pulse, perfect population transfer in this regime can be achieved regardless of the phase. However, in order to maintain this pulse area strong coupling is

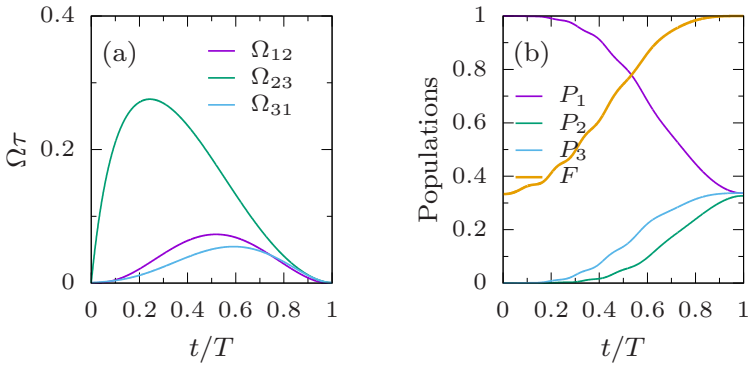


FIGURE 4.4: SNAP superposition scheme $|1\rangle \rightarrow \frac{1}{\sqrt{3}}(|1\rangle - i|2\rangle - |3\rangle)$ in the three-level approximation. $T/\tau = 400$. Sub-figures are the same as in figure 4.2 and the fidelity shown in (b) is defined as $F = |\langle\Psi_{\text{target}}|\Psi(t)\rangle|^2$.

required for very short processes, as the strength of Ω_{31} is inversely proportional to T. This might set a bound on how fast this shortcut can be implemented.

It is worth noting that this system also allows for the possibility of measuring the magnetic flux Φ_B, as the amount of transferred population oscillates as a function of the total phase Φ, which is directly related to the magnetic flux as $\Phi = \frac{q}{\hbar}\Phi_B$. As an example we show the occupation probabilities for $T/\tau = 48$ in each trap at the end of the process as a function of the phase in figure 4.3(b) . One can see that the populations strongly depend on the phase and over a large range of values one can therefore determine the magnetic flux. The exact relationship between the probabilities and the magnetic flux differs for different total times T.

4.5.2 Creation of a three-trap superposition

The second scheme we discuss highlights the generality of the Lewis–Riesenfeld invariant based method. In this scheme we create an equal superposition state between the particles being in all three traps, which means that the initial and target states are

$$|\Psi(0)\rangle = |1\rangle \quad \rightarrow \quad |\Psi_{\text{target}}\rangle = |\Psi(T)\rangle = \frac{1}{\sqrt{3}}(|1\rangle - i|2\rangle - |3\rangle). \tag{4.27}$$

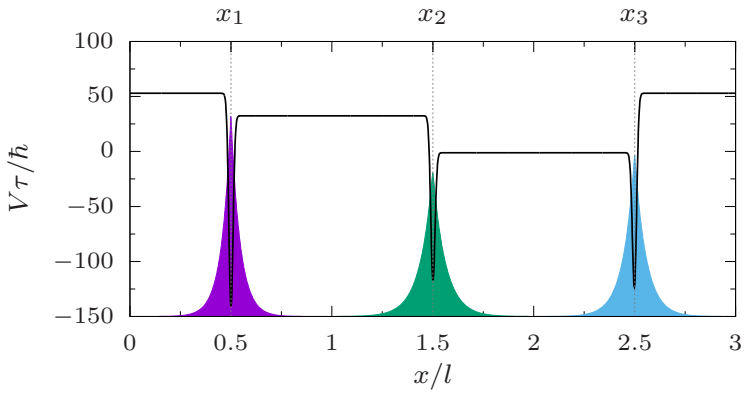


FIGURE 4.5: Schematic of the potential used in the numerical simulations (black line) with the localised states in each trap (coloured areas). The Gaussian shape of the traps is exaggerated here for clarity.

This can be realised by imposing the boundary conditions

$$\beta(0) = -\frac{\pi}{2}, \qquad \beta(T) = -\arctan\sqrt{2}, \tag{4.28}$$

$$\alpha(0) = 0, \qquad \alpha(T) = \frac{\pi}{4}, \tag{4.29}$$

on the auxiliary functions. A simple ansatz which fulfils these boundary conditions is a fourth order polynomial for $\beta(t)$ and third order polynomials for $\alpha(t)$ and $\Omega_{31}(t)$. The pulses are then obtained from (4.20) and (4.21) and their form is shown in figure 4.4(a). From figure 4.4(b) it can be seen that this choice creates the target state at the final time with perfect fidelity.

4.6 SNAP in the continuum model

While the three-level approximation discussed above gives a clear picture of the physics of the system, it does not include effects such as excitations to higher energy states that can occur during the process. We will therefore in the following test the approximation by numerically integrating the full Schrödinger equation in real space. For this, we will consider traps that are narrow enough to limit the system dynamics to an effectively one-dimensional setting along the azimuthal coordinate, $x = \varphi R$, i.e., around a circle of radius R, see figure 4.1. Moreover, we

will assume that the magnetic field is characterised by a vector potential in the azimuthal direction, $\vec{A} = A\hat{e}_\varphi$.

We are therefore dealing with a one-dimensional system of length $2\pi R$ with periodic boundary conditions, whose dynamics are described by the following Schrödinger equation

$$i\hbar\frac{\partial\psi}{\partial t} = \frac{1}{2m}\left(-i\hbar\frac{\partial}{\partial x} - qA\right)^2\psi + V(x)\psi. \tag{4.30}$$

We assume a constant vector potential throughout the dynamical part of the protocols, as any time-varying vector potential would produce an unwanted force due to the electric field $\vec{E} = -\partial_t\vec{A}$.

In order to be able to apply a well-defined phase we model the trapping sites as highly localised point-like potentials of depth ϵ_j at the positions $x_j = jl - l/2$ (see figure 4.5). They are separated by square barriers of heights $V_{jk}(t)$ (and length l), giving a total potential

$$V(x,t) = -\sum_{j=1}^{3}\epsilon_j(t)\delta(x-x_j) + \begin{cases} V_{31}(t) & \text{if} \quad 0 < x < x_1, \\ V_{12}(t) & \text{if} \quad x_1 < x < x_2, \\ V_{23}(t) & \text{if} \quad x_2 < x < x_3, \\ V_{31}(t) & \text{if} \quad x_3 < x < 3l. \end{cases} \tag{4.31}$$

Since point-like potentials are difficult to implement numerically, in the simulations below they are implemented as narrow Gaussians. It is important to note that this model is not designed to give realistic estimates for the fidelities or exactly reproduce the dynamics of the three-level approximation. It is a toy model to validate the basic underlying processes and show that SNAP schemes also make sense in the continuum.

As mentioned above, the tunnelling rates $\Omega_{jk}(t)$ in the three-level approximation are related to the barrier heights $V_{jk}(t)$ of the continuum model, see Appendix B.1. However, changing the barrier heights in order to achieve tunnelling will also affect the energies of the localised states in the neighbouring traps. Therefore,

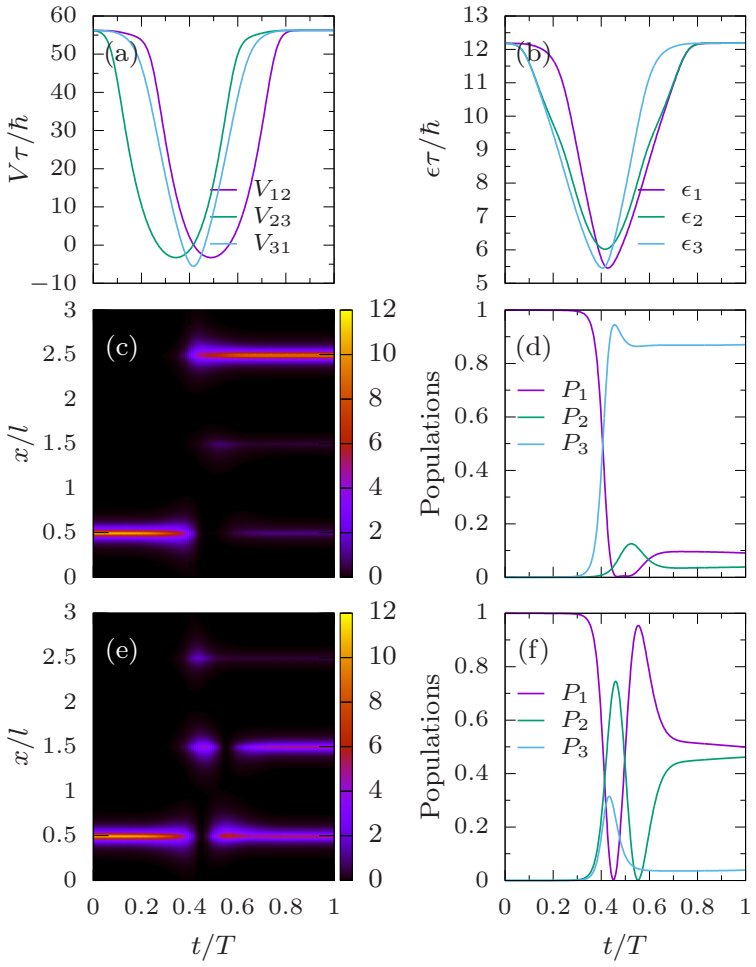


FIGURE 4.6: SNAP transport in the continuum model. $T/\tau = 100$. (a,b) Barrier heights and trap depths obtained by mapping the couplings in figure 4.2(a). (c) Evolution of the particle density $|\psi(x,t)|^2$. (d) Corresponding populations $P_i = |\langle i|\Psi(t)\rangle|^2$ in each trap and of the target state. (e,f) are the same as (c,d) but with the magnetic flux flowing in the opposite direction. The width of the Gaussian traps is $10^{-4}l$.

in order to reproduce the resonance of the three-level approximation (where the diagonal elements of the Hamiltonian are always zero) in the continuum model, the depths of the delta potentials ϵ_j have to be adjusted as the barriers' heights change, see figure 4.5. Finally, to map the barrier heights V_{jk} and trap depths ϵ_j parameters of the continuum model to the tunnelling rates Ω_{jk} of the three-level approximation, we numerically calculate the overlaps of neighbouring delta-trap eigenstates.

Results for transport of a particle using the shortcut scheme described in section

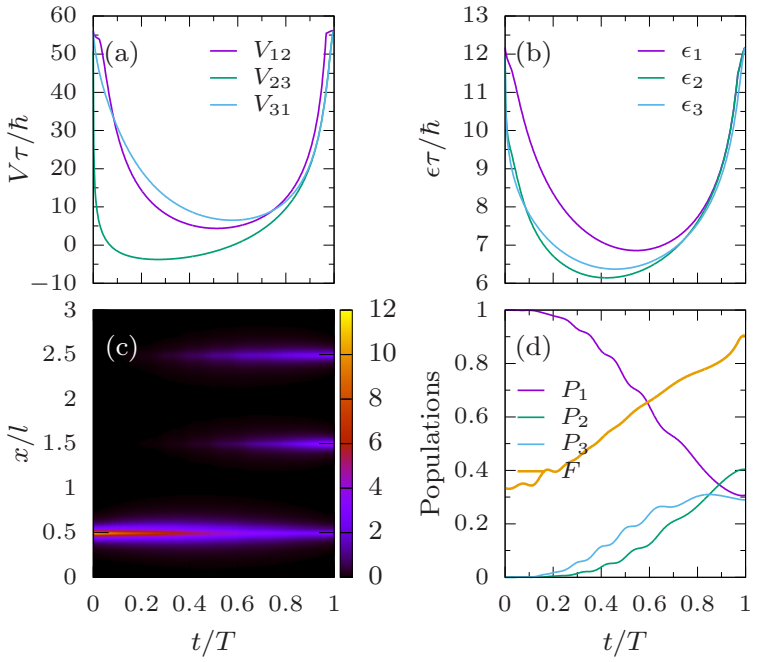


FIGURE 4.7: Same as figure 4.6(a-d) but for SNAP superposition scheme given in (4.27) in the continuum model. $T/\tau = 400$. $F = |\langle\psi_{\text{target}}|\psi(t)\rangle|^2$ is the fidelity of the process.

4.5.1 are shown in figure 4.6 and the barrier heights and trap depths used to match the pulses given in figure 4.2 are shown in figures 4.6(a,b). The probability density during the process can be seen in figure 4.6(c) and the populations in each trap are given in figure 4.6(d). While the process is not perfect, one can see that the particle is transported to the final trap with a fidelity of 87%. The effect of the magnetic field can be seen in figures 4.6(e,f), where we show results for the same process but with an inverted magnetic field (using a total phase of $\Phi = -\pi/2$). In this case the interference between the adiabatic and shortcut paths is destructive, and almost no population ends up in the final trap.

The results for the creation of the superposition state discussed in section 4.5.2 are shown in figure 4.7. The observed dynamics are very similar to the one in the three-level approximation and the process reaches a final fidelity of the target state of 91%.

Since the continuum model has many more degrees of freedom than the three-level model, it is not surprising that the fidelities obtained are lower. Nevertheless, the

basic functioning of the SNAP technique is clearly established from the calculations shown above. Optimising the fidelity in the continuum is an interesting task which, however, goes beyond the scope of the current work.

4.7 Conclusions

In this chapter, we have shown how complex tunnel frequencies in single-particle systems allow one to develop spatial non-adiabatic passage techniques that can lead to fast and robust processes for quantum technologies. In particular, we have discussed the case of a single, charged particle in a triple well ring system. The complex tunnelling couplings are obtained from the addition of a constant magnetic field, and have allowed us to generalise adiabatic state preparation protocols beyond the usual spatial adiabatic passage techniques [115]. This demonstrates that non-adiabatic techniques can be as efficient as their adiabatic counterparts, without requiring the long operation times.

In particular, we have discussed the implementation of the counter-diabatic term for spatial adiabatic passage transport via a direct coupling of all the traps. This was, in a second step, generalised to a flexible and robust method for preparing any state of the single-particle system by using Lewis–Riesenfeld invariants. As an example, we have shown that an equal spatial superposition state between the three wells can be created on a short time scale. Finally, by using a toy model for the mapping between the discrete approximation and the continuum model, we have presented numerical evidence that the SNAP process works beyond this approximation. It is worth noting that the complex tunnelling couplings we introduce can also be used to implement other techniques, e.g. those based on composite pulses [188].

In the next two chapters we will look at STA in continuous systems.

Chapter 5

Creating exotic angular momentum states by shaking an optical lattice

5.1 Overview

We propose a method to create higher orbital states of ultracold atoms in the Mott regime of an optical lattice. This is done by periodically modulating the position of the trap minima (known as shaking) and controlling the interference term of the lasers creating the lattice. These methods are combined with techniques of shortcuts to adiabaticity. As an example of this, we show specifically how to create an anti–ferromagnetic type ordering of angular momentum states of atoms. The specific pulse sequences are designed using Lewis–Riesenfeld invariants and a four–level model for each well. The results are compared with numerical simulations of the full Schrödinger equation.

This chapter is based on the following publication:
A. Kiely, A. Benseny, T. Busch and A. Ruschhaupt,
Shaken, not stirred: Creating exotic angular momentum states by shaking an optical lattice,

J. Phys. B: At. Mol. Opt. Phys. **49** 215003 (2016).
I derived the four–level Hamiltonian, the associated invariant and the required schemes. I also derived the six–level Hamiltonian and performed all the numerical simulations. Albert Benseny contributed in the discussions. All authors contributed to writing the manuscript.

5.2 Introduction

Optical lattices have proven to be highly versatile systems for investigating quantum many body physics [6, 189] and building quantum simulators [190, 191]. One of the first notable results was the observation of the phase transition between a superfluid and a Mott–insulator state [192–195], which was achieved for atoms trapped in the lowest band of the optical lattice. However, in the solid state, the orbital degree of freedom also plays an important role in many of the complex phases. For instance, many models in high temperature superconductivity involve higher orbital occupations [196–198]. As a result, there has been a lot of interest recently in the physics of higher bands of optical lattices [199, 200]. The bosonic Hubbard model describing the lowest band has been extended to incorporate higher Bloch bands [201] and Bose-Einstein condensation with nonzero orbital momenta has been studied [202, 203]. Many exotic phases have been predicted to occur due to the interplay of interactions and the higher bands [204].

Recently, first experiments have been performed realising multiorbital systems with ultracold atoms [205, 206] where the lifetimes of atoms in the excited state have been long enough to observe tunnelling dynamics. In particular, the formation of a superfluid in the higher bands has been experimentally achieved [207, 208]. The condensate formation in the higher bands has been used to investigate topologically induced avoided band crossing [209].

Engineering quantum states in higher bands is therefore of great interest and several techniques have been developed to manipulate the state of atoms in an optical lattice [200]. One example of this is periodic modulation of the lattice

amplitudes in order to induce controlled transitions to higher orbital states [210] or transitions to motional eigenstates [211]. Higher orbitals have also been populated by stimulated Raman transitions [206].

Another possibility is to shake the lattice in one direction, i.e., a periodic modulation of the position of the trap minima [212, 213]. The idea of shaking a single trap has been previously used for a variety of other tasks such as vibrational state inversion of a condensate in a trap [214] and Ramsey interferometry using the motional states of the condensate [215]. Shaking of an optical lattice in one direction has been explored theoretically for applications in quantum computing [216], to create artificial gauge fields [217] and to create higher orbital states in the lattice [218–220]. The latter has also been realised experimentally [221–223]. Recently there has been work which combines both amplitude and position modulation of the lattice potential using optimal control in order to transfer atoms between different vibrational states [224].

The goal of this chapter is to further develop the idea of shaking an optical lattice in order to create exotic states. This will be done by combining lattice shaking with the techniques of "Shortcuts to Adiabaticity" [65]. In general, performing fast and stable state preparation of quantum systems is very demanding. Adiabatic techniques are a common choice but have the drawback of needing extremely long times [113]. This has motivated the development of shortcuts to adiabaticity, which are protocols which reach fidelities of adiabatic processes in significantly shorter times. An important advantage of these methods is that they possess a certain freedom to optimise against noise, systematic error or unwanted transitions to higher levels [79, 88, 158, 160, 175]. In the following, we will show that combining optical lattice shaking with shortcut techniques can lead to schemes that are experimentally feasible (only requiring control over the relative phase and the polarisation of the lasers) and still have the freedom to be further optimised against the most relevant experimental noise sources. In particular, we will choose a staggered order angular momentum state as our target state, which has many physically interesting properties [201, 203, 204, 226]. This non-trivial state has an anti–ferromagnetic type ordering, which consist of each potential well

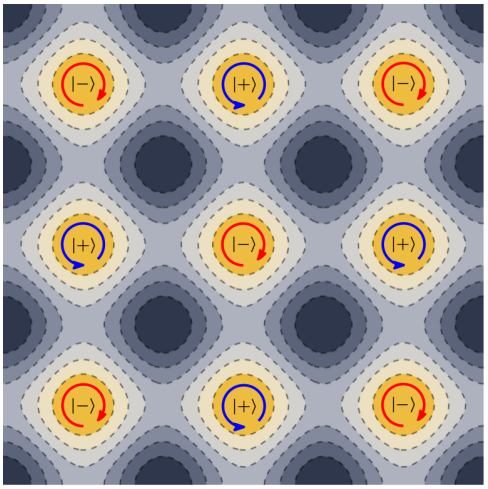


FIGURE 5.1: Diagram of final state of each atom in the lattice. Each site contains one atom in state $|\pm\rangle$ with angular momentum $\approx \pm\hbar$.

being occupied by a single atom, carrying alternating angular momentum $\approx \pm\hbar$ (see figure 5.1). We will propose a method which, starting from a Mott–insulator state, prepares such an anti–ferromagnetic type ordering by shaking the lattice. The state we create can be seen as a stepping stone towards more complex higher band states and the method we present is readily extendible to generate other states. It should be noted that shortcuts have been suggested previously for the creation of angular momentum in ultracold atom systems [112, 227].

The remainder of this chapter is structured as follows. In the subsequent section, we outline our model for the shaken optical lattice. In section 5.4, we review the method of Lewis–Riesenfeld invariants. In section 5.5, we outline the different schemes used in order to prepare the angular momentum state. In section 5.6, we perform numerical simulation of the full Schrödinger equation for a single atom in one site of an optical lattice in order to verify our assumptions. In section 5.7, we remark on some experimental considerations. Finally in section 5.8, we discuss our results.

5.3 Model

5.3.1 Optical lattice

We consider a two–dimensional optical lattice (in the x–y plane) generated by two pairs of counter–propagating laser beams. We assume a strong confinement in the z direction such that only dynamics in the x–y plane are relevant. We also assume that the atoms are in the Mott insulator regime i.e. each site is occupied by a single atom which is effectively independent of all the others. One can enter such a regime by having a large lattice depth so that tunnelling rates are small. While this means it is sufficient to consider each atom separately in the following, it is important to note that all the operations presented here are global and will affect all the atoms/sites simultaneously.

The complex amplitude of the electric field of the laser beams generating the two–dimensional optical lattice is

$$\vec{\mathcal{E}}(x,y,t) = \vec{\mathcal{E}}_0 \sin\left\{k\left[x - r_x(t)\right]\right\} + i\vec{\mathcal{E}}_0 e^{-i\rho(t)} \sin\left\{k\left[y - r_y(t)\right]\right\}, \tag{5.1}$$

where $r_x(t)$ and $r_y(t)$ define the position of the minimum of the central trap, and can be controlled by a time-dependent phase difference between the pair of laser beams in each direction. When these are modulated periodically, it results in a shaking of the lattice. We will see below that this shaking alone is insufficient to create the desired quantum state. Therefore, we assume in addition that the polarisation vectors in the two directions have an equal amplitude $\vec{\mathcal{E}}_0$, but with a slowly varying relative phase $\rho(t)$.

Similar to the one–dimensional case presented in section 2.1.2.1, the potential felt by an atom in the two–dimensional optical lattice is given by [189]

$$V(x,y) = \frac{1}{4\hbar\Delta}\left|\vec{\mu}\cdot\vec{\mathcal{E}}^*(x,y,t)\right|^2, \tag{5.2}$$

where $\vec{\mu}$ is the transition dipole moment of the atom and Δ (assumed to be large) is the detuning of the laser with respect to the atomic transition frequency. Defining the lattice depth as

$$V_0 = \frac{1}{4\hbar\Delta}\left|\vec{\mu}\cdot\vec{\mathcal{E}}_0^*\right|^2, \tag{5.3}$$

the potential can be written as

$$\begin{aligned} V(x,y) = \quad & V_0\sin^2\left\{k\left[x-r_x(t)\right]\right\} + V_0\sin^2\left\{k\left[y-r_y(t)\right]\right\} \\ & + V_\rho(t)\sin\left\{k\left[x-r_x(t)\right]\right\}\sin\left\{k\left[y-r_y(t)\right]\right\}, \end{aligned} \tag{5.4}$$

where $V_\rho(t) = 2V_0\sin\left[\rho(t)\right]$ is the amplitude of the interference term, restricted to the interval $[-2V_0, 2V_0]$. Without any loss of generality, we assume that the laser is blue detuned ($\Delta > 0$) so that V_0 is positive.

We now change from the lab frame to the lattice frame (see Appendix C.1 for details), where the Hamiltonian takes the form

$$\begin{aligned} H_{\text{lattice}}(t) &= H_0 + H_1(t), && (5.5)\\ H_0 &= -\frac{\hbar^2}{2m}\nabla^2 + V_0\sin^2(kx) + V_0\sin^2(ky), && (5.6)\\ H_1(t) &= m\ddot{r}_x(t)x + m\ddot{r}_y(t)y + V_\rho(t)\sin(kx)\sin(ky). && (5.7) \end{aligned}$$

It is worth noting that without the V_ρ term, the Hamiltonian would be separable in x and y coordinates and therefore be unable to produce an angular momentum state (which is not separable in x and y). We will assume the shaking of the lattice to be of the form

$$\begin{aligned} r_x(t) &= -g_x(t)\cos(\omega_x t), \\ r_y(t) &= g_y(t)\sin(\omega_y t), \end{aligned} \tag{5.8}$$

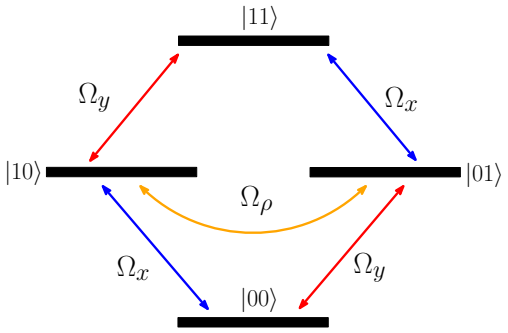


FIGURE 5.2: Energy level diagram for the four chosen energy eigenstates of H_0 and the various couplings between them.

where $g_{x,y}(t)$ are the time–dependent amplitudes and $\omega_{x,y}$ are the frequencies. By assuming that $g_{x,y}(t)$ vary slowly with time, $H_1(t)$ simplifies to

$$H_1(t) \quad = \quad f_x(t)\, x + f_y(t)\, y + V_\rho(t) \sin(kx) \sin(ky), \tag{5.9}$$

where

$$f_x(t) = m\omega_x^2 g_x(t) \cos(\omega_x t), \tag{5.10}$$

$$f_y(t) = -m\omega_y^2 g_y(t) \sin(\omega_y t). \tag{5.11}$$

In this case the shaking in the y direction is $\pi/2$ out of phase with the shaking in x direction.

5.3.2 Four–level approximation

Our aim is to derive the control schemes, i.e., the time dependence of the functions $r_x(t)$, $r_y(t)$ and $V_\rho(t)$, which will lead to a desired final state. To do this we will now derive a simplified model of the system by concentrating on a single atom in a single well of the lattice defined by $-\ell \leq x \leq \ell$ and $-\ell \leq y \leq \ell$, where $2\ell = \pi/k$ is the lattice constant. The situation where the neighbouring lattice potential wells can be neglected is very well realised in the Mott insulator regime.

Furthermore, we assume that the dynamics can be effectively described by a four–level approximation, considering only the four most relevant eigenstates of H_0

localised in the central site, $\{|00\rangle, |10\rangle, |01\rangle, |11\rangle\}$ (see figure 5.2). The validity of this and all subsequent approximations will be checked later by comparing with the numerical integration of the full Schrödinger equation. In coordinate representation, these basis states are given by

$$\langle \vec{r}|ij\rangle = \Gamma_i(x)\Gamma_j(y), \tag{5.12}$$

where $\Gamma_0(x)$ and $\Gamma_1(x)$ are, respectively, the localised ground and first excited states of a one–dimensional unperturbed optical lattice site. Note that this is only possible because H_0 is separable in x and y. Their respective energies are $E_{ij} = \hbar\omega_{ij}$, where $E_{00} < E_{01} = E_{10} < E_{11}$.

Let us now define a unitary transformation of the form

$$\begin{aligned} U(t) = \quad & e^{-i(\omega_{10}+\omega_x)t}|00\rangle\langle 00| + e^{-i(\omega_{10}+\omega_x-\omega_y)t}|01\rangle\langle 01| \\ & + e^{-i\omega_{10}t}|10\rangle\langle 10| + e^{-i\omega_{11}t}|11\rangle\langle 11|, \end{aligned} \tag{5.13}$$

under which the Hamiltonian changes as

$$H \quad \longrightarrow \quad U^\dagger H U - i\hbar U^\dagger \dot{U} = U^\dagger H_0 U - i\hbar U^\dagger \dot{U} + U^\dagger H_1(t) U = H_{4L}. \tag{5.14}$$

The first part of this is

$$U^\dagger H_0 U - i\hbar U^\dagger \dot{U} = \hbar(\omega_{00} - \omega_{10} - \omega_x)|00\rangle\langle 00| + \hbar(\omega_y - \omega_x)|01\rangle\langle 01|, \tag{5.15}$$

and the second part simplifies to

$$\begin{aligned} U^\dagger H_1(t) U = \quad & e^{-i\omega_x t}\gamma_1 f_x(t)|10\rangle\langle 00| + V_\rho(t)\gamma_2 e^{-i(\omega_x-\omega_y)t}|10\rangle\langle 01| \\ & + e^{i(\omega_x-\omega_y-\omega_d)t}\gamma_1 f_x(t)|01\rangle\langle 11| + e^{-i\omega_d t}\gamma_1 f_y(t)|10\rangle\langle 11| \\ & + e^{i\omega_y t}\gamma_1 f_y(t)|00\rangle\langle 01| + V_\rho(t)\gamma_2 e^{i(\omega_x-\omega_d)t}|00\rangle\langle 11| + \text{h.c.}, \end{aligned} \tag{5.16}$$

where we have defined

$$\begin{aligned}
\gamma_1 &= \int_{-\ell}^{\ell} \Gamma_0(x) x \Gamma_1(x) dx, && (5.17)\\
\gamma_2 &= \left[\int_{-\ell}^{\ell} \Gamma_0(x) \sin(kx) \Gamma_1(x) dx\right]^2, && (5.18)\\
\omega_d &= \omega_{10} - \omega_{00}. && (5.19)
\end{aligned}$$

Note that the symmetry of the unperturbed lattice gives $\omega_{11} = 2\omega_{10} - \omega_{00}$.

We now assume that the shaking of the lattice in both directions is done on resonance, i.e., $\omega_x = \omega_y = -\omega_d$. This allows us to write the four–level Hamiltonian as

$$\begin{aligned}
H_{4L}(t) = \quad & \frac{\hbar}{2}\Big[\Omega_x(t)\left(1 + e^{2i\omega_d t}\right)|10\rangle\langle 00| + \Omega_x(t)\left(1 + e^{-2i\omega_d t}\right)|01\rangle\langle 11| \\
& -i\Omega_y(t)\left(1 - e^{-2i\omega_d t}\right)|10\rangle\langle 11| - i\Omega_y(t)\left(1 - e^{-2i\omega_d t}\right)|00\rangle\langle 01| \\
& +\Omega_\rho(t)|10\rangle\langle 01| + \Omega_\rho(t)e^{-2i\omega_d t}|00\rangle\langle 11| + \text{h.c.}\Big], \qquad (5.20)
\end{aligned}$$

with the couplings

$$\begin{aligned}
\Omega_{x,y}(t) &= m\omega_d^2 \gamma_1 g_{x,y}(t)/\hbar, \\
\Omega_\rho(t) &= 2V_\rho(t)\gamma_2/\hbar. \qquad (5.21)
\end{aligned}$$

By making a rotating wave approximation, where the terms containing $e^{\pm 2i\omega_d t}$ average to 0, we arrive at our final four–level Hamiltonian (see figure 5.2)

$$H_{4L}(t) = \frac{\hbar}{2}\begin{pmatrix} 0 & \Omega_x & \Omega_\rho & -i\Omega_y \\ \Omega_x & 0 & -i\Omega_y & 0 \\ \Omega_\rho & i\Omega_y & 0 & \Omega_x \\ i\Omega_y & 0 & \Omega_x & 0 \end{pmatrix}, \qquad (5.22)$$

where we have used the following representation of the states

$$|10\rangle = \begin{pmatrix} 1 \\ 0 \\ 0 \\ 0 \end{pmatrix}, \quad |00\rangle = \begin{pmatrix} 0 \\ 1 \\ 0 \\ 0 \end{pmatrix}, \quad |01\rangle = \begin{pmatrix} 0 \\ 0 \\ 1 \\ 0 \end{pmatrix}, \quad |11\rangle = \begin{pmatrix} 0 \\ 0 \\ 0 \\ 1 \end{pmatrix}. \tag{5.23}$$

It is important to note that state $|11\rangle$ can not be neglected and should be included in the approximation, as it is resonantly coupled to $|01\rangle$ and $|10\rangle$.

5.3.3 Initial and target states

Our goal is to perform a state transfer from the ground state $|00\rangle$ to an angular momentum state of the form

$$|\pm\rangle = \frac{1}{\sqrt{2}} \left(|10\rangle \pm i|01\rangle \right). \tag{5.24}$$

If the harmonic approximation holds, $|\pm\rangle$ are eigenvectors of the z component of the angular momentum operator L_z with eigenvalues $\pm\hbar$.

One can see that the interference term in (5.7), which includes V_ρ, alternates sign at each lattice site in a checkerboard pattern. In the case where $\Omega_y = 0$, this can be seen as a change of basis $|01\rangle \to -|01\rangle$ and $|11\rangle \to -|11\rangle$ and hence one obtains either $|+\rangle$ or $|-\rangle$ in alternating sites, leading to the pattern in Fig. 5.1. For our schemes we will assume that $\Omega_y = 0$, although more general schemes might be derived in a similar way.

In the following, we will use the technique of Lewis–Riesenfeld invariants to derive shortcut schemes to implement the state transfer $|00\rangle \to |-\rangle$. An advantage of this method is that one still has a certain freedom to optimise the stability of the schemes against the most relevant error sources in a specific setting [79, 88, 158, 160, 175].

5.4 Lewis–Riesenfeld invariants for the four–level system

One possible technique to derive shortcuts to adiabaticity is based on Lewis–Riesenfeld invariants [116]. A Lewis–Riesenfeld invariant for a Hamiltonian $H(t)$ is a Hermitian operator $I(t)$ which satisfies

$$\frac{\partial I}{\partial t} + \frac{i}{\hbar}\left[H, I\right] = 0. \tag{5.25}$$

Recall from section 2.2.2 that because $I(t)$ is a constant of motion it can be shown that it has time–independent eigenvalues and that a particular solution of the Schrödinger equation,

$$i\hbar\frac{\partial}{\partial t}\left|\psi_n(t)\right\rangle = H(t)\left|\psi_n(t)\right\rangle, \tag{5.26}$$

can be written as

$$\left|\psi_n(t)\right\rangle = e^{i\beta_n(t)}\left|\phi_n(t)\right\rangle. \tag{5.27}$$

Here $\left|\phi_n(t)\right\rangle$ is an instantaneous eigenstate of $I(t)$ and

$$\beta_n(t) = \frac{1}{\hbar}\int_0^t \left\langle\phi_n(s)\right| \left|[i\hbar\partial_s - H(s)]\right| \left.\phi_n(s)\right\rangle ds \tag{5.28}$$

is the Lewis–Riesenfeld phase. Hence a general solution to the Schrödinger equation can be written as

$$\left|\psi(t)\right\rangle = \sum_n c_n \left|\psi_n(t)\right\rangle \tag{5.29}$$

where the c_n are independent of time.

The idea behind inverse engineering is that instead of following the instantaneous eigenstate of the Hamiltonian (as in the adiabatic case), one follows the instantaneous eigenstate of the invariant (up to the Lewis–Riesenfeld phase). Demanding that the invariant and the Hamiltonian commute at the start and the end of the process i.e., $[I(0), H(0)] = [I(T), H(T)] = 0$, one ensures that the eigenstates of the invariant and the Hamiltonian coincide at initial and final times. This leaves the freedom to choose how the state evolves in the intermediate time and then use

(5.25) to determine how the Hamiltonian should vary with time to ensure such a state evolution.

In the following we will derive the invariant for the Hamiltonian in (5.22) with $\Omega_y = 0$. For a more detailed review of Lewis–Riesenfeld invariants for four level systems see [228]. Following the general method proposed in [122, 229], we start with a closed Lie algebra $\{G_1, G_2, G_3, G_4\}$ of Hermitian operators

$$\begin{aligned} G_1 &= \begin{pmatrix} 0 & 1 & 0 & 0 \\ 1 & 0 & 0 & 0 \\ 0 & 0 & 0 & 1 \\ 0 & 0 & 1 & 0 \end{pmatrix}, G_2 = \begin{pmatrix} 0 & 0 & 1 & 0 \\ 0 & 0 & 0 & 0 \\ 1 & 0 & 0 & 0 \\ 0 & 0 & 0 & 0 \end{pmatrix}, \\ G_3 &= \begin{pmatrix} 0 & 0 & 0 & i \\ 0 & 0 & -i & 0 \\ 0 & i & 0 & 0 \\ -i & 0 & 0 & 0 \end{pmatrix}, G_4 = \begin{pmatrix} 0 & 0 & 0 & 0 \\ 0 & 0 & 0 & 1 \\ 0 & 0 & 0 & 0 \\ 0 & 1 & 0 & 0 \end{pmatrix}. \end{aligned} \tag{5.30}$$

This algebra was chosen so that the 4–level Hamiltonian and the associated Lewis–Riesenfeld invariant can now be written as a linear combination of these operators

$$H(t) = \frac{\hbar}{2}\Omega_x(t) G_1 + \frac{\hbar}{2}\Omega_\rho(t) G_2, \tag{5.31}$$

$$I(t) = \sum_{i=1}^{4} \alpha_i(t) G_i, \tag{5.32}$$

where $\alpha_i(t) \in \mathbb{R}$. Inserting this into (5.25), we get that the coupling strengths are given by

$$\Omega_x(t) = -\frac{\dot{\alpha}_2(t)}{\alpha_3(t)}, \tag{5.33}$$

$$\Omega_\rho(t) = \frac{2\dot{\alpha}_1(t)}{\alpha_3(t)}, \tag{5.34}$$

and that

$$\alpha_3(t) = \xi\sqrt{2C_2 - [\alpha_1^2(t) + \alpha_2^2(t)] + C_1\alpha_2(t)}, \tag{5.35}$$

$$\alpha_4(t) = C_1 - \alpha_2(t), \tag{5.36}$$

where $C_{1,2} \in \mathbb{R}$ are constants, $\xi = \pm 1$ and $\alpha_1(t), \alpha_2(t)$ are still arbitrary functions.

In order to be useful it is important to know the eigenvalues κ_i and eigenvectors $|\phi_i(t)\rangle$ of the invariant, i.e. $I(t) = \sum_{i=1}^{4} \kappa_i |\phi_i(t)\rangle\langle\phi_i(t)|$. We get that the eigenvalues are

$$\begin{aligned} \kappa_1 &= \frac{1}{2}\left(-C_1 - Q\right), \kappa_2 = \frac{1}{2}\left(C_1 - Q\right), \\ \kappa_3 &= \frac{1}{2}\left(-C_1 + Q\right), \kappa_4 = \frac{1}{2}\left(C_1 + Q\right), \end{aligned} \tag{5.37}$$

where $Q = \sqrt{C_1^2 + 8C_2}$. The corresponding eigenvectors are

$$|\phi_1(t)\rangle = \begin{pmatrix} -B_+D_- \\ -\frac{1}{2B_+} \\ B_+D_- \\ \frac{1}{2B_+} \end{pmatrix}, |\phi_2(t)\rangle = \begin{pmatrix} -B_-D_+ \\ \frac{1}{2B_-} \\ -B_-D_+ \\ \frac{1}{2B_-} \end{pmatrix}, \tag{5.38}$$

$$|\phi_3(t)\rangle = \begin{pmatrix} B_-D_- \\ -\frac{1}{2B_-} \\ -B_-D_- \\ \frac{1}{2B_-} \end{pmatrix}, |\phi_4(t)\rangle = \begin{pmatrix} B_+D_+ \\ \frac{1}{2B_+} \\ B_+D_+ \\ \frac{1}{2B_+} \end{pmatrix}, \tag{5.39}$$

where we have defined

$$B_\pm(t) = \sqrt{\frac{Q}{\pm C_1 + Q \mp 2\alpha_2}}, \tag{5.40}$$

$$D_\pm(t) = \frac{i}{Q}\left[\frac{2C_2 + (C_1 - \alpha_2)\alpha_2}{\pm i\alpha_1 + \xi\sqrt{2C_2 + (C_1 - \alpha_2)\alpha_2 - \alpha_1^2}}\right]. \tag{5.41}$$

Note that $Q, B_\pm \in \mathbb{R}$ and $D_+^* = -D_-$. We also assume a nonzero Q so that none of the above quantities diverge.

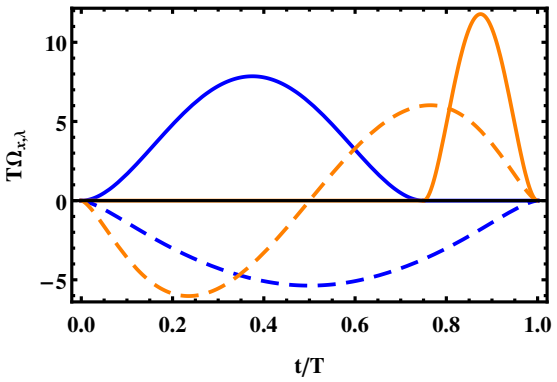


FIGURE 5.3: Coupling strengths against time for the two different schemes. Polynomial scheme: Ω_x (blue, dashed line) and Ω_ρ (orange, dashed line). Piecewise scheme ($t_S = 0.75T$): Ω_x (blue, solid line) and Ω_ρ (orange, solid line).

Finally, the Lewis-Riesenfeld phases [116] are given by

$$\begin{aligned} \beta_1(t) &= -\chi_+(t), \quad \beta_2(t) = \chi_-(t), \\ \beta_3(t) &= -\chi_-(t), \quad \beta_4(t) = \chi_+(t)\,, \end{aligned} \tag{5.42}$$

where we have defined

$$\chi_\pm(t) = \int_0^t \frac{2\alpha_1\left[C_1^2 + 4C_2 \pm C_1 Q \mp 2\left(\pm C_1 + Q\right)\alpha_2 + 2\alpha_2^2\right]\dot{\alpha}_2}{\left(C_1 \pm Q - 2\alpha_2\right)^3 \xi\left[2C_2 + \left(C_1 - \alpha_2\right)\alpha_2 - \alpha_1^2\right]^{\frac{1}{2}}} ds. \tag{5.43}$$

5.5 Shaking schemes for preparing an angular momentum state

In this section, we present two schemes which allow us to prepare our target state. In order to design the scheme we start by constructing a solution to the Schrödinger equation as a linear combination of two of the eigenvectors of the invariant

$$\begin{aligned} |\psi(t)\rangle &= \frac{1}{\sqrt{2}}\left[-|\phi_1(t)\rangle e^{i\beta_1(t)} + |\phi_4(t)\rangle e^{i\beta_4(t)}\right] \\ &= \frac{1}{\sqrt{2}}\left[-|\phi_1(t)\rangle e^{-i\beta_4(t)} + |\phi_4(t)\rangle e^{i\beta_4(t)}\right]. \end{aligned} \tag{5.44}$$

The initial and final state of the system are fixed as

$$|\psi(0)\rangle = |00\rangle, \tag{5.45}$$

$$|\psi(T)\rangle = |-\rangle, \tag{5.46}$$

which leads to the boundary conditions

$$\begin{aligned} \alpha_1(0) &= 0,\ \alpha_2(0) = (C_1 - Q)/2, \\ \alpha_1(T) &= 0,\ \alpha_2(T) = (C_1 + Q)/2,\ \beta_4(T) = 0, \end{aligned} \tag{5.47}$$

in the limits $t \to 0$ and $t \to T$.

We also demand that Ω_x, Ω_ρ and their first derivatives with respect to time are zero at the start and the end of the process. This requires that all the derivatives of $\alpha_1(t)$ and $\alpha_2(t)$ up to fourth order are zero at $t = 0$ and $t = T$, which gives 10 constraints to be fulfilled by $\alpha_1(t)$ and also 10 constraints for $\alpha_2(t)$.

5.5.1 Polynomial scheme

A convenient choice of ansatz for $\alpha_1(t)$ and $\alpha_2(t)$ which fulfills all the constraints is given by polynomials of the form

$$\begin{aligned} \alpha_1(sT) &= 1024W(-s^{10} + 5s^9 - 10s^8 + 10s^7 - 5s^6 + s^5), \\ \alpha_2(sT) &= \frac{1}{2}(C_1 - Q) + 70Qs^9 - 315Qs^8 + 540Qs^7 - 420Qs^6 + 126Qs^5, \end{aligned} \tag{5.48}$$

where $s = t/T$. To avoid the trivial solution $\alpha_1(sT) = 0$ we also demand $\alpha_1(T/2) = W \neq 0$. We are now allowed to arbitrarily pick $C_1 = 10$ and $C_2 = 11$ so that $Q \neq 0$ and $\alpha_3(t)$ is real for all times. We also set $\xi = +1$ and then numerically calculate W (≈ -2.74) so that $\beta_4(T) = 0$. The coupling strengths $\Omega_x(t)$ and $\Omega_\rho(t)$ can be calculated from Eqs. (5.33) and (5.34), and are shown in figure 5.3 (dashed lines).

Let us underline again that this is just one possible choice for the auxiliary functions $\alpha_1(t)$ and $\alpha_2(t)$ (and the constants C_1 and C_2). The advantage of this inverse–engineering ansatz is that it provides a lot of freedom in choosing these functions which can be used for further optimisations [79].

5.5.2 Piecewise scheme

The second example we introduce to generate our target state is a simple piecewise scheme. The idea is to first perform a π pulse in Ω_x (of duration t_S) which transfers all the population from $|00\rangle$ to $|10\rangle$, followed by a $\pi/2$ pulse in Ω_ρ (of duration $T - t_S$) which leads to the superposition $|-\rangle$. This method has the advantage that the state $|11\rangle$ is never populated, which reduces the chance of losing population to higher levels. However the rotating wave approximation will be more valid in the previous scheme. The amplitudes of the couplings are determined by t_S and are given by (see figure 5.3 (solid lines))

$$\begin{aligned}
\Omega_x(t) &= \begin{cases} \frac{30\pi t^2 (t-t_S)^2}{t_S^5} & 0 \le t \le t_S, \\ 0 & t_S < t \le T, \end{cases} \\
\Omega_\rho(t) &= \begin{cases} 0 & 0 \le t < t_S, \\ -\frac{15\pi (t-T)^2 (t-t_S)^2}{(t_S-T)^5} & t_S \le t \le T. \end{cases}
\end{aligned} \tag{5.49}$$

Since Ω_x and Ω_ρ are a π pulse and $\pi/2$ pulse respectively, we have that $\int_0^T \Omega_x(t)dt = \pi$ and $\int_0^T \Omega_\rho(t)dt = \pi/2$.

This can be seen as a particular case of schemes derived using invariant–based inverse engineering. In this case $\alpha_1(t)$ and $\alpha_2(t)$ are given by

$$\begin{aligned}
\alpha_1(t) &= \begin{cases} \epsilon & 0 \le t \le t_S, \\ \epsilon \cos\left[\frac{1}{2}\int_{t_S}^t \Omega_\rho(t')\,dt'\right] & t_S < t \le T, \end{cases} \\
\alpha_2(t) &= \begin{cases} \frac{1}{2}\left\{C_1 - \sqrt{C_1^2 + 8C_2 - 4\epsilon^2}\cos\left[\int_0^t \Omega_x(t')\,dt'\right]\right\} & 0 \le t < t_S, \\ \frac{1}{2}\left(C_1 + \sqrt{C_1^2 + 8C_2 - 4\epsilon^2}\right) & t_S \le t \le T, \end{cases}
\end{aligned} \tag{5.50}$$

and $\xi = -1$. Inserting Eqs. (5.50) in Eqs. (5.33) and (5.34) gives back Eqs. (5.49). The required boundary conditions of α_1 and α_2 are fulfilled in the limit $\epsilon \to 0^+$.

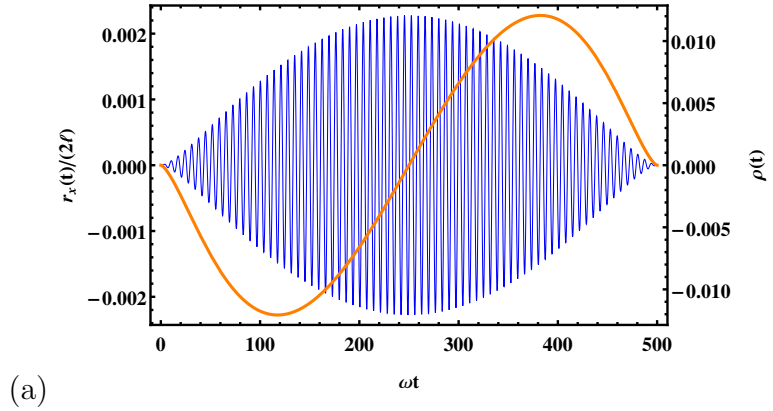
5.6 Numerical simulations of the shaking schemes

The presented schemes result in the desired state transfer exactly in the framework of the four–level Hamiltonian. In order to check the validity of all the approximations we have made to reach this model, we present below simulations of the full Schrödinger equation with Hamiltonian (5.5) in coordinate space for an atom initially in the ground state of a single lattice site.

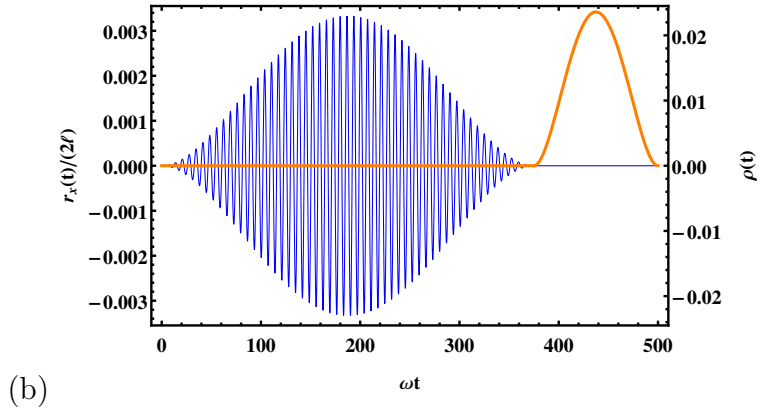
The evolution is performed by means of the Fourier split–operator method [145], where the initial ground state is found by imaginary–time evolution. For more details on these methods see section 2.3.3. In order to make all plots dimensionless we define $\omega = \sqrt{\frac{2V_0k^2}{m}}$, which is the frequency of the harmonic oscillator potential which approximates each well of the optical lattice. Note that the previously defined $\omega_d = \omega_{10} - \omega_{00}$ converges to ω for increasing lattice depth V_0. The rotating wave approximation and the slowly–varying shaking amplitude approximation can be combined in the condition $T \gg \omega_d^{-1} \approx \omega^{-1}$.

As we have assumed to be in the Mott–insulator regime, we restrict our simulations to the dynamics of an atom in a single well. We have checked the validity of this approximation by simulating our schemes in a 3×3 lattice. With the typical parameters used below, the shaking causes only about a 1% leakage into the neighbouring traps.

The control parameters in our system are the shaking function in the x direction, $r_x(t)$ (as stated above, we keep $r_y(t) = 0$), and the relative phase between the polarisation vectors in the x and y directions, $\rho(t)$. They relate to the couplings



(a)



(b)

FIGURE 5.4: Shaking function $r_x(t)$ with $\omega_x = -\omega_d$ (thin, blue line) and relative phase between the polarisation vectors $\rho(t)$ (thick, orange line) versus time for (a) the polynomial scheme and (b) the piecewise scheme ($t_S = 0.75T$). $V_0 = 3\hbar\omega$, $T = 500\omega^{-1}$ and $2\ell = \pi/k$ is the lattice constant.

as

$$r_x(t) = -\frac{\hbar}{m\omega_d^2\gamma_1}\Omega_x(t)\cos(\omega_x t)\,, \tag{5.51}$$

$$\rho(t) = \arcsin\left(\frac{\hbar}{4V_0\gamma_2}\Omega_\rho(t)\right). \tag{5.52}$$

The resulting functions for both the polynomial process and the piecewise process are shown in figure 5.4. One can see that the required amplitude of the shaking is only a small fraction of the lattice constant.

The results of the numerical simulation of both schemes are shown in figure 5.5, together with the ideal populations based on the four–level Hamiltonian in (5.22). Using the polynomial scheme, even for a short (relative to the time scale of the inverse trap frequency) total time $T = 100\omega^{-1}$ (figure 5.5(a)), the final population

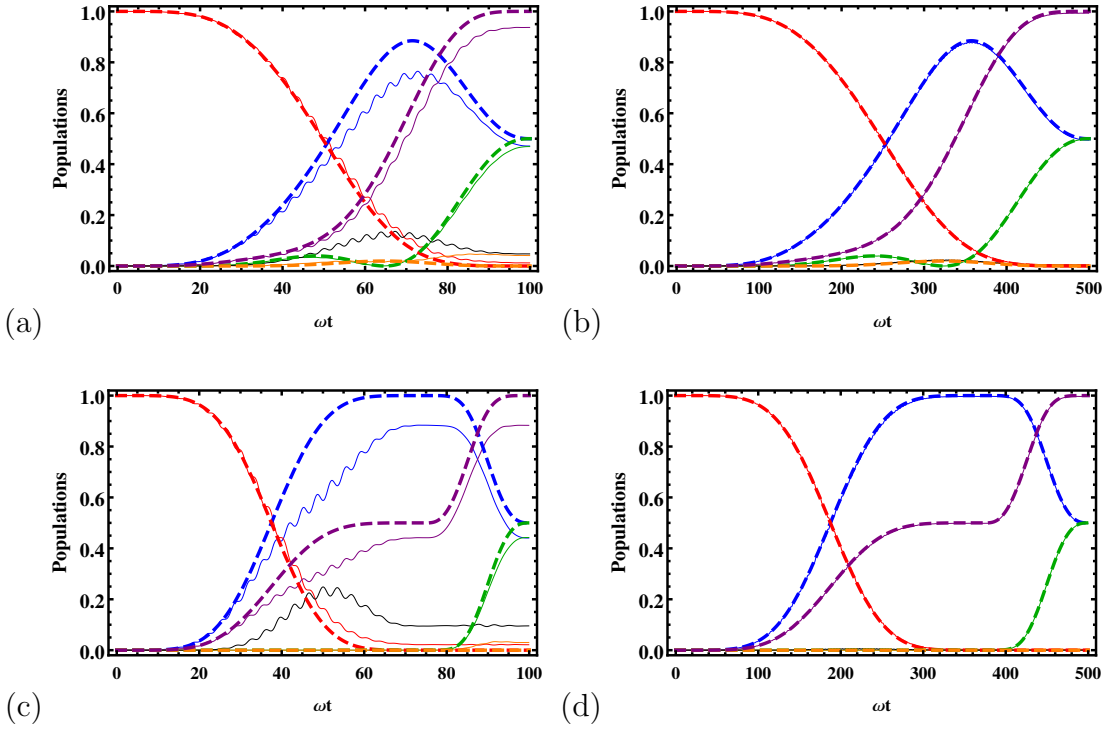


FIGURE 5.5: Populations against time calculated using the four–level approximation (dashed lines) and the full Schrödinger equation (solid lines) with $V_0 = 3\hbar\omega$ for the polynomial process with (a) $T = 100\omega^{-1}$ and (b) $T = 500\omega^{-1}$ and the piecewise process ($t_S = 0.75T$) with (c) $T = 100\omega^{-1}$ and (d) $T = 500\omega^{-1}$. Colours correspond to: $|\langle\psi(t)|00\rangle|^2$ (red), $|\langle\psi(t)|10\rangle|^2$ (blue), $|\langle\psi(t)|01\rangle|^2$ (green), $|\langle\psi(t)|11\rangle|^2$ (orange), $|\langle\psi(t)|-\rangle|^2$ (purple), and populations of higher levels, i.e., $1 - \sum_{i,j=0}^{1} |\langle\psi(t)|ij\rangle|^2$ (black).

in the desired state is already greater than 90%, with about 5% of population leaking to states outside of the four–level model. For a longer total time T (figure 5.5(b)), the agreement between the four–level Hamiltonian and the full dynamics is almost perfect, ending up with nearly 100% in the desired state.

Similarly for the piecewise scheme, the dynamics for a short total time (figure 5.5(c)) leads to oscillations and a non–perfect population of the target state, and approximately a 10% population of higher lying states. However, for longer T (figure 5.5(d)), the final fidelity is nearly 100%. Note that since the second pulse Ω_ρ in this scheme does not require the rotating wave approximation, it is beneficial to give the first pulse a longer duration. Hence the choice of $t_S = 0.75T$.

The fidelity of both schemes for different total times T and different lattice depths V_0 is shown in figure 5.6; the lattice constant $2\ell = \pi/k$ is varied in such a way that

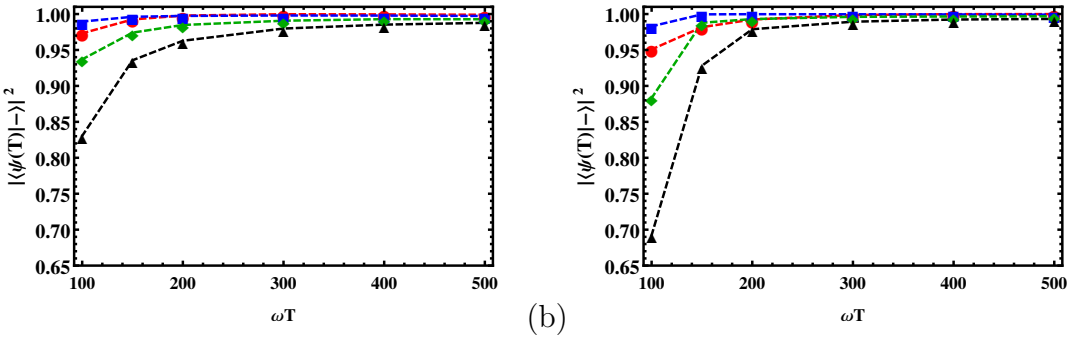


FIGURE 5.6: Fidelity $|\langle\psi(T)|-\rangle|^2$ against total time T for different lattice depths V_0 for a fixed trapping frequency ω. Points joined with lines: $V_0 = 2\hbar\omega$ (red circles), $V_0 = 2.5\hbar\omega$ (blue squares), $V_0 = 3\hbar\omega$ (green diamonds) and $V_0 = 3.5\hbar\omega$ (black triangles); (a) polynomial scheme, (b) piecewise scheme ($t_S = 0.75T$).

the trapping frequency $\omega = \sqrt{\frac{2V_0k^2}{m}}$ is kept fixed. From this we can see again how for a larger T we achieve higher fidelities, which is consistent with the rotating wave approximation and the slowly varying shaking amplitude approximation becoming more valid. We can also see that the fidelities decrease for deeper lattices because as the well becomes deeper it becomes more harmonic and hence has equally spaced energy levels. This leads to resonant coupling to higher energy levels (see Appendix C.2 for details).

In the following, we want to examine the stability of the schemes. In figure 5.7(a), we show the resonance curve for both processes, i.e., the fidelity against the detuning of the shaking frequency with respect to the frequency difference of the first two levels. We compare the four–level model (not assuming $\omega_x = -\omega_d$) against the full Schrödinger equation dynamics. As expected, one achieves high fidelity when the shaking frequency is on resonance. Perhaps surprisingly one can note that the highest fidelity of the full dynamics is achieved for a slightly off resonant shaking frequency. This is not true in the four–level model, as the corresponding curves have their maximum at resonance. The reason for this is the presence of an off resonant coupling to the state $|20\rangle$(which is not present in the four-level model). By slightly increasing the detuning of Ω_x with respect to the $|00\rangle \leftrightarrow |10\rangle$ transition, an even greater detuning in the coupling between $|10\rangle$ and $|20\rangle$ is created, leading to less leakage to these higher states. We can verify this by considering a six–level

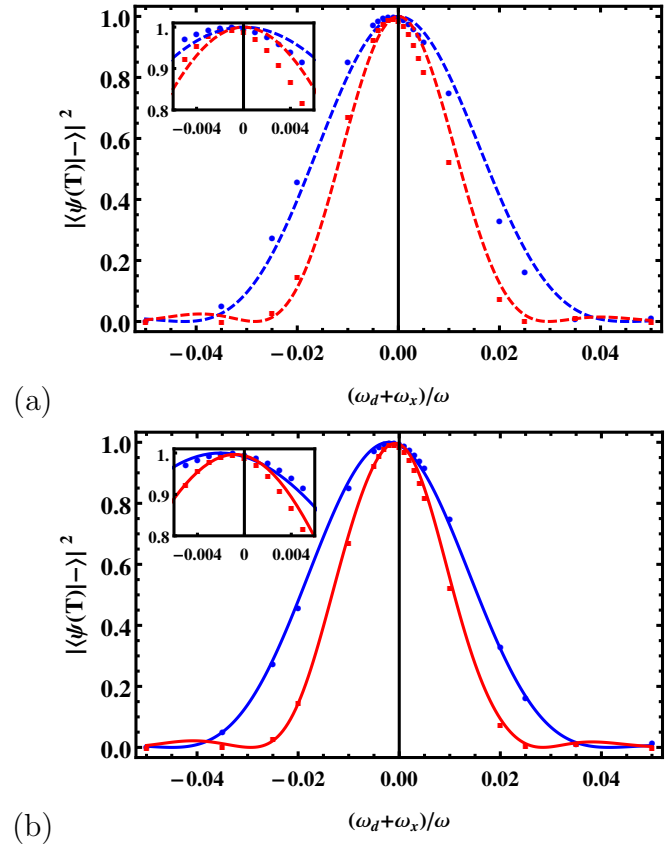


FIGURE 5.7: Fidelity $|\langle\psi(T)|-\rangle|^2$ against the deviation from resonant shaking $(\omega_x + \omega_d)/\omega$ for $V_0 = 3\hbar\omega$ and $T = 300\omega^{-1}$ (resonant shaking corresponds to $\omega_x = -\omega_d$). Polynomial scheme (red) and piecewise scheme with $t_S = 0.75T$ (blue). Points correspond to the full Schrödinger equation, dashed lines to the 4–level model and lines to the 6–level model (C.8).

model (see Appendix C.2), which can be seen to agree with the full Schrödinger equation dynamics (see figure 5.7(b))

Finally, we remark once again that in the case of more lattice sites, each containing a single atom, the schemes would result in the pattern in figure 5.1. As a brief aside, we now consider a single atom whose initial state is now a superposition of all ground states of all 9 wells of a 3×3 lattice; the single atom is delocalised across the entire lattice. Applying here the piecewise shaking scheme, one reaches the final state represented in figure 5.8. It can be clearly seen that a checkerboard pattern of left- and right-handed angular momentum states is produced, similar to figure 5.1. Note that we have adjusted the (physically irrelevant) global phase such that the branch cut is horizontal in this representation of the wave function.

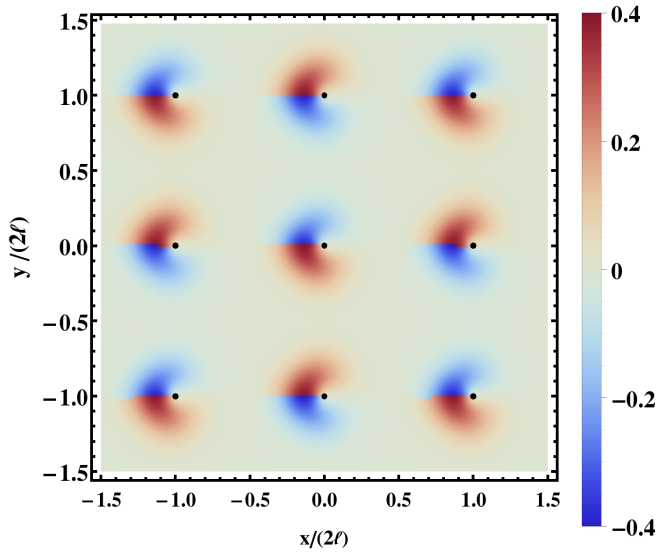


FIGURE 5.8: Final state after applying the piecewise process with $V_0 = 3\hbar\omega$, $T = 300\omega^{-1}$ and $t_S = 0.75T$. Shown is $|\Psi(x, y, T)| \cdot \arg[\Psi(x, y, T)]$, with the black dots indicating the minima of the lattice wells.

In this case, we have produced a final state for a single atom in which its position is entangled with the sign of the angular momentum in each well.

5.7 Experimental considerations

There are several options for experimentally implementing such a system depending on how one creates the two counter propagating beams for each direction. One option is to use a beam and a retro-reflecting mirror, in which case one can induce the shaking by mounting the mirror on a piezo-electric actuator which will then oscillate according to $r_x(t)$ [230–232]. In the case where the beam is split in two, one can introduce a small frequency difference $\Delta\nu(t)$ between the beams by using acousto-optic modulators to make the lattice move with a velocity $\Delta\nu(t)\lambda/2$, where λ is the wavelength of the laser [232, 233]. The shaking is then given by $r_x(t) = \frac{\lambda}{2}\int_0^t \Delta\nu(\tau)d\tau$.

Parameter values of $V_0/(\hbar\omega) = 3$ and $\omega T = 300$ could for example be reached using ^{133}Cs atoms with $\lambda = 1064\,\text{nm}$ lasers and a lattice depth of $36E_r$, where $E_r = \frac{\hbar^2k^2}{2m}$

is the recoil energy. The shaking frequency required would be $\omega_d/(2\pi) \approx 14\,\mathrm{kHz}$ and the total time required for the operation would be $T \approx 3\,\mathrm{ms}$. Under the assumption that $V_0 \gg E_r$ (i.e. that the well is deep), one can approximate the ground state tunnelling rate J_0 as [6, 234]

$$J_0 \approx \frac{4E_r}{\sqrt{\pi}} \left(\frac{V_0}{E_r}\right)^{3/4} e^{-2\sqrt{V_0/E_r}}. \tag{5.53}$$

For our scheme to work, the operation must be performed much faster than this tunnelling time, i.e, we want $T \ll \hbar/J_0 \approx 589\,\mathrm{ms}$ for the parameter values above. If one calculates the tunnelling rates using exact band structure calculations [201], one obtains a ground state tunnelling time of $\hbar/J_0 \approx 600\mathrm{ms}$ and an excited state tunnelling time of $\hbar/J_1 \approx 17\mathrm{ms}$. Being in the Mott insulator ground state (for ^{133}Cs) corresponds to a potential depth of about $22E_r$ [193] or greater. Being in the Mott state for both the ground state and the first excited state (i.e. atoms are localised in one well, regardless of being in the ground or first excited state) will not be affected by the shaking, as it has been shown both theoretically [235] and experimentally [236] that the shaking effectively reduces the tunnelling strength to the neighbouring wells. In addition, the anharmonic nature of the potential inhibits first order decay processes whereby two atoms in the first excited state collide, promoting one to the second excited state and the other to the ground state [201].

5.8 Conclusions

We have developed two schemes to prepare an exotic lattice state, namely a staggered order angular momentum state, starting from a Mott insulator state in an optical lattice. Both of these use shaking of the optical lattice together with a modulation of the interference term. The flexibility of the invariant–based approach makes it possible to extend the scheme presented in multiple directions. For instance, one could further optimise it to combat the most relevant errors in a given experimental implementation [79]. Since the atoms are in the Mott–insulator

regime the effects of atoms tunnelling into neighbouring wells and atom-atom interactions have been neglected. Nevertheless, these effects could possibly play a role in lattices with imperfect filling factors. It would be beneficial to generalise our scheme to become insensitive to such imperfections.

This work could be extended in several interesting directions. One possibility would be to prepare a state with equal angular momentum per lattice site. This could possibly be done by additionally shaking the lattice in the y direction resulting in a non-zero Ω_y term. Another would be to apply the process we describe above to a single delocalised atom, which would result in an entangled state where the well position is entangled with the sign of the angular momentum. Finally, atoms with angular momentum have recently been shown to be useful for generating complex tunnelling frequencies [237].

Chapter 6

Fast and stable manipulation of a charged particle in a Penning trap

6.1 Overview

In this chapter, we propose shortcuts to adiabaticity (STA) to achieve fast and stable control of the state of a charged particle in an electromagnetic field. In particular we design a non-adiabatic change of the magnetic field strength in a Penning trap which changes the radial spread without final excitations. We apply a streamlined version of the fast-forward formalism as well as an invariant based inverse engineering approach. We compare both methods and examine their stability.

This chapter is based on the following publication:
A. Kiely, J. P. L. McGuinness, J. G. Muga and A. Ruschhaupt,
Fast and stable manipulation of a charged particle in a Penning trap,
J. Phys. B: At. Mol. Opt. Phys. **48** 075503 (2015).
Justin McGuinness did preliminary calculations for generalising the fast-forward approach to the minimal coupling equation as part of his undergraduate dissertation. I did the definitive final analytical calculations, applied these results to the

Penning trap, made the connection to the invariant formalism and produced the figures. All authors contributed to the writing of the manuscript.

6.2 Introduction

The fast expansion or compression of a particle state driven by a time dependent trap frequency is one of the paradigmatic operations for which STA have been developed, both in theory [65, 238] and experiment [239, 240]. Interacting particles in an expanding/compressing external harmonic potential such as ion chains [241], Bose-Einstein condensates [69], or classical gases [22], have also been studied. There are many applications for fast expansion/compression, such as controlled cooling/heating of the state [242, 243], implementation of quantum engines and refrigerators based on cyclic expansions and compressions [244–246], fast switching between manipulations suited for a low trap frequency or for a high trap frequency configuration [241], or efficient sympathetic cooling [247, 248]. Fundamental aspects such as the quantification of the third law of thermodynamics [67, 244] have also been examined.

Real traps are of course three-dimensional, but most of the theory work deals with 1D traps with time dependent frequencies whose effective realization is not straightforward. Torrontegui et al. [249] studied the fast expansions of cold atoms in a three-dimensional Gaussian-beam optical trap. The radial and axial frequencies are coupled and as a consequence some shortcut schemes that work in 1D were in fact restricted to certain parameter domains, and others failed completely. Traps with uncoupled radial and axial frequencies are of interest to perform clean STA expansions/compressions and such a possibility is indeed provided by the Penning trap.

In this chapter, we will put forward shortcut schemes to control a charged particle in a Penning trap. Recall from section 2.1.2.2 that a Penning trap uses a combination of a uniform and unidirectional magnetic field and an electrostatic quadrupole potential. This potential is typically created using three electrodes

which are hyperboloids of revolution. Penning traps are commonly used for accurate measurement of the properties of different charged particles [250–253].

Since different operations on the trapped charged particle (preparation, measurement, or interactions) may require or benefit from different extensions of the density cloud, our aim is to change this extension rapidly without producing final excitations. Therefore, we shall construct schemes to decrease the radial extension of the particle's wave function, without producing final excitations, by changing the magnetic field intensity. We shall first design such shortcuts by means of the fast-forward formalism.

In the following section we will develop a streamlined version of the fast-forward formalism in the general case of a charged particle in an electromagnetic field. In section 6.4, we will review the known eigenstates of a particle in a a Penning trap. In section 6.5, we apply the streamlined formalism to change the state from an eigenstate of one magnetic field strength to that of a larger field strength. We also compare it with an inverse engineering approach based on Lewis-Riesenfeld invariants and examine the stability versus systematic errors in the magnetic field. Finally, in section 6.6 we discuss our results.

6.3 General streamlined formalism

We shall now put forward a streamlined version of the fast-forward formalism including an electromagnetic field [138]. This will extend what was reviewed in section 2.2.4.

6.3.1 Main equations

We consider a spinless charged particle as spin will not play any role in the trap configuration considered below. The Schrödinger equation for this particle in an

electromagnetic field is given by

$$i\hbar\frac{\partial}{\partial t}\Psi = H(t)\Psi, \tag{6.1}$$

where the Hamiltonian (expressed in some chosen gauge e.g. the Coulomb gauge) is given in coordinate representation by

$$H(t) = \frac{1}{2m}\left[\frac{\hbar}{i}\nabla - q\vec{A}(t,\vec{r})\right]^2 + q\phi(t,\vec{r}), \tag{6.2}$$

with q being the charge, $\vec{A}$ the vector potential and ϕ the scalar potential (both real). We write Ψ as

$$\Psi(t,\vec{r}) = \alpha(t,\vec{r})e^{i\beta(t,\vec{r})}, \tag{6.3}$$

where $\alpha(t,\vec{r}), \beta(t,\vec{r}) \in \mathbb{R}$. Note that $\Psi(t,\vec{r})$ corresponds to the fast-forwarded state Ψ_{FF} in [138]. $\vec{A}$ and $q\phi$ correspond to the driving potentials $\vec{A}_{FF}$ and V_{FF} in [138].

Inserting the ansatz (6.3) into (6.1) and then multiplying the equation by $e^{-i\beta(t,\vec{r})}$, we get for the real part of the result

$$0 = -\frac{\hbar^2}{2m}\Delta\alpha + \frac{1}{2m}\left(q\vec{A} - \hbar\nabla\beta\right)^2\alpha + \left(q\phi + \hbar\frac{\partial\beta}{\partial t}\right)\alpha, \tag{6.4}$$

and for the imaginary part

$$\hbar\frac{\partial\alpha}{\partial t} = \frac{\hbar}{2m}\nabla\left(q\vec{A} - \hbar\nabla\beta\right)\alpha + \frac{\hbar}{m}\left(q\vec{A} - \hbar\nabla\beta\right)\nabla\alpha. \tag{6.5}$$

To write these two equations in a more compact way, let us define

$$\vec{\chi} = \vec{A} - \frac{\hbar}{q}\nabla\beta,\ \Phi = \phi + \frac{\hbar}{q}\frac{\partial\beta}{\partial t}. \tag{6.6}$$

The electric and the magnetic fields are now given by

$$\vec{E} = -\nabla\Phi - \frac{\partial\vec{\chi}}{\partial t},\ \vec{B} = \nabla\times\vec{\chi}. \tag{6.7}$$

Using these definitions of $\vec{\chi}$ and Φ, the two equations (6.4) and (6.5) simplify to

$$\Phi = \frac{\hbar^2}{2mq\alpha}\Delta\alpha - \frac{q}{2m}\vec{\chi}^2, \tag{6.8}$$

and

$$\frac{\partial\alpha}{\partial t} - \frac{q}{2m}(\nabla\vec{\chi})\alpha - \frac{q}{m}\vec{\chi}\nabla\alpha = 0. \tag{6.9}$$

These are the two main equations.

Note that $\vec{\chi}$ and Φ as well as the main equations (6.8) and (6.9) are invariant under a gauge transformation Λ acting in the usual way

$$\vec{A} \to \vec{A} + \nabla\Lambda,\ \phi \to \phi - \frac{\partial\Lambda}{\partial t} \text{ and } \Psi \ \to \ e^{\frac{i}{\hbar}q\Lambda}\Psi, \tag{6.10}$$

i.e., $\beta \to \beta + \frac{q}{\hbar}\Lambda$ and α is unchanged.

6.3.2 Inverse engineering and boundary conditions

Let the initial state of the system $\psi_0(\vec{r}) \equiv \alpha_0(\vec{r})e^{i\beta_0(\vec{r})}$ be an eigenstate of the initial time independent Hamiltonian

$$H_0 = \frac{1}{2m}\left(\frac{\hbar}{i}\nabla - q\vec{A}_0\right)^2 + q\phi_0, \tag{6.11}$$

with eigenvalue $\mathcal{E}_0$. (The eigenstates of the Penning trap are reviewed in the following section.) The goal is to design a scheme ($\vec{A}(t,\vec{r})$ and $\phi(t,\vec{r})$) such that the final state (at $t = T$) of the system, $\psi_T(\vec{r}) \equiv \alpha_T(\vec{r})e^{i\beta_T(\vec{r})}$, is an eigenstate of the final (time independent) Hamiltonian

$$H_T = \frac{1}{2m}\left(\frac{\hbar}{i}\nabla - q\vec{A}_T\right)^2 + q\phi_T, \tag{6.12}$$

with eigenvalue $\mathcal{E}_T$. The Hamiltonian should be continuous at initial and final time, i.e., $H(0) = H_0$ and $H(T) = H_T$.

In the inversion protocol we first design $\alpha(t,\vec{r})$ and $\beta(t,\vec{r})$ fulfilling the boundary conditions

$$\begin{aligned}\alpha(0,\vec{r}) = \alpha_0(\vec{r}),\ \alpha(T,\vec{r}) = \alpha_T(\vec{r}),\\ \beta(0,\vec{r}) = \beta_0(\vec{r}),\ \beta(T,\vec{r}) = \beta_T(\vec{r}).\end{aligned} \tag{6.13}$$

In the next step, we have to solve for $\vec{\chi}$ in (6.9). The function Φ is then given by (6.8). Because the Hamiltonian should be changing continuously at initial and final time, $\vec{\chi}$ must fulfil the following boundary conditions

$$\vec{\chi}(0,\vec{r}) = \vec{A}_0 - \frac{\hbar}{q}\nabla\beta_0,\ \vec{\chi}(T,\vec{r}) = \vec{A}_T - \frac{\hbar}{q}\nabla\beta_T. \tag{6.14}$$

A consequence of these conditions can be seen by evaluating (6.9) at the initial and final time (see also Appendix D.1). This leads to

$$\frac{\partial\alpha}{\partial t}(0,\vec{r}) = 0,\ \frac{\partial\alpha}{\partial t}(T,\vec{r}) = 0. \tag{6.15}$$

The boundary conditions of Φ can be seen by evaluating (6.8) at initial and final time leading to (see also Appendix D.1)

$$\begin{aligned}\Phi(0,\vec{r}) = \phi_0(\vec{r}) - \frac{1}{q}\mathcal{E}_0 = \phi_0(\vec{r}) + \frac{\hbar}{q}\frac{\partial\beta}{\partial t}(0,\vec{r}),\\ \Phi(T,\vec{r}) = \phi_0(\vec{r}) - \frac{1}{q}\mathcal{E}_T = \phi_0(\vec{r}) + \frac{\hbar}{q}\frac{\partial\beta}{\partial t}(T,\vec{r}).\end{aligned} \tag{6.16}$$

These conditions are equivalent to

$$\frac{\partial\beta}{\partial t}(0,\vec{r}) = -\frac{1}{\hbar}\mathcal{E}_0,\ \frac{\partial\beta}{\partial t}(T,\vec{r}) = -\frac{1}{\hbar}\mathcal{E}_T. \tag{6.17}$$

Finally, the vector potential and the scalar potential in the chosen gauge are then given by

$$\vec{A}(t,\vec{r}) = \vec{\chi}(t,\vec{r}) + \frac{\hbar}{q}\nabla\beta(t,\vec{r}), \tag{6.18}$$

$$\phi(t,\vec{r}) = \Phi(t,\vec{r}) - \frac{\hbar}{q}\frac{\partial\beta}{\partial t}, \tag{6.19}$$

and the electric and magnetic fields are given by (6.7).

The above boundary conditions guarantee that the magnetic field is continuous at the initial and final time. To make the electric field continuous at the initial and final time, we also impose

$$\frac{\partial\vec{\chi}}{\partial t}(0,\vec{r})=0,\ \frac{\partial\vec{\chi}}{\partial t}(T,\vec{r})=0. \tag{6.20}$$

6.4 Energy Eigenstates of a Penning trap

Let us introduce cylindrical coordinates $\{r,\theta,z\}$ where $x=r\cos\theta$ and $y=r\sin\theta$, and define the orthogonal unit vectors

$$\hat{r}=\begin{pmatrix}\cos\theta\\ \sin\theta\\ 0\end{pmatrix},\ \hat{\theta}=\begin{pmatrix}-\sin\theta\\ \cos\theta\\ 0\end{pmatrix},\ \hat{z}=\begin{pmatrix}0\\ 0\\ 1\end{pmatrix}. \tag{6.21}$$

For the Penning trap, we assume a homogeneous magnetic field in z direction, $\vec{B}=B_z\hat{z}$, and an electrostatic field of the form $\vec{E}=E_r\hat{r}+E_\theta\hat{\theta}+E_z\hat{z}$, where

$$E_r=\frac{m\omega_z^2}{2q}r,\ E_\theta=0,\ E_z=-\frac{m\omega_z^2}{q}z. \tag{6.22}$$

The vector potential and the scalar potential can be written as

$$\vec{A}=\frac{rB_z}{2}\hat{\theta},\ \phi=\frac{m\omega_z^2}{4q}\left(2z^2-r^2\right). \tag{6.23}$$

The corresponding Hamiltonian reads

$$H=-\frac{\hbar^2}{2m}\Delta+\frac{m}{2}\widetilde{\omega}^2r^2-\omega L_z+\frac{1}{2}m\omega_z^2z^2, \tag{6.24}$$

where $\widetilde{\omega}^2=\omega^2-\omega_z^2/2$, $\omega=qB_z/(2m)$ (similar to the cyclotron frequency) and $L_z=\frac{\hbar}{i}\frac{\partial}{\partial\theta}$ is the z-component of the angular momentum operator. L_z commutes with the rest of the Hamiltonian, so it represents a conserved quantity. The

Hamiltonian (6.24) is separable into a Hamiltonian depending on r and θ and a Hamiltonian depending solely on z. The corresponding Schrödinger equation can be solved by a product of a function of r and θ and a function of z. The z-dependent function describes the dynamics of a harmonic oscillator with axial (angular) frequency ω_z which we assume to have a fixed value. Since we shall consider B_z as the time dependent external parameter, the non-trivial part of interest is the function that depends on r and θ. Hence we focus solely on this part. We also assume $qB_z > 0$. The energy eigenfunctions are

$$\psi_{N,M,l}(r,\theta) = f_{N,M,l}(r)\exp\left(iM\theta\right), \tag{6.25}$$

where

$$f_{N,M,l}(r) \;=\; \frac{1}{\sqrt{2\pi}}\sqrt{\frac{N!}{(N+|M|)!}}\frac{1}{l}\left[\frac{r}{\sqrt{2}l}\right]^{|M|}\exp\left(-\frac{r^2}{4l^2}\right)L_N^{|M|}\left(\frac{r^2}{2l^2}\right), \tag{6.26}$$

$N, M \in \mathbb{Z}$, $L_N^{|M|}(q)$ are the generalised Laguerre Polynomials, defined by

$$L_N^a(Q) = \frac{Q^{-a}e^Q}{N!}\frac{d^N}{dQ^N}(e^{-Q}Q^{N+a}), \tag{6.27}$$

and the constant l is defined by

$$l = \sqrt{\frac{\hbar}{2m\widetilde{\omega}}}. \tag{6.28}$$

M is the quantum number associated with the z component of the angular momentum operator (i.e. $L_z\psi_{N,M,l}(r,\theta) = M\hbar\psi_{N,M,l}(r,\theta)$) and N is a quantum number that determines the radial structure. $l \in \mathbb{R}$ is the characteristic radial length scale of the wavefunction; it is determined by the magnetic field B_z and the axial frequency ω_z via (6.28). The energy eigenvalues are

$$\mathcal{E}_{N,M} = \hbar\widetilde{\omega}\left(2N + |M| + 1\right) - \hbar\omega M, \tag{6.29}$$

where $N = 0, 1, ...$ and M is an integer. Alternatively, using $\widetilde{N} := 2N + |M|$, the energy eigenvalues are often written as $\mathcal{E} = \hbar\widetilde{\omega}(\widetilde{N}+1) - \hbar\omega M$ with $\widetilde{N} = 0, 1, ...$

and $M = -\widetilde{N}, -\widetilde{N}+2, ..., \widetilde{N}-2, \widetilde{N}$. For example, these eigenfunctions were previously found for $\widetilde{\omega} = \omega$ in [254].

6.5 Varying the magnetic field strength

We would like to design the time dependence of the magnetic field so that the system starts from the eigenstate $\psi_{N,M,l_0}(r,\theta)$ at initial time $t = 0$ with magnetic field $B_z(0) = B_{z,0}$ and ends in the eigenstate $\Psi_{N,M,l_T}(r,\theta)$ at final time $t = T$ with magnetic field $B_z(T) = B_{z,T}$, i.e. $\Psi(0,r,\theta) = \psi_{N,M,l_0}(r,\theta)$, $\Psi(T,r,\theta) = \psi_{N,M,l_T}(r,\theta)$, where $l_0 = \sqrt{\hbar/(2m\widetilde{\omega}(0))}$, $l_T = \sqrt{\hbar/(2m\widetilde{\omega}(T))}$, and $\widetilde{\omega}(t) = \sqrt{\left(qB_z(t)/(2m)\right)^2 - \omega_z^2/2}$. The frequency ω_z should be kept constant. Of course, this can be done in an adiabatic way but here we want to derive a shortcut to adiabaticity. As an example, we will examine a way to decrease the characteristic length scale, $l_0 \to l_T$.

6.5.1 Streamlined formalism

Following the algorithm presented in section 6.3, we start by choosing the following ansatz for the time evolution of the wavefunction

$$\alpha(t,r) = \sqrt{\frac{N!}{(N+|M|)!}}\frac{1}{\sqrt{2\pi}l(t)}\left(\frac{r}{\sqrt{2}l(t)}\right)^{|M|}\exp\left(-\frac{r^2}{4l(t)^2}\right)L_N^{|M|}\left(\frac{r^2}{2l(t)^2}\right), \tag{6.30}$$

and $\beta(t,\theta) = M\theta + \zeta(t)$. For the boundary conditions (6.13), it follows $\alpha(0,r) = f_{N,M,l_0}(r)$ and $\alpha(T,r) = f_{N,M,l_T}(r)$ and so we get the condition $l(0) = l_0$, $l(T) = l_T$. Moreover, we get $\zeta(0) = \zeta(T) = 0$.

As the next step, we have to solve the main equation (6.9). We assume that $\vec{\chi}$ does not depend on θ, i.e. $\vec{\chi} = \chi_r(t,r)\,\hat{r} + \chi_\theta(t,r)\,\hat{\theta}$. (6.9) then becomes

$$\frac{2mr}{q}\frac{\partial\alpha}{\partial t} - \chi_r\left(\alpha + 2r\frac{\partial\alpha}{\partial r}\right) - r\frac{\partial\chi_r}{\partial r}\alpha = 0, \tag{6.31}$$

and (6.8) becomes

$$\Phi = -\frac{q}{2m}\left(\chi_r^2+\chi_\theta^2\right)+\frac{\hbar^2}{2mq\alpha}\left(\frac{1}{r}\frac{\partial\alpha}{\partial r}+\frac{\partial^2\alpha}{\partial r^2}\right). \tag{6.32}$$

A solution of (6.9) is given by

$$\chi_r(t,r) = -\frac{2m}{q}\frac{1}{r\,\alpha^2}\int_r^\infty ds\, s\,\alpha\frac{\partial\alpha}{\partial t}(t,s). \tag{6.33}$$

The solution when α and $\vec{\chi}$ depend on θ can be found in Appendix D.2.

For α given by (6.30), we get from (6.33) that

$$\chi_r(t,r) = -\frac{m}{q}\frac{rl'(t)}{l(t)}, \tag{6.34}$$

where the prime indicates a derivative with respect to time. Note that this solution is independent of the quantum numbers N and M.

The components of the physical fields can be written as

$$B_z(t,r) = \frac{1}{r}\frac{\partial(r\chi_\theta)}{\partial r}, \tag{6.35}$$

$$E_r(t,r) = -\frac{\partial}{\partial r}\Phi-\frac{\partial\chi_r}{\partial t},\ E_\theta(t,r) = -\frac{\partial\chi_\theta}{\partial t}. \tag{6.36}$$

We want a uniform magnetic field and a constant radial electric field $\left(E_r=\frac{m\omega_z^2}{2q}r\right)$ during the whole process. To achieve a uniform magnetic field $B_z = B_z(t)$ we set

$$\chi_\theta(t,r) = \frac{r}{2}B_z(t)+\frac{g(t)}{r}, \tag{6.37}$$

with an arbitrary function g. The electric field component E_r is now

$$E_r = \frac{M^2\hbar^2-q^2g(t)^2}{mqr^3}+\frac{r}{4mq}\left(q^2B_z^2-\frac{\hbar^2}{l(t)^4}+\frac{4m^2l''(t)}{l(t)}\right). \tag{6.38}$$

The demand $E_r=\frac{m\omega_z^2}{2q}r$ leads to the choice $g(t)=-M\hbar/q$ and

$$B_z(t) = \frac{\sqrt{\hbar^2-4m^2l(t)^3l''(t)+2m^2\omega_z^2l(t)^4}}{ql(t)^2}, \tag{6.39}$$

where $qB_z(t) > 0$ is assumed. The electric field components are finally

$$E_r = \frac{m\omega_z^2}{2q} r,\ E_\theta = -\frac{r}{2} B_z'(t). \tag{6.40}$$

Now, we have

$$\chi(t,r) = \left[\frac{r}{2} B_z(t) - \frac{M\hbar}{qr}\right] \hat{\theta} - \frac{m}{q} \frac{r l'(t)}{l(t)} \hat{r}. \tag{6.41}$$

Following from (6.14), we get the boundary conditions for $\vec{\chi}$

$$\begin{aligned} \vec{\chi}(0,r) &= \vec{A}_0 - \frac{\hbar}{q}\nabla\beta_0 = \left(\frac{rB_0}{2} - \frac{\hbar M}{qr}\right)\hat{\theta}, \\ \vec{\chi}(T,r) &= \vec{A}_T - \frac{\hbar}{q}\nabla\beta_T = \left(\frac{rB_T}{2} - \frac{\hbar M}{qr}\right)\hat{\theta}. \end{aligned} \tag{6.42}$$

With the χ given in (6.41), this is fulfilled if $l'(0) = 0$, $l'(T) = 0$, $B_z(0) = B_0$, and $B_z(T) = B_T$. To fulfil the last two conditions, we have to demand $l''(0) = 0$, $l''(T) = 0$.

The boundary conditions of Φ are fulfilled if the conditions (6.17) are satisfied, i.e. if

$$\frac{\partial\zeta}{\partial t}(0) = -\frac{1}{\hbar}\mathcal{E}_0,\ \frac{\partial\zeta}{\partial t}(T) = -\frac{1}{\hbar}\mathcal{E}_T. \tag{6.43}$$

A simple choice of ζ may be a polynomial of degree 3 that obeys all of the boundary conditions on ζ. Note that the magnetic and the electric fields do not depend on the choice of the time dependent global phase $\zeta(t)$.

An additional boundary condition on $l(t)$ can be derived by enforcing that the electric field is continuous at $t = 0$ and $t = T$, see the conditions (6.20). This requires $B_z'(0) = 0$ and $B_z'(T) = 0$. Differentiating the expression (6.39) for $B_z(t)$ with respect to time gives

$$B_z'(t) = -\frac{2\Big(l'(t)\left[\hbar^2 - m^2 l(t)^3 l''(t)\right] + m^2 l(t)^4 l'''(t)\Big)}{q l^3(t)\sqrt{\hbar^2 - 4m^2 l(t)^3 l''(t) + 2m^2\omega_z^2 l(t)^4}}. \tag{6.44}$$

Noting the boundary conditions on l already derived, this requires, in addition, that $l'''(0) = 0$, $l'''(T) = 0$.

In summary, the boundary conditions for $l(t)$ are

$$l(0) = l_0 = \sqrt{\frac{\hbar}{2m\widetilde{\omega}\,(0)}},\ l'(0) = l''(0) = l'''(0) = 0,$$
$$l(T) = l_T = \sqrt{\frac{\hbar}{2m\widetilde{\omega}\,(T)}},\ l'(T) = l''(T) = l'''(T) = 0. \tag{6.45}$$

These conditions are independent of the quantum numbers N and M.

If $l(t)$ satisfies these boundary conditions, the corresponding magnetic field and electric field are given by equations (6.39) and (6.40), and fulfil $\nabla \cdot \vec{E} = 0$ and $\nabla \times \vec{B} = 0$. They are also independent of the quantum numbers N and M. If the system starts in the corresponding eigenstate and if these fields are implemented, then the system will end with fidelity 1 in the final state. We will show that these schemes which do not change the quantum number could be alternatively derived using an invariant based approach.

6.5.2 Invariant based approach

Recall from section 2.2.2, that a Lewis-Riesenfeld invariant is a Hermitian operator $I(t)$ fulfilling

$$\frac{\partial}{\partial t} I(t) = \frac{i}{\hbar} \left[I(t), H(t) \right], \tag{6.46}$$

where $H(t)$ is the Hamiltonian for the system. If we disregard again the z dependent part, we find the following invariant for the Hamiltonian (6.24),

$$I(t) \;=\; -\hbar^2 l(t)^2 \Delta - 2ml'(t)l(t) \left(\frac{\hbar}{i} \frac{\partial}{\partial r} \right) r + \left(m^2 l'(t)^2 + \frac{\hbar^2}{4l(t)^2} \right) r^2, \tag{6.47}$$

where the function $l(t)$ has to be a solution of the following Ermakov-like equation

$$4m^2\frac{l''(t)}{l(t)} + 4m^2\widetilde{\omega}(t)^2 - \frac{\hbar^2}{l(t)^4} = 0. \tag{6.48}$$

(In [116], the case $\widetilde{\omega} = \omega$ was examined and an invariant was constructed. Eigenstates of this invariant which are simultaneously eigenstates of L_z were also constructed indirectly.) An explicit expression of the eigenstates of I is

$$\begin{aligned}\Gamma_{N,M}(t,r,\theta) &= \frac{1}{\sqrt{2\pi}}\sqrt{\frac{N!}{(N+|M|)!}}\frac{1}{l(t)}\left[\frac{r}{\sqrt{2}l(t)}\right]^{|M|} L_N^{|M|}\left(\frac{r^2}{2l(t)^2}\right) \\ &\quad\times\exp\left(-\frac{r^2}{4l(t)^2} + \frac{iml'(t)}{2\hbar l(t)}r^2 + iM\theta\right)\end{aligned} \tag{6.49}$$

where $N, M \in \mathbb{Z}$ and $l(t)$ is a solution of (6.48). The corresponding eigenvalue of I is $(2N + |M| + 1)\hbar^2$ and the corresponding eigenvalue of L_z is $M\hbar$. A more general invariant (which allows for a time dependent mass) was described in [255]. An eigenstate of a Lewis-Riesenfeld invariant is a solution to the Schrödinger equation for $H(t)$ up to a time dependent phase $\Pi_{N,M}(t)$ [116], which is here given by

$$\Pi_{N,M}(t) = \int_0^t dt' \left(M\omega(t') - \frac{(N+1)\hbar}{2ml(t')^2}\right). \tag{6.50}$$

The idea is to do inverse-engineering by demanding that the system follows the state $\Psi(t,r,\theta) = \Gamma_{N,M}(t,r,\theta)e^{i\Pi_{N,M}(t)}$. First, we choose an auxiliary function $l(t)$ (which has to fulfil different conditions at initial and final time, see below) and then we get $\widetilde{\omega}(t)$ from (6.48). At initial and final time the eigenstates of the invariant should coincide with the eigenstates of the Hamiltonian, i.e. $[I(0), H(0)] = 0 = [I(T), H(T)]$. Therefore, we have to impose the following boundary conditions for the auxiliary function $l(t)$:

$$\begin{aligned} l(0) = l_0 &= \sqrt{\frac{\hbar}{2m\widetilde{\omega}\,(0)}},\ l'(0) = 0, \\ l(T) = l_T &= \sqrt{\frac{\hbar}{2m\widetilde{\omega}\,(T)}},\ l'(T) = 0. \end{aligned} \tag{6.51}$$

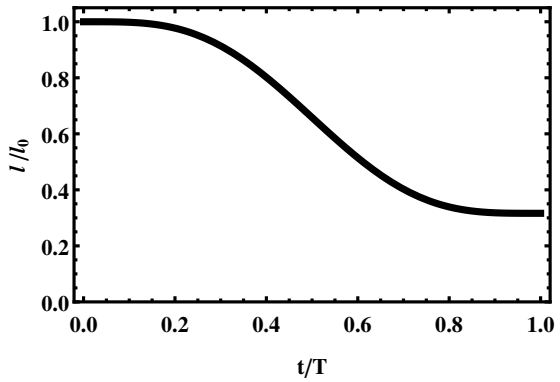


FIGURE 6.1: Auxiliary function $l(t)$ versus t.

From these boundary conditions and (6.48), it also follows that $l''(0) = 0$ and $l''(T) = 0$.

An additional boundary condition on $l(t)$ can be derived by enforcing that the electric field is continuous at $t = 0$ and $t = T$. This leads to $B_z'(0) = B_z'(T) = 0$ or $l'''(0) = l'''(T) = 0$. The complete list of boundary conditions is equivalent to (6.45) above. As already mentioned, we can now design first an auxiliary function $l(t)$ fulfilling the above boundary conditions and then calculate $\widetilde{\omega}(t)$ and hence the magnetic field strength $B_z(t)$ from (6.48). The resulting formula for $B_z(t)$ is the same as (6.39) above.

Summarising, the streamlined fast-forward formalism and the invariant based approach provide two ways to find the same boundary conditions for the auxiliary function $l(t)$ in this setting. So, for varying the magnetic field strength, both formalisms are equivalent as they both require that one chooses the auxiliary function $l(t)$ fulfilling these boundary conditions and then the corresponding physical potentials can be calculated in the same way. In the following we look at a numerical example of this procedure.

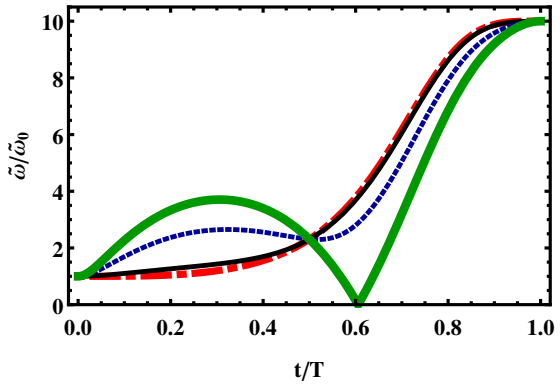


FIGURE 6.2: Frequency ratio $\widetilde{\omega}(t)/\widetilde{\omega}(0)$ versus t; $\mu \to \infty$ (red, dashed-dotted line), $\mu = 3$ (black, solid line), $\mu = 1$ (blue, dotted line), $\mu = 0.672$ (green, thick, solid line).

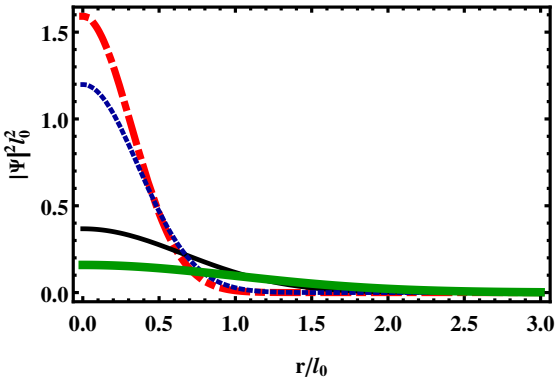


FIGURE 6.3: Time evolution of $|\Psi(t,r)|^2$ with $N = M = 0$; $t = 0$ (green, thick, solid line), $t = T/2$ (black, thin, solid line), $t = 3T/4$ (blue, dotted line), $t = T$ (red, dashed-dotted line).

6.5.3 Numerical Example

Let us first set $l(t) = l_0\lambda(\tau)$ where $\tau = t/T$. From the above formalism, the time dependence of $\widetilde{\omega}$ follows as

$$\widetilde{\omega}(t) = \widetilde{\omega}(0)\frac{1}{\lambda(\tau)^2}\sqrt{1 - \frac{\lambda(\tau)^3\lambda''(\tau)}{\mu^2}}, \tag{6.52}$$

where $\mu = T\widetilde{\omega}(0)$. μ can be seen as the final time in units of $1/\widetilde{\omega}(0)$. Therefore, decreasing μ corresponds to decreasing the total time T of the process, with fixed $\widetilde{\omega}(0)$ (i.e. fixed $\omega_0 = \frac{qB_z(0)}{2m} > 0$ and fixed ω_z). The limit $\mu \to \infty$ would correspond to the adiabatic limit where we get $\widetilde{\omega}(t)/\widetilde{\omega}(0) \to \frac{1}{\lambda^2(\tau)}$.

The corresponding magnetic field would then be given by (6.39) or in dimensionless variables

$$B_z(t) = \frac{\hbar}{q l_0^2} \frac{1}{\lambda(\tau)^2} \left[1 - \frac{\lambda(\tau)^3 \lambda''(\tau)}{\mu^2} + \frac{\nu^2}{2-\nu^2} \lambda(\tau)^4 \right]^{1/2} \tag{6.53}$$

where $\nu = \frac{\omega_z}{\omega_0}$ is the ratio between the two initial frequencies. This parameter ν is independent of the total time T. We want to have a trap setting at initial and final time, i.e. $\widetilde{\omega}(0)^2$ and $\widetilde{\omega}(T)^2$ should be positive. From this, ν must be in the range $0 \leq \nu < \sqrt{2}\min\{1, \omega_T/\omega_0\}$ where $\omega_T = \frac{qB_z(T)}{2m} > 0$.

Assuming a polynomial form of $\lambda(\tau)$ and using the above conditions, $\lambda(\tau)$ can be expressed as

$$\begin{aligned} \lambda(\tau) &= 1 - 20\,(l_T/l_0 - 1)\,\tau^7 + 70\,(l_T/l_0 - 1)\,\tau^6 \\ &\quad -84\,(l_T/l_0 - 1)\,\tau^5 + 35\,(l_T/l_0 - 1)\,\tau^4. \end{aligned} \tag{6.54}$$

The final value of the magnetic field is chosen in this example such that $\widetilde{\omega}(T)/\widetilde{\omega}(0) = c = 10$ (i.e. $l_T = l_0/\sqrt{10}$). The ratio between initial and final magnetic field is then

$$\frac{B_z(T)}{B_z(0)} = \sqrt{c^2 \left(1 - \frac{\nu^2}{2}\right) + \frac{\nu^2}{2}}.$$

Figure 6.1 is the corresponding plot of $l(t)$.

Figure 6.2 shows $\widetilde{\omega}(t)$ for different values of μ. For $\mu \approx 0.672$ (green, thick, solid line) $\widetilde{\omega}(t)^2 > 0$ is no longer fulfilled for all times. The requirement that $B_z(t) \in \mathbb{R}$ for all times results in a type of quantum speed limit of the form

$$\mu \geq \max_{\tau \in [0,1]} \left[\frac{\lambda(\tau)^3 \lambda''(\tau)}{1 + \nu^2 (2-\nu^2)^{-1} \lambda(\tau)^4} \right]^{1/2}. \tag{6.55}$$

Recently the topic of quantum speed limits has gained renewed interest in the literature. For example recent work has been done on extending the usual Mandelstam-Tamm(MT)[95, 96] and Margolus-Levitin(ML)[97] bounds for open system dynamics [256, 257]. It has also proven useful when using optimal control techniques

[258]. The quantum speed limit of our case is clearly more restrictive than the MT and ML bounds i.e. the minimal time of our speed limit is larger or equal than the time limit provided by those bounds.

As an example, the wavefunction at different times with $N = M = 0$ can be seen in figure 6.3. The shown time evolution is independent of μ, ν and depends only on the chosen form of $l(t)$.

6.5.4 Superposition

The electric and magnetic fields derived in the previous subsection are independent of the quantum numbers N and M. Therefore, the fields can be also applied to a superposition of different eigenstates with initial magnetic field B_0 and they will produce a superposition of eigenstates with final magnetic field B_T with the same populations as initially. Let us assume an initial wavefunction of the form

$$\Psi(0, r, \theta) = \sum_{N,M} c_{N,M} \Gamma_{N,M}(0, r, \theta), \tag{6.56}$$

where $\Gamma_{N,M}(t, r, \theta)$ are the eigenfunctions of the invariant given in (6.49) and $c_{N,M}$ are (constant) complex coefficients. Then it follows that the state at final time will be

$$\Psi(T, r, \theta) = \sum_{N,M} c_{N,M} e^{i\Pi_{N,M}(T)} \Gamma_{N,M}(T, r, \theta), \tag{6.57}$$

where $\Pi_{N,M}$ is given in (6.50), so the populations in the different eigenstates will be the same as initially, i.e. $\left|c_{N,M} e^{i\Pi_{N,M(t)}}\right|^2 = |c_{N,M}|^2$.

6.5.5 Stability

It is important that the scheme is not only fast but also stable concerning errors in the implementation. We want to examine the stability of the protocol if there is a systematic error in the magnetic field $B_z(t)$. We assume that the magnetic

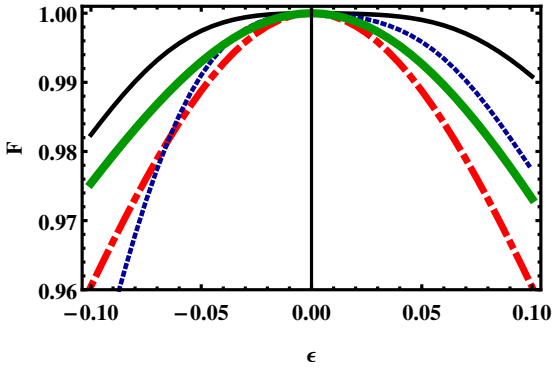


FIGURE 6.4: Fidelity F versus error ϵ; $\mu = 1, \nu = 0.1$ (blue, dotted line); $\mu = 1, \nu = 1$ (red, dashed-dotted line); $\mu = 3, \nu = 0.1$ (black, thin, solid line); $\mu = 3, \nu = 1$ (green, thick, solid line).

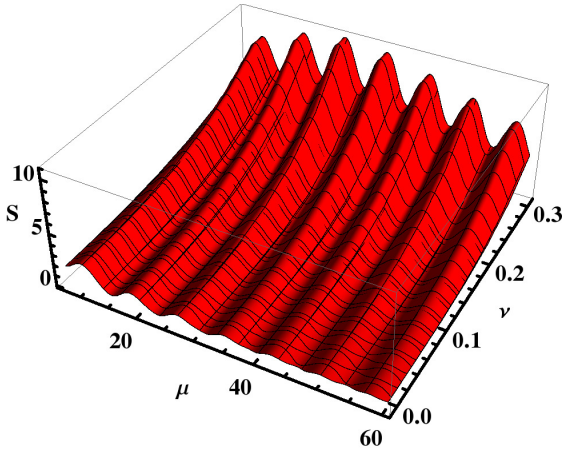


FIGURE 6.5: Systematic error sensitivity S versus μ and ν.

field is correctly implemented before and after the process, for $t \leq 0$ and $t \geq T$. Nevertheless, during the change of the magnetic field for for $0 < t < T$, we assume that an inaccurate magnetic field $\mathcal{B}_\epsilon(t) = B_z(t)(1+\epsilon)$ is implemented, where $B_z(t)$ is the correct one and ϵ a small relative systematic error which is unknown but constant.

We will examine the final fidelity as a function of ϵ for $N = M = 0$. The initial state is still $\Psi_\epsilon(0) = \psi_{N=0,M=0,l_0}$. The solution of the Schrödinger equation is then still given by $\Psi_\epsilon(t) = \Gamma_{0,0}(t)e^{i\Pi_{0,0}(t)}$ (see (6.49)) with $l(t)$ replaced by $\ell_\epsilon(t)$, a

solution of

$$4m^2\frac{\ell_\epsilon''(t)}{\ell_\epsilon(t)} + 4m^2\left[\left(\frac{q\mathcal{B}_\epsilon(t)}{2m}\right)^2 - \frac{\omega_z^2}{2}\right] - \frac{\hbar^2}{\ell_\epsilon(t)^4} = 0, \tag{6.58}$$

with $\ell_\epsilon(0) = l_0$ and $\ell_\epsilon'(0) = 0$. The fidelity at $t = T$ is now

$$\begin{aligned} F &= |\langle\Psi(T)|\Psi_\epsilon(T)\rangle| \\ &= \frac{2l(T)\ell_\epsilon(T)}{\sqrt{(l(T)^2 + \ell_\epsilon(T)^2)^2 + \frac{4m}{\hbar^2}l(T)^4\ell_\epsilon(T)^2\ell_\epsilon'(T)^2}}. \end{aligned} \tag{6.59}$$

Let $l(t)$ be given again as in (6.54). We once again fix $\widetilde{\omega}(T)/\widetilde{\omega}(0) = c = 10$, noting that the magnetic field is assumed to be error-free at the initial and final time. With these values fixed, the fidelity F only depends on μ, ν and ϵ. Note ν must be in the range $0 \leq \nu < \sqrt{2}$. The fidelity F for different combinations of μ and ν versus ϵ is shown in figure 6.4. One still gets a high fidelity even if there is a small, systematic error in the implementation of the magnetic field during the scheme. The scheme is, in some range, stable concerning this type of systematic error.

A sensitivity S of the scheme versus this systematic error can be defined as the negative curvature of the fidelity at $\epsilon = 0$, i.e. $S = -\frac{\partial^2 F}{\partial\epsilon^2}\big|_{\epsilon=0}$. This sensitivity S versus μ and ν is shown in figure 6.5. The sensitivity is increasing with increasing ratio ν for fixed μ. For fixed ν the sensitivity shows an oscillating behaviour with increasing μ. The sensitivity for arbitrary N and M is treated in Appendix D.3.

In order to have even more stability against systematic error in the magnetic field one could design a different $l(t)$ which minimises the sensitivity S and still fulfils the necessary boundary conditions (a similar strategy could also be applied to other types of systematic errors or random errors). As shown in Appendix D.3, it would be sufficient to minimise S only for $N, M = 0$.

6.6 Conclusion

In this chapter, we have put forward shortcuts to adiabaticity for a charged particle in an electromagnetic field focusing on a change of the radial spread in a Penning trap by modifying the magnetic field intensity. Two methods have been used for this: a streamlined version of the fast-forward formalism for an electromagnetic field, and an invariant based procedure. We have shown their equivalence for this operation. In general the fast-forward formalism presented in this chapter could be applied to other tasks for which the invariant approach is not well suited, such as transformations for individual states [136]. We also found that a type of quantum speed limit applies. Moreover, we have examined the scheme in the case of a systematic error in the magnetic field and shown its stability.

In the next chapter we will move on from STA processes to considering the effects of classical Poisson white noise on adiabatic processes.

Chapter 7

Effect of Poisson noise on adiabatic quantum control

7.1 Overview

We present a detailed derivation of the master equation describing a general time-dependent quantum system with classical Poisson white noise and outline its various properties. We discuss the limiting cases of Poisson white noise and provide approximations for the different noise strength regimes. We show that using the eigenstates of the noise superoperator as a basis can be a useful way of expressing the master equation. Using this we simulate various settings to illustrate different effects of Poisson noise. In particular, we show a dip in the fidelity as a function of noise strength where high fidelity can occur in the strong noise regime for some cases. We also investigate recent claims [31] that this type of noise may improve rather than destroy adiabaticity.

This chapter is based on the following publication:
A. Kiely, J. G. Muga and A. Ruschhaupt,
Effect of Poisson noise on adiabatic quantum control,
Phys. Rev. A **95** 012115 (2017).

7.2 Introduction

Understanding the effect of noise is of great interest for creating many of the predicted quantum technologies, e.g., for quantum metrology, quantum cryptography and quantum computation [2]. Almost all quantum systems suffer from decoherence in one form or another as it is impossible to isolate a system completely. Moreover interactions are needed to prepare, manipulate or read off the state of a system. Many recent publications have focused on combating different forms of decoherence by designing control schemes which are stable against specific forms of decoherence. Different strategies have been followed to design such schemes, e.g, dynamical decoupling [259], composite pulses [25–27], "shortcuts to adiabaticity" [21], and optimal control schemes [28–30].

There are different possible approaches for modelling this decoherence. One is based on a system-bath theory, where the bath dynamics are traced out under the Born-Markov approximation [260, 261]. Another approach is to assume a "classical noise", whereby the effect of the bath is described by a stochastic temporal evolution of a closed system. It has been shown for random telegraph noise (also known as a two-state Markov process or dichotomic Markov process) acting on a qubit, that these descriptions lead to equivalent dynamics [262]. Classical noise can of course also occur from classical fluctuations in the experimental system parameters. This noise could also be purposefully used to perform quantum simulations of environmentally induced decoherence [263]. Hence understanding the effect of classical noise on a quantum system can be quite useful.

In this chapter we will consider the effect of classical Poisson white noise (sometimes referred to as white shot noise) [264]. It is a sequence of random Markovian strikes with exponential inter-arrival times, i.e., which are Poisson distributed in time. It can be shown that if a general point process is boundedly finite and non-null, has complete independence and is stationary then it must be a Poisson point process [265]. There are also many other convergence results where Poisson processes emerge [266], which explain why it is so widely applicable. Poisson noise is useful for modeling noise processes which occur as a result of a small number

of discrete events, e.g., photons for electromagnetic radiation or electrons for electrical current. For a large number of events, the Poisson distribution tends to a Normal or Gaussian distribution.

White shot noise has already been widely discussed in the context of classical physics [267–269]. It has been applied to a variety of settings, e.g., micromechanical resonators [270], the statistics of current through Josephson junctions [271, 272], modelling random impulsive excitations [273], and its effects on transport of Brownian particles [274, 275]. It has also been used to model the effect of light intensity fluctuations on photochemical reactions [276] and radiation pressure shot noise in optomechanical systems [277, 278]. It was first considered in a quantum setting in [279] and has since been proposed as a power source for a quantum heat engine [280, 281]. It is also a special case of random telegraph noise with vanishing correlation time [282]. General random telegraph noise has been used to investigate noise effects on tunneling dynamics [283], model the environmental noise of a quantum dot [284], and model decoherence of qubits in general [285]. A master equation for random telegraph noise has been derived for time independent systems [286].

Previous works have mainly focussed on Gaussian noise for stochastic Hamiltonian evolution [287]. Hence, it would be interesting to have a tractable master equation for a more general non-Gaussian noise. Here we will present a general master equation for classical Poisson white noise and show how it simplifies in two-level systems [280, 281] and reduces to Gaussian white noise in the appropriate limits [264].

In a recent paper by Jing et al. [31], it is claimed that Poisson noise can counterintuitely help improve adiabaticity for increasing noise strength. We will show that what is referred to as strong noise is actually a large noise bias which implies a stronger Hamiltonian. By coherently increasing the energy of the system (for a fixed total time), one will of course improve the adiabaticity. However, we will also show that for a general quantum system with Poisson noise, the system will follow specific eigenstates of the noise superoperator (in the limit of strong noise) in a

manner analogous to the adiabatic theorem. This has been previously outlined for the case of Gaussian white noise and has been connected to the effect of repeated measurements or the quantum Zeno effect [288–292].

The rest of this chapter is outlined as follows. In the next section, the master equation for a general time-dependent quantum system with Poisson noise is derived and its general properties discussed including the special case of a two-level system. In section 7.4, we review the adiabatic approximation for density matrices and derive approximations for the cases of weak and strong Poisson noise. In section 7.5, we solve the master equation numerically for several cases, including the setting described in [31] and Stimulated Raman adiabatic passage (STIRAP) [113] type schemes in three-level systems. The examples we present will illustrate the different effects of Poisson noise. Finally, in section 7.6, we summarize our work and make some concluding remarks.

7.3 Master equation for Poisson noise

We will first derive the master equation for Poisson noise. Let us consider a Hamiltonian

$$H(t) = H_0(t) + z(t) H_1(t), \tag{7.1}$$

where $z(t)$ is a real function, given by classical Poisson white noise

$$z(t) = \sum_{i=1}^{N(t)} \xi_i \delta(t - t_i). \tag{7.2}$$

The probability of the number of strikes $N(t)$ is given by a Poissonian counting process such that the probability of n strikes after a time t is

$$Q(N(t) = n) = (\nu t)^n \frac{e^{-\nu t}}{n!}, \tag{7.3}$$

and the random times t_i are uniformly distributed on the interval $(0, t)$. The strength of the strikes ξ_i are statistically independent of the times and are distributed according to a probability density $P(\xi)$. The quantity ν (which corresponds to the quantity W in [31]) can be thought of as the average frequency of the noise shots. Note that $z(t)$ is dimensionless and the strength of a strike ξ_i has dimensions of time. The average and two-time correlation function are given by

$$\langle z(t)\rangle = \nu\langle\xi\rangle, \tag{7.4}$$

$$\langle z(t)z(s)\rangle - \langle z(t)\rangle\langle z(s)\rangle = \nu\langle\xi^2\rangle\delta(t-s). \tag{7.5}$$

For a particular realization of the noise $z\,(t)$, the Liouville-von Neumann equation for the density matrix $\rho_z\,(t)$ is given by

$$\dot{\rho}_z\,(t) = -\frac{i}{\hbar}\left[H(t), \rho_z\,(t)\right]. \tag{7.6}$$

By taking the average over all realizations of $z\,(t)$ and defining a new density matrix $\rho\,(t) = \langle\rho_z\,(t)\rangle_z$ this becomes

$$\dot{\rho}\,(t) = -\frac{i}{\hbar}\left[H_0(t), \rho\,(t)\right] - \frac{i}{\hbar}\left\langle z\,(t)\left[H_1(t), \rho_z\,(t)\right]\right\rangle_z. \tag{7.7}$$

From Eq. (7.6) it can be seen that $\rho_z(t)$ remains a positive matrix for all times. Since ρ is an average of positive matrices and positivity is preserved under summation, it follows that ρ is also positive for all times.

We now apply the Klyatskin-Tatarsky formula [279, 293] (one could also consider using the Shapiro-Loginov formula [294]) which has the following form for a Poisson process

$$\langle z(t)R[z]\rangle_z = \nu\int_{-\infty}^{\infty} d\xi P(\xi)\int_0^{\xi} d\eta\langle\exp\left[\eta\frac{\delta}{\delta z(t)}\right]R[z]\rangle_z, \tag{7.8}$$

where $R[z]$ is some functional of $z(t)$. In this case $R[z] = [H_1, \rho_z]$. From (7.6), the functional derivative is

$$\frac{\delta}{\delta z(t)}\rho_z(t) = -\frac{i}{\hbar}\left[H_1(t), \rho_z(t)\right], \tag{7.9}$$

and

$$\exp\left[\eta\frac{\delta}{\delta z(t)}\right]\rho_z(t) = A_\eta \rho_z(t) A_\eta^\dagger, \tag{7.10}$$

where $A_\eta = e^{-i\eta H_1(t)/\hbar}$. From this we arrive at the master equation (where the explicit time dependence has been dropped),

$$\dot{\rho} = -\frac{i}{\hbar}\left[H_0, \rho\right] + \nu\int_{-\infty}^{\infty} d\xi\, P(\xi)\left(A_\xi \rho A_\xi^\dagger - \rho\right), \tag{7.11}$$

where the following identity has been used

$$\int_0^\xi d\eta\left[H_1, A_\eta \rho A_\eta^\dagger\right] = i\hbar\left(A_\xi \rho A_\xi^\dagger - \rho\right). \tag{7.12}$$

Note that (7.11) is very close to Lindblad form [295], where the operators A_ξ correspond to the Lindblad operators and the sum has been replaced by an integral. By now applying the Hadamard lemma [296], we get the final form of the master equation,

$$\dot{\rho} = \mathcal{L}_0(\rho) + \mathcal{L}_1(\rho), \tag{7.13}$$

where

$$\mathcal{L}_0(\rho) = -\frac{i}{\hbar}\left[H_0, \rho\right], \tag{7.14}$$

$$\mathcal{L}_1(\rho) = \nu\sum_{s=1}^{\infty}\frac{1}{s!}\left(-\frac{i}{\hbar}\right)^s\langle\xi^s\rangle\left[H_1, \rho\right]_s, \tag{7.15}$$

$[H_1, \rho]_s = \left[H_1, [H_1, \rho]_{s-1}\right]$ and $[H_1, \rho]_0 = \rho$. Note that $\mathcal{L}_0$ and $\mathcal{L}_1$ commute when the two Hamiltonians (H_0 and H_1) commute. It is clear from the form of the master equation that it is linear in ρ, and by taking the trace of (7.13), we get

that $\partial_t \mathrm{tr}\rho = 0$ and hence the trace is preserved.

Gaussian white noise is recovered if one takes the limit $\nu \to \infty$ such that $\nu \langle \xi \rangle \to \widetilde{J}$, a constant, $\nu \langle \xi^2 \rangle \to 2\widetilde{D}$, a positive constant, and $\nu \langle \xi^s \rangle \to 0 \; \forall s > 2$ [264]. As an explicit example where this happens, let us choose a Laplace distribution $P(\xi) = \left(\frac{1}{2A}\right) \exp\left(-|\xi|/A\right)$ with $A > 0$. Since the distribution is symmetric, the odd moments are 0, i.e., $\langle \xi^{2n+1} \rangle = 0$ for $n \in \mathbb{N}$ and the even ones are given by $\langle \xi^{2n} \rangle = (2n)!\, A^{2n}$. From this we can see that $\langle \xi \rangle = 0$ and that, setting $A = \sqrt{\frac{\widetilde{D}}{\nu}}$, then $\nu \langle \xi^2 \rangle = 2\widetilde{D}$. In general we get that $\nu \langle \xi^{2n} \rangle = (2n!)\, \widetilde{D}^n \nu^{1-n}$, hence, $\nu \langle \xi^s \rangle \to 0 \; \forall s > 2$ as $\nu \to \infty$. In this case (and in general taking this limit), the master equation simply reduces to a master equation for Gaussian white noise,

$$\dot{\rho} = -\frac{i}{\hbar}\left[H_0 + \widetilde{J} H_1, \rho\right] - \frac{\widetilde{D}}{\hbar^2}\left[H_1, [H_1, \rho]\right], \tag{7.16}$$

which could also be derived directly using Novikov's theorem [297].

7.3.1 General properties of $\mathcal{L}_0$ and $\mathcal{L}_1$

We will now outline some general properties of $\mathcal{L}_0$ and $\mathcal{L}_1$. In the following, the density matrix $\rho(t)$ will be represented as a vector $|\rho\rangle\rangle$ in a larger Hilbert space such that the scalar product is preserved, i.e., for two operators M_1 and M_2, $\langle\langle M_1 | M_2 \rangle\rangle = \mathrm{tr}\left(M_1^\dagger M_2\right)$. The equivalence between the two representations will be indicated as $|\rho\rangle\rangle \equiv \rho(t)$. The superoperators $\mathcal{L}_0$ and $\mathcal{L}_1$ can be then seen as linear operators acting on the vector $|\rho\rangle\rangle$.

Let us start by examining $\mathcal{L}_0$, see (7.14). Let $|\phi_n^{(0)}(t)\rangle$ be an instantaneous eigenvector of H_0 with eigenvalue $E_n^{(0)}(t)$ and $n \in \mathbb{N}$ (assuming discrete eigenvalues). Defining $|A_{n,m}(t)\rangle\rangle \equiv |\phi_n^{(0)}(t)\rangle\langle\phi_m^{(0)}(t)|$, we get

$$\mathcal{L}_0(t)|A_{n,m}(t)\rangle\rangle = \alpha_{n,m}(t)|A_{n,m}(t)\rangle\rangle, \tag{7.17}$$

where $\alpha_{n,m} = -\frac{i}{\hbar}\left(E_n^{(0)} - E_m^{(0)}\right)$ for all $n, m \in \mathbb{N}$. Therefore, $|A_{n,m}\rangle\rangle$ is an eigenvector of the superoperator $\mathcal{L}_0$ with eigenvalue $\alpha_{n,m}$. Because the eigenvalues $\alpha_{n,m}$ are purely imaginary, $\mathcal{L}_0$ is anti-Hermitian, i.e., $\mathcal{L}_0^\dagger = -\mathcal{L}_0$.

Let us now examine $\mathcal{L}_1$, see (7.15). Let $|\phi_n^{(1)}(t)\rangle$ be an eigenvector of H_1 with eigenvalue $E_n^{(1)}(t)$. Defining $|B_{n,m}(t)\rangle\rangle \equiv |\phi_n^{(1)}(t)\rangle\langle\phi_m^{(1)}(t)|$, we get

$$\begin{aligned}\mathcal{L}_1|B_{n,m}(t)\rangle\rangle &= \nu\sum_{s=1}^{\infty}\frac{1}{s!}\left(-\frac{i}{\hbar}\right)^s\langle\xi^s\rangle\left(E_n^{(1)} - E_m^{(1)}\right)^s|B_{n,m}(t)\rangle\rangle \\ &= \beta_{n,m}(t)|B_{n,m}(t)\rangle\rangle. \end{aligned} \tag{7.18}$$

Therefore, $|B_{n,m}\rangle\rangle$ is an eigenvector of the superoperator $\mathcal{L}_1$ with eigenvalue

$$\begin{aligned}\beta_{n,m} &= \nu\sum_{s=1}^{\infty}\frac{1}{s!}\left(-\frac{i}{\hbar}\right)^s\langle\xi^s\rangle\left(E_n^{(1)} - E_m^{(1)}\right)^s \\ &= \nu\left[C_\xi\left(\frac{E_m^{(1)} - E_n^{(1)}}{\hbar}\right) - 1\right], \end{aligned} \tag{7.19}$$

where $C_\xi(x) = \langle e^{i\xi x}\rangle$ is the characteristic function of the probability distribution $P(\xi)$.

We now recall some properties of a general characteristic function which are $|C_\xi(x)| \leq 1$, $C_\xi(0) = 1$ and $C_\xi(-x) = C_\xi(x)^*$ for real x. From the last property, it follows that $\beta_{n,m} = \beta_{m,n}^*$. Moreover, $-2\nu \leq \mathrm{Re}(\beta_{n,m}) \leq 0$ and $-\nu \leq \mathrm{Im}(\beta_{n,m}) \leq \nu$ for all n, m and $\beta_{n,n} = 0$ for all n. For a symmetric probability distribution, i.e., $P(\xi) = P(-\xi)$, $\mathcal{L}_1$ is Hermitian and negative. In general, $\mathcal{L}_1$ is always diagonalizable but not necessarily Hermitian.

For numerical treatment it is often useful to represent the master equation in the eigenbasis of $\mathcal{L}_1$, i.e., $|\rho\rangle\rangle = \sum_{n,m} d_{n,m}|B_{n,m}\rangle\rangle$. Using (7.13) we get the following

equation for the coefficients of $|\rho\rangle\rangle$ in this basis

$$\begin{aligned}
&\dot{d}_{n,m} - \beta_{n,m} d_{n,m} \\
&\quad + \sum_{i,j} \left[\delta_{m,j} \left(\langle \phi_n^{(1)} | \dot{\phi}_i^{(1)} \rangle + \frac{i}{\hbar} \langle \phi_n^{(1)} | H_0 | \phi_i^{(1)} \rangle \right) d_{i,j} \right. \\
&\quad \left. + \delta_{n,i} \left(\langle \dot{\phi}_j^{(1)} | \phi_m^{(1)} \rangle - \frac{i}{\hbar} \langle \phi_j^{(1)} | H_0 | \phi_m^{(1)} \rangle \right) d_{i,j} \right] = 0.
\end{aligned} \tag{7.20}$$

In this representation the total contribution from $\mathcal{L}_1$ arises solely from the eigenvalues $\beta_{n,m}$. The condition for ρ to remain Hermitian is simply $d_{n,m} = d_{m,n}^*$ and for it to be pure is $\sum_{n,m} |d_{n,m}|^2 = 1$. By taking the complex conjugate of (7.20) we see that ρ will indeed remain Hermitian. So in summary, the master equation is linear and preserves both the trace and Hermiticity.

7.3.2 Special case: Two-level quantum system

As a special case, consider a two-level quantum system with Hamiltonians given by

$$H_0(t) = \frac{\hbar}{2} \begin{pmatrix} -\Delta(t) & \Omega_R(t) - i\Omega_I(t) \\ \Omega_R(t) + i\Omega_I(t) & \Delta(t) \end{pmatrix}, \tag{7.21}$$

$$H_1(t) = \frac{\hbar}{2} \begin{pmatrix} -\widetilde{\Delta}(t) & \widetilde{\Omega}_R(t) - i\widetilde{\Omega}_I(t) \\ \widetilde{\Omega}_R(t) + i\widetilde{\Omega}_I(t) & \widetilde{\Delta}(t) \end{pmatrix}. \tag{7.22}$$

Physically, the Hamiltonian H_0 could, for example, correspond to an atom illuminated by a laser which couples only two atomic levels. In that case, $\Omega_R + i\Omega_I$ would be the Rabi frequency of the coupling and Δ would be the detuning of the laser. Possible physical motivations of H_1 will be given in the examples in section 7.5.

The eigenvalues of H_0 and H_1 are $E_\pm^{(0)} = \pm\frac{\hbar}{2}\sqrt{\Omega_R^2 + \Omega_I^2 + \Delta^2}$ and $E_\pm^{(1)} = \pm\frac{\hbar}{2}\sqrt{\widetilde{\Omega}_R^2 + \widetilde{\Omega}_I^2 + \widetilde{\Delta}^2}$ respectively. The master equation, (7.11), can now be simplified further by applying the Hadamard lemma [296] to the integrand of the last term and noticing a recursion relation between nested commutators (see Appendix E.1). We get

$$\begin{aligned}\dot{\rho} &= -\frac{i}{\hbar}\left[H_0, \rho\right] - \frac{D}{\hbar^2}\left[H_1, \left[H_1, \rho\right]\right] - \frac{i}{\hbar}J\left[H_1, \rho\right] \\ &= -\frac{i}{\hbar}\left[(H_0 + JH_1), \rho\right] - \frac{D}{\hbar^2}\left[H_1, \left[H_1, \rho\right]\right], \end{aligned} \tag{7.23}$$

where

$$\begin{aligned} J &= \nu\frac{\hbar}{2\sqrt{\chi}}\int_{-\infty}^{\infty} d\xi\, P\left(\xi\right)\sin\left(\frac{2}{\hbar}\xi\sqrt{\chi}\right) = \nu\sum_{l=0}^{\infty}\frac{\chi^l}{(2l+1)!}2^{2l}\left(-\frac{i}{\hbar}\right)^{2l}\left\langle\xi^{2l+1}\right\rangle, \\ D &= \frac{\nu\hbar^2}{2\chi}\int_{-\infty}^{\infty} d\xi\, P\left(\xi\right)\sin^2\left(\frac{1}{\hbar}\xi\sqrt{\chi}\right) = -\nu\hbar^2\sum_{k=1}^{\infty}\frac{\chi^{k-1}}{(2k)!}2^{2(k-1)}\left(-\frac{i}{\hbar}\right)^{2k}\left\langle\xi^{2k}\right\rangle, \end{aligned} \tag{7.24}$$

and $\chi = \left(E_\pm^{(1)}\right)^2$. This is the final version of the master equation for Poisson noise in a two-level quantum system. J and D depend on the odd and even moments of $P(\xi)$ respectively. Note that the *noise bias* J (which is dimensionless) only modifies the coherent evolution whereas the *noise strength* D (which has dimensions of time) has a decoherent effect. In this case the eigenvalues of the superoperator $\mathcal{L}_1$ (see (7.19)) are given by

$$\beta_{n,m} = -\frac{i}{\hbar}J(E_n^{(1)} - E_m^{(1)}) - \frac{D}{\hbar^2}(E_n^{(1)} - E_m^{(1)})^2, \tag{7.25}$$

where $n = \pm$ and $m = \pm$.

The master equation for a two-level system with Poisson noise has the same form as the case of Gaussian white noise (see (7.16)) apart from different expressions for the constant coefficients J and D. In the limit in which Poisson noise converges to Gaussian noise, then $J \to \widetilde{J}$ and $D \to \widetilde{D}$.

7.4 Approximations for weak and strong Poisson noise

In this section we consider the different regimes of adiabaticity with no noise, weak noise and strong noise.

7.4.1 Adiabatic approximation without noise

We will first review the adiabatic approximation without noise. The master equation is then

$$\frac{d}{dt}|\rho(t)\rangle\rangle = \mathcal{L}_0(t)|\rho(t)\rangle\rangle. \tag{7.26}$$

We are interested in the dynamics for a slowly varying $\mathcal{L}_0$, i.e., for large total time T. In the usual adiabatic approximation for the Schrödinger equation with an initial state $|\psi(0)\rangle = \sum_n a_n|\phi_n^{(0)}(0)\rangle$, the state evolves as

$$\begin{aligned} |\psi(T)\rangle &\approx |\psi_{ad}(T)\rangle \\ &= \sum_n a_n \exp\left[-\frac{i}{\hbar}\int_0^T ds\, E_n^{(0)}(s) - \int_0^T ds \langle\phi_n^{(0)}(s)|\dot{\phi}_n^{(0)}(s)\rangle\right] |\phi_n^{(0)}(T)\rangle \end{aligned} \tag{7.27}$$

for large T. To simplify the notation, we will now assume that the time-dependent phase of $|\phi_n^{(0)}(t)\rangle$ has been chosen such that $\langle\phi_n^{(0)}(t)|\dot{\phi}_n^{(0)}(t)\rangle = 0$ for all n and t, i.e., the parallel transport condition. This condition can always be fulfilled. While it is always true that $\langle\langle A_{n,n}(t)|\dot{A}_{n,n}(t)\rangle\rangle = 0$, with this assumption about $|\phi_n^{(0)}(t)\rangle$, it also follows $\langle\langle A_{n,m}(t)|\dot{A}_{n,m}(t)\rangle\rangle = 0$ for all n, m.

Motivated by (7.27), we now use the ansatz

$$|\rho(t)\rangle\rangle = \sum_{n,m} b_{n,m}(t) \exp\left[\Lambda_{n,m}(t)\right] |A_{n,m}(t)\rangle\rangle, \tag{7.28}$$

for the density matrix, where $b_{n,m}(t)$ are time-dependent coefficients and

$$\Lambda_{n,m}(t) = \int_0^t ds\, \alpha_{n,m}(s). \tag{7.29}$$

Inserting this into (7.26), it follows that

$$\dot{b}_{n,m}(t) = - \sum_{\substack{l,k \\ (l,k)\neq(n,m)}} \exp\left[\Lambda_{l,k}(s) - \Lambda_{n,m}(s)\right] \langle\langle A_{n,m}|\dot{A}_{l,k}\rangle\rangle b_{l,k}(t). \tag{7.30}$$

By assuming a large value of T and following similar steps as in the derivation of the adiabatic approximation for pure states, we get that $b_{n,m}(T) \approx b_{n,m}(0) = \langle\langle A_{n,m}(0)|\rho(0)\rangle\rangle$. Therefore the adiabatic approximation is

$$|\rho(T)\rangle\rangle \approx \sum_{n,m} b_{n,m}(0) \exp\left[\Lambda_{n,m}(T)\right] |A_{n,m}(T)\rangle\rangle. \tag{7.31}$$

Let us consider that the system starts in a pure state $|\psi(0)\rangle = \sum_n a_n |\phi_n^{(0)}(0)\rangle$ (where $\sum_n |a_n|^2 = 1$). It follows that $|\rho(0)\rangle\rangle \equiv |\psi(0)\rangle\langle\psi(0)|$ and so $b_{n,m}(0) = a_n a_m^*$. Then,

$$\begin{aligned} |\rho(T)\rangle\rangle &\approx \sum_{n,m} a_n a_m^* \exp\left[\Lambda_{n,m}(T)\right] |A_{n,m}(T)\rangle\rangle \\ &\equiv |\psi_{ad}(T)\rangle\langle\psi_{ad}(T)|, \end{aligned} \tag{7.32}$$

where $|\psi_{ad}(T)\rangle$ is given in (7.27). If the system starts in an energy eigenstate of H_0, we get that $|\rho(0)\rangle\rangle = |A_{N,N}(0)\rangle\rangle \equiv |\phi_N^{(0)}(0)\rangle\langle\phi_N^{(0)}(0)|$ for a fixed N. It follows $b_{n,m}(0) = \delta_{n,N}\delta_{m,N}$. Therefore the adiabatic approximation becomes

$$|\rho(T)\rangle\rangle \approx |A_{N,N}(T)\rangle\rangle \tag{7.33}$$

since $\alpha_{N,N}(t) = 0$.

7.4.2 Approximation for weak noise in an adiabatic process

In this section, we will consider the effect of weak Poisson noise on an adiabatic process. We start with the general master equation for Poisson noise

$$\frac{d}{dt}|\rho(t)\rangle\rangle = [\mathcal{L}_0(t) + \kappa\mathcal{L}_1(t)]\,|\rho(t)\rangle\rangle, \tag{7.34}$$

where we have included a dimensionless coefficient κ which is an auxiliary variable used to perform a series expansion. It corresponds to the strength of the noise superoperator $\mathcal{L}_1$ and will be assumed to be a small quantity in this section.

We assume that the system starts at $t = 0$ in a pure state $|\rho(0)\rangle\rangle \equiv |\psi(0)\rangle\langle\psi(0)|$, where $|\psi(0)\rangle = \sum_n a_n|\phi_n^{(0)}(0)\rangle$. It should end at $t = T$ in the state $|\rho_{ad}\rangle\rangle \equiv |\psi_{ad}(T)\rangle\langle\psi_{ad}(T)|$. We define a fidelity F, such that $F^2 = \langle\langle\rho_{ad}|\rho(T)\rangle\rangle = \langle\psi_{ad}(T)|\rho(T)|\psi_{ad}(T)\rangle$. We can expand this in terms of the small quantity κ to get the approximation

$$F(\kappa) \approx F(0) + \kappa F'(0), \tag{7.35}$$

where the noise sensitivity is

$$F'(0) = \frac{1}{2F(0)}\int_0^T dt\langle\langle\widetilde{\rho}(t)|\mathcal{L}_1(t)|\rho_0(t)\rangle\rangle. \tag{7.36}$$

We have defined $|\widetilde{\rho}(t)\rangle\rangle = \mathcal{U}_0(t,T)|\rho_{ad}\rangle\rangle$ and $|\rho_0(t)\rangle\rangle = \mathcal{U}_0(t,0)|\rho(0)\rangle\rangle$, where $\mathcal{U}_0(t_2,t_1) = \mathcal{T}\exp\left[\int_{t_1}^{t_2} ds\mathcal{L}_0(s)\right]$ is the noise-less time-evolution operator and $\mathcal{T}$ is the time ordering operator. Note that we do not assume perfect adiabatic transfer in the unperturbed case.

If the system starts at $t = 0$ in an energy eigenstate of H_0, i.e., $|\rho(0\rangle\rangle = |A_{NN}(0)\rangle\rangle \equiv |\phi_N^{(0)}(0)\rangle\langle\phi_N^{(0)}(0)|$, the target state is $|\rho_{ad}\rangle\rangle = |A_{NN}(T)\rangle\rangle \equiv |\phi_N^{(0)}(T)\rangle\langle\phi_N^{(0)}(T)|$. In this case, the noise sensitivity is

$$F'(0) = \frac{1}{2F(0)}\int_0^T dt\langle\langle\widetilde{A}_{NN}(t)|\mathcal{L}_1(t)|\rho_0(t)\rangle\rangle, \tag{7.37}$$

where $|\widetilde{A}_{NN}(t)\rangle\rangle = \mathcal{U}_0(t,T)|A_{NN}(T)\rangle\rangle$. In the following examples, the noise sensitivity $F'(0)$ is negative. This shows that in these cases a small amount of noise will not improve the fidelity, contrary to the claim in [31].

7.4.3 Strong noise limit

In this section, we will consider the case of strong noise, i.e., where $\mathcal{L}_1$ is dominant. Note that this is not the same as the Gaussian noise limit. The master equation is once again given by

$$\frac{d}{dt}|\rho(t)\rangle\rangle = [\mathcal{L}_0(t) + \kappa\mathcal{L}_1(t)]\,|\rho(t)\rangle\rangle, \tag{7.38}$$

where κ is again an auxiliary variable (which corresponds to the strength of the superoperator $\mathcal{L}_1$) used for the purposes of approximation. In this case it will be assumed to be large. A discussion of the adiabatic condition for non-unitary evolution can be found in [299]. However the setting in (7.38) differs from this in the sense that only part of the right-hand side is dominant. Note that $\mathcal{L}_0(t)$ and $\mathcal{L}_1(t)$ can always be diagonalized (see section 7.3.1). The case of an adiabatic approximation where the superoperator can only be tranformed in a Jordan canonical form can be found in [298].

Recall that the instantaneous eigenvectors of $\mathcal{L}_1$ are $|B_{n,m}\rangle\rangle \equiv |\phi_n^{(1)}\rangle\langle\phi_m^{(1)}|$ with corresponding eigenvalues $\beta_{n,m}$ (see section 7.3.1). To simplify the notation, we will assume that $\langle\phi_n^{(1)}(t)|\dot{\phi}_n^{(1)}(t)\rangle = 0$ for all n and t. It then follows that $\langle\langle B_{n,m}(t)|\dot{B}_{n,m}(t)\rangle\rangle = 0$ for all n, m. Moreover, we assume a symmetric probability distribution $P(\xi)$ which results in real negative eigenvalues $\beta_{n,m}$ and $\mathcal{L}_1$ Hermitian. While it is always the case that $\beta_{n,n} = 0$, we also assume that $\beta_{n,m} = 0$ if and only if $n = m$. This is fulfilled if the eigenvalues of H_1 are non-degenerate and $C_\xi(x) = 1$ if and only if $x = 0$.

If the initial state is expressed as $|\rho(0)\rangle\rangle = \sum_{n,m} c_{n,m}(0)|B_{n,m}(0)\rangle\rangle$ (where $c_{n,m}(0) = \langle\langle B_{n,m}(0)|\rho(0)\rangle\rangle$), then motivated by the usual adiabatic theorem in quantum mechanics and by [298] we use the general ansatz

$$|\rho(t)\rangle\rangle = \sum_{n,m} c_{n,m}(t) \exp\left[\tilde{\Lambda}_{n,m}(t)\right] |B_{n,m}(t)\rangle\rangle, \tag{7.39}$$

where

$$\tilde{\Lambda}_{n,m}(t) = \int_0^t ds\ \left[\kappa\beta_{n,m}(s) + \langle\langle B_{n,m}(s)|\mathcal{L}_0|B_{n,m}(s)\rangle\rangle\right]. \tag{7.40}$$

If we now insert this into (7.38), we get that

$$\dot{c}_{n,m}(t) = \sum_{\substack{l,k \\ (l,k)\neq(n,m)}} \exp\left[\tilde{\Lambda}_{l,k}(t) - \tilde{\Lambda}_{n,m}(t)\right] M_{n,m,l,k}(t) c_{l,k}(t), \tag{7.41}$$

where

$$M_{n,m,l,k}(t) = \langle\langle B_{n,m}|\mathcal{L}_0|B_{l,k}\rangle\rangle - \langle\langle B_{n,m}|\dot{B}_{l,k}\rangle\rangle. \tag{7.42}$$

For large noise κ (see Appendix E.2 for details)

$$|\rho(t)\rangle\rangle \approx \sum_{n,m} c_{n,m}(0) \exp\left[\tilde{\Lambda}_{n,m}(t)\right] |B_{n,m}(t)\rangle\rangle. \tag{7.43}$$

Note that $\tilde{\Lambda}_{n,n}(t) = 0$. If $n \neq m$, $\exp\left[\tilde{\Lambda}_{n,m}(t)\right] \to 0$ in the limit of $\kappa \to \infty$. Hence the final result is

$$\begin{aligned} |\rho(t)\rangle\rangle &\approx \sum_n c_{n,n}(0)|B_{n,n}(t)\rangle\rangle \\ &= |\rho_\infty(t)\rangle\rangle. \end{aligned} \tag{7.44}$$

We define the strong noise limit fidelity F_∞ as $F_\infty^2 = \langle\langle \rho_\infty|\rho\rangle\rangle$. The only remaining elements are those which are not affected by $\mathcal{L}_1$, i.e., $\mathcal{L}_1|B_{n,n}\rangle\rangle = 0$. These are the diagonal elements of the density matrix in the eigenbasis of H_1. For example, if $H_1 = H_0$, the noise term simply projects on the eigenstates of H_0. Hence, if

the state starts in an eigenstate of H_0, it will remain in that eigenstate in the strong noise regime. However, a superposition of eigenstates will not survive, as the noise term clearly kills any coherence terms (or off-diagonal elements of the density matrix). This is different from the adiabatic approximation applied to $\mathcal{L}_0$ for large time in a previous subsection.

The purity of the general ansatz, (7.39), becomes

$$\langle\langle\rho(t)|\rho(t)\rangle\rangle \to \sum_n c_{n,n}(0)^2 \tag{7.45}$$

in the limit $\kappa \to \infty$. The system will remain in a pure state in the strong noise limit if the density matrix is diagonal in the H_1 eigenbasis at $t = 0$.

7.5 Poisson noise effect on adiabaticity

In this section, we will present different types of effects of Poisson noise on adiabaticity using several illustrating examples.

7.5.1 Phase-changing scheme in a two-level system

We start by examining the setting which is also considered in [31], i.e., a two-level quantum system with Poisson white noise. While the Poisson noise used in [31] is always Gaussian, we will continue to use the notation for Poisson white noise since obtaining the results for Gaussian white noise only requires a relabelling $J \to \widetilde{J}$ and $D \to \widetilde{D}$. The noise Hamiltonian is $H_1 = H_0$ such that the master equation is

$$\dot{\rho} = -\frac{i}{\hbar}\left[(1+J)H_0, \rho\right] - \frac{D}{\hbar^2}\left[H_0, [H_0, \rho]\right]. \tag{7.46}$$

Instead of averaging over different realizations of the noise as is done in [31], we will directly solve this master equation numerically. This avoids any convergence issues that could arise when numerically averaging over multiple realizations. We

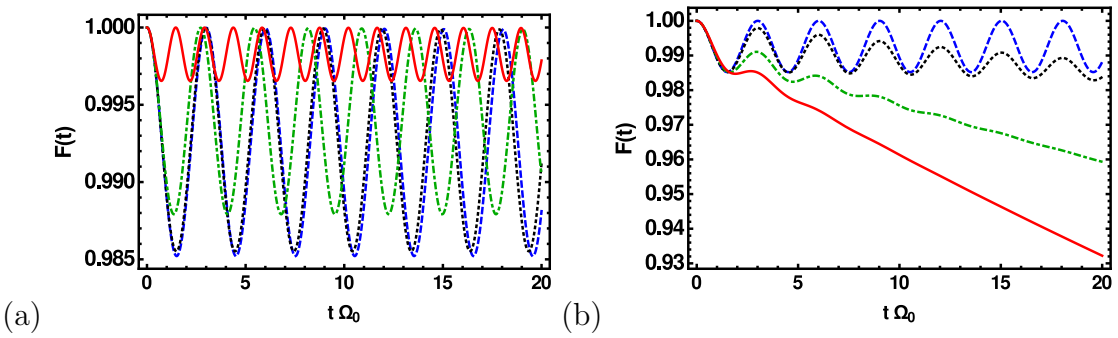


FIGURE 7.1: Phase changing scheme. Fidelity $F(t)$ versus time t. (a) $J = 0$ (blue, dashed line), $J = 0.01$ (black, dotted line), $J = 0.1$ (green, dot-dashed line), $J = 1$ (red, solid line), $D\Omega_0 = 10^{-4}$ in all cases. (b) $J = 0$; $D = 0$ (blue, dashed line), $D\Omega_0 = 0.01$ (black, dotted line), $D\Omega_0 = 0.05$ (green, dot-dashed line), $D\Omega_0 = 0.1$ (red, solid line). $\Omega = 0.4\,\Omega_0$ and $T\Omega_0 = 20$.

use the following scheme from [31]:

$$\Omega_R(t) = 2\Omega_0 \cos(\Omega t)\,,\ \Omega_I(t) = 2\Omega_0 \sin(\Omega t)\,,\ \Delta = -\Omega_0. \tag{7.47}$$

This scheme only changes the relative phase of the state and not the populations. The goal is to follow adiabatically the eigenstate $|\phi_+^{(0)}\rangle$ of H_0.

We now simulate the master equation (7.46), and plot the fidelity $F(t) = \sqrt{\langle\phi_+^{(0)}(t)|\rho(t)|\phi_+^{(0)}(t)\rangle}$ versus time. In figure 7.1(a), the fidelity is plotted for different values of the noise bias J with a very small noise strength $D\Omega_0 = 10^{-4}$. The corresponding plot is qualitatively similar to Fig. 1 in [31] as we have used similar parameter values. The fidelity increases with increasing noise bias J for a fixed, small noise strength D (this is also discussed in detail in [31]). This can be easily understood from the master equation (7.46); increasing J (with a fixed and almost negligible D) has just the same effect as increasing the strength of the Hamiltonian H_0 which clearly results in a better adiabatic behavior.

The outcome is completely different if we fix $J = 0$ and increase D. This can be seen in figure 7.1(b). Good adiabaticity, i.e., high fidelity, is only found for small D. In general the fidelity is decreasing with increasing D. This agrees with the natural intuition that noise typically destroys adiabaticity. In the following, the

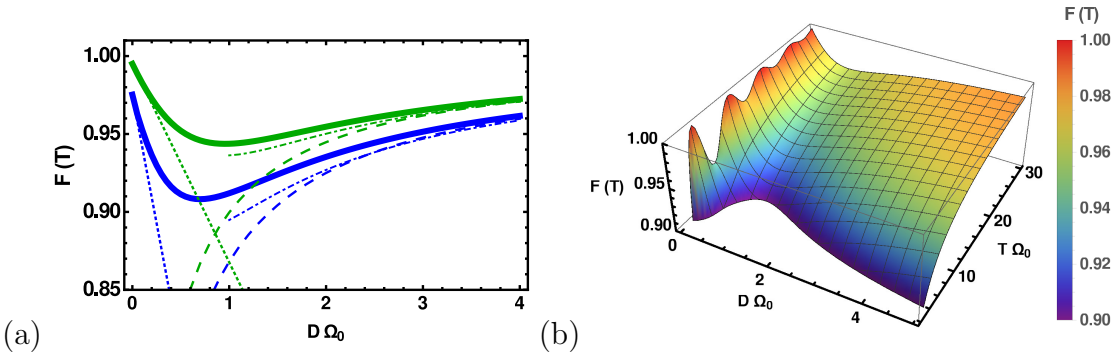


FIGURE 7.2: RAP scheme in a two-level system with $H_0 = H_1$. (a) Fidelity $F(T)$ against noise strength D, $\delta_0 = 3.5\,\Omega_0$(blue) and $\delta_0 = 1\,\Omega_0$(green). Numerically exact solution (solid lines), small noise approximation (7.35) (dotted lines), Naive strong noise approximation (dashed lines) and strong noise approximation (E.10) (dot-dashed line); $T\Omega_0 = 20$. (b) Fidelity $F(T)$ against both noise strength D and total time T; $\delta_0 = 1\,\Omega_0$.

effect of the noise strength D on adiabatic schemes is investigated further. From this point on, $J = 0$ always since it only changes the coherent evolution.

7.5.2 Population transfer in a two-level system

In this section, we continue to consider a two-level system but now for a population transfer scheme. We assume the following Rapid Adiabatic Passage(RAP) protocol [300–302]

$$\begin{aligned} \Omega_R(t) &= \Omega_0 \sin\left(\frac{\pi t}{T}\right), \\ \Omega_I(t) &= 0, \\ \Delta(t) &= -\delta_0 \cos\left(\frac{\pi t}{T}\right), \end{aligned} \tag{7.48}$$

which produces a population inversion in the bare basis. The system starts in an instantaneous energy eigenstate $|\phi_+^{(0)}(t)\rangle$ of $H_0(t)$. We use the same definition of fidelity as in the previous subsection. We now simulate (7.23).

First consider the case $H_1 = H_0$. Physically, this could originate from Poisson noise in the total Hamiltonian, or from Poisson noise in the timing of the process.

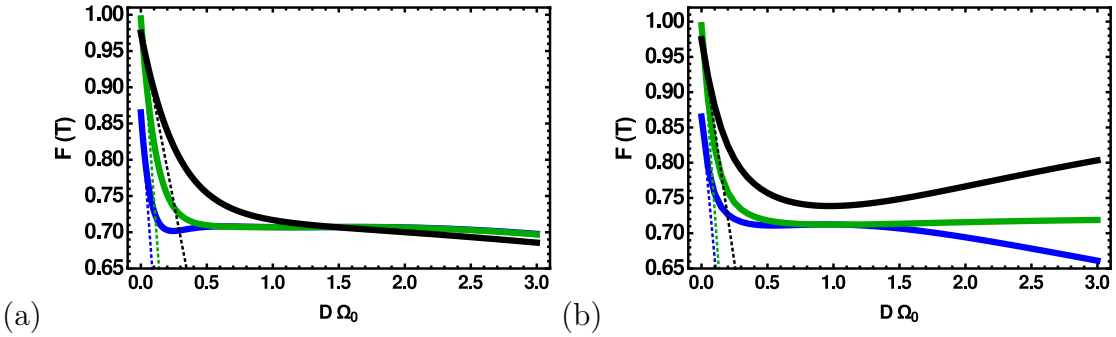


FIGURE 7.3: RAP scheme in a two-level system with $H_0 \neq H_1$. $\delta_0 = 3.5\,\Omega_0$(black), $\delta_0 = 1\,\Omega_0$(green), $\delta_0 = 0.5\,\Omega_0$(blue). Numerically exact solution (solid lines) and small noise approximation (7.35) (dotted lines). (a) Fidelity $F(T)$ against noise strength D for frequency error. (b) Fidelity $F(T)$ against noise strength D for both timing and frequency error with $c = 1$.

In figure 7.2(a), the fidelity is decreasing for small noise, i.e., the noise sensitivity (see (7.37)) is negative. This shows that a small amount of noise will not improve the fidelity as one would expect. The fidelity is decreasing with increasing noise strength D.

However, at some point the fidelity begins to increase again due to the effect of strong noise. Even though the noise bias J is zero, there is a convergence to the strong noise limit fidelity $F_\infty = 1$ in this case. The strong noise approximation (E.10) (which is only plotted in the strong noise regime $D \geq 1$) is compared to the naive strong noise solution (which is the solution of the equation $\dot{\rho} = \mathcal{L}_1(\rho)$). While only heuristic, this naive approach works well in the limit of strong noise. However, it is clearly not as accurate as the approach presented in Appendix E.2.

In figure 7.2(b), the same fidelity plotted against both noise strength D and total time T is shown. For $D = 0$, the fidelity oscillates slowly towards 1 for increasing T, i.e., the adiabatic limit. In general the fidelity increases both for increasing T (adiabatic limit) and increasing D (strong noise limit). The same dip in figure 7.2(a) is present here also.

We also consider examples where $H_1 \neq H_0$. Firstly we consider an absolute error in the detuning which could be due to an error in the laser frequency. In this case

$$\widetilde{\Omega}_R(t) = 0,\ \widetilde{\Omega}_I(t) = 0,\ \widetilde{\Delta}(t) = \Omega_0. \tag{7.49}$$

This is shown in figure 7.3(a). For all values of δ_0 the fidelity decreases for increasing noise strength. In particular the value of the fidelity in the strong noise limit is $F_\infty = 0$ for all cases. However there are some cases whereby the fidelity can increase again for large noise strengths even though $H_1 \neq H_0$.

One possible example of this is a case where there is both noise in the detuning $z(t)$ and noise in the timing of the process $\tilde{z}(t)$. In this case we assume that the different noises are proportional $z(t) = c\tilde{z}(t)$ and ignore higher order terms to get a noise Hamiltonian

$$H_1(t) = \frac{\hbar}{2}\begin{pmatrix} -(\Delta(t) + c\widetilde{\Delta}) & \Omega_R(t) - i\Omega_I(t) \\ \Omega_R(t) + i\Omega_I(t) & \Delta(t) + c\widetilde{\Delta} \end{pmatrix}. \tag{7.50}$$

In figure 7.3(b), we can see the fidelity is plotted against noise strength D for $c = 1$. The examples shown represent $c\widetilde{\Delta} < \delta_0$, $c\widetilde{\Delta} = \delta_0$ and $c\widetilde{\Delta} > \delta_0$. The limiting solution for $c\widetilde{\Delta} > \delta_0$ is $F_\infty = 1$ as H_0 and H_1 have the same eigenvectors at initial and final times, i.e., $t = 0$ and $t = T$. The limiting solution for $c\widetilde{\Delta} < \delta_0$ is $F_\infty = 0$ since H_0 and H_1 have eigenvectors which are exactly opposite at the initial time but the same at the final time. If $c\widetilde{\Delta} = \delta_0$, there is a degeneracy in H_1 at $t = 0$. This leads to a maximally mixed state in the strong noise limit with $F_\infty = 1/\sqrt{2}$.

While this example is perhaps not the most realistic (since it is assumed that both noise terms are proportional and higher terms can be neglected), it provides a nice example of the different possible effects noise may have on the fidelity. In particular it is possible to achieve high fidelity for strong noise even when $H_1 \neq H_0$.

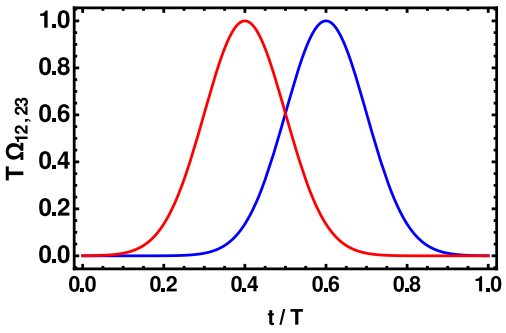


FIGURE 7.4: STIRAP pulse sequence with $T\Omega_0 = 1$ and $\tau\Omega_0 = 0.1$; Ω_{12}(blue) and Ω_{23}(red).

In the two-level model, the previous results can be also applied if the Poisson noise becomes Gaussian noise because the change from Poisson noise to Gaussian noise just corresponds to a reinterpretation $J \to \widetilde{J}$ and $D \to \widetilde{D}$. A third example, using a more complex quantum system will be considered in the next subsection. The master equation for Poisson white noise will no longer be of the same form as that for Gaussian white noise.

7.5.3 STIRAP process in a three-level system

Consider now a three-level quantum system and a STIRAP scheme for population transfer. In this setting the master equation for Poisson noise does not simplify to a form similar to the Gaussian noise master equation. The Hamiltonian is now

$$H_0(t) = \frac{\hbar}{2}\begin{pmatrix} 0 & \Omega_{12}(t) & 0 \\ \Omega_{12}(t) & 0 & \Omega_{23}(t) \\ 0 & \Omega_{23}(t) & 0 \end{pmatrix}, \tag{7.51}$$

where all functions are assumed to be real. The typical counter-intuitive ordering of a STIRAP transfer is given by

$$\Omega_{12} = \Omega_0 g\left[t - T(1/2 + \tau)\right], \tag{7.52}$$

$$\Omega_{23} = \Omega_0 g\left[t - T(1/2 - \tau)\right], \tag{7.53}$$

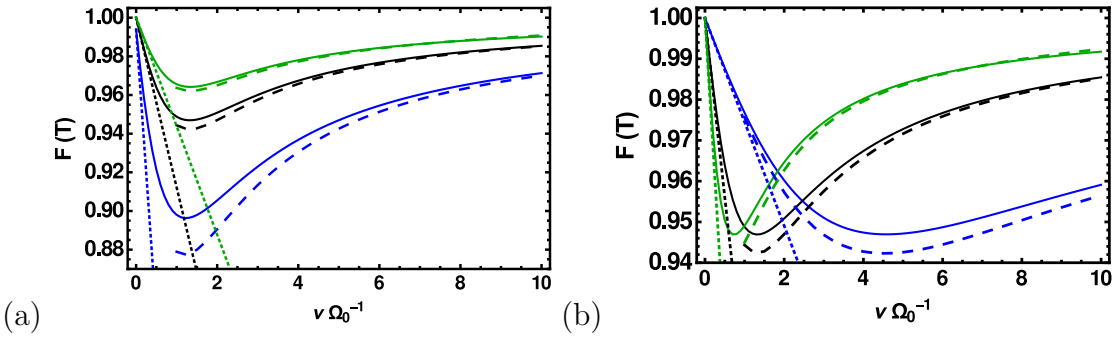


FIGURE 7.5: STIRAP population transfer in a three-level system with $H_0 = H_1$, $\tau\Omega_0 = 0.1$. Numerically exact solution (solid lines), small noise approximation (7.35) (dotted lines) and strong noise approximation (E.10) (dashed line) (a) Fidelity F versus frequency ν for $\sigma\Omega_0 = 2$ and $T\Omega_0 = 100, 200, 300$ blue, black and green respectively. (b) Fidelity F versus frequency ν for $T\Omega_0 = 200$ and $\sigma\Omega_0 = 1, 2, 3$ blue, black and green respectively.

where $g(t) = \exp\left[-(t/T)^2/0.02\right]$ and the pulses are shown in figure 7.4. The goal is to follow the usual dark state $|\phi_2^{(0)}\rangle$ which has eigenvalue 0 always. Hence we define $|\psi_{ad}(t)\rangle = |\phi_2^{(0)}(t)\rangle$.

A Gaussian distribution is assumed for the strike strength of the noise $P(\xi) = \frac{1}{\sqrt{2\pi}\sigma}\exp\left(-\frac{\xi^2}{2\sigma^2}\right)$ with mean $\langle\xi\rangle = 0$ and width σ. The eigenvalues of $\mathcal{L}_1$ can be found from the characteristic function of $P(\xi)$, namely

$$\beta_{n,m} = \nu\left\{\exp\left[-\frac{\sigma^2}{2}\left(\frac{E_n - E_m}{\hbar}\right)^2\right] - 1\right\}. \tag{7.54}$$

To numerically solve this, the master equation is represented in the eigenbasis of $\mathcal{L}_1$.

Different settings of the noise Hamiltonian are now considered. In the first case, let $H_1 = H_0$. In figure 7.5, the fidelity F at final time $t = T$ against the frequency of the strikes ν is shown. The dip in the fidelity is present here again. In figure 7.5(a) the fidelity is shown for different total times T. One can see that the amount that the fidelity drops is dictated by the adiabaticity (or equivalently the total time for the process). In figure 7.5(b) the fidelity is shown for different distribution widths σ. The location of the turning point is determined by σ. In all cases the fidelity in

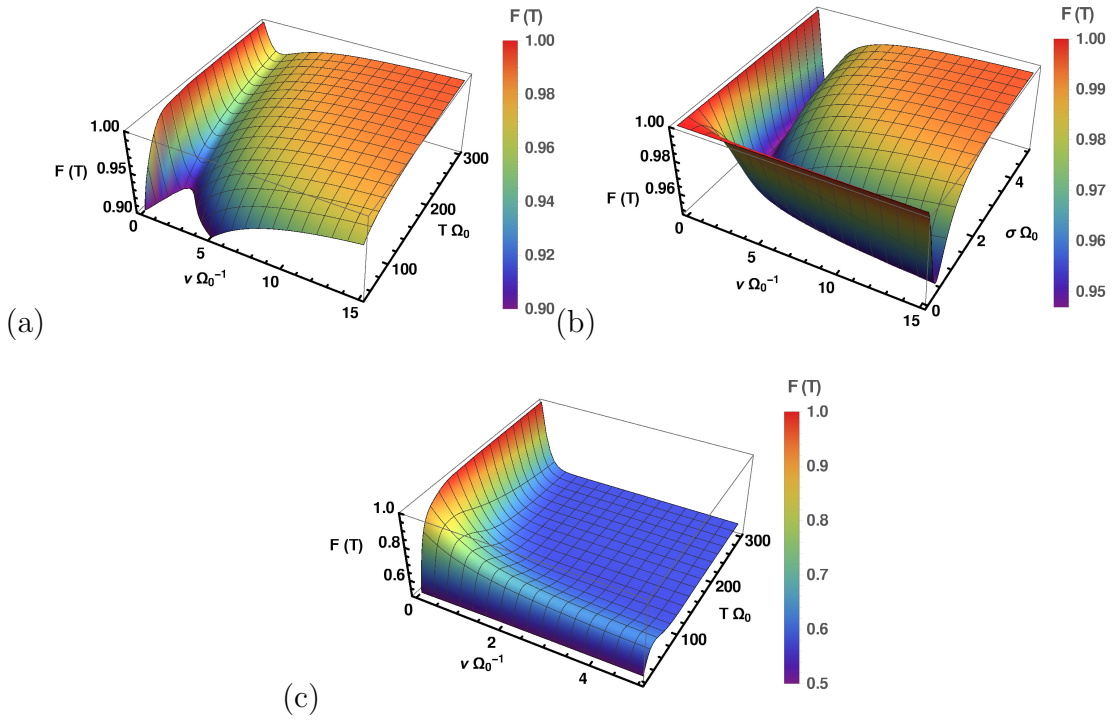


FIGURE 7.6: STIRAP population transfer in a three-level system. (a) Fidelity F versus noise parameter ν and final time T for $H_1 = H_0$; $\sigma\Omega_0 = 2$. (b) Fidelity F versus noise parameter ν and distribution width σ for $H_1 = H_0$; $T\Omega_0 = 200$. (c) Fidelity F versus noise parameter ν and final time T for the case of phase fluctuations; $\sigma\Omega_0 = 2$. $\tau\Omega_0 = 0.1$ in all cases

the strong noise limit is $F_\infty = 1$. The strong noise approximation (E.10), is seen to represent accurately the dynamics in the strong noise regime $\nu\Omega_0^{-1} \geq 1$.

In figure 7.6(a) and (b) the fidelity is shown versus the final time T, the frequency of strikes ν and the variation in their strength σ. We can see again a dip which comes from the fact that small noise disturbs the adiabaticity while strong noise acts as a projector on the eigenstates of the noise Hamiltonian.

As an example where there is only decay in the fidelity consider the noise Hamiltonian

$$H_1 = \frac{\hbar}{2}\begin{pmatrix} 0 & 0 & 0 \\ 0 & 0 & i\Omega_{23}(t) \\ 0 & -i\Omega_{23}(t) & 0 \end{pmatrix}. \tag{7.55}$$

This could arise from random fluctuations in the phase of the Rabi frequency, i.e., $\Omega_{23}e^{i\kappa z(t)} \approx \Omega_{23}\left(1 + i\kappa z(t)\right)$ for $\kappa \ll 1$. The fidelity in this case, plotted in figure 7.6(c), goes down to a fixed value for increasing noise strength.

7.6 Conclusion

Let us now summarize the work of the chapter. We have presented a master equation for Poisson noise in a general time dependent quantum system and outlined various properties associated with it. We have outlined the behaviour in three regimes, namely adiabatic processes with no noise, weak noise and strong noise. We have also shown that previous claims in [31], that white shot noise can improve the adiabatic condition, may be misleading. Standard adiabaticity only improves when the noise bias is increased, i.e., when the Hamiltonian is made stronger, without necessarily implying a strong noise. For very strong noise a different type of adiabaticity (in operator space rather than in the usual state space) emerges which implies the decay of coherences. Finally we have provided some numerical examples where this master equation can be used for non-trivial systems such as a three-level system (where Poisson noise differs from standard Gaussian noise). In some examples, a dip in the fidelity as a function of noise strength is present where high fidelity still occurs for large noise strengths. Our results may also be relevant to continuous measurements, which are described by master equations which are formally similar to those describing decoherence [303–305]. For example, (7.23) could also describe a continuous measurement of the operator H_1, where the magnitude of $\widetilde{D}$ is determined by the strength and frequency of measurement.

Chapter 8

Summary and outlook

This thesis has focussed on applying the techniques of shortcuts to adiabaticity (especially those using Lewis-Riesenfeld invariants) to a variety of quantum systems for the purpose of state transfer. In this chapter we will summarise the work presented in the previous chapters and provide an outlook for further work that could be done in the future.

8.1 Inhibiting unwanted transitions

In chapter 3, we designed control schemes which are both fast and stable in two- and three-level quantum systems. The schemes are stable against an unwanted uncontrollable transition. This was done by exploiting the freedom associated with invariant based inverse engineering techniques. A transition sensitivity was derived and minimised using this freedom.

The schemes developed are made stable up to second order in the strength of the unwanted transition by minimizing the transition sensitivity. One could also consider calculating (and then minimising) even higher orders, similar to [158]. Other constraints could be easily imposed such as demanding that the pulses are smooth everywhere and are zero at the start and the end of the process.

The results of this chapter could also be extended in several other ways. Firstly one could consider combining the results with numerical optimisation techniques such as the well known chopped random basis (CRAB) algorithm [306] where the transition sensitivity would be a cost function. One could also use the Lewis-Riesenfeld invariant formalism to define several additional cost functions (where each could be associated with a different noise or error as in [79]) and then attempt to determine a scheme which minimises both the transition sensitivity and these new cost functions simultaneously.

While the work could be extended to different level structures with multiple unwanted transitions, it is likely that the least detuned transition will play a dominant role over the others. More generally it would be interesting to investigate how one can minimise transitions outside a certain subspace, i.e., how to make a subspace effectively closed. This problem often arises when using a truncated Hilbert space approach to modelling a system as was done in chapters 4 and 5.

8.2 Spatial non-adiabatic passage

In chapter 4, we presented schemes for manipulating a charged particle in a system of three tunnel coupled quantum wells. Using the presence of a static magnetic field we were able to create complex tunnelling frequencies and show how these are useful for the purposes of control. In particular we showed how to create a superposition of the particle between all sites.

As an outlook, it would be useful to determine another mapping to the three-level model which leads to analytical expressions but remains as straightforward to invert. Alternatively, a similar system (using four sites for symmetry reasons) might prove useful as an interferometer [179]. Finally, finding an implementation where several of these systems could exist and interact would be useful for quantum computation. One possibility could be using artificial gauge fields with triangular optical lattices [307].

8.3 Creating exotic angular momentum states

In chapter 5, a method of creating higher orbital states of ultracold atoms in an optical lattice was proposed. The main idea is to periodically modulate the position of the lattice. This "shaking" allows one to create controlled excitations in the motional state of the atoms. The specific schemes were designed using a four-level model for each localised atom and invariant-based shortcuts to adiabaticity. The example used is that of an anti-ferromagnetic type ordering of angular momentum states. The results of the four-level model were found to agree with numerical simulations of the full Schrödinger equation.

There are some obvious next steps one could take in this direction such as designing schemes to achieve a state with all atoms having the same angular momentum or states containing even higher orbitals by using the six-level model (presented in Appendix C.2).

Since the atoms are in the Mott insulator regime, the effect of interactions was completely neglected in this work. It would be interesting to consider interaction as a perturbative effect on the process. Simulating the whole system of atoms in a numerically exact way is much too demanding. However one could consider as an intermediate step, to simulate the many body case using a non-standard Bose-Hubbard type model, see [200, 308] for example.

Atoms have finite lifetimes in higher orbital states before they decay back to the ground state. Current theoretical [201] and experimental [206] work estimates lifetimes in the first excited state to be between 10 and 100 times longer than the natural tunnelling time. It would be useful to explore ways of extending the lifetime further.

Other interesting extensions of this work could include making a connection to the effect of Bloch oscillations [309, 310]. Although the time dependence of the system is only quasi-periodic, Floquet theory might still be exploited in this chapter's setting [311, 312]. Finally, in order to break the symmetry of the lattice we use the

interference term of the two beams. One could perhaps think of other approaches for this such as changing the angle between the lasers in time.

8.4 Manipulation of a particle in a Penning trap

In chapter 6, we outlined a way to change the radial spread (or equivalently the motional frequency) of a single ion wavefunction in a Penning trap simply by changing the strength of the magnetic field in time. We made use of the fast-forward method and show that in this setting it can be equivalently formulated using the formalism of Lewis-Riesenfeld invariants. This result has been further explored in [139] to filter ions of different mass or charge.

It would be useful for several reasons to extend these results to the case of many ions. In this setting different types of operations would benefit from such a change between higher and lower motional frequencies. High motional frequencies lead to small ion separation distance and small Lamb-Dicke parameters. This benefits Doppler laser cooling (as the mean phonon number is lower for tighter traps [313]) and operations requiring a spectrally resolved motional normal mode (since the frequency difference between modes is proportional to the trap curvature [314]). However operations which are best performed with a low motional frequency include single ion addressing (as they are spaced further apart) and resolved sideband cooling (as the rate of cooling is proportional to the Lamb-Dicke parameter squared [315]). Therefore, being able to change between a high and low frequency trapping potential for several ions would be beneficial.

In order to achieve an ideal harmonic trap, the electrodes of a Penning trap must in principle be hyperbolic sheets of revolution. However different electrode geometries are often easier to manufacture, align and allow better optical access to the trapped ions [47]. For Penning traps the choice is often segmented cylindrical electrodes. This leads to trapping potentials which are slightly anharmonic. This unwanted effect could reduce the fidelity obtained by the schemes in chapter 6 and bound the

speed at which operations could be performed. Therefore, an extension of these schemes for slightly anharmoic potentials would be fruitful.

Other possible extensions to this work include optimising the stability of the scheme for systematic errors in the magnetic field or designing schemes which could change the principal or angular momentum quantum number of the state (which is possible in the fast-forward formalism [316]). One could also consider other applications of the streamlined fast-forward formalism for the minimal coupling equation such as the Paul trap.

8.5 Effect of classical Poisson noise

In chapter 7, we presented the master equation which describes a general quantum system in the presence of classical Poisson white noise and outlined its properties. Various limiting cases were discussed and approximations were introduced for different noise strength regimes. Simulations of some simple systems in the presence of Poisson noise were also provided.

The effect of Poisson noise was only investigated for adiabatic processes. It might be interesting to extend this to non-adiabatic processes. As random telegraph noise [282] is commonly used to model noise in many systems [284, 285, 317], it would also be interesting to see how well the master equation for Poisson noise approximates the effect of random telegraph noise with short correlation time and if using this could provide some analytic insight into designing schemes which are stable against this noise.

Appendix A

Properties of Lewis–Riesenfeld invariants

In this section, we will derive the main properties of Lewis–Riesenfeld invariants. Since the invariant I is Hermitian, all its eigenvalues are real. We can write its spectral decomposition as $I(t) = \sum_k \lambda_k(t) |\phi_k(t)\rangle \langle\phi_k(t)|$. We can now show that these eigenvalues are also time independent as follows

$$\begin{aligned}
\partial_t \lambda_k &= \frac{d}{dt} \langle \phi_k(t) | I(t) | \phi_k(t) \rangle \\
&= \left(\frac{d}{dt} \langle \phi_k(t) | \right) I |\phi_k(t)\rangle + \langle \phi_k(t)| \dot{I}(t) |\phi_k(t)\rangle + \langle \phi_k(t)| I \left(\frac{d}{dt} |\phi_k(t)\rangle \right) \\
&= \lambda_k \left(\frac{d}{dt} \langle \phi_k(t)| \right) |\phi_k(t)\rangle - \frac{i}{\hbar} \langle \phi_k(t)| (H\lambda_k - \lambda_k H) |\phi_k(t)\rangle \\
&+ \lambda_k \langle \phi_k(t)| \left(\frac{d}{dt} |\phi_k(t)\rangle \right) \\
&= \lambda_k \frac{d}{dt} [\langle \phi_k(t) \mid \phi_k(t)\rangle] \\
&= 0
\end{aligned} \tag{A.1}$$

since the eigenvectors are normalised.

Secondly, we wish to show that the eigenvectors of the invariant are solutions of the Schrödinger equation up to a time dependent phase. We start by taking the

time derivative of $I|\phi_k\rangle = \lambda_k|\phi_k\rangle$ which gives

$$\begin{aligned}\lambda_k|\dot{\phi}_k\rangle &= \dot{I}|\phi_k\rangle + I|\dot{\phi}_k\rangle \\ &= -\frac{i}{\hbar}\left[H, I\right]|\phi_k\rangle + I|\dot{\phi}_k\rangle \\ &= -\frac{i}{\hbar}\lambda_k H|\phi_k\rangle + \frac{i}{\hbar}IH|\phi_k\rangle + I|\dot{\phi}_k\rangle. \end{aligned} \tag{A.2}$$

Now we apply $\langle\phi_p|$ from the left,

$$\lambda_k\langle\phi_p|\dot{\phi}_k\rangle = -\frac{i}{\hbar}\lambda_k\langle\phi_p|H|\phi_k\rangle + \frac{i}{\hbar}\lambda_p\langle\phi_p|H|\phi_k\rangle + \lambda_p\langle\phi_p|\dot{\phi}_k\rangle. \tag{A.3}$$

This can be rewritten as

$$i\hbar\left(\lambda_k - \lambda_p\right)\langle\phi_p|\dot{\phi}_k\rangle = \left(\lambda_k - \lambda_p\right)\langle\phi_p|H|\phi_k\rangle. \tag{A.4}$$

In the case where $\lambda_k \neq \lambda_p$ we get that

$$i\hbar\langle\phi_p|\dot{\phi}_k\rangle = \langle\phi_p|H|\phi_k\rangle. \tag{A.5}$$

If this equation held for both the case of $\lambda_k \neq \lambda_p$ and $\lambda_k = \lambda_p$, the eigenvector $|\phi_k\rangle$ would clearly be a solution of the Schrödinger equation for the Hamiltonian H.

We can always add a time dependent phase to any eigenvector. With this in mind we consider $|\psi_k(t)\rangle = e^{i\alpha_k(t)}|\phi_k(t)\rangle$. In the case where I does not contain any time derivative operators, these new states are also eigenvectors of the invariant. By taking the time derivative we see that

$$\begin{aligned} i\hbar\partial_t|\psi_k(t)\rangle &= i\hbar\partial_t\left[e^{i\alpha_k(t)}|\phi_k(t)\rangle\right] \\ &= -\hbar\dot{\alpha}_k(t)e^{i\alpha_k(t)}|\phi_k(t)\rangle + i\hbar e^{i\alpha_k(t)}|\dot{\phi}_k(t)\rangle. \end{aligned} \tag{A.6}$$

Since this must equal $He^{i\alpha_k(t)}|\phi_k(t)\rangle$ in order to be a solution we get that $\dot{\alpha}_k = \frac{1}{\hbar}\langle\phi_k(t)|\left[i\hbar\partial_t - H(t)\right]|\phi_k(t)\rangle$. After integrating this we get that the Lewis–Riesenfeld

phase is given by

$$\alpha_k(t) = \frac{1}{\hbar}\int_0^t ds\langle\phi_k(s)|\left[i\hbar\partial_s - H(s)\right]|\phi_k(s)\rangle. \tag{A.7}$$

Appendix B

Supplementary calculations for chapter 4

B.1 Mapping continuum model to the three-level approximation

In this appendix we give more details on how to connect the parameters of the three-level approximation and the continuum model. For clarity, we set $\hbar = m = 1$ in the following. Let us first recall the eigenfunctions of a single asymmetric delta potential given by

$$V(x) = -\epsilon\delta(x) + \begin{cases} V_L & x < 0 \\ V_R & x \geq 0. \end{cases} \tag{B.1}$$

This potential has only one bound state (as long as $2\epsilon^2 > |V_L - V_R|$) which is of the form

$$\psi(x) = \begin{cases} \phi_L(x) & x < 0 \\ \phi_R(x) & x \geq 0 \end{cases}, \tag{B.2}$$

where

$$\phi_L(x) = \exp\left[\frac{(2\epsilon^2 + V_L - V_R)\,x}{2\epsilon}\right] \frac{\sqrt{4\epsilon^4 - (V_L - V_R)^2}}{2\epsilon^{3/2}}, \tag{B.3}$$

$$\phi_R(x) = \exp\left[-\frac{(2\epsilon^2 + V_R - V_L)\,x}{2\epsilon}\right] \frac{\sqrt{4\epsilon^4 - (V_L - V_R)^2}}{2\epsilon^{3/2}}, \tag{B.4}$$

with an energy

$$E = -\frac{4\epsilon^4 + (V_L - V_R)^2 - 4\epsilon^2\,(V_L + V_R)}{8\epsilon^2}. \tag{B.5}$$

In our work we use these eigenstate as the localised basis states in each of the three delta trap potentials. For example, the basis state $\psi_1(x)$ for the first trap can be constructed from the substitutions $\epsilon \to \epsilon_1$, $V_L \to V_{13}$, $V_R \to V_{12}$ and $x \to x - l/2$ (see figure 4.5) and the states $\psi_2(x)$ and $\psi_3(x)$ for the other two wells can be obtained in a similar manner. While choosing a basis for the system this way does not necessarily lead to an orthogonal basis set, we have checked numerically that the states are approximately orthogonal at all times during our simulations. This allows us to approximate the Hamiltonian associated with (4.30) as (4.6).

The coupling constants between each pair of neighbouring traps can be determined by calculating the overlap between the two respective trap states in the barrier region between them, i.e.,

$$\Omega_{12} \approx -2\int_{l/2}^{3l/2} \psi_1(x)\left[-\frac{1}{2}\partial_x^2\psi_2(x) + V_{12}\psi_2(x)\right] dx, \tag{B.6}$$

$$\Omega_{23} \approx -2\int_{3l/2}^{5l/2} \psi_2(x)\left[-\frac{1}{2}\partial_x^2\psi_3(x) + V_{23}\psi_3(x)\right] dx, \tag{B.7}$$

$$\Omega_{31} \approx -2\int_{5l/2}^{7l/2} \psi_1(x-3l)\left[-\frac{1}{2}\partial_x^2\psi_3(x) + V_{31}\psi_3(x)\right] dx. \tag{B.8}$$

Similarly, the on-site energies (or diagonal elements) are approximated by considering only the regions for which the basis states are significant, e.g.,

$$E_2 \approx \int_{l/2}^{3l/2} \psi_2(x) \left[-\frac{1}{2}\partial_x^2 \psi_2(x) + V_{12}\psi_2(x) \right] dx + \int_{3l/2}^{5l/2} \psi_2(x) \left[-\frac{1}{2}\partial_x^2 \psi_2(x) + V_{23}\psi_2(x) \right] dx \tag{B.9}$$

and correspondingly for the energies E_1 and E_3. We can then tabulate sets of values for the barrier heights, $\{V_{12}, V_{23}, V_{13}\}$, trap depths, $\{\epsilon_1, \epsilon_2, \epsilon_3\}$, and tunnelling rates, $\{\Omega_{12}, \Omega_{23}, \Omega_{13}\}$, such that the energies all match a fixed reference value, i.e., $E_1 = E_2 = E_3 = E_0$ where E_0 is fixed to some constant value. Since for a given protocol the required tunnelling rates are known, we can finally numerically invert the table in order to determine how the barrier heights and trap depths have to vary in time.

Appendix C

Supplementary calculations for chapter 5

C.1 Transformation into lattice frame

To transform our Hamiltonian in the lab frame,

$$H_{\text{lab}}(t) = \frac{\vec{p}^{\,2}}{2m} + V(\vec{r} - \vec{R}_0(t), t), \tag{C.1}$$

to the lattice frame we follow the procedure outlined in [232]. The relationship between the two Hamiltonians is given by a unitary transformation $\mathcal{U}$,

$$H_{\text{lattice}}(t) = \mathcal{U} H_{\text{lab}} \mathcal{U}^\dagger - i\hbar \mathcal{U} \partial_t \mathcal{U}^\dagger, \tag{C.2}$$

which can be expressed as three separate unitary operators $\mathcal{U} = U_3 U_2 U_1$. These are a translation operator,

$$U_1 = \exp\left[\frac{i}{\hbar}\vec{R}_0(t)\vec{p}\right], \tag{C.3}$$

a momentum shift operator,

$$U_2 = \exp\left[-\frac{i}{\hbar} m \dot{\vec{R}}_0(t)\vec{r}\right], \tag{C.4}$$

and an operator that removes a time–dependent energy shift from the Hamiltonian,

$$U_3 = \exp\left[-\frac{i}{\hbar}\frac{m}{2}\int_0^t dt' \dot{\vec{R}}_0(t')^2\right]. \tag{C.5}$$

From this we arrive at the Hamiltonian in the lattice frame,

$$H_{\text{lattice}}(t) = \frac{\vec{p}^{\,2}}{2m} + V(\vec{r},t) + m\ddot{\vec{R}}_0(t)\vec{r} \tag{C.6}$$

We impose that $\vec{R}_0(0) = \vec{R}_0(T) = 0$ and $\dot{\vec{R}}_0(0) = \dot{\vec{R}}_0(T) = 0$, such that $\mathcal{U}$ becomes the identity (up to a global phase) at the initial and final times.

C.2 Six–level approximation

If one were to include more levels to approximate the Hamiltonian (5.5), the natural choice would be $|20\rangle$ and $|02\rangle$. A six–level Hamiltonian to describe our system can be obtained following a derivation similar to the one presented in section 5.3.2, but using the unitary operator

$$\begin{aligned} U(t) \;=\; & e^{-i\omega_{10}t}|10\rangle\langle 10| + e^{-i(\omega_{10}+\omega_x)t}|00\rangle\langle 00| + e^{-i(\omega_{10}+\omega_x-\omega_y)t}|01\rangle\langle 01| \\ & + e^{-i\omega_{11}t}|11\rangle\langle 11| + e^{-i\omega_{20}t}|20\rangle\langle 20| + e^{-i\omega_{02}t}|02\rangle\langle 02| \end{aligned} \tag{C.7}$$

and setting $\Omega_y = 0$. One then arrives at the Hamiltonian

$$H_{6L} = \frac{\hbar}{2}\begin{pmatrix} 0 & \Omega_x\theta_x^- & \Omega_\rho & 0 & \delta_1 & 0 \\ \Omega_x\theta_x^+ & -2\left(\omega_d+\omega_x\right) & 0 & \Omega_\rho e^{i(\omega_x-\omega_d)t} & 0 & 0 \\ \Omega_\rho & 0 & 0 & \Omega_x\theta_x^+ & 0 & 0 \\ 0 & \Omega_\rho e^{-i(\omega_x-\omega_d)t} & \Omega_x\theta_x^- & 0 & \delta_2 & \delta_2 \\ \delta_1^* & 0 & 0 & \delta_2^* & 0 & 0 \\ 0 & 0 & 0 & \delta_2^* & 0 & 0 \end{pmatrix} \tag{C.8}$$

in the ordered basis $\{|10\rangle, |00\rangle, |01\rangle, |11\rangle, |20\rangle, |02\rangle\}$, where

$$\theta_x^\pm = \left(\frac{\omega_x}{\omega_d}\right)^2\left(1+e^{\pm 2i\omega_x t}\right), \tag{C.9}$$

$$\delta_1 = \left[\int_{-\ell}^{\ell}\Gamma_2(x)x\Gamma_1(x)dx\right]\gamma_1^{-1}\Omega_x e^{i(\omega_{10}-\omega_{20}+\omega_x)t}\theta_x^-, \tag{C.10}$$

$$\delta_2 = \left[\int_{-\ell}^{\ell}\Gamma_2(x)\sin(kx)\Gamma_1(x)dx\right]\frac{1}{\sqrt{\gamma_2}}\Omega_\rho e^{-i(\omega_{20}-\omega_{11})t}. \tag{C.11}$$

One can see that for deep (i.e. harmonic) potential wells $\omega_{10} - \omega_{20} = -\omega_d$ and $\omega_{20} = \omega_{11}$. For $\omega_x = -\omega_d$ and in the rotating–wave approximation, one gets

$$H_{6L} = \frac{\hbar}{2}\begin{pmatrix} 0 & \Omega_x & \Omega_\rho & 0 & \sqrt{2}\Omega_x & 0 \\ \Omega_x & 0 & 0 & 0 & 0 & 0 \\ \Omega_\rho & 0 & 0 & \Omega_x & 0 & 0 \\ 0 & 0 & \Omega_x & 0 & \sqrt{2}\Omega_\rho & \sqrt{2}\Omega_\rho \\ \sqrt{2}\Omega_x & 0 & 0 & \sqrt{2}\Omega_\rho & 0 & 0 \\ 0 & 0 & 0 & \sqrt{2}\Omega_\rho & 0 & 0 \end{pmatrix}. \tag{C.12}$$

This clearly shows that for deep lattices a strong resonant coupling to levels $|20\rangle$ and $|02\rangle$ exists, and therefore the four–level approximation becomes invalid in this limit.

Appendix D

Supplementary calculations for chapter 6

D.1 Boundary conditions for $\Phi(t, \vec{r})$

Because $\psi_0(\vec{r}) \equiv \alpha_0(\vec{r})e^{i\beta_0(\vec{r})}$ should be an energy eigenvector of the Hamiltonian H_0 with eigenvalue $\mathcal{E}_0$, it follows from the real part of the corresponding stationary Schrödinger equation that

$$0 = -\frac{\hbar^2}{2m}\Delta\alpha_0 + \frac{1}{2m}\left(q\vec{A}_0 - \hbar\nabla\beta_0\right)^2 \alpha_0 + (q\phi - \mathcal{E}_0)\,\alpha_0, \tag{D.1}$$

and from the imaginary part that

$$0 = \frac{\hbar}{2m}\nabla\left(q\vec{A}_0 - \hbar\nabla\beta_0\right)\alpha_0 + \frac{\hbar}{m}\left(q\vec{A}_0 - \hbar\nabla\beta_0\right)\nabla\alpha_0. \tag{D.2}$$

Equation (6.9) at initial time becomes

$$\frac{1}{q}\frac{\partial\alpha}{\partial t}(0,\vec{r}) \;=\; \frac{1}{2m}(\nabla\vec{\chi}_0)\alpha_0 + \frac{1}{m}\vec{\chi}_0\nabla\alpha_0 = 0, \tag{D.3}$$

because of (D.2), and $\vec{\chi}_0 = \vec{A}_0 - \frac{\hbar}{q}\nabla\beta_0$.

Equation (6.8) at initial time becomes

$$\Phi(0,\vec{r}) \;=\; \frac{\hbar^2}{2mq\alpha_0}\Delta\alpha_0 - \frac{q}{2m}\vec{\chi}_0^2 = \phi_0 - \frac{\mathcal{E}_0}{q} \tag{D.4}$$

because of (D.1). Similar calculations also apply to the final time.

D.2 Solution of the main equations in polar coordinates

We assume that $\alpha(t,r,\theta)$ is given. We set

$$\vec{\chi} = \chi_r(t,r,\theta)\,\hat{r} + \chi_\theta(t,r,\theta)\,\hat{\theta}. \tag{D.5}$$

The main equation (6.9) now becomes

$$\frac{2mr}{q}\frac{\partial\alpha}{\partial t} - 2\chi_\theta\frac{\partial\alpha}{\partial\theta} - \frac{\partial\chi_\theta}{\partial\theta}\alpha - \chi_r\left(\alpha + 2r\frac{\partial\alpha}{\partial r}\right) - r\frac{\partial\chi_r}{\partial r}\alpha = 0 \tag{D.6}$$

and (6.8) becomes

$$\Phi = -\frac{q}{2m}\left(\chi_r^2+\chi_\theta^2\right) + \frac{\hbar^2}{2mq\alpha}\left(\frac{1}{r^2}\frac{\partial^2\alpha}{\partial\theta^2} + \frac{1}{r}\frac{\partial\alpha}{\partial r} + \frac{\partial^2\alpha}{\partial r^2}\right). \tag{D.7}$$

A solution of the main equation (D.6) for χ_r in terms of $w=\alpha^2$ and χ_θ can be written down,

$$\chi_r = -\frac{1}{rw}\int_r^\infty ds\,\left[\frac{ms}{q}\frac{\partial w}{\partial t}(t,s,\theta) - \chi_\theta(t,s,\theta)\frac{\partial w}{\partial\theta}(t,s,\theta) - w(t,s,\theta)\frac{\partial\chi_\theta}{\partial\theta}(t,s,\theta)\right]. \tag{D.8}$$

Thus a function χ_θ can be chosen to determine (together with the chosen α) the function χ_r. Alternatively, a solution of the main equation for χ_θ in terms of α

and χ_r is given by

$$\begin{aligned}\chi_\theta &= -\frac{f_\theta(r,t)}{\alpha}+\frac{1}{\alpha}\int_0^\theta d\rho\left\{\frac{mr}{q}\frac{\partial w}{\partial t}(r,\rho,t)\right.\\ &\left.-r\chi_r(r,\rho,t)\frac{\partial w}{\partial r}(r,\rho,t)-w(r,\rho,t)\left[\chi_r(r,\rho,t)+r\frac{\partial \chi_r}{\partial r}(r,\rho,t)\right]\right\},\end{aligned} \tag{D.9}$$

where $\chi_\theta(r,\theta+2\pi,t)=\chi_\theta(r,\theta,t)$.

D.3 Fidelity and sensitivity for arbitrary N and M

For arbitrary N and M we get for the fidelity $F_{N,M}$, by using [142],

$$F_{N,M}=|\langle\Psi(T)|\Psi_\epsilon(T)\rangle|=Q^{1+|M|}\left|P_N^{(|M|,0)}(1-2Q^2)\right|, \tag{D.10}$$

where P are Jacobi's polynomials and

$$Q=\frac{2l(T)\ell_\epsilon(T)}{\sqrt{(l(T)^2+\ell_\epsilon(T)^2)^2+\frac{4m}{\hbar^2}l(T)^4\ell_\epsilon(T)^2\ell'_\epsilon(T)^2}}. \tag{D.11}$$

The result is valid for an arbitrary function $l(t)$. Note that $F_{N=0,M=0}=Q=F$, this is the special case given in (6.59).

The general sensitivity $S_{N,M}=-\left.\frac{\partial^2 F_{N,M}}{\partial\epsilon^2}\right|_{\epsilon=0}$ is

$$S_{N,M}=\left.\frac{\partial F_{N,M}}{\partial Q}\right|_{Q=1}\times S_{N=0,M=0}, \tag{D.12}$$

where $S_{N=0,M=0}=S$ is the special case discussed in the main text. The factor $\left.\frac{\partial F_{N,M}}{\partial Q}\right|_{Q=1}$ only depends on N and M and is independent of the chosen $l(t)$.

Appendix E

Supplementary calculations for chapter 7

E.1 Commutator recursion relation in two-level systems

Let us first define $\lambda = -(i/\hbar)\,\xi$ and then split the sum into even and odd terms,

$$\begin{aligned}
e^{\lambda H_1}\rho e^{-\lambda H_1} &= \rho + \sum_{n=1}^{\infty}\frac{\lambda^n}{n!}\left[H_1,\rho\right]_n \\
&= \rho + \sum_{k=1}^{\infty}\frac{\lambda^{2k}}{(2k)!}\left[H_1,\rho\right]_{2k} + \sum_{l=0}^{\infty}\frac{\lambda^{2l+1}}{(2l+1)!}\left[H_1,\rho\right]_{2l+1} \\
&= \rho + \sum_{k=1}^{\infty}\frac{\lambda^{2k}}{(2k)!}\chi^{k-1}2^{2(k-1)}\left[H_1,[H_1,\rho]\right] \\
&+ \sum_{l=0}^{\infty}\frac{\lambda^{2l+1}}{(2l+1)!}\chi^{l}2^{2l}\left[H_1,\rho\right] \\
&= \rho + \left[\frac{-\sin^2\left(-\frac{1}{\hbar}\xi\sqrt{\chi}\right)}{2\chi}\right]\left[H_1,[H_1,\rho]\right] \\
&+ i\left[\frac{\sin\left(-\frac{2}{\hbar}\xi\sqrt{\chi}\right)}{2\sqrt{\chi}}\right]\left[H_1,\rho\right]. \qquad \text{(E.1)}
\end{aligned}$$

We now need to prove the second last step. Let's do each case separately. For n odd it can be proved by induction that

$$[H_1, \rho]_n = 2^{n-1} \chi^{(n-1)/2} [H_1, \rho] \,. \tag{E.2}$$

Clearly this is true for the case of $n = 1$. It can also be shown by explicit calculation to be true for $n = 3$. Now let us show that if it is true for n it is true for $n + 2$,

$$\begin{aligned} [H_1, \rho]_{n+2} &= [H_1, [H_1, [H_1, \rho]_n]] \\ &= 2^{n-1} \chi^{(n-1)/2} [H_1, \rho]_3 \\ &= 2^{n-1} \chi^{(n-1)/2} 4\chi [H_1, \rho] \\ &= 2^{(n+2)-1} \chi^{((n+2)-1)/2} [H_1, \rho] \,. \end{aligned} \tag{E.3}$$

Hence it is true for all n odd.

For n even we claim that

$$[H_1, \rho]_n = 2^{n-2} \chi^{(n-2)/2} [H_1, [H_1, \rho]] \,. \tag{E.4}$$

For $n = 2$ and $n = 4$ this holds true. Now let us show that if it is true for n it is true for $n + 2$,

$$\begin{aligned} [H_1, \rho]_{n+2} &= [H_1, [H_1, [H_1, \rho]_n]] \\ &= 2^{n-2} \chi^{(n-2)/2} [H_1, \rho]_4 \\ &= 2^{(n+2)-2} \chi^{((n+2)-2)/2} [H_1, [H_1, \rho]] \,. \end{aligned} \tag{E.5}$$

Hence it is true for all n even.

E.2 Derivation of strong noise limit

In this section a more detailed overview of the derivation of the strong noise limit will be presented. Let us start by integrating (7.41),

$$\begin{aligned} c_{n,m}(T) &= c_{n,m}(0) \\ &+ \sum_{\substack{l,k \\ (l,k)\neq(n,m)}} \int_0^T dt \exp\left[\tilde{\Lambda}_{l,k}(t) - \tilde{\Lambda}_{n,m}(t)\right] M_{n,m,l,k}(t) c_{l,k}(t). \end{aligned} \quad \text{(E.6)}$$

We then change to the coefficients

$$d_{n,m}(t) = c_{n,m}(t) \exp\left[\tilde{\Lambda}_{n,m}(t)\right], \quad \text{(E.7)}$$

where $d_{n,m}(0) = c_{n,m}(0)$ since $\tilde{\Lambda}_{n,m}(0) = 0$. By now rewriting (E.6) with these coefficients it becomes

$$\begin{aligned} d_{n,m}(T) &= d_{n,m}(0) \exp\left[\tilde{\Lambda}_{n,m}(T)\right] \\ &+ \sum_{\substack{l,k \\ (l,k)\neq(n,m)}} \int_0^T dt \exp\left[\tilde{\Lambda}_{n,m}(T,t)\right] M_{n,m,l,k}(t) d_{l,k}(t), \end{aligned} \quad \text{(E.8)}$$

where

$$\begin{aligned} \tilde{\Lambda}_{n,m}(T,t) &= \tilde{\Lambda}_{n,m}(T) - \tilde{\Lambda}_{n,m}(t) \\ &= \int_t^T ds \, \left[\kappa\beta_{n,m}(s) + \langle\langle B_{n,m}(s)|\mathcal{L}_0|B_{n,m}(s)\rangle\rangle\right]. \end{aligned} \quad \text{(E.9)}$$

This has the property that $\mathrm{Re}\left(\tilde{\Lambda}_{n,m}(T,t)\right) \leq 0$ for $T \geq t$ and $\tilde{\Lambda}_{n,n}(T,t) = 0$. By using (E.8) recursively one obtains the approximation

$$\begin{aligned} d_{n,m}(T) &\approx d_{n,m}(0)\exp\left[\tilde{\Lambda}_{n,m}(T)\right] \\ &+ \sum_{\substack{l,k \\ (l,k)\neq(n,m)}} \int_0^T dt \exp\left[\tilde{\Lambda}_{n,m}(T,t) + \tilde{\Lambda}_{l,k}(t)\right] M_{n,m,l,k}(t) d_{l,k}(0) \\ &+ \sum_{\substack{l,k \\ (l,k)\neq(n,m)}} \sum_{\substack{q,r \\ (q,r)\neq(l,k)}} \int_0^T dt \int_0^t ds M_{n,m,l,k}(t) \\ &\times \exp\left[\tilde{\Lambda}_{n,m}(T,t) + \tilde{\Lambda}_{l,k}(t,s) + \tilde{\Lambda}_{q,r}(s)\right] M_{l,k,q,r}(s) d_{q,r}(0), \end{aligned} \tag{E.10}$$

where the real part of all terms in the exponentials are negative. One can of course continue this process to obtain a series expansion on the right hand side. However for our purposes it is enough to understand the general form of the expansion so further terms are neglected.

For times $t_2 > t_1$ it is clear that $\exp\left[\tilde{\Lambda}_{n,m}(t_2,t_1)\right] \to 0$ as $\kappa \to \infty$ if $n \neq m$. However for $n = m$, $\exp\left[\tilde{\Lambda}_{n,n}(t_2,t_1)\right] = 1$ for all κ. Recall that we assume $\beta_{n,m} = 0$ if and only if $n = m$. It is then straightforward to see that $d_{n,m}(T) \to 0$ as $\kappa \to \infty$ for $n \neq m$. An approximation to this is $d_{n,m}(T) \approx d_{n,m}(0)\exp\left[\tilde{\Lambda}_{n,m}(T)\right]$. Converting back to the original coefficients we get that $c_{n,m}(T) \approx c_{n,m}(0)$ for large κ.

The result is more difficult to see if $n = m$. By explicit calculation it is found that

$$M_{n,n,l,k}(t) = \begin{cases} \frac{i}{\hbar}\langle\phi_k^{(1)}|H_0|\phi_n^{(1)}\rangle - \langle\dot{\phi}_k^{(1)}|\phi_n^{(1)}\rangle & l = n, k \neq n \\ -\frac{i}{\hbar}\langle\phi_n^{(1)}|H_0|\phi_l^{(1)}\rangle - \langle\phi_n^{(1)}|\dot{\phi}_l^{(1)}\rangle & l \neq n, k = n \\ 0 & l \neq n, k \neq n \\ 0 & l = n, k = n \end{cases}. \tag{E.11}$$

Therefore all cases where $M_{n,n,l,k}(t) \neq 0$ have $l \neq k$. However in this case $\exp\left[\tilde{\Lambda}_{l,k}(t,0)\right] \to 0$ in the limit where $\kappa \to \infty$. In terms of the original coefficients

this gives $c_{n,n}(T) \approx c_{n,n}(0)$ for large κ. So in general we get that $c_{n,m}(T) \approx c_{n,m}(0)$ for all n, m in the case of strong noise i.e. large κ.

Bibliography

[1] Einstein A, Podolsky B, and Rosen N 1935 *Phys. Rev.* **47** 777

[2] Scheich W P et al. 2016 *Appl. Phys. B* **122** 130

[3] `http://www.nobelprize.org/nobel_prizes/physics/laureates/2012/index.html`

[4] Oliveira I S, Bonagamba T J, Sarthour R S, Freitas J C C, and deAzevedo R R 2007, *NMR Quantum Information Processing* (Elsevier, Amsterdam)

[5] Jones J A 2011 *Prog. Nucl. Magn. Reson. Spectrosc.* **59** 91

[6] Bloch I, Dalibard J, and Zwerger W 2008 *Rev. Mod. Physics* **80** 885

[7] Walther H et al 2006 *Rep. Prog. Phys.* **69** 1325

[8] Pethick C J and Smith H 2001, *Bose–Einstein Condensation in Dilute Gases* (Cambridge University Press, Cambridge)

[9] Bassi A and Ghirardi G C 2003 *Phys. Rep.* **379** 257

[10] Bassi A, Lochan K, Satin S, Singh T P, and Ulbricht H 2013 *Rev. Mod. Phys.* **85** 471

[11] Nielsen M A and Chuang I L 2000 *Quantum Computation and Quantum Information* (Cambridge University Press, Cambridge)

[12] `http://www.idquantique.com`

[13] `http://magiqtech.com`

[14] Shor P W 1997 *SIAM J. Comput.* **26** 1484

[15] Grover L K 1996 *Proceedings, 28th Annual ACM Symposium on the Theory of Computing* 212

[16] Cronin A D, Schmiedmayer J, and Pritchard D E 2009 *Rev. Mod. Physics* **81** 1051

[17] Fogarty T, Kiely A, Campbell S, Busch T 2013 *Phys. Rev. A* **87** 043630

[18] Ludlow A D et al. 2015 *Rev. Mod. Physics* **87** 637

[19] DiVincenzo D P 1997, *Mesoscopic Electron Transport* (Kluwer Ac. Publ., Dordrecht)

[20] Born M and Fock V A 1928 *Zeitschrift für Physik A* **51** 165

[21] Torrontegui E, Ibáñez S, Martínez-Garaot S, Modugno M, del Campo A, Guéry-Odelin D, Ruschhaupt A, Chen X and Muga J G 2013 *Adv. At. Mol. Opt. Phys.* **62** 117

[22] Guéry-Odelin D, Muga J G, Ruiz-Montero M J, and Trizac E 2014 *Phys. Rev. Lett.* **112** 180602

[23] Deffner S 2016 *New J. Phys.* **18** 012001

[24] Song X K, Deng F G, Lamata L, Muga J G, ArXiv:1612.03033

[25] Torosov B T, Kyoseva E S, and Vitanov N V 2015 *Phys. Rev. A* **92** 033406

[26] Ivanov S S and Vitanov N V 2015 *Phys. Rev. A* **92** 022333

[27] Torosov B T and Vitanov N V 2014 *Phys. Rev. A* **90** 012341

[28] Glaser S et al. 2015 *Eur. Phys. J. D* **69** 279

[29] van Frank S et al., ArXiv:1511.02247

[30] Doria P, Calarco T, and Montangero S 2011 *Phys. Rev. Lett.* **106** 190501

[31] Jing J, Wu L A, Yu T, You J Q, Wang Z M and Garcia L 2014 *Phys. Rev. A* **89** 032110

[32] Schleich W P 2001, *Quantum Optics in Phase Space* Wiley-VCH Verlag)

[33] Takamoto M, Hong F L, Higashi R and Katori H 2005 *Nature* **435** 321

[34] Kay A, Pachos J K 2004 *New Journal of Physics* **6** 126

[35] Calarco T, Dorner U, Julienne P, Williams C, and Zoller P 2004 *Phys. Rev. A* **70** 012306

[36] Shimizu F 2004 *Japanese Journal of Appl. Phys.* **43** 8376

[37] Lewenstein M, Sanpera A, Ahufinger V, Damski B, Sen(De) A and Sen U 2007 *Adv. Phys.* **56** 243

[38] Bakr W S, Gillen J I, Peng I, Folling S, and Greiner M 2009 *Nature* **462** 74

[39] Sherson J F, Weitenberg C, Endres M, Cheneau M, Bloch I, and Kuhr S 2010 *Nature* **467** 68

[40] Jaksch D, Bruder C, Cirac J I, Gardiner C W, and Zoller P 1998 *Phys. Rev. Lett.* **81** 3108

[41] Bloch I and Greiner M 2005 *Adv. At. Mol. Opt. Phys.* **52** 1

[42] Fisher M P A, Weichman P B, Grinstein G, and Fisher D S 1989 *Phys. Rev. B* **40** 546

[43] Paul W 1990 *Rev. Mod. Physics* **62** 531

[44] Penning F M 1936 *Physica* **3** 873

[45] Fischer E 1959 *Z. Phys.* **156** 1

[46] Paul W , Osberghaus O and Fischer E 1958 *Forschungsberichte des Wirtschaftsund Verkehrsministeriums Nordrhein-Westfalen* **415** (Köln and Opladen, Westdeutscher Verlag)

[47] Castrejon-Pita J R, Ohadi H, Crick D R, Winters D F A, Segal D M and Thompson R C 2007 *Journal of Modern Optics* **54** 1581

[48] Griffiths D J 2013, *Introduction to Electrodynamics* (Pearson)

[49] Wineland D J, Itano W M and van Dyck Jr. R 1983 *Adv. in Atomic and Molecular Physics* **19** 135

[50] Brown L S and Gabrielse G 1986 *Rev. mod. Phys.* **58** 233

[51] Graff G , Major F G , Roeder R W H and Werth G 1968 *Phys. Rev . Lett* **21** 340

[52] Dehmelt H G and Walls F L 1968 *Phys. Rev. Lett* **21** 127

[53] Britton J W, Sawyer B C, Keith A C, Wang C C J, Freericks J K, Uys H, Biercuk M J, and Bollinger J J 2012 *Nature* **484** 489

[54] Goodwin J F, Brown B J, Stutter G, Dale H, Thompson R C, and Rudolph T 2015 *Phys. Rev. A* **92** 032314

[55] Porras D and Cirac J I 2006 *Phys. Rev. Lett.* **96** 250501

[56] Mooser A, Ulmer S, Blaum K, Franke K, Kracke H, Leiteritz C, Quint W, Rodegheri C C, Smorra C, and Walz J 2014 *Nature* **509** 596

[57] DiSciacca J et al. 2013 *Phys. Rev. Lett.* **110** 130801

[58] Goodwin J F, Stutter G, Thompson R C, and Segal D M 2016 *Phys. Rev. Lett.* **116** 143002

[59] Metcalf H J and van der Straten P 1999, *Laser Cooling and Trapping* (Springer)

[60] Chu S 1998 *Rev. Mod. Phys.* **70** 685

[61] Cohen-Tannoudji C 1998 *Rev. Mod. Phys.* **70** 707

[62] Phillips W D 1998 *Rev. Mod. Phys.* **70** 721

[63] Monroe C, Meekhof D M, King B E, Jefferts S R, Itano W M, and Wineland D J 1995 *Phys. Rev. Lett.* **75** 4011

[64] Eschner J, Morigi G, Schmidt-Kaler F, and Blatt R 2003 *J. Opt. Soc. Am. B* **20** 1003

[65] Chen X, Ruschhaupt A, Schmidt S, del Campo A, Guéry-Odelin D, and Muga J G 2010 *Phys. Rev. Lett.* **104** 063002

[66] Muga J G, Chen X, Ibáñez S, Lizuain I, and Ruschhaupt A 2010 *J. Phys. B: At. Mol. Opt. Phys.* **43** 085509

[67] Chen X and Muga J G 2010 *Phys. Rev. A* **82** 053403

[68] Stefanatos D, Ruths J, and Li J S 2010 *Phys. Rev. A* **82** 063422

[69] Muga J G, Chen X, Ruschhaupt A and Guéry-Odelin D 2009 *J. Phys. B: At. Mol. Opt. Phys.* **42** 241001

[70] Torrontegui E, Chen X, Modugno M, Schmidt S, Ruschhaupt A, Muga J G 2012 *New J. Phys.* **14** 013031

[71] Stefanatos D and Li J S 2012 *Phys. Rev. A* **86** 063602

[72] Torrontegui E, Ibáñez S, Chen X, Ruschhaupt A, Guéry-Odelin D, Muga J G 2011 *Phys. Rev. A* **83** 013415

[73] Chen X,Torrontegui E, Stefanatos D, Li J S, Muga J G 2011 *Phys. Rev. A* **84** 043415

[74] Sarandy M S, Duzzioni E I, Serra R M 2011 *Phys. Lett. A* **375** 3343

[75] Lau H K and James D F V 2012 *Phys. Rev. A* **85** 062329

[76] Torrontegui E, Martínez-Garaot S, Modugno M, Chen X, Muga J G 2013 *Phys. Rev. A* **87** 033630

[77] Chen X, Lizuain I, Ruschhaupt A, Guéry-Odelin D, Muga J G 2010 *Phys. Rev. Lett.* **105** 123003

[78] Chen X and Muga J G 2012 *Phys. Rev. A* **86** 033405

[79] Ruschhaupt A, Chen X, Alonso D, Muga J G 2012 *New J. Phys.* **14** 093040

[80] Ban Y, Chen X, Sherman E Y, Muga J G 2012 *Phys. Rev. Lett.* **109** 206602

[81] Herrera M, Sarandy M S, Duzzioni E I, and Serra R M 2014 *Phys. Rev. A* **89** 022323

[82] Yuce C 2012 *Phys. Lett. A* **376** 1717

[83] Ozcakmakli Z,Yuce C 2012 *Phys. Scr.* **86** 055001

[84] del Campo A 2011 *Phys. Rev. A* **84** 031606

[85] del Campo A, Boshier M G 2012 *Sci. Rep.* **2** 648

[86] del Campo A, Rams M M, Zurek W H 2012 *Phys. Rev. Lett.* **109** 115703

[87] Julia-Diaz B, Torrontegui E, Martorell J, Muga J G, Polls A 2012 *Phys. Rev. A* **86** 063623

[88] Lu X J, Muga J G, Chen X, Poschinger U G, Schmidt-Kaler F, Ruschhaupt A 2014 *Phys. Rev. A* **89** 063414

[89] Lu X J, Palmero M, Ruschhaupt A, Chen X, Muga J G 2015 *Physica Scripta* **90** 074038

[90] Palmero M, Martínez-Garaot S, Leibfried D, Wineland D J, Muga J G arXiv:1609.01892

[91] Li Y, Wu L A, Wang Z D 2011 *Phys. Rev. A* **83** 043804

[92] Zhang J Q, Li Y and Feng M 2013 *J. Phys.: Condens. Matter* **25** 142201

[93] Lin T Y, Hsiao F C, Jhang Y W, Hu C, Tseng S Y 2012 *Opt. Exp.* **20** 24085

[94] Tseng S Y, Chen X 2012 *Opt. Lett.* **37** 5118

[95] Mandelstam L and Tamm I G 1945 *I. Phys. USSR* **9** 249

[96] K Bhattacharyya 1983 *J. Phys. A: Math. Gen.* **16** 2993

[97] Margolus N and Levitin L B 1998 *Physica D: Nonlinear Phenomena* **120** 188

[98] Bender C M, Brody D C, Jones H F, Meister B K 2007 *Phys. Rev. Lett.* **98** 040403

[99] Schaff J F, Song X L, Vignolo P, and Labeyrie G 2010 *Phys. Rev. A* **82** 033430

[100] Schaff J F, Song X L, Capuzzi P, Vignolo P and Labeyrie G 2011 *Europhysics Letters* **93** 23001

[101] Schaff J F, Capuzzi P, Labeyrie G and Vignolo P 2011 *New J. Phys.* **13** 113017

[102] Bason M G, Viteau M, Malossi N, Huillery P, Arimondo E, Ciampini D, Fazio R, Giovannetti V, Mannella R and Morsch O 2012 *Nature Phys.* **8** 147

[103] Zhang J, Shim J H, Niemeyer I, Taniguchi T, Teraji T, Abe H, Onoda S, Yamamoto T, Ohshima T, Isoya J, and Suter D 2013 *Phys. Rev. Lett.* **110** 240501

[104] An S, Lv D, del Campo A and Kim K 2016 *Nature Communications* **7** 12999

[105] Du Y X, Liang Z T, Li Y C, Yue X X, Lv Q X, Huang W, Chen X, Yan H and Zhu S L 2016 *Nature Communications* **7** 12479

[106] Kato T 1950 *Journal of the Physical Society of Japan* **5** 435

[107] Avron J E and Elgart A 1999 *Communications in Mathematical Physics* **203** 445

[108] Sarandy M and Lidar D 2005 *Phys. Rev. A* **71** 012331

[109] Bransden B H and Joachain C J 2000, *Quantum Mechanics* (Person Education)

[110] Messiah A 1959, *Quantum Mechanics* (Dunod, Paris)

[111] Comparat D 2009 *Phys. Rev. A* **80** 012106

[112] Martínez-Garaot S, Ruschhaupt A, Gillet J, Busch T, and Muga J G 2015 *Phys. Rev. A* **92** 043406

[113] Bergmann K, Theuer H, and Shore B W 1998 *Rev. Mod. Phys.* **70** 1003; Bergmann K, Vitanov N V, and Shore B W 2015 *J. Chem. Phys.* **142** 170901; Vitanov N V, Rangelov A A, Shore B W, and Bergmann K, arXiv:1605.00224

[114] Gaubatz U et al. 1990 *J. Chem. Phys.* **92** 5363

[115] Menchon-Enrich R, Benseny A, Ahufinger V, Greentree A D, Busch T, and Mompart J 2016 *Rep. Prog. Phys.* **79** 074401

[116] Lewis H R and Riesenfeld W B 1969 *J. Math. Phys.* **10** 1458

[117] Gao X C, Xu J B, Qian T Z 1991 *Phys. Rev. A* **44** 7016

[118] Gao X C, Xu J B, Qian T Z 1992 *Phys. Rev. A* **46** 3626

[119] Lohe M A 2009 *J. Phys. A: Math. Theor.* **42** 035307

[120] Ibáñez S, Martínez-Garaot S, Chen X, Torrontegui E, Muga J G 2011 *Phys. Rev. A* **84** 023415; Erratum: [*Phys. Rev. A* **84** 023415] *Phys. Rev. A* **86** 019901(E)

[121] Fasihi M A, Wan Y, Nakahara M 2012 *J. Phys. Soc. Jpn.* **81** 024007

[122] Torrontegui E, Martínez-Garaot S, and Muga J G 2014 *Phys. Rev. A* **89** 043408

[123] Lewis H R and Leach P G 1982 *J. Math. Phys.* **23** 2371

[124] Ermakov V P 1880 *Univ. Izv. (Kiev)* **20** 1

[125] Berry M V 2009 *J. Phys. A* **42** 365303

[126] Demirplak M and Rice S A *J. Phys. Chem. A* **107** 9937

[127] Zheng Y, Campbell S, De Chiara G, Poletti D 2016 *Phys. Rev. A* 94 042132

[128] Campbell S and Deffner S ArXiv:1609.04662

[129] Campbell S, De Chiara G, Paternostro M, Palma G M, and Fazio R 2015 *Phys. Rev. Lett.* **114** 177206

[130] Vacanti G et al 2014 *New J. Phys.* **16** 053017

[131] Ibáñez S, Chen X, Torrontegui E, Muga J G, Ruschhaupt A 2012 *Phys. Rev. Lett.* **109** 100403

[132] Opatrný T and Mølmer K 2014 *New J. Phys.* **16** 015025

[133] Opatrný T, Saberi H, Brion E, Mølmer K 2016 *Phys. Rev. A* **93** 023815

[134] Masuda S and Nakamura K 2008 *Phys. Rev. A* **78** 062108

[135] Masuda S and Nakamura K 2010 *Proc. R. Soc. A* **466** 1135

[136] Torrontegui E, Martínez-Garaot S, Ruschhaupt A, and Muga J G 2012 *Phys. Rev. A* **86** 013601

[137] Masuda S, Nakamura K, and del Campo A 2014 *Phys. Rev. Lett.* **113** 063003

[138] Masuda S and Nakamura K 2011 *Phys. Rev. A* **84** 043434

[139] Masuda S and Rice S A 2015 *The Journal of Physical Chemistry B* **119** 11079

[140] Razavy M 2003, *Quantum Theory of Tunneling* (World Scientific)

[141] Gati R, Albiez M, Fölling J, Hemmerling B and Oberthaler M K 2006 *Appl. Phys. B* **82** 207

[142] Gradshteyn I S and Ryzhik I M 2007 *Table of Integrals, Series, and Products* (Elsevier, Amsterdam)

[143] Galindo A and Pascual P 1991, *Quantum Mechanics II* (Springer-Verlag Berlin Heidelberg)

[144] Ballentine L 1998 *Quantum Mechanics: A Modern Development* (World Scientific Publishing Co. Pte. Ltd)

[145] Fleck J A, Morris J R, and Feit M D 1976 *Appl. Phys.* **10** 129

[146] Hutson V, Pym J S, and Cloud M 2005, *Applications of functional analysis and operator theory, Mathematics in Science and Engineering* **200** (Elsevier)

[147] `http://www.nvidia.com/object/cuda_home_new.html`

[148] Olver P 2013, *Introduction to Partial Differential Equations* (Springer)

[149] Bouwmeester D, Ekert A and Zeilinger A 2000 *The Physics of Quantum Information: Quantum Cryptography, Quantum Teleportation, Quantum Computation* (Berlin: Springer-Verlag)

[150] Allen L and Eberly J H 1987 *Optical Resonance and Two-Level Atoms* (New York: Dover)

[151] Levitt M H 1986 *Prog. Nucl. Magn. Reson. Spectrosc.* **18** 61

[152] Collin E, Ithier G, Aassime A, Joyez P, Vion D and Esteve D 2004, *Phys. Rev. Lett.* **93** 157005

[153] Torosov B T, Guérin S and Vitanov N V 2011 *Phys. Rev. Lett.* **106** 233001

[154] Vitanov N V, Fleischhauer N, Shore B W and Bergmann K 2001 *Adv. At. Mol. Opt. Phys.* **46** 55

[155] Vitanov N V, Halfmann T, Shore B W and Bergmann L 2001 *Ann. Rev. Phys. Chem* **52** 763

[156] Guérin S and Jauslin H R 2003 *Adv. Chem. Phys* **125** 147

[157] Ruschhaupt A and Muga J G 2013 *J. Mod. Optics* DOI: 10.1080/09500340.2013.846431

[158] Daems D, Ruschhaupt A, Sugny D and Guérin S 2013 *Phys. Rev. Lett.* **111** 050404

[159] Ibáñez S, Chen X and Muga J G 2013 *Phys. Rev.* A **87** 043402

[160] Lu X J, Chen X, Ruschhaupt A, Alonso D, Guérin S, Muga J G 2013 *Phys. Rev. A* **88** 033406

[161] Genov G T and Vitanov N V 2013 *Phys. Rev. Lett.* **110** 133002

[162] Lu T, Miao X and Metcalf H 2007 *Phys. Rev.* A **75** 063422

[163] Miao X, Wertz E, Cohen M G and Metcalf H 2007 *Phys. Rev.* A **75** 011402(R)

[164] Carroll C E and Hioe F T 1990 *Phys. Rev.* A **42** 1522

[165] Eckert K, Lewenstein M, Corbalán R, Birkl G, Ertmer W, and Mompart J 2004 *Phys. Rev. A* **70** 023606

[166] Eckert K, Mompart J, Corbalán R, Lewenstein M, and Birkl G 2006 *Opt. Commun.* **264** 264; McEndoo S, Croke S, Brophy J and Busch T 2010 *Phys. Rev. A* **81** 043640; Benseny A, Fernández-Vidal S, Bagudà J, Corbalán R, Picón A, Roso L, Birkl G, and Mompart J 2010 *Phys. Rev. A* **82** 013604; Gajdacz M, Opatrný T, and Das K K 2011 *Phys. Rev. A* **83** 033623; Benseny A, Gillet J, and Busch T 2016 *Phys. Rev. A* **93** 033629

[167] Menchon-Enrich R, McEndoo S, Busch T, Ahufinger V, and Mompart J 2014 *Phys. Rev. A* **89** 053611

[168] Menchon-Enrich R, McEndoo S, Mompart J, Ahufinger V, and Busch T 2014 *Phys. Rev. A* **89** 013626

[169] Greentree A D, Cole J H, Hamilton A R, and Hollenberg L C L 2004 *Phys. Rev. B* **70** 235317

[170] Fountoulakis A and Paspalakisa E 2013 *J. Appl. Phys.* **113** 174301

[171] Seaman B T, Krämer M, Anderson D Z, and Holland M J 2007 *Phys. Rev. A* **75** 023615; Pepino R A, Cooper J, Anderson D Z, and Holland M J 2009 *Phys. Rev. Lett.* **103** 140405

[172] Jaksch D, Briegel H J, Cirac J I, Gardiner C W, and Zoller P 1999 *Phys. Rev. Lett.* **82** 1975

[173] Loiko Y, Ahufinger V, Menchon-Enrich R, Birkl G and Mompart J 2014 *Eur. Phys. J. D* **68** 147

[174] Longhi S 2006 *Phys. Rev. E* **73** 026607; Longhi S, Della Valle G, Ornigotti M and Laporta P 2007 *Phys. Rev. B* **76** 201101

[175] Kiely A and Ruschhaupt A 2014 *J. Phys B* **47** 115501

[176] Hsieh C Y, Shim Y P, Korkusinski M, and Hawrylak P 2012 *Rep. Prog. Phys.* **75** 114501

[177] Domínguez F, Platero G, and Kohler S 2010 *Chem. Phys.* **375** 284

[178] Huneke J, Platero G, and Kohler S 2013 *Phys. Rev. Lett.* **110** 036802

[179] Jong L M and Greentree A D 2010 *Phys. Rev. B* **81** 035311; Mousolou V A arXiv:1510.05306; Zeng Q B, Chen S, Lü R, arXiv:1608.00065.

[180] Braakman F R, Barthelemy P, Reichl C, Wegscheider W, and Vandersypen L M K 2013 *Nat. Nanotechnol.* **8** 432

[181] Seidelin S et al. 2006 *Phys. Rev. Lett.* **96** 253003

[182] Aharonov Y and Bohm D 1959 *Phys. Rev.* **115** 485

[183] Graf M and Vogl P 1995 *Phys. Rev. B* **51** 4940; Ismail-Beigi S et al. 2001 *Phys. Rev. Lett.* **87** 087402; Cehovin A et al. 2004 *Phys. Rev. B* **69** 045411

[184] Carroll C E and Hioe F T 1988 *J. Opt. Soc. Am. B* **5** 1335

[185] Unanyan R G, Yatsenko L P, Bergmann K, and Shore B W 1997 *Opt. Commun.* **139** 48

[186] Dalibard J, Gerbier F, Juzeliūnas G, and Öhberg P 2011 *Rev. Mod. Phys.* **83** 1523

[187] Polo J, Mompart J, and Ahufinger V 2016 *Phys. Rev. A* **93** 033613

[188] Torosov B T and Vitanov N V 2011 *Phys. Rev. A* **83** 053420

[189] Lewenstein M, Sanpera A, and Ahufinger V 2012, *Ultracold Atoms in Optical Lattices: Simulating Quantum Many-Body Systems* (Oxford University Press, Oxford)

[190] Gorshkov A V et al. 2010 *Nature Physics* **8** 289

[191] Cappellini G et al. 2014 *Phys. Rev. Lett.* **113** 120402

[192] Bakr W S, Peng A, Tai M E, Ma R, Simon J, Gillen J I,Fölling S, Pollet L, and Greiner M 2010 *Science* **329** 547

[193] Gemelke N, Zhang X, Hung C L and Chin C 2009 *Nature* **460** 995

[194] Greiner M, Mandel O, Esslinger T, Hänsch T W and Bloch I 2002 *Nature* **415** 39-44

[195] Spielman I B, Phillips W D and Porto J V 2007 *Phys. Rev. Lett.* **98** 080404

[196] Kamihara Y, Hiramatsu H, Hirano M, Kawamura R, Yanagi H, Kamiya T, and Hosono H 2006 *J. Am. Chem. Soc.* **128** 10012

[197] Luke G M, Fudamoto Y, Kojima K M, Larkin M I, Merrin J, Nachumi B, Uemura Y J, Maeno Y, Mao Z Q, Mori Y, Nakamura H, and Sigrist M 1998 *Nature* **394** 558

[198] Ohtomo A and Hwang H Y 2004 *Nature* **427** 423

[199] Lewenstein M and Liu W V 2011 *Nat. Phys.* **7** 101

[200] Li X and Liu W V 2016 *Rep. Prog. Phys.* **79** 116401

[201] Isacsson A and Girvin S M 2005 *Phys. Rev. A* **72** 053604

[202] Kuklov A B 2006 *Phys. Rev. Lett.* **97** 110405

[203] Liu W V and Wu C 2006 *Phys. Rev. A* **74** 013607

[204] Hébert F, Cai Z, Rousseau V G, Wu C, Scalettar R T, and Batrouni G G 2013 *Phys. Rev. B* **87** 224505

[205] Browaeys A, Häffner H, McKenzie C, Rolston S L, Helmerson K, and Phillips W D 2005 *Phys. Rev. A* **72** 053605

[206] Müller T, Fölling S, Widera A, and Bloch I 2007 *Phys. Rev. Lett.* **99** 200405

[207] Wirth G, Ölschläger M and Hemmerich A 2011 *Nat. Phys.* **7** 147

[208] Ölschläger M, Wirth G and Hemmerich A 2011 *Phys. Rev. Lett.* **106** 015302

[209] Ölschläger M, Wirth G, Kock T, and Hemmerich A 2012 *Phys. Rev. Lett.* **108** 075302

[210] Sowinski T 2012 *Phys. Rev. Lett.* **108** 165301

[211] Holder B and Reichl L E 2007 *Phys. Rev. A* **76** 013420

[212] André Eckardt arXiv:1606.08041

[213] Dum R, Sanpera A, Suominen K A, Brewczyk M, Kuś M, Rzaążewski K, and Lewenstein M 1998 *Phys. Rev. Lett.* **80** 3899

[214] Bücker R, Berrada T, van Frank S, Schaff J F, Schumm T, Schmiedmayer J, Jäger G, Grond J and Hohenester U 2013 *J. Phys B* **46** 104012

[215] van Frank S, Negretti A, Berrada T, Bücker R, Montangero S, Schaff J F, Schumm T, Calarco T, and Schmiedmayer J 2014 *Nat. Commun.* **5** 4009

[216] Schneider P I and Saenz A 2012 *Phys. Rev. A* **85** 050304(R)

[217] Stuck J et al. 2012 *Phys. Rev. Lett.* **108** 225304

[218] Zhang S-L and Zhou Q 2014 *Phys. Rev. A* **90** 051601

[219] Sträter C and Eckardt A 2015 *Phys. Rev. A* **91** 053602

[220] Zhang S L, Lang L J, and Zhou Q 2015 *Phys. Rev. Lett.* **115** 225301

[221] Weinberg M et al. 2015 *Phys. Rev. A* **92** 043621

[222] Parker C V, Ha L-C, and Chin C 2013 *Nat. Phys.* **9** 769

[223] Khamehchi M A, Qu C, Mossman M E, Zhang C, and Engels P 2016 *Nat. Commun.* **7** 10867

[224] Hallaji M, Zhuang C, Hayat A, Motzoi F, Khani B,Wilhelm F K and Steinberg A M 2015 arXiv: 1510.09186

[225] Lu X J, Chen X, Ruschhaupt A, Alonso D, Guérin S, Muga J G 2013 *Phys. Rev. A* **88** 033406

[226] Collin A, Larson J, and Martikainen J P 2010 *Phys. Rev. A* **81** 023605

[227] Schloss J, Benseny A, Gillet J, Swain J, and Busch T 2016 *New J. Phys.* **18** 035012

[228] Güngördü U, Wan Y, Ali Fasihi M and Nakahara M 2012 *Phys. Rev. A* **86** 062312

[229] Martínez-Garaot S, Torrontegui E, Chen X, and Muga J G 2014 *Phys. Rev. A* **89** 053408

[230] Ivanov V V et al 2008 *Phys. Rev. Lett.* **100** 043602

[231] Zenesini A, Lignier H, Ciampini D, Morsch O, Arimondo E 2009 *Phys. Rev. Lett.* **102** 100403

[232] Arimondo E, Ciampini D, Eckardt A, Holthaus M, Morsch O 2012 *Adv. At. Mol. Opt. Phys.* **61** 515

[233] Sias C, Lignier H, Singh Y P , Zenesini A, Ciampini D, Morsch O, Arimondo E 2008 *Phys. Rev. Lett.* **100** 040404

[234] Zwerger W 2003 *J. Opt. B* **5** S9

[235] Eckardt A, Weiss C, and Holthaus M 2005 *Phys. Rev. Lett.* **95** 260404

[236] Lignier H et al. 2007 *Phys. Rev. Lett.* **99** 220403

[237] Polo J, Mompart J and Ahufinger V 2016 *Phys. Rev. A* **93** 033613

[238] Deffner S, Jarzynski C, and del Campo A 2014 *Phys. Rev. X* **4** 021013

[239] Schaff J F, Song X L, Vignolo P, and Labeyrie G, 2010 *Phys. Rev. A* **82** 033430; 2011 *Phys. Rev. A* **83** 059911(E)

[240] Schaff J F, Song X L, Capuzzi P, Vignolo P, and Labeyrie G 2011 *Europhys. Lett.* **93** 23001

[241] Palmero M, Martínez-Garaot S, Alonso J, Home J P, and Muga J G, 2015 *Phys. Rev. A* **91** 053411

[242] Li Y, Wu L A, and Wang Z D 2011 *Phys. Rev. A* **83** 043804

[243] Zhang J-Q, Yong L, and Feng M 2013 *J. Phys.: Condens. Matter* **25** 142201

[244] Salamon P, Hoffmann K H, Rezek Y, and Kosloff R 2009 *Phys. Chem. Chem. Phys.* **11** 1027

[245] Hoffmann K H, Salamon P, Rezek Y, and Kosloff R 2011 *Europhys. Lett.* **96** 60015

[246] del Campo A, Goold J, and Paternostro M 2013 *Sci. Rep.* **4** 6208

[247] Choi S, Onofrio R, and Sundaram B 2011 *Phys. Rev. A* **84** 051601(R)

[248] Choi S, Onofrio R, and Sundaram B 2012 *Phys. Rev. A* **86** 043436

[249] Torrontegui E, Chen X, Modugno M, Ruschhaupt A, Guéry-Odelin D, and Muga J G 2012 *Phys. Rev. A* **85** 033605

[250] K Blaum, Novikov Yu N, and Werth G 2010 *Contemporary Physics* **51** 149

[251] Quint W and Vogel M 2014 *Fundamental Physics in Particle Traps* (Springer)

[252] Werth G, Gheorghe V N, and Major F G 2009 *Charged Particle Traps* (Springer)

[253] Blaum K and Herfurth F 2008 *Trapped Charged Particles and Fund. Interactions* (Springer)

[254] de Brito P E and Nazareno H N 2007 *Eur. J. Phys.* **28** 9

[255] Fiore G and Gouba L 2011 *J. Math. Phys.* **52** 103509

[256] del Campo A, Egusquiza I L, Plenio M B, and Huelga S F 2013 *Phys. Rev. Lett.* **110** 050403

[257] Deffner S and Lutz E 2013 *Phys. Rev. Lett.* **111** 010402

[258] Deffner S 2014 *J. Phys. B: At. Mol. Opt. Phys.* **47** 145502

[259] Lidar D A 2014 *Quantum Information and Computation for Chemistry: Advances in Chemical Physics* **154** 295

[260] Breuer H P and Petruccione F 2002, *The theory of open quantum systems* (Oxford)

[261] Carmichael H J 1999, *Statistical Methods in Quantum Optics 1: Master Equations and Fokker-Planck Equations* (Springer)

[262] Saira O P, Bergholm V, Ojanen T, and Möttönen M 2007 *Phys. Rev. A* **75** 012308

[263] Chenu A, Beau M, Cao J, and del Campo A, ArXiv:1608.01317.

[264] Hänggi P 1980 *Z. Physik B* **36** 271

[265] D. J. Daley and D. Vere-Jones, *An Introduction to the Theory of Point Processes: Volume II : Elementary Theory and Methods* (Springer, New York, 2008)

[266] D. J. Daley and D. Vere-Jones, *An Introduction to the Theory of Point Processes: Volume II: General Theory and Structure* (Springer, New York, 2008)

[267] Kim C, Lee E K, Hänggi P, and Talkner P 2007 *Phys. Rev. E* **76** 011109

[268] Dykman M I 2010 *Phys. Rev. E* **81** 051124

[269] Ichiki A, Tadokoro Y, and Dykman M I 2013 *Phys. Rev. E* **87** 012119

[270] Zou J, Buvaev S, Dykman M, and Chan H B 2012 *Phys. Rev. B* **86** 155420

[271] Huard B, Pothier H, Birge N O, Esteve D, Waintal X, and Ankerhold J 2007 *Ann. Phys.* **16** 736

[272] Sukhorukov E V and Jordan A N 2009 *Phys. Rev. Lett.* **102** 086806

[273] Khovanova N A and Khovanov I A 2011 *Appl. Phys. Lett.* **99** 144101

[274] Czernik T, Kula J, Luczka J, and Hänggi P 1997 *Phys. Rev. E* **55** 4057

[275] Spiechowicz J, Luczka J, and Hänggi P 2013 *J. Stat. Mech.* P02044

[276] Horsthemke W and McCarty P 1986 *Physics Letters A* **117** 1

[277] Børkje K, Nunnenkamp A, Zwickl B M, Yang C, Harris J G E, and Girvin S M 2010 *Phys. Rev. A* **82** 013818

[278] Purdy T P, Peterson R W, and Regal C A 2013 *Science* **339** 801

[279] Luczka J and Niemiec M 1991 *J. Phys. A: Math. Gen.* **24** L1021

[280] Levy A and Kosloff R 2012 *Phys. Rev. Lett.* **108** 070604

[281] Levy A and Kosloff R 2014 *Annual Review of Physical Chemistry* **65** 365

[282] Van Den Broeck C 1983 *J. Stat. Phys.* **31** 467

[283] Ankerhold J and Pechukas P 2000 *Europhys. Lett.* **52** 264

[284] Gurvitz S, Aharony A, and Entin-Wohlman O 2016 *Phys. Rev. B* **94** 075437

[285] Cheng B, Wang Q H, and Joynt R 2008 *Phys. Rev. A* **78** 022313

[286] Luczka J 1991 *Czech. J. Phys.* **41** 289

[287] Budini A A 2001 *Phys. Rev. A* **64** 052110

[288] Pascazio S 2004 *Journal of Modern Optics* **51** 925

[289] Facchi P, Fazio R, Florio G, Pascazio S, and Yoneda T 2006 *Found. Phys.* **36** 500

[290] Nakazato H and Pasczio S 1999 *Journal of Superconductivity* **12** 843

[291] Facchi P and Pascazio S 2003, *The Physics of Communication - Proceedings of the XXII Solvay Conference on Physics* (World Scientific, Singapore)

[292] Facchi P and Pascazio S 2002 *Phys. Rev. Lett.* **89** 080401

[293] Klyatskin V L and Tatarsky V I 1973 *Teor Mat. Fiz.* **17** 273

[294] Shapiro V E and Loginov V M 1978 *Physicsa* **91A** 563

[295] Lindblad G 1976 *Commun. Math. Phys.* **48** 119

[296] Mandel L and Wolf E 1995, *Optical Coherence and Quantum Optics* (Cambridge University Press,Cambridge)

[297] Novikov E A 1965 *Soviet physics, J. Exp. Theor. Phys.* **20** 5

[298] Sarandy M S and Lidar D A 2005 *Phys. Rev. A* **71** 012331

[299] Ibáñez S and Muga J G 2014 *Phys. Rev. A* **89** 033403

[300] Lu T X, Miao X, and Metcalf H 2007 *Phys. Rev. A* **75** 063422

[301] Miao X, Wertz E, Cohen M G, and Metcalf H 2007 *Phys. Rev. A* **75** 011402

[302] Lu T S 2011 *Phys. Rev. A* **84** 033411

[303] Mensky M B 2003 *Proceedings TH2002 Supplement* **197** 205

[304] Mensky M B 1993, *Continuous Quantum Measurements and Path Integrals* (CRC Press)

[305] Mensky M B 2013, *Quantum Measurements and Decoherence: Models and Phenomenology* (Springer Science and Business Media)

[306] Caneva T, Calarco T, Montangero S 2011 *Phys. Rev. A* **84** 022326

[307] Struck J et al. 2013 *Nature Physics* **9** 738

[308] Dutta O et al 2015 *Rep. Prog. Phys.* **78** 066001

[309] Dekorsy T, Ott R, Kurz H, and Köhler K 1995 *Phys. Rev. B* **51** 17275

[310] Morsch O, Muller J H, Cristiani M, Ciampini D, and Arimondo E 2001 *Phys. Rev. Lett.* **87** 140402

[311] Verdeny A, Puig J and Mintert F, arXiv:1603.03923

[312] Novicenko V, Anisimovas E and Juzeliunas G, arXiv:1608.08420

[313] Stenholm S 2009 *Rev. Mod. Phys.* **58** 699

[314] Home J P, Hanneke D, Jost J D, Leibfried D, and Wineland D J 2011 *New J. Phys.* **13** 073026

[315] Leibfried D, Blatt R, Monroe C, and Wineland D J 2003 *Rev. Mod. Phys.* **75** 281

[316] Martínez-Garaot S, Palmero M, Muga J G, Guéry-Odelin D, arXiv:1609.01887

[317] Eroms J, van Schaarenburg L C, Driessen E F C, Plantenberg J H, Huizinga C M, Schouten R N, Verbruggen A H, Harmans C J P M, and Mooij J E 2006 *Appl. Phys. Lett.* **89** 122516